Evolutionary Competition in Microbial Communities:

From Population Dynamics to Single-Cell Behavior

Nuno Miguel Oliveira

A thesis submitted for the degree of *Doctor of Philosophy*

University of Oxford, Merton College

Trinity term 2015





Statement of Originality

I declare that this thesis was composed by myself and that the work contained herein is my own except where explicitly stated in the text. This work has not been submitted for any degree or professional qualification except as specified.

Nuno Miguel Oliveira, Trinity 2015

For Mom and Dad.



And for the animalcules too!

Acknowledgments

Newton's expression '*If I have seen further, it is by standing on the shoulders of Giants'*, is typically associated with the idea of using the understanding accumulated by other scientists to make intellectual progress. I have plenty of those 'Giants', who I cite throughout this thesis. But I also have many others to whom I am deeply grateful.

Clearly, 'if I have seen further', it only happened because of my supervisor Kevin for giving me complete freedom in my research, freedom to explore and make mistakes, while remaining supportive and offering (a lot of) time-consuming supervision throughout. And obviously for putting up with me and my bad temper, which is likely even harder to deal with than my very many and regular queries on the biology of our little bugs. I am very glad I chased you until you accepted being my supervisor, and I would do it again if I had to start from scratch. Thanks for sharing your wisdom with me, and for your patience. I will have to come back to you still (below).

Then, I have to thank Rene and Mack for all their help, and for being co-authors of most of my work. As 'co-authors' suggests, it only happened because of you as well.

I have to thank all the comments and discussion from many colleagues, friends and collaborators, including: Judith Armitage, Howard Berg, Mette Burmolle, Jim Collins, Dan Cornforth, Julian Davies, Vlad Denic, Alex Flecher, Steve Frank, Eamonn Gaffney, Ashleigh Griffin, Jeffery Guasto, Roberto Kolter, Michael Laub, Richard Lenski, Craig MacLean, Esteban Martinez-Garcia, Jeff Morris, Andrew Murray, Timothy Pedley, Gail Preston David Queller, Katharina Ribbeck, Joel Sachs, Linus Schumacher, Soren Sorensen, Bodo Stern, Roman Stocker, Joan Strassmann, Harris Wang, Stu West, Gerard Wong and João Xavier.

I cannot forget all the students and post-docs of the Foster, West, Griffin and MacLean labs for their feedback and constant support, as well as for their patience regarding my overuse of incubators, robot and microscope. In particular, I have to thank Wook, Sara, Despoina, Diego, Alvaro, Vitoria, Lorenzo, Tom, Mila, Danna, Jonas, Kat, Jamie, Oliver, Rose, Isabel, Melanie, Karl, QQ, Michael, Nick, John and David.

And because a PhD is not just about the work we produce but also the journey and the overall experience, I have to thank the folks in DTC, particularly Hima and Georg for being annoyingly clever and very hard to beat, my fellow Mertonians and all the staff of Merton College for sharing with me the grounds of the best college in Oxford, and obviously the rowing and triathlon clubs of Oxford University for pushing the limits of my game. You have all contributed to make Oxford such a unique experience. Whatever happens from here, my heart will always be dark blue.

I cannot forget my parents, to whom this thesis is dedicated, for their constant encouragement and support, as well as DTC/EPSRC, FCT and ERC for funding.

Finally, I must thank my friend Jorge Carneiro from IGC for his inspiring words on the importance of exploring and opening new doors in Science. To him, and my supervisor Kevin who never limited that quest, I dedicate my last data chapter that represents, I really hope, true novelty. And obviously, I cannot forget the animalcules for sharing with me some of their secrets. This is clearly all your fault, and it was a privilege.

Publications and statement of authorship

The majority of each data chapter in this thesis has been my own work but I have received help from other people. Several publications arose from this work and I am the first author in all of them. However, I clarify below the contribution of others to each data chapter and respective publication.

Chapter 2 has been published as:

Oliveira NM, Niehus R, Foster KR (2014) Evolutionary limits to cooperation in microbial communities. *PNAS* 111(50):17941-17946.

Rene Niehus helped with the analysis; Kevin Foster was involved in the interpretation of results and has commented on the manuscript.

Chapter 3 has been published as:

Oliveira NM, Martinez-Garcia E, Xavier J, Durham WM, Kolter R, Kim W, Foster KR (2015) Biofilm formation as a response to ecological competition. *PLoS Biology* 13(7):e1002191.

Esteban Martinez-Garcia, João Xavier and Kevin Foster helped with data collection and analysis; all authors helped with the interpretation and commented on the manuscript.

Chapter 4 is currently in review as:

Oliveira NM, Durham WM, Foster KR. Single-cell twitching chemotaxis during biofilm formation. In review.

William Durham helped with data collection and analysis; both William Durham and Kevin Foster helped with the interpretation and commented on the manuscript.

Chapter 5 is currently in preparation for submission as:

Oliveira NM, Durham WM, Foster KR. Bacterial chemotaxis towards antibiotics results in extreme phenotypic resistance. In prep.

William Durham and Kevin Foster helped with the interpretation and commented on the manuscript.

For convenience I retain the format of the respective journal for each data chapter of my thesis, which includes *PNAS* (Chapter 2, published), *PLoS Biology* (Chapter 3, published), *Nature* (Chapter 4, in review) and *Cell* (Chapter 5, in prep). Published works by the time of submission of this thesis are included in the Appendix in their published format.

ABSTRACT

Microbial life in nature is typically associated with two distinctive features: (i) the formation of densely packed groups, mostly on surfaces, within which social interactions are rife, and (ii) mixing with multiple strains and species, which brings with it the potential for strong evolutionary conflict. However, most microbiology still rests upon the study of single genetic backgrounds, often in shaking flasks. There is a need then to better integrate the natural ecology and evolution of microbes into microbiological studies. My thesis combines ecoevolutionary theory with the empirical study of both population dynamics and single-cell behavior to understand social interactions within microbial communities. This systems biology approach suggests that competition, not cooperation, is central to understanding diverse microbial communities and can explain key social phenotypes including cross-feeding, biofilm formation and antibiotic resistance. Specifically, I study the theoretical limits for cooperation within microbial communities and conclude that natural selection will rarely favor cooperation between genotypes; I show that antibiotic competition between strains is an important driver of biofilm formation, which is consistent with the idea of competition sensing (the ability to use antibiotics, or more generally any form of biotic stress, as a cue to detect and respond to ecological competition); I establish the behavioral and genetic basis of chemotaxis on surfaces at the single-cell level and discuss how this phenotype can be useful in the social milieu of microbial communities where positioning is a major determinant for evolutionary competition; and finally, I show that bacteria are able to climb antibiotic gradients via twitching chemotaxis and achieve an unprecedented level of resistance in a few hours by simply modulating their physiology. Again, and as for antibiotic-induced biofilm formation, I argue that this perplexing phenotype has its natural roots in competition sensing. The study of microbial interactions has emphasized the importance of cooperation between cells of a single genotype. My thesis shows the need to consider the other side of microbial interactions: evolutionary competition. A cell will commonly face intense competition from other strains and species, and only by appreciating this evolutionary conflict will we fully understand microbes and their complex communities.

TABLE OF CONTENTS

Chapter

1.	Introduction	9
2.	Evolutionary limits to cooperation in microbial communities	20
3.	Biofilm formation as a response to ecological competition	42
4.	Single-cell twitching chemotaxis during biofilm formation	73
5.	Bacterial chemotaxis towards antibiotics results in extreme phenotypic resistance	86
6.	Discussion and Conclusion	113
7.	Bibliography	129
8.	Appendix	149

1. Introduction

Hail to the animalcules 9

Genetic diversity and sociality within microbial communities 10

Evolutionary ecology of microbial responsiveness 14

***Pseudomonas aeruginosa* as model organism** 16

Thesis outline 17

Hail to the animalcules

The study of microbes encompasses members of the domain Bacteria and Archaea (Achtman and Wagner, 2008), but can also include some members of the domain Eukarya such as unicellular algae, fungi, protists (Martiny et al., 2006) and even small animals such as rotifers (Robeson et al., 2011). It is clear, however, that 'microbe' and 'macrobe' are not used as biologically coherent or evolutionary meaningful terms (O'malley, 2009). The reason for such diversity in the classification is that microbes here are defined by size, as being microscopic living organisms, rather than phylogeny. It was pioneers like Antony van Leeuwenhoek who first classified microbes based upon the latest imaging technology of the day. Leeuwenhoek did not himself use the term microbes, however, but the term 'animalcules' (Dobell, 1960): *'and I then most always saw, with great wonder, that in the sad matter there were very little living animalcules, very prettily a-moving'*. What is striking is that these early observations already included an appreciation of both diversity and motility in microbial groups, and curiously this 'sad matter' that Leeuwenhoek refers to was actually a fragment of a surface-attached community from his own mouth. While these properties were mostly ignored during the emergence of microbiology as a research field, typically focusing

on single genetic backgrounds in well-mixed flasks, they are central to my thesis. I present next a general introduction to social evolution in microbial communities, and each data chapter comes with dedicated introduction for the main topics of study.

Genetic diversity and sociality within microbial communities

One of the most distinctive features of natural microbial communities is their impressive genetic diversity (Figure 1A). In natural systems as varied as soil, thermal vents, stromatolites and, with relevance for us, the human gut or oral cavity, microbes mix with multiple and diverse strains and species as suggested by metagenomic analysis (Baumgartner et al., 2009; Gans et al., 2005; Lozupone and Knight, 2007; Roesch et al., 2007; Sogin et al., 2006; Yooseph et al., 2007). Such genetic diversity can reach astonishing proportions: a simple gram of soil can contain one million different species, and even inside us it can reach one thousand (Murray et al., 2014), suggesting that the paradigm of classical microbiology of studying pure cultures will rarely hold outside the lab. This impressive genetic diversity is particularly striking in surface-associated communities, often called 'biofilms' (Mitri et al., 2011; Nadell et al., 2009), which are a central feature of this thesis (Chapters 3, 4 and 5).

Recognizing this vast diversity within microbial communities is important as evolutionary and ecological theories teach us it should have strong impact on microbial life (Hamilton, 1964a, b; May and McLean, 2007). Specifically, diversity is considered central to predicting 'social' interactions within microbial communities. In evolutionary biology, social behaviors are those that affect the survival and reproduction of both the 'actor' and 'recipient' in a biological interaction (West et al., 2007b). They are often categorized as mutually beneficial traits (actor/recipient: +/+), selfish (actor/recipient: +/−), altruistic (actor/recipient: −/+) and spiteful

(actor/recipient: −/−). More generally, mutually beneficial and altruistic behaviors are associated with *cooperation* between individuals while selfish and spiteful traits with *competition*. Throughout this thesis I will mainly talk about competition and cooperation but I included here the above terminology for completeness.

Diversity is considered fundamental to understanding social phenotypes in microbes because genetic diversity reduces the average relatedness, i.e. frequency of clonemates, of the group leading to the potential for strong social interactions, which typically promote competition and conflict and conversely limit cooperation (Hamilton, 1964a, b). Arguably one of the clearest illustrations of this mixing effect in the microbial world is the evolution of antibiotics, namely narrow killing spectrum bacteriocins that specifically target closely related strains of the producing individuals (Figure 1B,C,D). The widespread production of such antimicrobials across phylogenies (Riley and Wertz, 2002) is indicative of how important interactions with genetically similar genotypes is for microbial evolution, and consistent with recent overviews on the microbial diversity of environments such as the soil where related genotypes typically co-occur (Lozupone and Knight, 2007).

However, social phenotypes in microbes extend beyond antibiotic warfare, including not only growth rate regulation such as the switches between prudent and wasteful metabolic states that are often associated with the pace and yield of growth, but also the widespread secretion of other compounds that can either enhance or inhibit the growth of neighbors, namely digestive secretions, siderophores, communication molecules, quorum quenchers and polymeric substances for protection or smothering other genotypes, just to cite a few examples (Crespi, 2001; Nadell et al., 2009; West et al., 2007a).

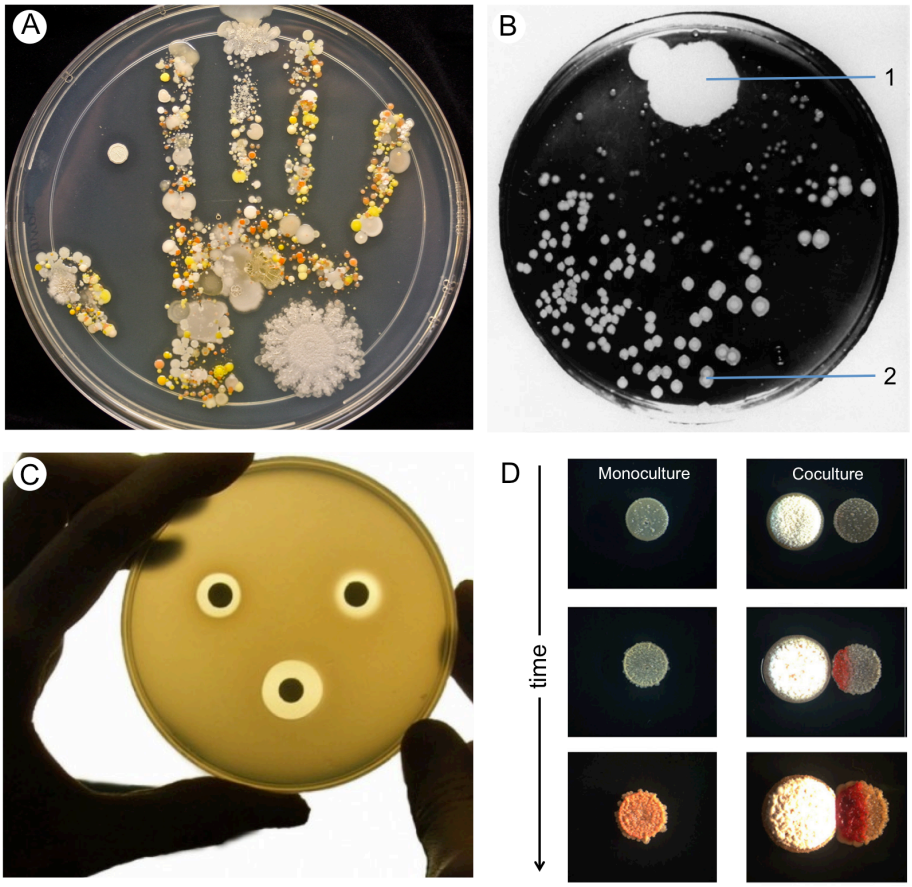

Figure 1: Interacting Microbes. (**A**) Handprint of 8-year-old's child on a TSA plate after playing outdoors. It shows the glory of the microbial world lurking everywhere. Note the diversity of colors and shapes of bacterial colonies, which likely belong to very different phylogenies. Credits to Tasha Sturm. (**B,C,D**) Interference competition via antibiotic production. (**B**) Antibiotic discovery was associated with warfare between microbes. Alexander Fleming discovered penicillin after observing that fungi (1, *Peniccilium notatum* colony) produced a factor, also named 'mold juice' at that time, which created a clear zone of inhibition around producers, preventing the growth of bacteria (2, *Staphylococcus aureus* colony). (**C**) Pictured are zones of inhibition in a lawn of a susceptible genotype (*Escherichia coli* BZB1011) surrounding filter disks soaked with antibiotic (top-left, penicillin), bacteriocin (top-right, colicin E1) and a combination of the two (bottom). Picture courtesy of Margaret Riley. (**D**) Bacteria fight back when threatened. Images show that *Streptomyces coelicolor* produce the antibiotic prodiginine (dark red pigment) when cocultured with other competing strains. Adapted from (Traxler et al., 2013).

The study of social interactions then is fundamental to understanding a wide range of microbial phenotypes and impacts. Perhaps the clearest examples of impacts are the phenotypes that affect microbial virulence and antibiotic resistance, including

biofilm formation and the production of extracellular secretions that can be used to exploit the host, often via quorum-sensing regulation (Nadell et al., 2009; West et al., 2007a). Importantly, many diseases do not have a single etiological agent, and there is the potential for strong synergism in polymicrobial infections (Murray et al., 2014). There is a clear need to understand interactions within disease-associated microbial communities and how they affect perturbations, both environmental and anthropogenic (Foster, 2005; Mitri and Foster, 2013; Murray et al., 2014; Nadell et al., 2009).

Social interactions are clearly common in the microbial world, but are they driven by cooperation or conflict between interacting individuals? Undoubtedly both are important. Theory suggests that cooperation should primarily be seen between members of the same genotype, because these are like cells within a multicellular organism, while competition should dominate between different strains and species (Cornforth and Foster, 2013; Mitri and Foster, 2013; Nadell et al., 2009).

The importance of cooperation within genotypes has been demonstrated in an extensive number of theoretical and empirical studies (Brown and Johnstone, 2001; Buckling et al., 2007; Chuang et al., 2009; Cremer et al., 2012; Datta et al., 2013; Diggle et al., 2007; Griffin et al., 2004; Nadell et al., 2010; Rainey and Rainey, 2003; Van Dyken et al., 2013; West and Buckling, 2003; Xavier et al., 2011). Moreover, large empirical surveys of microbial communities support this 'genotypic view' and suggest that competition is important for interactions between species (Foster and Bell, 2012; Freilich et al., 2011; Vetsigian et al., 2011). However, there are also many recent laboratory studies suggesting that between genotype cooperation is both common and can easily evolve in microbial groups (Andersson et al., 2008; Burmolle et al., 2014; Burmolle et al., 2006; Elias and Banin, 2012; Lee et al., 2014; Little et al., 2008; Moller et al., 1998; Ren et al., 2014a; Ren et al., 2014b; Zelezniak et al., 2015). The

lack of consensus in the field, and the absence of dedicated mathematical theory, prompted me to develop a theoretical framework to specifically address the relative importance of cooperation and competition in microbial communities (Chapter 2).

Evolutionary ecology of microbial responsiveness

When cells meet and mix with other genotypes there is a clear evolutionary incentive to develop adaptations that improve competitive ability (Mitri and Foster, 2013). An interesting corollary of this idea is that there should be an incentive for a cell to detect competitors and respond accordingly, either by protecting itself, fleeing, or engaging in counter attack. But how could a cell detect other genotypes? One way is to detect specific molecules that are secreted or otherwise released by other genotypes. A good documented example of the latter includes the use of peptidoglycan fragments by *P. aeruginosa* as a cue to stimulate the production of several extracellular factors including the antibiotic pyocyanin (Korgaonkar et al., 2013; Korgaonkar and Whiteley, 2011). The logic is that peptidoglycan shedding will typically inform on the rising threat of Gram-positive bacteria in natural communities that need to be outcompeted.

Another way to detect other strains is by directly detecting the fitness effects of a nearby genotype. This is the idea that has been called 'competition-sensing', which suggests that bacteria use the well-studied regulatory networks associated with sensing stress to reliably detect and respond to evolutionary competition, where responding cells are effectively detecting the harmful effects driven by competitors (Cornforth and Foster, 2013). The key prediction from this hypothesis is that bacteria will counter-attack and consistent with this, antibiotic production is often upregulated by stress responses associated with biotic stress such as nutrient limitation (stringent and general stress responses) and cell damage (envelope, DNA damage and oxidative stress

responses), while similar regulatory effect is not common for those associated with the abiotic environment such as heat and osmotic stress (Cornforth and Foster, 2013).

An important aspect of the competition-sensing hypothesis is that stress responses have two major advantages over other forms of sensing competitors: (i) the detection mechanism is general, and thus with broad range applications (here read, it can be used for detecting multiple genotypes, which can be a strength in diverse microbial communities), and (ii) it directly detects harmfulness, arguably the most important effect of a competitive interaction (Cornforth and Foster, 2013). Moreover, the authors argue that cell damage is likely the best indicator for detecting evolutionary competition in microbial communities given that the information on nutrient limitation cannot typically discern between self and other genotypes. This simple and elegant argument drove me to investigate the effects of interference competition associated with cell damage on other important microbial phenotypes to add on the initial focus of the authors, antibiotic kickback (Cornforth and Foster, 2013). My hypothesis was that, if cell damage has such predominance in the evolutionary ecology of microbial groups, then one would expect it also influences other major social traits, not just antibiotic production. In particular it could influence important phenotypes associated with protection or even retreat from the attack.

Consistent with this idea, one of the most widespread responses reported in bacteria is the formation of biofilms upon treatment with sub-lethal concentrations of antibiotics (Elliott et al., 2010; Haddadin et al., 2010; Hoffman et al., 2005; Kaplan, 2011; Kaplan et al., 2012; Kumar and Ting, 2013; Linares et al., 2006; Wang et al., 2010). This observation and the above rational drove me to study what is arguably the key social phenotype of bacteria, biofilm formation (Chapter 3), and how it is affected by competition between strains. From there, I became interested in the classical

example of cellular-decision making in the microbial world, motility control via chemotaxis (Berg, 2004; Porter et al., 2011; Wadhams and Armitage, 2004), and how this behavior is affected by social cues such as antibiotic stress (Chapters 4 and 5).

Pseudomonas aeruginosa as model organism

This thesis is a result of a mixture of theory and empirical work and the latter focuses on one key species, the opportunistic pathogen *Pseudomonas aeruginosa*, as model organism. *P. aeruginosa* is a versatile and ubiquitous gram-negative bacterium that became a workhorse of microbial sociobiology. From intensive efforts to understand the social life of this species, it is now clear it often produces a wide range of costly secretions, such as quenching molecules like siderophores (Buckling et al., 2007; Griffin et al., 2004; Julou et al., 2013; Kummerli and Brown, 2010), digestive enzymes and quorum-sensing signals (Diggle et al., 2007; Sandoz et al., 2007), along with a variety of antimicrobials, including both broad spectrum antibiotics such as pyocyanin (Korgaonkar et al., 2013; Korgaonkar and Whiteley, 2011) and cyanide (Wang et al., 2015), and narrow killing spectrum bacteriocins called pyocins (Inglis et al., 2009; Waite and Curtis, 2009). Additionally, *P. aeruginosa* is one of the most well-studied biofilm-forming organisms (Harmsen et al., 2010; O'Toole and Kolter, 1998), and biofilm formation is a key phenotype of study throughout this thesis (Chapters 3, 4, and 5). It inhabits a wide range of habitats (Kiewitz and Tummler, 2000), where it likely meets a wide diversity of genotypes.

P. aeruginosa is an important pathogen too. In humans it is one of the most common causes of nosocomial infections and a major cause of morbidity and mortality in immunocompromised individuals (Bodey et al., 1983; Stover et al., 2000), being particularly infamous for the formation of robust and multi-drug resistant biofilms that

may cause lethal airway infections in Cystic Fibrosis patients (Folkesson et al., 2012). And here too, inside of us, *P. aeruginosa* can meet a wide diversity of genotypes, from different strains of the same species, resulting from different colonization events at the early-staged infections (Burns et al., 2001; Mahenthiralingam et al., 1996; Renders et al., 2001), to different species that often interact strongly and affect pathogenesis (Murray et al., 2014). Accordingly, *P. aeruginosa* has become an important model organism to study polymicrobial infections (Baldan et al., 2014; Filkins et al., 2015; Korgaonkar et al., 2013; Mashburn et al., 2005; Pernet et al., 2014).

Thesis outline

As discussed above, the heart of the thesis is to study evolutionary competition in microbial communities and understand its impacts on a diversity of phenotypes. I adopt a broad systems approach that combines mathematical theory of population dynamics with the empirical study of microbial groups. I begin with a theoretical study of when to expect cooperation or competition between individuals (Chapter 2). I then move to the empirical study of how strain competition affects biofilm formation (Chapter 3). The study of single cells during biofilm formation led to the discovery of chemotaxis on surfaces and motivated the final two data chapters: I start by documenting chemotaxis of surface-attached cells in developing biofilms (Chapter 4), and then study how chemotaxis relates to competition by studying bacterial motility in gradients of antibiotics (Chapter 5). I briefly summarize each data chapter below.

Chapter 2: Microbes typically meet many strains and species forming dense groups where social interactions are both common and strong. But how cooperative - on average - are cells in such genetically diverse collectives? This is a major open

question for microbiology, and here I develop mathematical theory that aims to specifically address it. I study the potential for the evolution of cooperative cross-feeding between microbial genotypes and show that natural selection will not typically support such engagement. Autonomous strains are favored instead. And when cross-feeding evolves, it is more related with competition than with canonical cooperation as each genotype is effectively exploiting the others.

Chapter 3: Biofilm formation is arguably the key social phenotype in microbes and has traditionally been pictured as a cooperative enterprise where genotypes work together towards a common goal. Here I provide an alternative model: biofilm formation can be used as a response to ecological competition. In particular, I study the effect of mixing different natural isolates of the pathogenic bacterium *Pseudomonas aeruginosa* and show that strain mixing is associated with both strong competition and increases in biofilm formation. Moreover, I show that antibiotics produced by competing strains are the drivers of mixing-induced biofilm formation. Importantly, I find similar responses to clinical antibiotics and argue that the widely reported effects of sub-lethal concentrations of antibiotics on bacteria may have their natural roots in competition sensing and the ability to detect and respond to other strains.

Chapter 4: Bacterial chemotaxis is a major adaptation in the planktonic state and a paradigm for cellular-decision making. Cells can control the rotation of their flagella via thoroughly studied chemosensory systems to direct their motion towards, or away from, chemicals. However, bacteria typically live on surface-associated communities, and there the possibility for chemotaxis remains unexplored. This surprising and major gap in our knowledge drove me to investigative directed motility of surface-attached *P.*

aeruginosa in developing biofilms. I use microfluidic platforms and automated cell tracking to show that individual cells can effectively climb chemical gradients during biofilm formation via pili-based ('twitching') motility and the Chp chemosensory system. Behaviorally, cells are able to control their speed and the rate at which they reverse the direction of their motion, to position themselves at favored locations in the biofilm with submicron precision. Such active behavior agrees with the idea of positioning as a major basis for evolutionary competition in microbial communities.

Chapter 5: My final data chapter asks how bacterial competition and chemotaxis interact. Given that chemotaxis typically allows individuals to move towards beneficial compounds, and away from harmful ones, one might expect cells to avoid antibiotic competition from other strains. Surprisingly, I found the opposite: individual *P. aeruginosa* use twitching chemotaxis to move towards increasing concentrations of antibiotics. Moreover, within 20 hours susceptible cells can reach, move and grow at concentrations 1000 times superior than their MIC (minimal inhibitory concentration), seemingly by modulating their efflux physiology as they move along the antibiotic gradient. As for antibiotic-induced biofilm formation, I argue that such *antibiotic taxis* may have its natural origins in the ability to detect and respond to the evolutionary competition from threatening genotypes - competition sensing.

2. Evolutionary limits to cooperation in microbial communities

Abstract	20
Significance	21
Introduction	21
Results and Discussion	24
Conclusions	36
Materials and Methods	39

Abstract

Microbes produce many compounds that are costly to a focal cell but promote the survival and reproduction of neighboring cells. This observation has led to the suggestion that microbial strains and species will commonly cooperate by exchanging compounds. Here we examine this idea with an ecoevolutionary model where microbes make multiple secretions, which can be exchanged among genotypes. We show that cooperation between genotypes only evolves under specific demographic regimes, characterized by intermediate genetic mixing. The key constraint on cooperative exchanges is a loss of autonomy: strains become reliant on complementary genotypes that may not be reliably encountered. Moreover, the form of cooperation we observe arises through mutual exploitation that is related to cheating and Black Queen evolution for a single secretion. A major corollary is that the evolution of cooperative exchanges reduces community productivity relative to an autonomous strain that makes everything it needs. This prediction finds support in recent work from synthetic communities. Overall, our work suggests that natural selection will often limit

cooperative exchanges in microbial communities and that, when exchanges do occur, they can be an inefficient solution to group living.

Significance

Microbes form dense and diverse communities that affect every aspect of our lives. Microbial communities are often viewed as cooperative networks with species working together toward a common goal. Here we critically evaluate this view using an ecoevolutionary model. We show that cooperating with other species can be a poor evolutionary strategy because it renders a cell dependent upon species that may not be nearby. Moreover, when cooperative exchanges do evolve, they are inefficient and reduce the productivity of the community. Evolution by natural selection then limits the potential for productive cooperation between microbial species. We argue that understanding these limits, and how to overcome them, will be key to engineering microbial communities for our own ends.

> *'Benefit-of-the-species' arguments [...] provide for the reader an escape from inner conflict, exacting nothing emotionally beyond what most of us learn to accept in childhood, that most forms of life exploit and prey on one another.*
>
> Hamilton, 1975

Introduction

Microbes typically live in dense communities containing many strains and species. These genetically diverse societies are widespread and central to how microbes affect us, including examples such as the gut microbiome, polymicrobial infections and communities vital to bioremediation and nutrient cycling (Costerton, 2007; Lopez et al., 2010). In these collectives, ecological interactions are thought to be both common

and strong given that cell density is typically high and that microbes possess many phenotypes that influence the reproduction and survival of surrounding cells (West et al., 2007a; West et al., 2006). Such social traits include many secretions, such as extracellular enzymes and scavenging molecules (Nadell et al., 2009; West et al., 2007a; West et al., 2006), and other beneficial 'leaky' traits such as detoxification agents (Morris et al., 2012) or amino acids (Mee et al., 2014; Pande et al., 2013).

A central explanation for cooperative phenotypes in microbes is that they function to help cells of the same genotype (Hamilton, 1964a, b), which is backed up by a growing body of theory and experiments (Brown and Johnstone, 2001; Datta et al., 2013; Diggle et al., 2007; Griffin et al., 2004; Nadell et al., 2010; Van Dyken et al., 2013; West and Buckling, 2003). However, it is also clear that in nature microbes commonly interact with many different genotypes (both different strains and species) in complex ecological networks (Gans et al., 2005; Roesch et al., 2007; Santelli et al., 2008). Do these different microbial genotypes cooperate with one another? Understanding this is central to building models of microbial communities and how they will respond to both environmental and anthropogenic perturbations (Mitri and Foster, 2013).

Studies involving genetically engineered (Mee et al., 2014; Pande et al., 2013; Shou et al., 2007; Wintermute and Silver, 2010) and/or artificially selected communities (Harcombe, 2010; Hillesland and Stahl, 2010; Shou et al., 2007) emphasize how easily cooperation between genotypes can be achieved in the laboratory. Additionally, there are a growing number of suggestions that cooperation should commonly evolve between microbial strains and species (Elias and Banin, 2012; Little et al., 2008; Sachs and Hollowell, 2012; Schink, 2002). This view contrasts with empirical surveys of natural bacterial communities, which suggest that

competitive interactions predominate over cooperative interactions (Foster and Bell, 2012). However, it has also been suggested that cooperation between different genotypes may explain the unculturability of many species in the lab when in monoculture (D'Onofrio et al., 2010; Ernebjerg and Kishony, 2012; Kaeberlein et al., 2002). If correct, studies with culturable species could underestimate cooperativity in microbial communities.

The potential for cooperation between different microbial genotypes then remains unclear. Indeed, we even lack clear predictions of what to expect. There is a need for general theory on cooperation between microbial genotypes. One microbial interaction that has been explored theoretically is syntrophy, where one species produces a toxic waste product that another species consumes (Bull and Harcombe, 2009; Estrela et al., 2012; Fennell and Gossett, 1998; Kreikenbohm and Bohl, 1986). Syntrophy is likely to be ecologically important and, under some conditions (Estrela et al., 2012), can benefit both species. However, syntrophic species need not pay energetic costs to interact: one species is producing waste and the other species is feeding. Such byproduct cooperation can, therefore, readily evolve but is fundamentally different to the exchange of costly secretions (Foster and Wenseleers, 2006; Sachs et al., 2004). Other models have analyzed when costly cooperation between species is expected in microbes and other organisms (Bull and Harcombe, 2009; Foster and Wenseleers, 2006; Frank, 1994). However, these models assume that there is no opportunity for one partner to express the beneficial trait of the other. While this will sometimes occur, there is considerable functional overlap in the cooperative traits of microbial species (Morris et al., 2012). In addition, the potential for horizontal gene transfer in microbes means that there is a broad scope for a focal strain to pick up

the phenotypes of co-occurring strains and species (Nogueira et al., 2009; Papke and Gogarten, 2012; Rankin et al., 2011).

Here we examine the potential for microbial cooperation between different strains and species. We base our work on the well-established models of within-genotype microbial cooperation for a single public good (Brown and Johnstone, 2001; Chuang et al., 2009; Cremer et al., 2012; Frank, 2010; West and Buckling, 2003), so that the relationship to previous work is clear (see SI Materials and Methods). We add one key feature to these models: we allow cells to invest in multiple distinct cooperative secretions, such that there is the potential for different genotypes to exchange secretions with one another. Our analysis shows that the degree of genetic mixing defines the potential for cooperation both within and between genotypes. Low mixing favors genotypes that produce all secretions, whereas high mixing favors genotypes that do not produce any at all. Only for intermediate levels of genetic mixing do we find between-genotype cooperation where strains produce a subset of secretions and rely on other genotypes for the complementary traits. Moreover, the form of cooperation that emerges is inefficient and results in a loss of productivity relative to one genotype making all secretions. Natural selection limits both the occurrence and effectiveness of cooperation within microbial communities.

Results and Discussion

Logic of the model. We are interested in the potential for the evolution of cooperative exchanges in microbial communities. Cooperative phenotypes can be central to growth in microbes (Crespi, 2001; Nadell et al., 2009; West et al., 2007a), both in natural (Cordero et al., 2012a; Cordero et al., 2012b; Raymond et al., 2012) and disease (Rumbaugh et al., 2009) settings. These phenotypes are typically costly to produce but

provide large shared benefits that increase the yield of all cells in a neighborhood (Crespi, 2001; Nadell et al., 2009; West et al., 2007a; West et al., 2006). To reflect these strong benefits, we focus on secretions that are essential for bacterial growth and set final population yield (see Materials and Methods), although our conclusions also hold for nonessential secretions (Figure S1). Whereas our analysis is phrased in terms of secretions, like enzymes that liberate nutrients, it also captures a range of other leaky beneficial traits, such as detoxifying enzymes like catalase (Morris et al., 2012) or amino acids (Mee et al., 2014; Pande et al., 2013).

Figure 1 outlines the logic of our ecoevolutionary model. For two secretions our model has four genotypes: a producer of both traits [1,1], a producer of the first trait [1,0], a producer of the second trait [0,1] and a nonproducer [0,0], where for simplicity 1 and 0 denote production or no production of a given secretion, respectively, thus labeling each genotype.

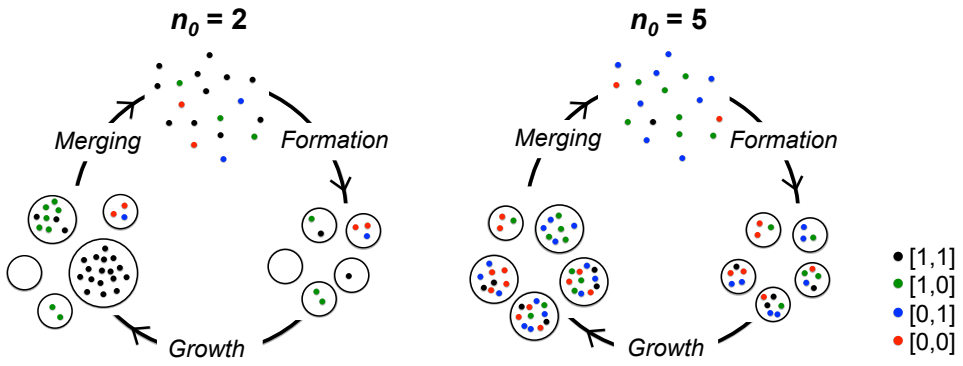

Figure 1: Ecoevolutionary model of microbial lifecycle. We considered three cyclically recurrent phases to model the evolutionary dynamics of a microbial population that depends on multiple secretions to grow: (*i*) formation, stochastic seeding of M separate subpopulations following a Poisson process with mean n_0; (*ii*) growth, independent evolution of each group following logistic growth, where the carrying capacity of the environment is proportional to the concentration of secretions in the focal group; (*iii*) merging, M groups merge, and the cycle starts again after updating the genotypic frequencies. As an illustrative example, we show the effect of two different n_0 values in a two-trait model of four genotypes, [1,1], [1,0], [0,1] and [0,0], which make both secretions, one secretion, the other secretion, and none, respectively.

Our modeling is intended to capture two related scenarios. The first scenario is a single strain that makes multiple secretions where loss of function mutations can generate the above trait combinations. The second scenario is where the different genotypes come from a combination of interacting strains and species that have similar ecologies. This latter case has clear potential for complexities that we do not represent, but we can, nevertheless, capture the evolutionary dynamics that would be driven by the focal traits.

In addition to extending models of single secretions, our model is intended to formalize the hypothesis that cooperation can arise by different genotypes losing the genes for different secretions (Sachs and Hollowell, 2012). This hypothesis was developed from the idea of 'Black Queen' evolution (Morris et al., 2012). Specifically, if many strains all make and use the same 'leaky' trait, some strains can lose the trait and rely on others to grow. For a single trait, Black Queen evolution then has similarities to the evolution of cheating, where a diverse network of species may be involved either as a producer or receiver of a particular trait.

When microbes possess multiple leaky traits, it raises the possibility that two genotypes may reciprocally exchange beneficial traits when one loses one trait and one loses another (Sachs and Hollowell, 2012). Linked to this scenario, a key assumption in our analysis is that it is possible for a cell to make all secretions if favored by natural selection (i.e. in a system relying on two secretions, for example, there is always the possibility of a [1,1] genotype). Although not always the case, this possibility seems likely to be common, because many secretion systems are associated with horizontal gene transfer (Nogueira et al., 2009; Rankin et al., 2011). However, we discuss later the effect of some secretions only being achievable by some genotypes.

Between-genotype cooperation emerges with intermediate levels of genotypic mixing. We are interested in understanding the effects of natural selection when microbes produce more than one fitness-promoting secretion. In particular, we are interested in whether strains will evolve to exchange costly secretions. Figure 2 gives the final (steady-state) frequencies of each of the different secretion genotypes as a function of the degree of genotypic mixing.

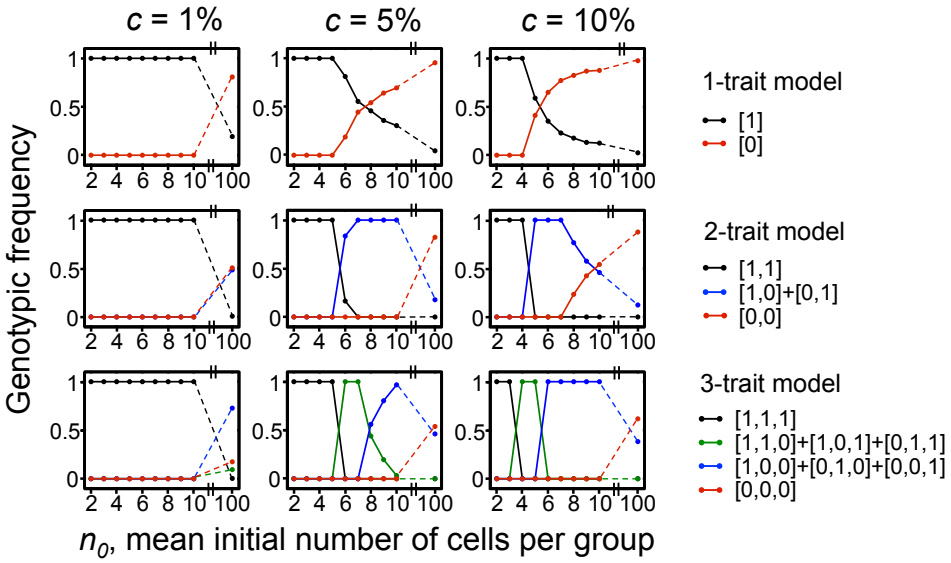

Figure 2: The evolution of within- and between-genotype cooperation in microbial communities. We show steady-state frequencies of different genotypes as a function of the average number of cells founding each group (n_0) and cost of each trait (c) in systems that depend on one, two and three secretions to grow. Genotypes are labeled with one and zero to show whether they invest or not in a given secretion. [1], [1,1] and [1,1,1] have advantage at low n_0, while [0], [0,0] and [0,0,0] have advantage at high n_0. Cross-feeding genotypes that cooperatively exchange secretions dominate at intermediate values of n_0 (a proxy for mixing among genotypes), particularly for secretions with high cost (c).

We include a model of a single secretion, which recapitulates the well-known cooperator-cheater dynamics where limited genotypic mixing (high relatedness) leads to the evolution of secretion, whereas high genotypic mixing (low relatedness) leads to a loss of secretion (Chuang et al., 2009; Cremer et al., 2012; Frank, 2010; Griffin et al.,

2004; Nadell et al., 2010; West and Buckling, 2003). What happens when cells can produce two secretions? At low mixing, the genotype that produces all secretions dominates, and at high mixing, one sees the opposite (the genotype that does not produce any secretions dominates). Interestingly, however, at intermediate levels of genotypic mixing, there is natural selection for partial secretors that produce only a subset of the secretions, such as [1,0], which rely on the complementary strain, [0,1], for the other secretion. The emergence of such cross-feeding between partial secreting genotypes represents a simple form of between-genotype cooperation.

Why do complementary genotypes dominate nonsecretors at intermediate genotypic mixing? The answer is in the demographics of the system and the potential for something known as Simpson's Paradox (Chuang et al., 2009; Cremer et al., 2012). Within any one group, nonsecretors outcompete secretor genotypes because of the costs associated with making the secretions. However, the groups containing more secretors make more cells in total to seed new groups. Then, at intermediate levels of genetic mixing, complementary genotypes are associated with more productive groups relative to nonsecretors and, therefore, can outcompete them. Additionally, because there is a significant amount of mixing, one partial secretor genotype [0,1] will often meet their partner genotype [1,0] within a given group, allowing them to outcompete full secretors [1,1] that grow more slowly in order to make both traits. Partial secretors compete best against full secretors [1,1] when the costs of secretions are relatively high, because there is a more significant growth advantage from not making a secretion (Figure 2).

The behavior of the model for two, three and four secretions is broadly similar (Figure 2 and Figure S2). However, adding more secretions to the system increases the scope for cross-feeding genotypes to outcompete other genotypes. A key reason for

this is that increasing the number of secretions increases the associated costs, which promotes cross-feeders over full secretors (Figure 2). The importance of costs is shown by changing the number of secretions in the system while keeping the total cost of all secretions constant (Figure S2). A general prediction then is that raising the costs of secretions, either through a single secretion that is very costly or by the expression of many individually-costly secretions, can favor cross-feeders relative to full secretors. As we show below, however, using many secretions also creates problems, because cross-feeders need to reliably find multiple partners to be successful. This makes cross-feeding with many secretions particularly fragile to factors that limit access to other genotypes (Figure S3).

Our model assumes that all strains compete for the same niche. Although this seems reasonable given the competition observed between strains and species from a common environment (Foster and Bell, 2012; Vetsigian et al., 2011), the extent of niche overlap will vary between different genotypes. We, therefore, decided to test the importance of complete niche overlap for our conclusions. We did this by modeling two sets of interacting strains. All strains can cooperate with one another, but only within a set do the strains compete. Between sets, there is no resource competition consistent with each set occupying a different niche. Importantly, this model shows the same qualitative behavior as our simpler single-niche model: between-genotype cooperation requires intermediate levels of genotypic mixing to evolve by natural selection (Figure S4).

In sum, we find that between-genotype cooperation can evolve by natural selection, particularly with high costs to secretions and intermediate levels of mixing of microbial genotypes.

Between-genotype cooperation is associated with reduced group productivity. The two-way exchanges of secretions that emerge in the model can be viewed in at least two different ways. The first way is cooperation for mutual benefit. Indeed, if two complementary strains or species were examined in a laboratory experiment, one would find that each cannot grow alone but together they would grow well, a result that is commonly used to diagnose cooperation or mutualism (De Mazancourt et al., 2005; Foster and Bell, 2012). However, another aspect of the interaction is competitive, where each partial secretor is acting as a cheater on full secretors and its complementary partner. Can one then quantify the impact of this competition? A simple but powerful way to assess the effects of competition is to look at overall group performance, which can be harmed by genotypes investing in competitive traits instead of cooperative traits that benefit the group (Foster, 2004).

Figure 3 shows the evolved group productivities as a function of founder cell number (the degree of genotypic mixing). The emergence of cross-feeding exchanges with increased genetic mixing is associated with a loss of group productivity - a diagnostic of wasteful competition that is inefficient at the group level. The greater the potential for between-genotype cross-feeding, therefore, the lower the group performance relative to a single strain that makes all secretions. Accordingly, any factor that promotes cross-feeding exchanges, such as increasing the cost or number of secretions, leads to greater losses in group productivity. Why this reduction? The emergence of this type of cross-feeding is associated with a loss of genes for secretion in each partner. This means that less of the secretion will accumulate in a cross-feeding group relative to a group of cells that all make all secretions.

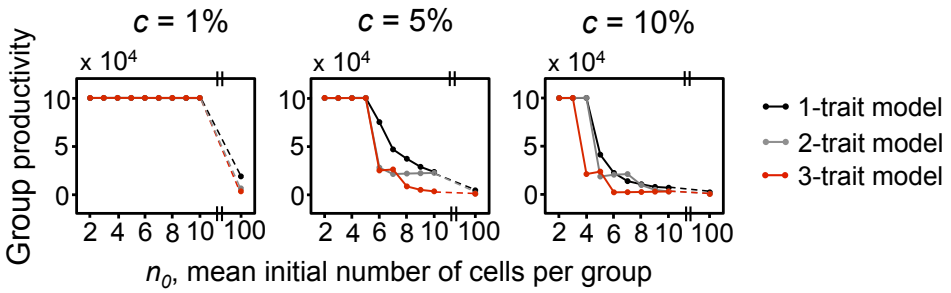

Figure 3: Evolved average group productivity as a function of founder cell number (n_0). The emergence of cooperative exchanges between genotypes is associated with a loss of group productivity (two- and three-trait models). This occurs for the same reason that cheaters harm group function in single-secretion models (one-trait model). This outcome is particularly clear for secretions with high cost (c), and high number of traits. Average group productivities were obtained from 1000 independent subpopulations. SE bars are smaller than the plotting dots and, therefore, are not shown.

The model does not allow strains to modulate the amount of secretion that they make. If allowed, will cross-feeders compensate for their low productivity by increasing their investment in cooperation? We evaluated this in two ways. First, we extended our model to allow strains to invest in three different levels of secretion (0.5, 1, 2). Second, we developed a new model that allows strains to invest any amount in secretions by considering mutations that can change the level of investment (see Materials and Methods). Rather than increasing group productivity, however, allowing strains to modulate secretion levels only makes things worse for cross-feeders (Figure 4 and Figure S5). The evolution of cross-feeding is now associated with even greater losses in group productivity, because cross-feeders evolve to invest less in each secretion than full secretors. In sum, the evolution of cross-feeding cooperation is associated with significant levels of competition and mutual exploitation.

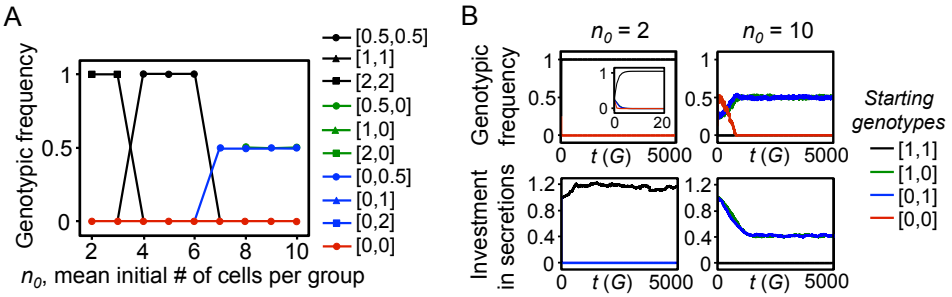

Figure 4: Evolved investment into secretion production as a function of founder cell number (n_0). Allowing for differential investment in secretion production amplifies the tragedy-of-the-commons because cross-feeders evolve to invest less in secretions than strains that make all secretions. (**A**) Discrete model. Genotypes that invest twice as much in secretions, [2,2] instead of [1,1], reach fixation when genetic mixing is low. However, at high mixing, the genotypes that fixate are cross-feeders that invest less in secretions than in the original model, [0.5,0] and [0,0.5] instead of [1,0] and [0,1], respectively. (**B**) Continuous model. If cells continuously tune their investments into secretion production, we find the same patterns, where cross-feeding strains invest less in cooperation than strains that make all secretions. *Upper* shows the genotypic frequencies of systems for low and high mixing, whereas *Lower* shows the mean investment in secretions. *Inset* clarifies that genotypic frequencies are identical at the beginning, but producers of both traits quickly reach fixation. SE bars for steady-state investments are smaller than the plotting lines and therefore, are not shown. We set the cost per trait (c) at 5%.

The idea that a cooperative interaction between genotypes can arise by exploitation has a precedent in discussions of mutualism and host-parasite evolution (De Mazancourt et al., 2005). There it has been observed that a chronic parasite might produce a factor that a host evolves to depend upon. Under these conditions, removing a parasite can harm a host, although the original basis for the interaction was strongly negative for the host. These situations, like in our system, can be viewed either as competitive or cooperative depending on the comparison taken. Specifically, if an experimenter simply removes a partner, he or she will diagnose the relationship as cooperative. However, this diagnosis will hide the evolutionary history and the fact that the partnership originally evolved through competition and exploitation. This historical effect of competition is not merely a definitional issue; it predicts that the

productivity of microbial communities relying on cross-feeding exchanges will be low relative to their full potential.

Constraints on the evolution of between-genotype cooperation. The evolution of cooperation between genotypes is predicted with relatively high costs to secretions and intermediate levels of mixing of microbial genotypes. The fitness cost of secretion can be highly variable in strongly regulated traits, such as siderophores, dependent upon how much a cell makes (Jiricny et al., 2010). Nevertheless, estimates of costs of secretions are often low, in the range of a few percent of growth rate or less (Drescher et al., 2014; Morris et al., 2011; Xavier et al., 2011). Low-cost secretions are expected whenever prudent regulation limits secretion to times when it is cheap to do so (Xavier et al., 2011). The effect of costs are also limited when secretions have a private component that benefits a secreting cell more than other cells (Gore et al., 2009). If low-cost secretions are the norm in nature, then our model suggests that the emergence of between-genotype cooperation will be limited. Potential exceptions to this prediction are if cells use many relatively-costly secretions (Figure 2 and Figure S2) or indeed, if using multiple secretions is, for some reason, disproportionally costly (Figure S6).

What about the levels of genetic mixing in microbial communities? This key variable is still poorly understood (Mitri and Foster, 2013; Nadell et al., 2009). However, what is clear is that many natural microbial communities display spatial structure, whereby microbes attach to surfaces and to each other and grow (Hallatschek et al., 2007; Nadell et al., 2010). This will affect genetic mixing and is not accounted for in our model that assumes that genetic mixing within any one microbial group is perfect. To examine the impacts of spatial structure, we implemented an individual-

based version of our two-secretion model, where cells are seeded on a lattice and divide if they have space around them and access to both public goods (see Materials and Methods). In particular, we focus on parameter ranges that strongly promote cross-feeding pairs in the absence of spatial structure within the group.

We first use the individual based model to recapitulate the well-mixed model by allowing secretions to diffuse a long distance so that cells have access to all secretions. We then implement a low diffusion scenario so that secretions only reach a limited range. This simple change has a strong qualitative effect on predictions: now the genotype that produces both secretions is dominant (Figure 5A). The reason for this effect is intuitive: spatial structure limits the potential for interactions with other genotypes. Cross-feeders are now less likely to interact with their complementary partner, which means they will often lack secretions that they need for their growth.

Spatial structure then tends to limit cooperation between microbial genotypes, which is consistent with recent empirical work showing that spatial structure can limit positive interactions between microbial genotypes (Hillesland and Stahl, 2010; Saxer et al., 2009). This effect contrasts with the typical conclusion that spatial structure promotes cooperation (Datta et al., 2013; MacLean and Gudelj, 2006; Nadell et al., 2010; Nowak and May, 1992; Van Dyken et al., 2013) by increasing the probability of interacting with the same genotype (Hamilton, 1964a, b). However, cooperation between genotypes in our multi-trait model emerges under the same conditions as cheating in the classical models. Accordingly, we find that spatial structure simultaneously inhibits between-genotype cooperation and promotes within-genotype cooperation.

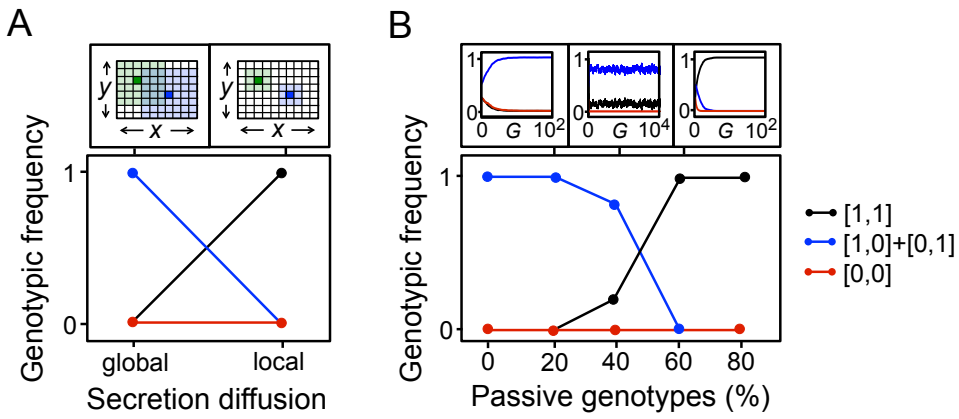

Figure 5: Effect of spatial structure and social insulation on the evolution of between-genotype cooperation. (**A**) Spatial structure (individual-based model). Space hinders the evolution of between-genotype cooperation with local diffusion of secretions, because genotypes are prevented from interacting. *Upper* shows cartoons to illustrate the diffusibility of secretions. (**B**) Social insulation modeled in well-mixed groups. The presence of passive genotypes, which do not compete with focal genotypes and do not contribute with traits, can prevent the evolution of between-genotype cooperation. *Upper* illustrates temporal dynamics (in generations *G*) for the three outcomes of the model. The cost per secretion was set at 5%.

Another assumption of our model, which is important for genetic mixing, is that all interacting genotypes in the system make use of the secretions. This assumption is likely to be broken, because the extreme genetic diversity associated with natural microbial communities suggests that there will often be many species present that do not use or make the secretions of our focal genotypes (Mitri et al., 2011). In models of a single secretion, it has been shown that such passive genotypes can insulate a focal genotype from interacting with other genotypes that might use its secretions - social insulation (Mitri et al., 2011). Figure 5B shows the effect of introducing passive genotypes that do not use the secretions or resources of the focal group. Like the effect of introducing space, the presence of passive genotypes decreases the probability that cross-feeding genotypes interact with their complementary partner, thereby favoring strains that can function effectively in isolation. Put another way, passive genotypes

reduce the group size of the focal interacting genotypes, which reduces the effective level of genetic mixing and promotes autonomous genotypes like [1,1].

We saw earlier that a high number of secretions can promote cross-feeding (Figure 2 and Figure S2). However, it is important to note that the introduction of passive genotypes has a disproportionately strong effect when cells use a high number of secretions (Figure S3). With many secretions, each cross-feeder has to find multiple partners, and passive genotypes become more of a problem than when a cell has to find just one partner. In sum, the use of many traits presents cross-feeders with two problems. First, cross-feeding involving many traits is associated with greater reductions in group productivity than with fewer traits; communities become more inefficient (Figure 3). Second, relying on many traits makes cross-feeding networks fragile in the sense that each cross-feeder will typically require multiple other genotypes nearby in order to grow (Figure S3).

Although we expect the effect of passive genotypes to be strong, mechanisms that promote association between complementary strains will improve the prospects of cross-feeding evolution. Candidate mechanisms that promote association include emergent sorting that can occur if two strains grow more in each other's presence than when alone (Mitri and Foster, 2013; Mitri et al., 2011; Momeni et al., 2013), chemotaxis towards partner genotypes, or even direct attachment (Wanner et al., 2008). The importance of such assortment processes in nature is not known, but it is an interesting area for future studies.

Conclusions

Our models identify conditions under which different microbial genotypes evolve to exchange fitness-promoting secretions. This outcome might occur through the selective

loss of costly but leaky traits via Black Queen dynamics (Morris et al., 2012; Sachs and Hollowell, 2012). The Black Queen Hypothesis was developed to explain the genome streamlining often seen among free-living bacteria (Morris et al., 2011; Morris et al., 2012). It suggests that microbes will lose functions that are costly but can be obtained from other genotypes because of their leaky nature (Morris et al., 2012). This process leads to the evolution of dependencies among genotypes, and potentially interdependent networks of cooperation in microbial communities (Sachs and Hollowell, 2012). However, consideration of the costs of secretions and the levels of genetic mixing in natural communities suggests that the evolution of such cooperative networks is not always expected. Instead, our models predict that may often be beneficial for a microbial genotype to produce all secretions that it needs.

Constraints may sometimes prevent a microbe from evolving all of the cooperative traits it needs (i.e. a [1,1] strain cannot evolve). This scenario makes cooperative exchanges with other genotypes much more likely and corresponds to the typical view of mutualism between species (Figure S7). However, the widespread potential for horizontal gene transfer (Nogueira et al., 2009; Papke and Gogarten, 2012; Rankin et al., 2011) suggests that the evolution of multiple traits should often be possible. Possessing multiple traits is beneficial in our model, because it removes reliance on other strains that may not be encountered. This benefit of autonomy then has the potential to limit both between genotype cooperation and the evolution of cheating genotypes (Griffin et al., 2004; Hamilton, 1964a, b; MacLean and Gudelj, 2006; Mitri et al., 2011).

Does the between-genotype cooperation we see in our model ever evolve in nature? An interesting corollary of the similarity between cheating and between-genotype cooperation in our model (Figure 2) is that the discovery of one in nature

should help to identify conditions that favor the other. A phenotype often associated with both cheating (Griffin et al., 2004) and Black Queen evolution (Morris et al., 2012) is siderophore production, which are secreted iron-scavenging molecules. Studies of marine assemblages suggest that bacterial strains often evolve to not secrete siderophores, while retaining the import proteins to take up siderophores made by other strains and species (Cordero et al., 2012a; D'Onofrio et al., 2010). In addition, siderophores appear particularly amenable to cheating and cross-feeding because they can be both costly (Jiricny et al., 2010) and diffusible (Figures 2, 5A). Siderophore interactions, therefore, may be unusually prone to the evolution of between-genotype cooperation.

Amino acids are another potential currency for cooperative exchange in microbial communities. Many bacteria lack the ability to make certain amino acids, particularly those that are costly to make (Mee et al., 2014). This raises the possibility that cooperative networks of amino acid exchange occur in microbial communities, which was recently demonstrated for synthetic communities of up to 14 different auxotrophic genotypes of *Escherichia coli* (Mee et al., 2014). What is critical for our arguments, however, is that the WT *E. coli* that makes all amino acids grows at least 1.5 to 2 times faster than the cooperating communities. If these networks of amino acid exchange do evolve in nature, therefore, then they are likely to be relatively inefficient.

Cooperation between cells of a single genotype appears common, which is likely explained by the clonal and patchy nature of microbial growth that guarantees frequent association between genetically-identical cells within microbial communities (Datta et al., 2013; Kim et al., 2014; Nadell et al., 2010; Van Dyken et al., 2013). Here we have shown that cooperation between microbial genotypes is expected under different conditions (intermediate levels of genetic mixing), and it remains to be seen how often

these conditions arise in nature. Both spatial structure and social insulation can cause problems finding a cooperating partner. Moreover, we show that even when cooperation does emerge between strains and species, it can be exploitative and wasteful relative to single-genotype cooperation. This prediction has implications for synthetic ecology and our ability to engineer microbial communities for our own ends (Klitgord and Segre, 2011; Mitri and Foster, 2013). If cooperative interactions in natural microbial communities are both limited and inefficient, there should be a broad scope for improving community productivity using strategies that promote positive interactions between species. More generally, our work cautions strongly against a view where microbial communities are dominated by networks of species working together in harmony. Competition is likely to be central to many microbial interactions, perhaps even the cooperative ones.

Materials and Methods

Ordinary differential equation models with fixed investment into secretion. We model the population dynamics of microbial genotypes growing in a well-mixed environment using systems of ordinary differential equations (see also SI Materials and Methods). Briefly, each system is composed by 2^s equations, where *s* is number of secretions in a given model and each equation represents the population dynamics of a given microbial genotype in each subpopulation. For a system of two cooperative secretions the four genotypes, [1,1], [1,0], [0,1] and [0,0], grow according to the following general form:

$$\frac{dg_{ij}}{dt} = (r - (i + j) \cdot c) \cdot g_{ij} \cdot \left(1 - \frac{\sum g}{K}\right)$$

where g_{ij} represents the density of individuals of genotype [i,j] in each subpopulation, $[(\mathrm{i},\mathrm{j}) \in \{1,0\}^s]$, r is the intrinsic growth rate (here assumed 1 for simplicity) and c the cost of producing each trait. Here, we assume additive costs for secretion production, but we also considered nonlinear costs, both accelerating and decelerating (Figure S6). K, the carrying capacity of the environment, is a function of the secretions available in each subpopulation (Figure S8).

We consider a standard life-cycle of microbes (see the work by Cremer and colleagues (Cremer et al. 2012) and references therein for further discussion of the lifecycle): (*i*) formation, where a random number of cells is allocated to each subpopulation (based on a Poisson process with mean n_0, Figure S9), in a set of M subpopulations, and the identity of each cell follows a uniform distribution based on the frequency of each genotype; (*ii*) growth, where genotypes in each group proliferate according to logistic dynamics (until saturation is reached), and (*iii*) merging, where the M groups are merged together and the global genotypic frequencies are updated. After a full cycle of seeding, growth and merging (equivalent to one generation), new patches are seeded according to the re-calculated genotypic frequency. These cycles are repeated for G generations, until genotypic frequencies reach equilibrium.

***ODE models with variable investment into secretion*.** We implemented two different frameworks, here called discrete and continuous models for the evolution of investment. In the discrete version we extended our model described above to allow strains to invest in three different levels of secretion to give genotypes: [0.5,0.5], [1,1], [2,2], [0.5,0], [1,0], [2,0], [0,0.5], [0,1], [0,2] and [0,0]. In Figure 4 full producers invest the same in both secretions, but we find the same qualitative results when we drop this assumption (Figure S5). The continuous version uses the same lifecycle but

we add a mutation phase, where a mutation can either increase or decrease the investment into cooperation. The lifecycle is then, (*i*) formation; (ii) mutation, where each cell of the subpopulation mutates its parameter *x*, which governs how much a cell invests into its public goods; (iii) growth; and (iv) merging. Each cell type proliferates as before but we additionally consider its investment in secretions:

$$\frac{dg_{x,ij}}{dt} = (r - (i + j) \cdot x \cdot c) \cdot g_{x,ij} \cdot \left(1 - \frac{\sum g}{K}\right)$$

where $g_{x,ij}$ represents the density of cell type with genotype [i,j] and investment *x*. Thus the genotypes are now effectively $x \cdot g_{ij}$, not g_{ij} as before. For example, if $x = 2$, a strain [1,1] will behave as a genotype [2,2].

Individual-based model. We use spatial simulations of 2D lattices with periodic boundaries. Cells can only divide into empty spaces of their closest neighborhood, and the effect of a public good is limited to a neighborhood of a certain size around the producer cell. At each sampled time step, a focal individual is selected with uniform probability, and the cell divides with probability directly proportional to growth rate, which depends on population density and public goods level, following logistic kinetics. As for the deterministic version with fixed investment, cells undergo our standard three-step lifecycle (see SI Materials and Methods).

3. Biofilm formation as a response to ecological competition

Abstract	42
Author Summary	43
Introduction	44
Results and Discussion	46
Conclusions	63
Methods	65

Abstract

Bacteria form dense surface-associated communities known as biofilms that are central to their persistence and how they affect us. Biofilm formation is commonly viewed as a cooperative enterprise, in which strains and species work together for a common goal. Here we explore an alternative model: biofilm formation is a response to ecological competition. We co-cultured a diverse collection of natural isolates of the opportunistic pathogen *Pseudomonas aeruginosa* and studied the effect on biofilm formation. We show that strain mixing reliably increases biofilm formation compared to unmixed conditions. Importantly, strain mixing leads to strong competition: one strain dominates and largely excludes the other from the biofilm. Furthermore, we show that pyocins, narrow-spectrum antibiotics made by other *P. aeruginosa* strains, can stimulate biofilm formation by increasing the attachment of cells. Side-by-side comparisons using microfluidic assays suggest that the increase in biofilm occurs because of a general response associated with cellular damage: the biofilm response to pyocins that disrupt membranes is comparable to the response to different commercial

antibiotics that damage DNA, inhibit protein synthesis or inhibit transcription. Our data show that bacteria increase biofilm formation in response to ecological competition that is detected by antibiotic stress. This is inconsistent with the idea that sub-lethal concentrations of antibiotics are cooperative signals that coordinate microbial communities, as is often concluded. Instead, our work is consistent with competition sensing where low-levels of antibiotics are used to detect and respond to the competing genotypes that produce them.

Author Summary

Bacteria often attach to each other and to surfaces and make biofilms. These dense communities occur everywhere, including on us and inside us, where they are central to both health and disease. Biofilm formation is often viewed as the coordinated action of multiple strains that work together in order to prosper and protect each other. In this study, we provide evidence for a very different view: biofilms are formed when bacterial strains compete with one another. We mixed together different strains of the widespread pathogen *Pseudomonas aeruginosa* and found that pairs often make bigger biofilms than either one alone. Rather than working together, however, we show that one strain normally kills the other off and that biofilm formation is actually a response to the damage of antibiotic warfare. Our work helps to explain the widespread observation that treating bacteria with clinical antibiotics can stimulate biofilm formation. When we treat bacteria, they respond as if the attack is coming from a foreign strain that must be outnumbered and outcompeted in a biofilm.

Introduction

While the traditional model for bacterial life was one of cells swimming in liquid, it is now realized that bacteria commonly live in surface-associated communities known as biofilms (Costerton, 1995; Kolter and Greenberg, 2006; Monds and O'Toole, 2009; Nadell et al., 2009). These groups of bacteria carry significant medical and economic importance that includes a role in chronic diseases, antibiotic tolerance, biofouling, and waste-water treatment (Hall-Stoodley et al., 2004; Lopez et al., 2010; Romling et al., 2014). The importance of biofilms has led to their intensive study in many species of bacteria. However, this work has revealed that the genetic and biochemical mechanisms underlying biofilm formation are extremely variable across strains and growth conditions (Beloin and Ghigo, 2005; Karatan and Watnick, 2009). This variability has made it difficult to identify common principles of biofilm formation across species.

One property common to the biofilms of many bacterial species, both gram-negative and gram-positive, is that they are induced by sub-lethal concentrations of antibiotics (Elliott et al., 2010; Haddadin et al., 2010; Hoffman et al., 2005; Kaplan, 2011; Kaplan et al., 2012; Kumar and Ting, 2013; Linares et al., 2006; Wang et al., 2010). The diversity of the species displaying this response is striking (Kaplan, 2011) and suggestive of the general principles that so often elude the study of biofilms. This, and the observation that sub-lethal antibiotics induce a range of other physiological changes (Andersson and Hughes, 2014), has led to the hypothesis that antibiotics may not function as killing agents in nature. Instead, it is suggested that antibiotics may function as cooperative signals between species that contribute to the homeostasis of bacterial communities (Davies et al., 2006; Fajardo and Martinez, 2008; Kaplan, 2011; Linares et al., 2006; Yim et al., 2007). In parallel, there are a growing number of

studies concluding that natural microbial communities are cooperative enterprises in which strains and species work together, both in biofilm formation and metabolism (Andersson et al., 2008; Burmolle et al., 2014; Burmolle et al., 2006; Elias and Banin, 2012; Lee et al., 2014; Little et al., 2008; Moller et al., 1998; Pande et al., 2013; Ren et al., 2014a; Ren et al., 2014b).

Cooperative phenotypes - such as secreted enzymes or polymers - are important in biofilms for cells of a single genotype (Chandler et al., 2012; Drescher et al., 2014; Mitri and Foster, 2013; Nadell and Bassler, 2011; Nadell et al., 2009). However, evolutionary theory and ecological experiments caution against the idea that this cooperation will always extend to cells of different genotypes (Chandler et al., 2012; Foster and Bell, 2012; Hibbing et al., 2010; Mitri and Foster, 2013; Oliveira et al., 2014). Competition between strains and species appears to be commonplace and it is not clear how cooperative signaling via antibiotics could widely evolve (Ratcliff and Denison, 2011). An alternative to the idea that sub-lethal antibiotics are cooperative signals between species is that they are cues used by competing species to detect competitors and respond appropriately (Bernier and Surette, 2013; Cornforth and Foster, 2013; Ratcliff and Denison, 2011). Under the cue model, antibiotics are not secreted in order to signal to others (Keller and Surette, 2006; Maynard Smith and Harper, 2003), they are secreted to attack but can inadvertently provide information to others at low concentration. The idea that bacteria use antibiotics and other factors as cues of competition is central to the idea of 'competition sensing' (Cornforth and Foster, 2013). This is based on the observation that both nutrient and antibiotic stress, which are associated with ecological competition, often cause bacteria to release their own antibiotics. Bacteria appear to attack back when they are themselves attacked.

If sub-lethal concentrations of antibiotics are cues of competition from other strains, and biofilms are induced by such concentrations, this implies that biofilm formation can be a response to ecological competition from other strains. Here we test this hypothesis by co-culturing natural isolates of the opportunistic pathogen *Pseudomonas aeruginosa* and studying the effects on biofilm formation. We focus on members of a single species here because these are expected to have the strongest ecological overlap and, therefore, the strongest ecological competition; something first noted by Darwin: "*The struggle almost invariably will be most severe between the individuals of the same species, for they frequent the same districts, require the same food, and are exposed to the same dangers*" (Darwin, 1859). More concretely, data from the cystic fibrosis lung suggest that different isolates can colonize and, at least temporarily, co-exist in young patients (Burns et al., 2001; Mahenthiralingam et al., 1996; Renders et al., 2001), which is consistent with different strains meeting. *P. aeruginosa* also forms robust biofilms that have been intensively studied (Lopez et al., 2010; O'Toole and Kolter, 1998). The co-culture of *P. aeruginosa* strains then provides a test case to evaluate the link between ecological competition and biofilm formation. Specifically, if biofilm formation is a response to ecological competition, we expect to observe (i) evidence of competition between strains and (ii) evidence of increased biofilm formation in co-cultures relative to monocultures.

Results and Discussion

Both clinical antibiotics and mixing strains promote biofilm formation. We begin by recapitulating the known effects of antibiotic stress on bacterial survival and biofilm formation. Figure 1 (panels A, B) shows the effects of antibiotics on *Pseudomonas aeruginosa* where we use optical density as a qualitative indicator of cell number. As

expected, increasing the concentration of three widely used clinical antibiotics - ciprofloxacin, rifampicin and tetracycline - monotonically reduces the optical density of shaking cultures. However, as previously shown, this monotonic decrease is not seen when the same concentrations are applied to standing cultures. In standing cultures, the liquid is not agitated and cells can readily attach to the edge of the well and establish biofilms. Under this condition, biofilm formation actually increases for many concentrations of the antibiotics, until the concentrations become so high that toxicity dominates (Kaplan, 2011).

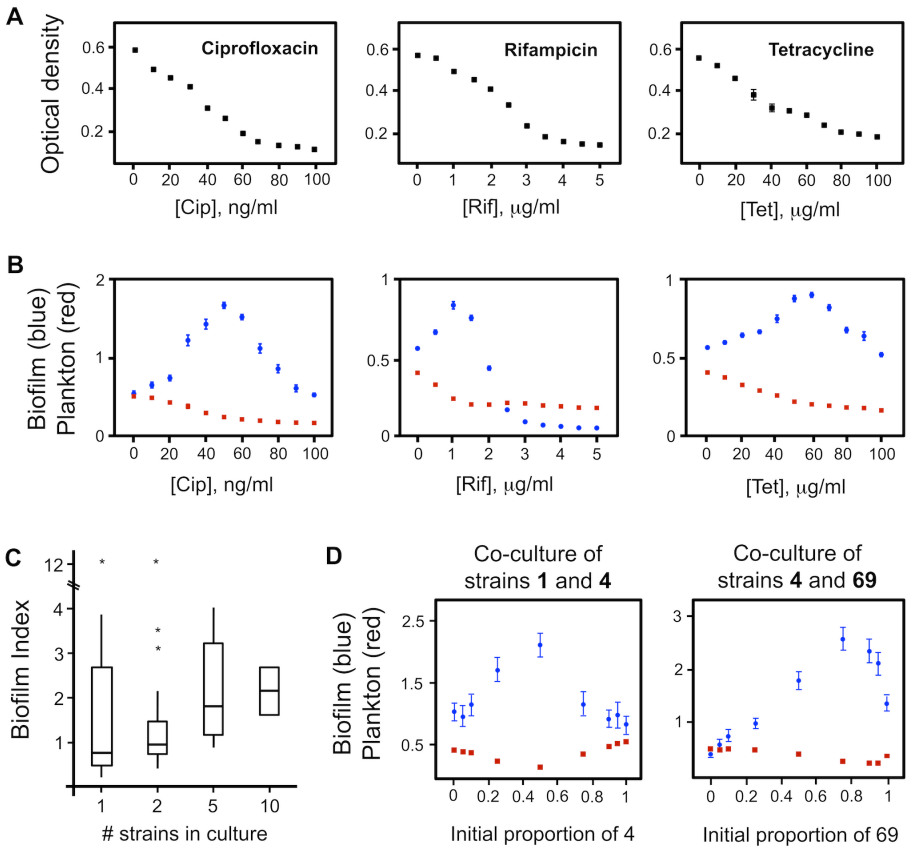

Figure 1. Effect of clinical antibiotics and strain mixing on biofilm formation of *P. aeruginosa*. (**A**) Increasing concentrations of three antibiotics from different classes, ciprofloxacin ('Cip'), rifampicin ('Rif'), and tetracycline ('Tet'), reduce the optical density of strain PAO1 shaking cultures. (**B**) Under static conditions, sub-lethal concentrations of antibiotics induce biofilm formation. (**C**) Mixing different natural isolates of *P. aeruginosa*

induces biofilm formation in an assay with increasing numbers of strains. The *y*-axis of box plots represents the biofilm index of each strain and mixtures, which is the ratio of biofilm to planktonic cell density (A_{595}/A_{600}). This measure controls for the large variability in overall growth between the strains and is a way to assess biofilm relative to the amount of planktonic cells (Savoia and Zucca, 2007). The biofilm index increases with the more strains present (2-tailed Spearman rank correlation, non-normal data, $n = 52$, $\rho = 0.305$, $p = 0.025$). (**D**) Mixing increases biofilm formation in two pairwise combinations of strains (1 + 4 and 4 + 69) in which the initial proportion of each strain was varied. Panels A, B, and D show means and 95% confidence intervals. Error bars are too small to see in some cases, particularly for the planktonic data.

Applying sub-lethal concentrations of antibiotics then leads to an increase in biofilm formation. Can we understand these widely reported biofilm responses to antibiotics in terms of ecological competition? We tested this by mixing natural isolates of *P. aeruginosa* in standing cultures and studying the impact on biofilm formation. Consistent with the hypothesis that biofilm formation is a response to ecological competition, we find that biofilm formation is increased in mixed cultures compared to pure cultures, both in a broad scale survey that mixed combinations of 22 natural isolates (Figure 1C, Table S1) and in defined pairwise comparisons in which we show that the strength of the biofilm response depends on the relative proportion of each strain at the start of the co-cultures (Figure 1D).

Competitive Exclusion Is Common in Pairwise Mixtures. The observed biofilm response is consistent with a competitive response. However, an alternative hypothesis is that the strains cooperate with one another to produce more biofilm (see Introduction). In order to better assess whether the strains were cooperating to make more biofilm, we labeled five of our *P. aeruginosa* natural isolates with constitutive fluorescent proteins (cyan fluorescent protein, CFP, and yellow fluorescent protein, YFP) by putting a single copy of the desired fluorescent protein gene at a specific site in the genome (Lambertsen et al., 2004). We then set up a round-robin tournament, in

which the five strains were mixed in all combinations, and measured biofilm formation, planktonic growth, and the relative frequency of the two strains (Figure 2). This revealed a strong competitive effect with one strain typically dominating after 24 hours (median proportion of dominant strain in biofilm = 0.98, Wilcoxon-signed rank test versus 0.5, $n = 10$, $p < 0.01$). Thus, the biofilm response is a manifestation of competition between strains rather than a cooperative synergy in which both strains benefit from the presence of one another (Mitri and Foster, 2013).

There are some cases in which biofilm formation in the mixture is less than that expected from the average of the two starting strains (Figure 2). However, accounting for which strain actually makes the final biofilm reveals that mixing nearly always causes an increase in biofilm formation by the dominant strain. For example, mixtures of strains 7 and 19 result in less biofilm than monocultures of strain 19. However, strain 7 eliminates strain 19 in co-cultures, producing more biofilm than it does when alone (Figure 2). More generally, we can calculate the expected biofilm formation from the pure culture data using a weighted average, which weights by the frequencies of the two strains in the biofilm after competition. This reveals that the mixed culture biofilm normally increases relative to the expectation based upon pure cultures (9/10 mixes increase, Wilcoxon signed rank test of expected/observed biofilm against a null of 1, $n = 10$, $p < 0.01$), while the amount of cells in the planktonic phase decreases ($n = 10$, $p < 0.01$). Moreover, the increases in biofilm and decreases in plankton that we observe upon mixing strains are significantly negatively correlated across the different strain mixtures (Spearman rank correlation, $n = 10$, $r = -0.782$, $p < 0.01$). This correlation agrees with recent observations on multispecies interactions during biofilm formation (Ren et al., 2014b).

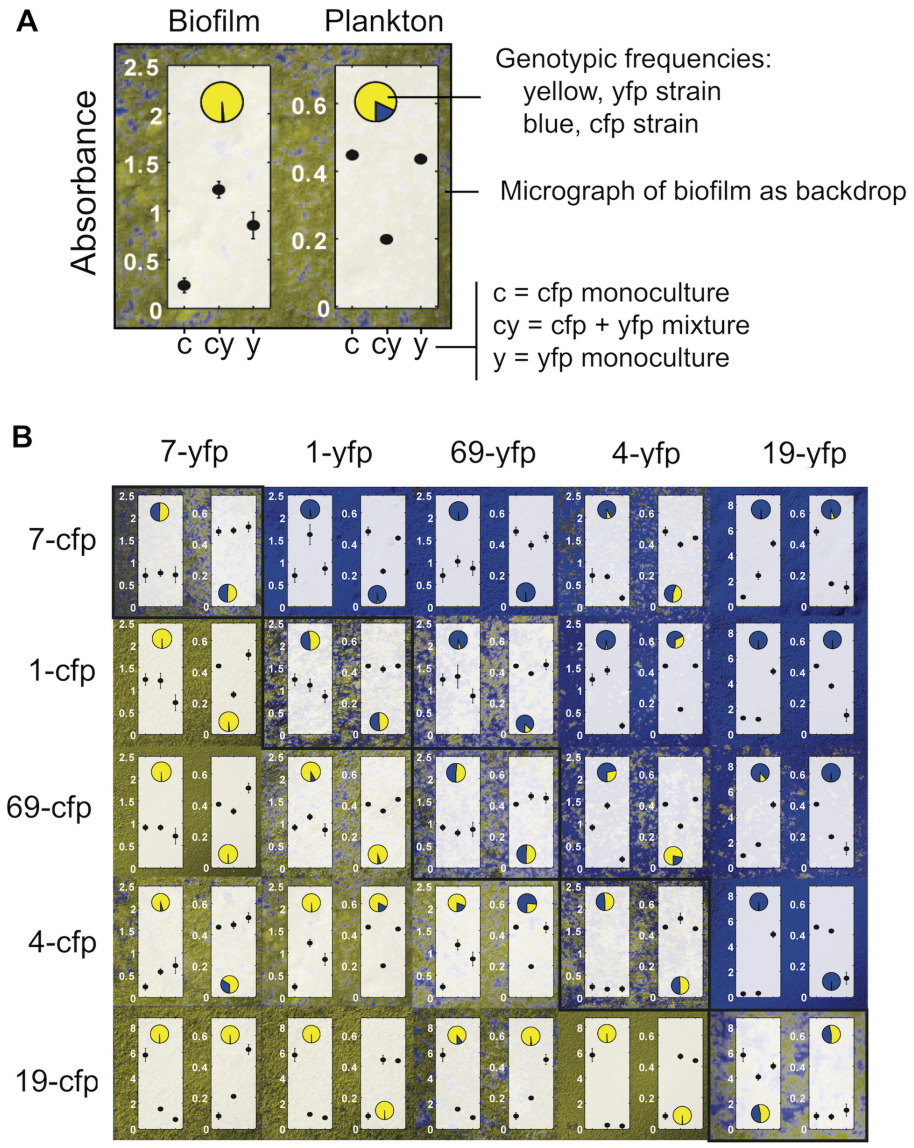

Figure 2. Round-robin tournament among natural isolates of *P. aeruginosa* showing strong competitive effects upon strain mixing. Five isolates were mixed together in all pairwise combinations and data from each mixture are shown in a corresponding panel. (**A**) Example data from strains 4 and 1 illustrating the different measures in a given mixture. In this example, mixing the two strains increases biofilm, decreases planktonic cells, and strain 1 (*yfp*-labeled) strain strongly outcompetes strain 4 (*cfp*-labeled) strain. (**B**) All data from the round-robin tournament. As in panel A, the backdrop to each panel is an epifluorescence image of the co-culture biofilm from a coverslip. All other data shown are from 96-well microtiter experiments. Specifically, the left-hand side graph in each panel shows information about the biofilm. Here, the plotted points show biofilm formation in the crystal violet assay by the *cfp*-labeled strain alone, both strains together, and the *yfp*-labeled strain alone, from left to right. The pie chart on the left shows frequencies of the two strains in the biofilm. The right-hand

side of each panel - graph and pie chart - shows the planktonic cell data from the same experiments as the biofilms measurements. *cfp* and *yfp* stand for cyan and yellow fluorescent protein, respectively. Plotted data show means and 95% confidence intervals.

The biofilm response is not an idiosyncrasy of our particular growth medium. Figure S1 shows the effect of varying levels of nutrients, buffering, and soluble iron for two genotype mixtures. Despite the success of strains in pairwise competition being strongly dependent on the environment, the biofilm response is detected across all conditions in at least one of the two strain combinations, but typically in both.

Pyocins serve as a cue for biofilm formation. We next focus on the cue that drives the increase in biofilm formation in co-cultures. We first examined whether the biofilm response requires cell-cell contact by growing pairs of strains on either side of a 0.4 μm permeable membrane (Figure 3A). Increased biofilm is observed across the membrane in most cases. In one case, there is a strong inhibitory effect on both biofilm and planktonic growth, which is consistent with the responder strain losing in co-culture (specifically, strain 4 is inhibited and outcompeted by strain 1, Figure 2). We also found that the biofilm response is recapitulated by the addition of cell-free culture supernatant of different strains. We focus on strain 4, which responds robustly to the addition of the supernatant from other strains (Figure 3B). The nature of the response is dose dependent: lower concentrations tend to induce biofilm formation while high concentrations inhibit both planktonic growth and biofilm formation.

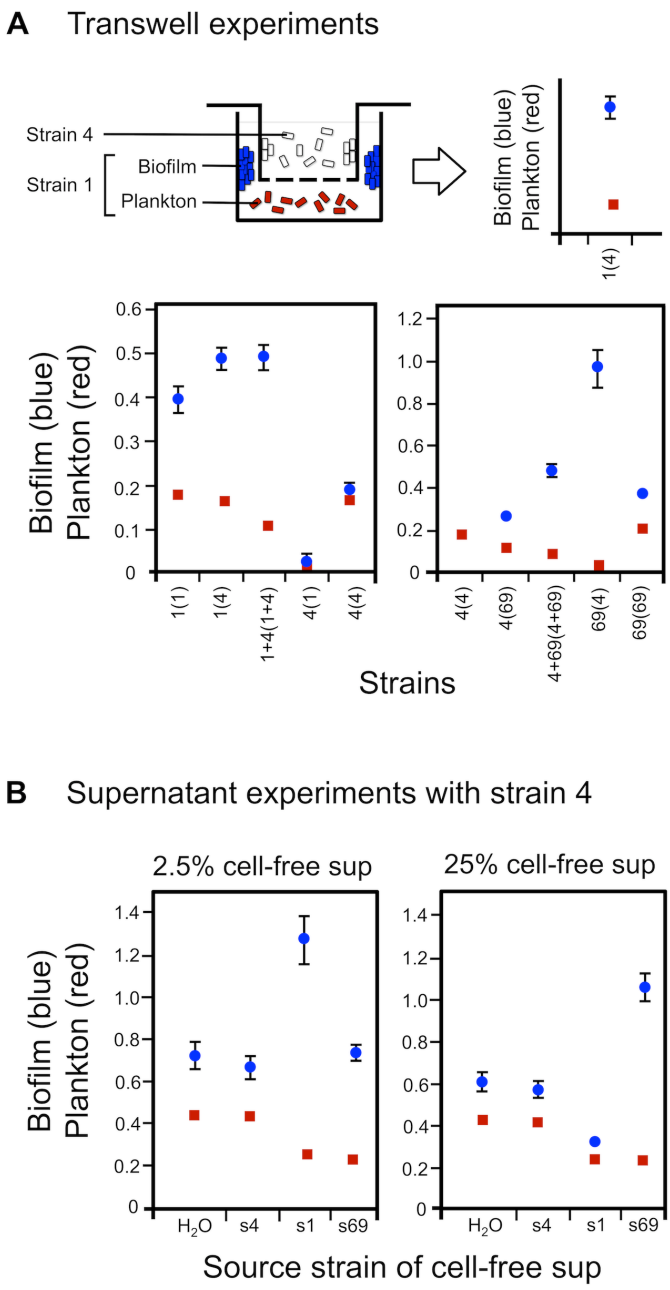

Figure 3. Increased biofilm in co-cultures is not dependent on cellular contact between strains. (**A**) Membrane-separated growth using Transwell plates (see Methods). Top diagram shows experimental design (left) and how results are plotted (right). On the axes, the first number refers to the responder strain for which the data are shown, while the number in parentheses is the inducer strain that is grown above, across the membrane. (**B**) Increased biofilm due to cell-free culture supernatants. Data are for strain 4 growing in the presence of various supernatants ('H_2O' is water in place of the supernatant, and 's4', 's1', and 's69' indicate the supernatant from strains 4, 1, and 69, respectively). Two concentrations of the supernatant are shown: 2.5% (left) and 25% (right). Data show means and 95% confidence intervals.

In order to identify the active component within the supernatant, we first performed anion exchange chromatography on the supernatant of strain 69 as it generates a robust response in strain 4 (Figure 3B). The active fraction that induced biofilm formation in strain 4 was further separated based on size by gel filtration. A single fraction (C9) appeared to contain the bulk of the active component as it strongly inhibited growth in strain 4, while the two flanking fractions C8 and C10 (i.e., lower concentrations of the effector) induced the biofilm response (Figure 4A). We subjected fraction C9 to protein mass spectrometry (see Methods). Of the proteins identified, three are notable for their known role in microbial interactions: homologs (PA14_8070, PA14_8090, PA14_8210) of the R and F pyocins in *P. aeruginosa* strain PA14 (Table S2) (Michel-Briand and Baysse, 2002). Given that PA14 is a well-characterized strain, we next sought to explore how the pyocins of PA14 induce the biofilm response in our natural isolates.

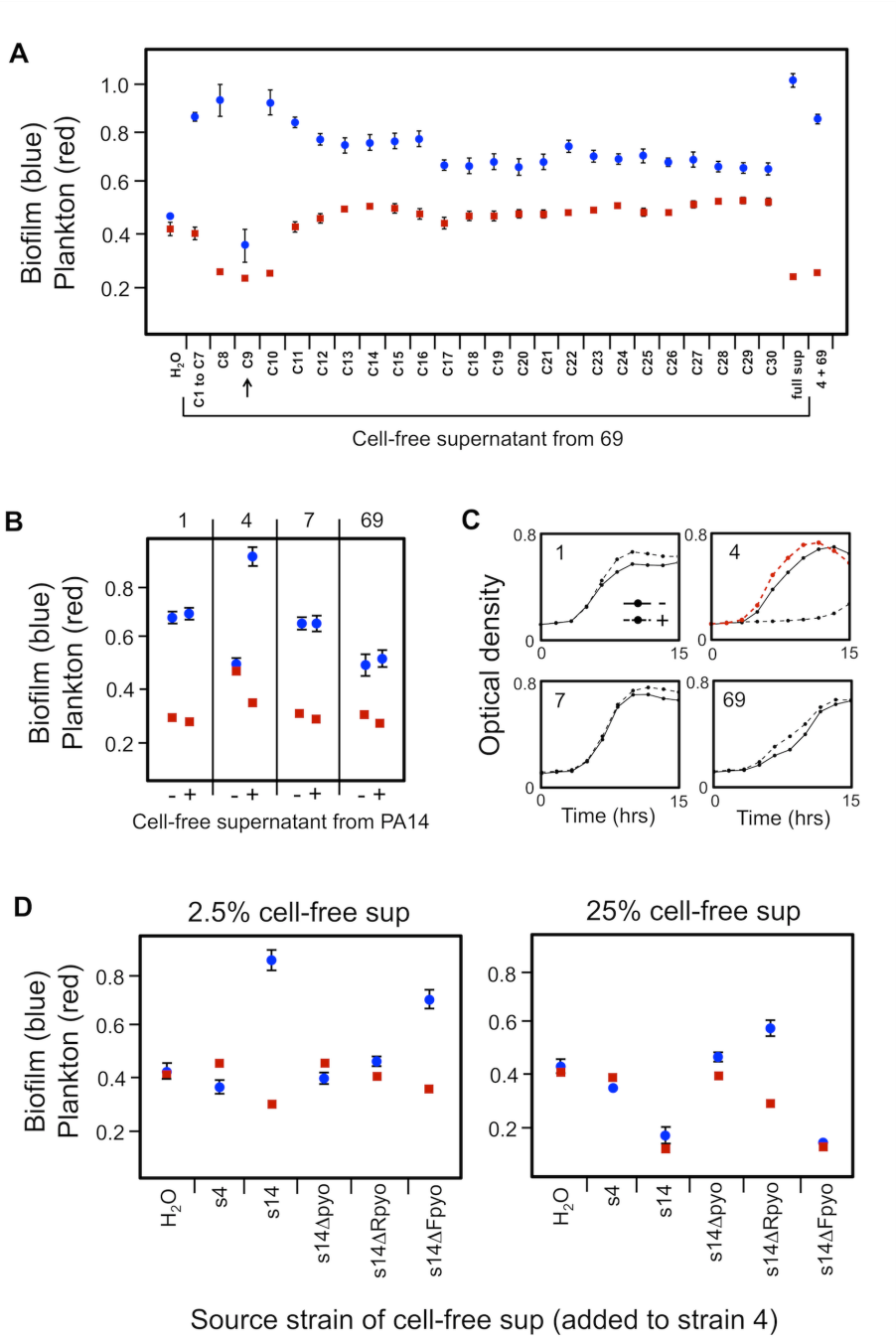

Figure 4. Pyocins are drivers of biofilm formation in co-cultures. (**A**) Size-based separation of the cell-free culture supernatant from strain 69 isolates fractions that induce biofilm formation at low concentrations and growth inhibition at high concentrations. Adding the unfractionated supernatant ('full sup') induces biofilm in strain 4, which is comparable to direct mixtures of strains 4 and 69 (here labeled as '4 + 69'). Mass spectrometry analysis of fraction C9 (arrow) identified three proteins that are homologous to R and F pyocins in strain PA14. Compared to manufacturer size standards for the column, fraction C9 is expected to be >600 kDa. (**B**) Cell-free culture supernatant at 2.5% in tryptone broth from PA14 ('+') causes increased biofilm formation in strain 4 relative to tryptone broth with the same amount of

water added ('-'), but this effect is not seen for strains 1, 7, or 69. (**C**) The supernatant from PA14 is toxic to only strain 4, causing a strong population growth lag. This suggests that some degree of cell damage is needed for the biofilm response. Supernatant from a PA14 pyocin-null mutant (PA14 *prtR*^{S153A}) does not cause any growth lag in strain 4 (red curve), confirming that the toxicity to strain 4 is driven by pyocins. (**D**) R pyocins, and F pyocins to a lesser degree, drive the biofilm response in strain 4. At 2.5%, the supernatant from both PA14 ('s14') and F-pyocin-null mutant ('s14ΔFpyo') elicit a strong biofilm response in strain 4, which is largely removed by mutating either a master regulator of pyocins ('s14Δpyo') or R pyocins ('s14ΔRpyo') in PA14 (left panel). At a higher concentration (25%), supernatant that contains R pyocins is strongly toxic to strain 4, and R pyocin-free supernatant now induces biofilm formation, which is consistent with the effects of other pyocins/toxins. Data from biofilm assays are means and 95% confidence intervals. Growth curves are means of eight replicates.

We first evaluated the effects of cell-free culture supernatant from PA14 on biofilm formation in the five strains from the round robin tournament. Strain 19, which was isolated from a cystic fibrosis infection, is a very poor competitor (Figure 2) and showed no detectable growth in our supernatant assays. It was therefore excluded from further analysis. Among the remaining strains, increased biofilm was observed in only strain 4 (Figure 4B), and we confirmed that direct mixtures of PA14 and strain 4 also lead to increased biofilm formation (Figure S2). Why is the biofilm response absent in the other three strains? To address this question, we grew the four strains in shaking culture in the presence or absence of the supernatant from PA14 and followed their growth over time. The results obtained show that the strains that do not show the biofilm response to the supernatant of PA14 also are not harmed by it (Figure 4C). This correlation between toxicity and increased biofilm helps to explain the lack of response in the three strains. Cell damage appears to be required for the biofilm response.

We next studied the effect of various mutants of pyocin production in PA14 on their ability to damage and induce the biofilm response in strain 4. We focused particularly on a strain of PA14 that has the gene coding for repressor of pyocins (PrtR) mutated to a version that is constitutively active (Table S3) (Penterman et al.,

2014b). We added cell-free supernatant of the PA14 *prtR* mutant to strain 4 and compared the effect to the addition of WT PA14 supernatant by propidium iodide staining. Propidium iodide preferentially enters cells with envelope damage (see Methods), and this assay confirmed that the pyocins produced by PA14 cause cell damage to strain 4 (Figure S3), which agrees with published literature on pyocin-driven lethality (Michel-Briand and Baysse, 2002). Moreover, additional experiments showed that the pyocins of PA14 are the major effectors of both population growth inhibition (Figure 4C) and the biofilm response of strain 4 (Figure 4D).

Focusing on the biofilm response, the use of mutants that lack only one class of pyocin suggested that F pyocins have some effect on biofilm formation at high concentrations, but it is particularly the R pyocins that strongly stimulate biofilm formation. This is, furthermore, consistent with the importance of cell damage because R pyocins are known to be efficient killers that can contribute significantly to competition among *P. aeruginosa* strains (Heo et al., 2007; Kohler et al., 2010). To further explore the potential of cell damage being required for the biofilm response, we screened 12 natural isolates for inhibition by the supernatant of PA14 in shaking culture and found that three strains were inhibited like strain 4. We randomly selected two of the inhibited strains for further study in the biofilm assay. This revealed that both exhibit a biofilm response comparable to that of strain 4 and, again, the response occurs in a pyocin-dependent manner (Figure S3). We also tested the response of the strain PAK under the same conditions. This serves as a good control case since PAK is known to be inhibited by the pyocins produced by PA14 (Heo et al., 2007). Again, we find evidence of pyocin-driven biofilm formation (Figure S4).

These data further support the idea that pyocin-driven damage under these conditions is sufficient to drive the biofilm response. We note, however, that this does

not exclude the possibility that there are additional mechanisms by which *P. aeruginosa* strains damage and induce biofilm in other susceptible strains. Indeed, the link between pyocin-based cell damage and the biofilm response is consistent with experiments using clinical antibiotics, in which antibiotic resistant mutants may require higher concentrations of antibiotics to elicit the biofilm response (Kaplain 2011). To confirm this effect in our assays, we tested a rifampicin resistant mutant of PAO1, with defined mutations in *rpoB* (Qi et al., 2014) and found that it does not respond to the same concentrations of rifampicin that trigger the biofilm responses in the wild type (Figure S5). In sum, we see comparable effects on biofilm formation from diverse forms of cell damage. This suggests that cell damage from a diverse range of bacteria interactions, both between strains and between species, has the potential to promote biofilm formation.

The biofilm response is observed in microfluidic experiments. Our experiments so far have utilized the crystal violet microtiter dish assay of standing cultures (O'Toole and Kolter, 1998). Although this experimental approach is widely used to quantify biofilm responses to antibiotics (Kaplan, 2011), it comes with two notable limitations. Firstly, indirect proxies are used to estimate biofilm formation (crystal violet staining) and planktonic cell numbers (optical density). Secondly, the presence of a large planktonic population in the standing culture means that the planktonic cells can affect the biofilm, and vice versa, in an undefined manner throughout the experiment. We, therefore, sought to recapitulate our results in a more defined assay using flow cells and direct imaging of the biofilms (Figure 5A).

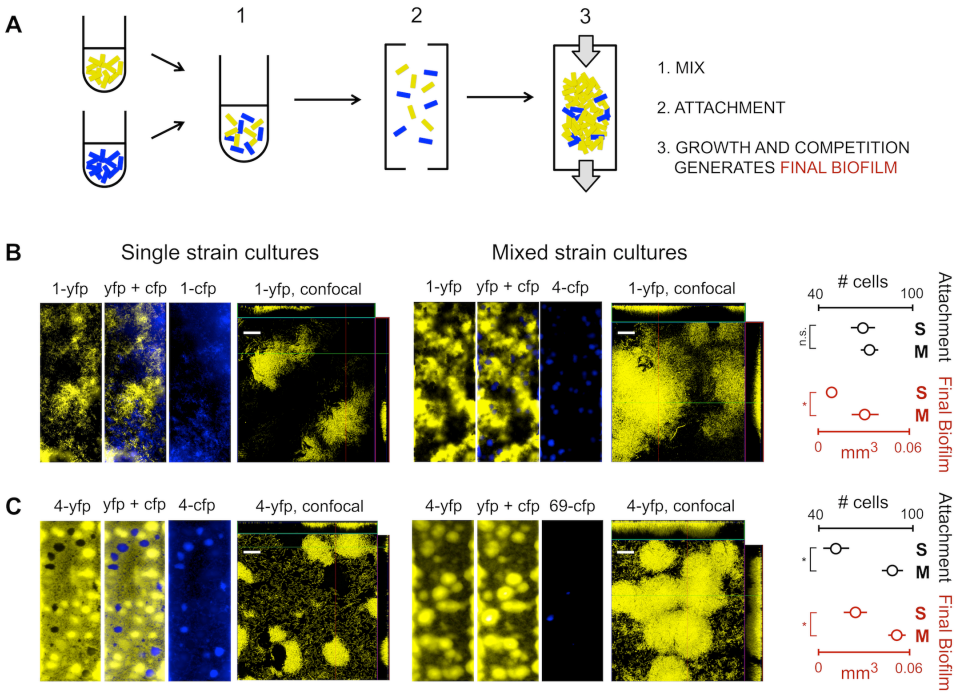

Figure 5. Strain mixing induces biofilm formation in *P. aeruginosa* in flow cells. (**A**) Schematic of the experimental design, which involves mixing genotypes, initial attachment in the absence of flow, and finally, growth and competition under constant flow. Grey arrows represent the flow of nutrient media (tryptone broth). (**B**) PAO1 biofilm compared to a mixed biofilm of PAO1 (strain 1) and strain 4. Within each image panel are three representative 10X epifluorescence micrographs of the flow cell channel showing the individual and merged YFP and CFP signals, and one 40X confocal image (scale bar is 30 μm) showing only the numerically-dominant *yfp* strain (autofluorescence in the CFP channel leads to a poor confocal signal). The charts at the far right show the initial attachment and final volume of biofilm of strain 1-*yfp* in single strain cultures (S) where 1-*yfp* is mixed with 1-*cfp* and in mixed strain cultures (M) where 1-*yfp* is mixed with 4-*cfp*. In both mixed and single cultures, the two differently-colored strains were initially mixed at a 1:1 ratio, *yfp*:*cfp*. Strain 1-*yfp* shows increased biofilm accumulation when mixed with 4, but cellular attachment is identical between single strain and mixed strain cultures. (**C**) Strain 4 biofilm compared to a mixed biofilm of strain 4 and strain 69. In both mixed and single strain conditions, two differently-colored strains were initially mixed at a 3:1 ratio, *yfp*:*cfp*. Strain 4-*yfp* attaches more and makes more biofilm when mixed with 69. Error bars are 95% confidence intervals of the mean from six replicates, which combines data from two different days. *, $p < 0.05$ and n.s., not significant in a *t* test.

We begin by studying one of our focal combinations, strain 1 (PAO1) and strain 4. As we find in the standing culture assay (Figures 1D and 2), PAO1 dominates strain 4 and largely excludes it from the biofilm after 24 h (Figure 5B). Moreover, we

observe an increase in the volume of biofilm formed by PAO1. Our observations in the less-defined crystal violet assays, therefore, are recapitulated in flow cell biofilms: strain-mixing results in a single strain dominating and an increase in biofilm formation. Do we also observe this biofilm response in strain 4, which was the focus of detailed analyses in the previous section? In order to study this, we needed to create a condition where strain 4 is not eliminated from the biofilm. Preliminary tests with our two focal mixtures (1 + 4, 4 + 69, Figure 1D) revealed that strain 4 will persist with strain 69, if it is over-represented at inoculation. We, therefore, tested strain 4 mixed with strain 69 in the flow cells at a 3:1 initial ratio. Under these conditions, strain 4 dominates the biofilms and largely excludes strain 69 and, most importantly, we see a clear increase in biofilm formation in strain 4 here when compared to its single-strain counterpart (Figure 5C).

Experiments using flow cells have a separate attachment phase at the beginning of the experiment to seed the surface with bacteria (see Methods). Counting attached cells after the attachment phase revealed that strain 4 attaches more in the presence of strain 69 but strain 1 does not attach more in the presence of strain 4 (Figure 5). Both initial attachment and subsequent biofilm accumulation, then, contribute to the response to strain mixing but while we always see increased biofilm formation, we do not always see an initial difference in attachment (also see next section). In sum, the flow cell experiments provide validation from a second assay that *P. aeruginosa* strains increase biofilm formation in response to the presence of competing strains.

Antibiotic gradients as drivers of biofilm formation. Our data suggest that bacteriocins produced by natural isolates of *P. aeruginosa* act as a cue that drives biofilm formation. This raises the possibility that the widely reported biofilm responses

to clinical antibiotics (Elliott et al., 2010; Haddadin et al., 2010; Hoffman et al., 2005; Kaplan, 2011; Kaplan et al., 2012; Kumar and Ting, 2013; Linares et al., 2006; Wang et al., 2010) also have their origins in responses to ecological competition from strains and species. But does the addition of antibiotics, or cell-free culture supernatant from competitors, also result in increased biofilm formation in a microfluidic device?

Experiments with a single concentration of antibiotic revealed that the addition of cell-free culture supernatant or clinical antibiotics commonly results in cell detachment at the initial stage of the experiment. This is consistent with the effects of supernatants and antibiotics in the crystal violet assay being strongly concentration dependent, whereby lower concentrations cause the biofilm response and higher concentrations cause growth inhibition (Figure 3). We, therefore, developed a more robust method to study the effects of cell-free supernatant and antibiotics on biofilms in microfluidic devices. We moved to use microfluidic platforms with two inlet channels in which only one of the two inlets contains the antibiotics (Figure 6A).

The goal of this experimental approach was to create a gradient inside the main chamber with a wide range of antibiotic concentrations, from sub-lethal to lethal (see Methods). Our protocol always allows some parts of the chamber to contain negligible amounts of the antibiotic, which ensures that not all cells detach when antibiotics are flowed through. Importantly, the cells will experience a wide range of concentrations of antibiotic in a single experiment, and we can directly observe how they respond. Under these conditions, we observe a large increase in biofilm formation upon the addition of multiple classes of antibiotics in multiple strain backgrounds (Figures 6, S6, and S7). Our data show that antibiotics do indeed promote biofilm formation in flow cells. In addition, they support the value of studying gradients for understanding cellular responses to stress. Such gradients are common in biofilms (Stewart and

Franklin, 2008; Tseng et al., 2013), but their effects can be missed by static culture assays.

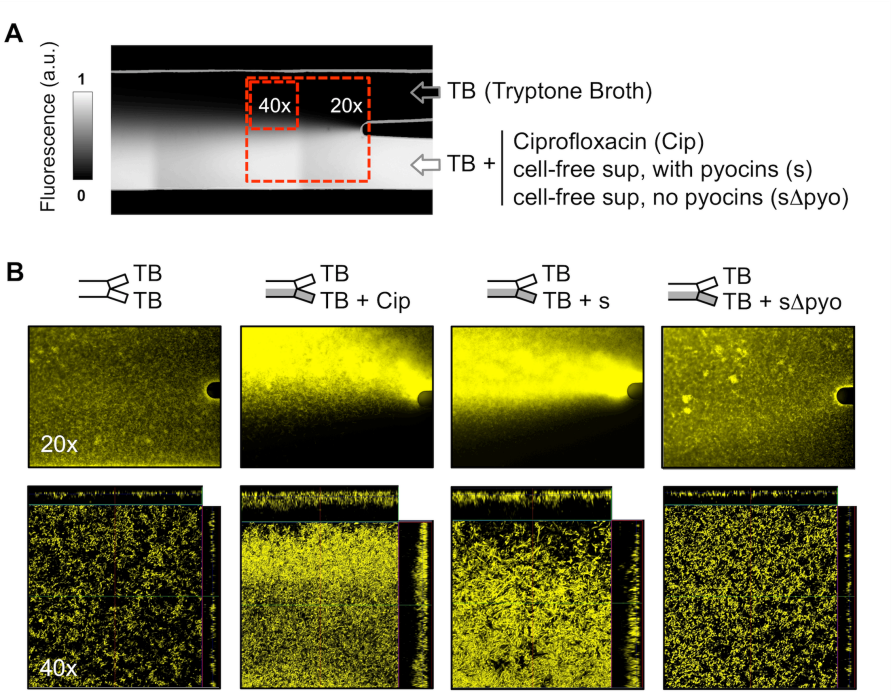

Figure 6. Antibiotic gradients drive biofilm formation. (**A**) Image of the double inlet flow cell. Growth medium (tryptone broth) flows through both inlets but one also contains the test compound, which generates a gradient of the compound in the main chamber. Arrows indicate the direction of the flow. A fluorescent dye (fluorescein) has been added in this particular example (white) to illustrate the gradient created, but this is not present in the experiments in which we study the response of cells to antibiotics and cell-free supernatant (a.u., arbitrary units). (**B**) Images corresponding to the red boxes shown in panel A, captured using a 20X objective (epifluorescence microscopy) and a 40X objective (confocal microscopy), respectively. 20X images are 350 μm by 450 μm, and 40X are 182 μm by 182 μm. Identical image collection and processing settings were used in all images to illustrate that ciprofloxacin ('Cip') and cell-free culture supernatant from strain PA14 ('s') both enhance the yellow signal when compared to controls at 20X magnification ('sΔpyo' is cell-free supernatant from the pyocin-null mutant and 'TB' is tryptone broth, the standard medium). The confocal microscopy shows that the increase in the YFP signal in the epifluorescence images is explained by an increase in both cell density and volume of the biofilm.

We next asked whether pyocins are also capable of promoting biofilm formation in our dual inlet experiment. In support of this outcome, we find that flowing the cell-

free culture supernatant of PA14 over strain 4 results in increased biofilm formation, but not when we use the supernatant of the pyocin null-mutant (Figure 6). What drives the increase in biofilm? Increased biofilm accumulation could occur through stronger attachment and better retention of cells throughout the experiment, or through the acceleration of cell division. In order to test the impact of pyocins on attachment, we allowed strain 4 cells to attach in the presence of cell-free supernatant of PA14 and compared this to the effect of cell free supernatant of the PA14 pyocin null-mutant (Figure S8). This shows that pyocins do indeed lead to increased attachment. This phenotype is not simply sedimentation of damaged cells. We flush unattached cells out before imaging and, importantly, we see increased attachment in the presence of pyocins both on the bottom and the top of the channel (Figure S9). Moreover, propidium iodide staining shows that, concurrently, there is increased cell damage from the supernatant of PA14 than with the supernatant of the pyocin null mutant (Figure S8), consistent with what we found for shaking culture (Figure S3). We see, therefore, that pyocins from competitors both cause cell damage (Figures S3 and S8) and an increase in biofilm formation (Figures 4, 6, S4, S8, and S9).

The attachment experiments (Figures S8 and S9) suggest that the biofilm response may occur via an increased propensity for cells to attach, and subsequently persist, in the biofilm. An increased rate of cell division could also contribute to the biofilm response in some or all strains. Direct assessments of cell division in three-dimensional biofilms is challenging and was not possible with our current methods. However, there is evidence from *Escherichia coli* that sub-lethal levels of antibiotics can increase growth rate (Migliore et al., 2013). More generally, there is evidence for widespread transcriptional and metabolic changes in response to antibiotics (Dwyer et al., 2014; Dwyer et al., 2007; Goh et al., 2002; Kohanski et al., 2010a; Kohanski et al.,

2010b; Kohanski et al., 2007; Kohanski et al., 2008; Linares et al., 2006; Tsui et al., 2004), which have recently been the focus of intense debate (Ezraty et al., 2013; Imlay, 2015; Keren, 2013; Kohanski et al., 2010b; Liu and Imlay, 2013) but still lack evolutionary explanation. If these changes are also involved in the responses to other bacterial strains and species, it would suggest that many of the physiological and metabolic changes seen upon antibiotic use have their natural origins in competition sensing (Cornforth and Foster, 2013) and the ecology of the species concerned.

Conclusions

Biofilms are central to microbiology. Despite this, we still understand relatively little about the drivers of biofilm formation in a natural context. Our data suggest that a major factor in biofilm formation in nature is ecological competition with other strains. We have shown that co-culturing strains of *P. aeruginosa* often leads to increased biofilm (Figures 1, 2, and 5). We have also shown that this increase in *P. aeruginosa* should not be interpreted as a cooperative interaction between strains. Mixing pairs of strains shows that one of the two strains is largely eliminated during the process of biofilm formation (Figures 2 and 5). Moreover, our data suggest that biofilm formation is stimulated as a response to cell damage caused by other strains: cell-free supernatant of one strain only induces biofilms in another strain when it also causes cell damage (Figures 4, S3, and S8).

In pairwise mixtures of natural isolates, we have shown that one driver of the biofilm response are R and F pyocins, the narrow-spectrum antibiotics produced by *P. aeruginosa*. We, therefore, expect that pyocin-mediated competition will often be an inducer of biofilm formation in *P. aeruginosa*. However, our work also emphasizes that the biofilm responses to clinical antibiotics are highly comparable to those seen

with pyocins. The different sets of antibiotics studied here have very different modes of action, including inhibition of DNA replication (ciprofloxacin), transcription (rifampicin), or translation (tetracycline) and, in the case of R and F pyocins, disruption of membrane potentials. The responses we observe, therefore, are very general and suggest that any toxin made by one *P. aeruginosa* strain has the potential to induce biofilm formation in another. Is there a common mechanism linking the diverse forms of cell damage to the biofilm response? Bacteria have a number of stress responses that are triggered by cell damage, which have been proposed as candidates for sensing the presence of competing strains (Cornforth and Foster, 2013). Perhaps most notably, this includes the responses to oxidative stress, which is associated with the action of clinical antibiotics and diverse damaging agents from competing microbes (Dong et al., 2015; Dwyer et al., 2014; Imlay, 2013, 2015; Kohanski et al., 2010b).

What is the evolutionary basis of *P. aeruginosa* strains increasing biofilm formation in response to ecological competition? Mechanistically, our experiments suggest that the biofilm response is caused, at least in part, by an increase in surface-attachment in the presence of other strains. Whether a biofilm response is caused by differential attachment or another mechanism, the key effect is to increase the frequency of the responder relative to competing genotypes. We hypothesize that the evolutionary advantage of this increase in frequency is that it allows strains to better defend against and attack other genotypes. Biofilms are known to promote resistance to a wide range of stressors, including R pyocins (Penterman et al., 2014a). In addition, the competitive ability in a biofilm is expected to be linked to the relative density of each strain. At high density, cells can better control the environment with secreted products that favor their genotype over others (Nadell et al., 2009; West et al., 2006). Dominating a biofilm early, then, is likely to enable a genotype to dominate in the long

term. In this model, the well-known biofilm responses to antibiotics (Elliott et al., 2010; Haddadin et al., 2010; Hoffman et al., 2005; Kaplan, 2011; Kaplan et al., 2012; Kumar and Ting, 2013; Linares et al., 2006; Wang et al., 2010) have their roots in natural selection to detect competing genotypes and respond in a manner that maximizes the ability to defend and attack (Cornforth and Foster, 2013; Ratcliff and Denison, 2011).

The fact that antibiotics are known to induce biofilm formation in diverse species suggests that ecological competition may increase biofilm formation in many microbial communities in which many strains and species meet. Consistent with this prediction, recent work on assemblage of multiple species, including known antibiotic producers, found that strain mixing increases biofilm formation (Lee et al., 2014; Ren et al., 2014a; Ren et al., 2014b), although it was interpreted there as cooperation between species. Understanding the effects of ecological competition on biofilm formation also has implications for health and disease. An important new idea in the treatment of microbial disease is that we can harness ecological competition between microbes to our advantage (Callaway et al., 2008; Kamada et al., 2013). Probiotic supplements for the gut are already an important industry (Gareau et al., 2010), and a major goal of synthetic biology is to arm benign bacteria with the antibiotics they need to combat disease-causing strains (Saeidi et al., 2011). We must be cautious, then, that this escalation of ecological competition does not result in the outcomes that we observe here: a more abundant pathogen.

Methods

Strains. A total of 22 strains of *Pseudomonas aeruginosa* were used, including both clinical and environmental isolates from the Kolter strain collection (Table S1). A

subset of these strains was subject to detailed analyses, including the well-studied clinical strain PAO1 (here referred to as strain 1), and strains 4, 7, 19, and 69. These five strains were chromosomally tagged with constitutively-expressed fluorescent tags (*cfp* or *yfp*) using the mini-*Tn*7 system (Lambertsen et al., 2004). The pyocin-null *prtR*^{S153A} (constructed as in (Penterman et al., 2014b)), producing constitutively active repressor, and its parental strain PA14 were kindly provided by Jon Penterman. The R and F pyocin mutants are from the PA14 Non-Redundant Transposon Insertion Mutant Set (Liberati et al., 2006). We found no differences in our assays between the two sources of PA14 strains and only show the data from the Penterman source in the figures. Other strains are described in S3 Table.

Static biofilm assays. These assays were based on standard protocols (O'Toole and Kolter, 1998). Briefly, cells from overnight cultures of *P. aeruginosa* were sub-cultured and from these, exponential phase cells were inoculated in peg-lidded 96-well plates (Nunc, conical bottom) in 100 µl tryptone broth (10 g Bacto triptone per 1 l water) at starting optical density of 0.0025 (A_{600}), and allowed to grow at 22 ºC. After 24 h, 50 µl of medium was removed and the optical density at A_{600} was measured to estimate the density of planktonic cells. Pegs were then washed, stained with 0.1% crystal violet, washed again, and then the remaining stain was dissolved with 200 µl of 33% acetic acid. Finally, the optical density at A_{595} was measured and used as a proxy for biofilm formation. For direct strain-mixing experiments (Figures 1C, 1D, and 2), we used plates without pegs because this allows cells to be more easily removed and sampled from the biofilms when required (see below). The only substantive difference is that the biofilm on the edge of the well is assessed using crystal violet rather than the biofilm on a peg. We confirmed that the two assays give very similar results (Figure

S10). While the experiments presented in the main text were done in tryptone broth, the biofilm response was also investigated in other standard bacterial growth media, including Luria broth (LB), *Pseudomonas* minimal medium (PMM) and casamino acid (CAA) medium, along with different concentrations of iron or buffer, which did not have qualitative effects in the cellular responses to mixing (Figure S1).

Antibiotics. Three antibiotics belonging to different structural families, namely ciprofloxacin, rifampicin, and tetracycline, were chosen to recapitulate the effect of sub-inhibitory concentrations of antibiotics on biofilm formation of *P. aeruginosa* (Kaplan, 2011). Stock solutions of each antibiotic (obtained from Sigma Chemical Company) were stored at -20 ºC and diluted to the desired concentration on the day of each experiment. All antibiotics experiments used tryptone broth as the growth medium. Biofilm formation and growth in shaking culture were assayed as detailed in the sections 'Static biofilm assays' (above) and 'Growth curves' (below), respectively. For the dual-flow microfluidic experiments (Figure 6) we injected through one of the inlets an antibiotic concentration ten times the concentration that inhibited growth in shaking culture (according to Figure 1). These concentrations are thus 1 μg/ml for ciprofloxacin, 50 μg/ml for rifampicin, and 1000 μg/ml for tetracycline.

Strain mixing experiments. The initial survey of how strain mixing affects biofilm formation was based on 22 strains of *P. aeruginosa*. Biofilm formation after 24 h was evaluated in 22 single strains, 22 pair-wise combinations, 8 combinations of 5 strains, and 2 of 10 strains. Strains were evenly mixed based upon the optical density of stationary phase cultures. The strain combinations in the mixtures were chosen to ensure a near-even representation of the strains across the mixtures. Each strain

occurred twice in the pairs, twice in the mixtures of fives (with one strain appearing only once), and once in a mixture of ten (with one strain excluded). Sixteen replicates were performed in each experiment for each strain or mixture, to give a total of 432 biofilm assays in each experiment. All treatments were performed on two different days.

The second set of experiments mixed five fluorescently-labeled strains in all combinations. We assessed biofilm formation and planktonic cell density in 96 well plates after 24 h. Samples of planktonic cells and biofilm cells were taken from each treatment to record the frequency of the two strains using fluorescence microscopy. The biofilm sample was taken by vigorously shaking the washed plates in phosphate buffer for one hour (experiments revealed that this treatment gives identical frequency estimates as shaking with 500 μm glass beads and removing the whole biofilm). In addition, direct images of the biofilms were taken by growing strains in 2 ml of media containing 25 x 25 mm^2 glass coverslips in 6-well plates under conditions otherwise identical to the 96-well plate assay. The bacteria form a biofilm on the coverslip slightly below the air-water interface, which is then visualized by fluorescent microscopy (Figure 2).

All experiments were repeated twice on different days. Comparison of these data with the pair-wise mixtures in the first experiments (above) confirmed that the mixing responses were not affected by fluorescent labeling. All methods were the same as before with the addition that we diluted overnight cultures of each strain and grew them for 2 h to obtain exponential phase cells to inoculate the biofilm assays (Figure 2). This did not affect biofilm formation, but it helped reduce variability in the strain frequency in the mixtures. For the two large-scale strain-mixing experiments (Figures

1C and 2), we present data that is the combination of the two repeats from different days, as variability between days was relatively high.

Microfluidic biofilm assays. Biofilm formation was also monitored under laminar flow conditions using the BioFlux 200 system (Fluxion Biosciences, South San Francisco, CA, United States). Experiments were performed essentially as described elsewhere (Benoit et al., 2010). First, microfluidic channels (350 μm x 75 μm x 4.89 mm for width, height, and length, respectively) were primed with growth media, here tryptone broth, to prevent air bubbles from entering the channels on subsequent loading steps, and just after, inoculated with cells at the exponential phase. The concentration of these cultures was adjusted so that the optical density at 600 nm in tryptone broth was 0.25. Then, after the attachment period without flow (20 min at 22 °C), fresh medium was pumped from inlet wells through the channels to outlet, firstly with a flow rate of 40 μl/h for 20 min to flush out planktonic cells, and then with a constant flow rate of 4 μl/h until the end of the experiments (24 or 48 h). To address the effect of pyocins on cellular attachment we allowed cells to attach in the channels for 20 minutes with tryptone broth made with 10% cell-free supernatant, either from strain PA14 WT or a mutant that has the gene coding the repressor of pyocins (PrtR) mutated to a version that is constitutively active (Table S3). We then flushed out planktonic cells, as explained above, and imaged to assess attachment.

For consistency, we used only one plate type for all microfluidic experiments, the 'Invasion' plate of Fluxion Biosciences that has two parallel inlets and one outlet (Figure 6). When studying co-cultures, the two inlets contained the same medium, and when studying the effect of antibiotic gradients we added the required concentration of the antibiotic (or cell-free culture supernatant) to one of the inlets only, thus creating a

gradient of the compound being tested in the main chamber. Each experiment was repeated twice, on different days, and the images of biofilms taken come from the middle of the channels, where the channels are the flattest, when accessing the effects of strain mixing. In all treatments, images were taken at the same distance from the respective inlets. When accessing the effect of antibiotics or cell-free supernatant we imaged directly downstream of the inlets, as shown in Figure 6, where the chemical gradient is the steepest.

Study of diffusible substances. To access the effects of diffusible substances in the biofilm response, two sets of experiments were performed. First, we used 96-well Transwell plates (Corning) with two different inlays separated by a 0.4 μm pore size membrane. In these experiments, the strain in the bottom of the well was inoculated at an optical density of 0.0025 (A_{600}) in 75 μl of media. This bottom strain was the tester strain in which biofilm formation was analyzed. The top strain was the inducer and was inoculated at a higher density of 0.1 (A_{600}) with 50 μl media. This assay revealed cell-to-cell contact is not strictly necessary for the biofilm response (Figure 3A). To investigate this further, we studied responses of strains to cell-free supernatants from other strains. The supernatant of the strains were obtained as follows. Exponential phase cells of all strains were inoculated in 6-well plates in 4 ml of tryptone broth at starting optical density of 0.025 (A_{600}), and allowed to grow at 22 ºC for 21 h. Cultures were then spun down (3,000 g during 10 min) and filtrated using 0.22 μm filters (Millipore). The spent media assay followed the same methods used for the biofilm assay, except that exponential phase cells of the responder strain were inoculated in media containing (2.5/25%) cell-free culture supernatant from itself or others.

Fractionation of the cell free supernatant was performed by GE 1 ml resource Q anion exchange chromatography (buffer A: 50 mM Tris-HCl [pH 7.5], 2% glycerol, 2 mM β-mercaptoethanol; buffer B: buffer A + 1 M NaCl) followed by GE Superdex 200 10/300 GL gel filtration in SEC buffer. The active fraction, as determined by the crystal violet assay (Figure 4), was subject to mass spectrometry by the FAS Center for Systems Biology Core Facilities, Harvard University, US. Briefly, the sample was reduced, carboxyamidomethylated and digested with trypsin. Peptide sequence analysis of each digestion mixture was then performed by microcapillary reversed phase high-performance liquid chromatography coupled with nanoelectrospray tandem mass spectrometry (μLC-MS/MS) on an LTQ-Orbitrap mass spectrometer (ThermoFisher Scientific, San Jose, CA, United States).

Growth curves. Exponential phase cells from overnight cultures were inoculated in flat-bottomed 96-well plates (Nunc) in 200 μl of tryptone broth at the starting optical density (A_{600}) of 0.0025, as for the biofilm assays, and allowed to grow at 22 ºC, shaking, inside a plate reader (Tecan, Infinite M200 Pro). Test treatments were supplemented with 25% of cell-free supernatant from PA14, the respective pyocin-null, or distilled water (control). The optical density at A_{600} was measured automatically every 500 s. When required, cell damage was assessed by staining shaking cultures or attached cells in a microfluidic device with propidium iodide, at the final concentration of 3 μl/ml (Webb et al., 2003). Propidium iodide-stained cells were visualized using epifluorescence microscopy with DsRed-based filters.

Fluorescence and Confocal Microscopy. Images of BioFlux biofilms were obtained using a Zeiss confocal laser scanning microscope (LSM 700), a digital camera

(AxioCam MRm), and the associated Zen 2011 software (blue or black edition, for fluorescence or confocal microscopy, respectively). Objectives used were 10X, 20X, or 40X, as specified in the figure legends.

Image Analysis. A MATLAB (MathWorks) script was used to determine the number of attached cells on the surface of microfluidics, along with the volume of biofilms after 24 h of incubation. The volume calculation uses the area of fluorescence signal of biofilms in each confocal slice, which is then summed across the slices in *z*-plane.

4. Single-cell twitching chemotaxis during biofilm formation

Abstract 73

Main text[1] 74

Abstract

Free-swimming bacteria navigate their environments using finely tuned chemosensory systems, which regulate the rotation of their flagella (Porter et al., 2011; Wadhams and Armitage, 2004). While this form of chemotaxis has been intensively studied, bacteria commonly live in surface-attached communities known as biofilms, which are central to their biology and how they affect us (Costerton et al., 1995; Kolter and Greenberg, 2006). Biofilm bacteria experience strong chemical gradients (Stewart and Franklin, 2008) and use grappling hook-like appendages (type IV pili) to move (Klausen et al., 2003; O'Toole and Kolter, 1998), but it has been concluded that individual cells cannot chemotax on surfaces (Taylor and Welch, 2008; Zhang et al., 2012). Here we use microfluidic chemical gradients and massively-parallel automated tracking to study the chemotactic behavior of *Pseudomonas aeruginosa* during biofilm formation. Experiments reveal that individual cells can efficiently move towards a chemoattractant source using their pili-based 'twitching' motility and the Chp chemosensory system. Analysis of tens of thousands of trajectories show that cells climb gradients by reversing the direction of their motility more frequently when they

[1] Format of journal *Nature*. Find Extended Data Figures, Videos and Supplementary Methods in the Appendix.

are moving away from a chemoattractant source. These corrective maneuvers are triggered rapidly, often before a wayward cell has ventured a small fraction of its body length away from the chemoattractant source. Cells lacking the response regulator PilG, a homologue of CheY from *Escherichia coli*, rarely reverse and are incapable of chemotaxis. Moreover, wild-type cells move faster when travelling towards a chemoattractant source, while Δ*pilG* cells traveling towards or away from a chemoattractant source move at the same speed. Our findings overturn the view that individual bacteria cannot direct their motion when attached to surfaces and reveal the hidden potential for chemotaxis within biofilms.

Main Text

Flagella-driven chemotaxis in bacteria has been thoroughly dissected (Adler, 1966; Berg, 2004; Berg and Brown, 1972; Wadhams and Armitage, 2004) leading to its emergence as a paradigm of both signal transduction and cellular decision-making (Porter et al., 2011; Wadhams and Armitage, 2004). However, many key phenotypes of bacteria occur when cells are not swimming. In particular, planktonic cells commonly attach to surfaces and form communities, known as biofilms, which are central to health, disease, agriculture, industry and the environment (Costerton et al., 1995; Kolter and Greenberg, 2006). Biofilms often contain steep chemical gradients that result from cell metabolism, hampered diffusion and the secretion of a wide variety of compounds (Stewart and Franklin, 2008). While biofilm cells can be highly motile (Klausen et al., 2003), surprisingly, we do not know whether individual cells within biofilms can perform chemotaxis. Surface-based chemotaxis involving collectives of cells is well known in the social bacterium *Myxococcus xanthus* during swarming and fruiting body formation (Shi et al., 1993; Zhang et al., 2012). In addition, *P.*

aeruginosa colonies in Petri dishes form asymmetrical shapes in gradients of phospholipids and unsaturated long-chain fatty acids, which has led to the suggestion that, as for *M. xanthus*, collectives of surface-attached *P. aeruginosa* cells can chemotax (Sampedro et al., 2014). However, in sharp contrast to swimming bacteria, studies of cell movement on surfaces have suggested that chemotaxis requires the collective interaction of many cells and that solitary bacteria are incapable of biasing their motility in response to chemical gradients (Taylor and Welch, 2008; Zhang et al., 2012). Moreover, previous observations of surface-based chemotaxis use agar-based colony assays and we lack direct tests of chemotaxis within biofilms where cells actively attach to, and grow from, a surface (O'Toole and Kolter, 1998).

Here we ask whether single cells of *P. aeruginosa* can respond to gradients of chemoattractants as they form a surface-attached biofilm. *P. aeruginosa* is an intensely studied opportunistic pathogen and a canonical model for the study of biofilms (O'Toole and Kolter, 1998). After attaching to surfaces, *P. aeruginosa* cells are highly motile and move by pulling themselves along via the extension and retraction of their type IV pili, a process known as twitching motility (Burrows, 2012). This form of movement is common throughout biofilm formation (Klausen et al., 2003; Zhao et al., 2013), and we focus here on the early stages of biofilm formation so that we can isolate the behavior of individual cells and map this to the chemical gradients they experience. We follow the movement of surface-attached cells within microfluidic devices and use flow to generate stable chemical gradients (Figure 1a, Extended Data Figure 1). Many bacterial chemoattractants strongly promote growth (Adler et al., 1973), which in our experiments leads to a crowded surface and a limited ability to analyze single cell behavior. We, therefore, focus here on dimethyl sulfoxide (DMSO), which does not strongly affect growth. We also confirm key observations using gradients of succinate,

which is the preferred carbon source of *P. aeruginosa* (Rojo, 2010) and a potent chemoattractant of this pathogen in the planktonic state (Moulton and Montie, 1979).

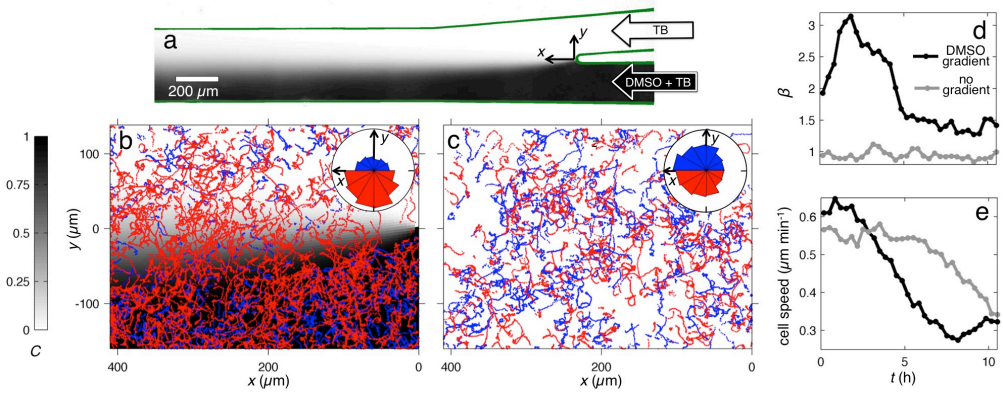

Figure 1: Surface-attached *P. aeruginosa* cells direct their movement up gradients of dimethyl sulfoxide (DMSO). (**a**) A two-inlet microfluidic device generates a stable chemical gradient via molecular diffusion. Tryptone broth (TB) is continuously injected through one of the inlets, whilst DMSO at a concentration of C_{max} = 350 mM and TB are continuously injected through the other inlet. Here $C = C'/C_{max}$ where C' is the local concentration of DMSO which was quantified using fluorescein in a separate experiment (Supplementary Methods). (**b**) Cell trajectories over the first five hours of the experiment (t = 0 – 5 h) show that motility is biased towards increasing concentrations of DMSO. Trajectories with net movement toward larger C (i.e. in $-y$) are shown in red and those with net movement towards smaller C (i.e. in $+y$) are shown in blue. The background shows C computed by a mathematical model (Supplementary Methods, Extended Data Figure 1). Inset shows probability density functions of the angle from each trajectory's origin to final position and red (blue) bins denote movement in the $-y$ ($+y$) direction. This inset also shows slight preferential movement in the $+x$ direction, which likely results from interactions with flow (Shen et al., 2012). (**c**) Control shows there is no bias in the y direction without DMSO. (**d,e**) A time series of the chemotactic bias, β, defined as the number of cells that move in $-y$ divided by the number moving in $+y$, peaks at $t \approx 2$ h (**d**) and then declines as the surface becomes more crowded and cell speed is attenuated (**e**).

We used automated cell tracking to follow *P. aeruginosa* cells in a stable gradient of DMSO during biofilm formation (Figure 1a, Extended Data Figure 1). This revealed that cell movement is strongly biased in the direction of increasing DMSO concentration (Figure 1b, Supplementary Video 1), which contrasts with their random motility in the absence of chemical gradients (Figure 1c). After two hours of incubation the chemotactic bias peaks, with more than three times as many cells

moving towards the chemoattractant source than moving away from it (β=3.1), but a significant bias is maintained even as the surface becomes more crowded with cells (Figure 1d,e). These data show single cells can direct their motility along chemical gradients and reveal that attached cells are capable of chemotaxis (*sensu* Adler (Adler, 1966)) during biofilm formation.

In our experiments both cell division and motility cause cells to preferentially accumulate on the side of the device with the chemoattractant (Supplementary Video 1). To test whether the biased motility we observe is an artifact of the variation in cell density, which has been shown coordinate surface motility in *M. xanthus* (Kaiser, 2003), we exposed cells to a chemoattractant gradient that switched directions every three hours (Supplementary Methods). When the chemoattractant gradient was inverted cells responded by changing the direction of their bias (Figure 2, Supplementary Video 2), indicating that cell movement is a direct response to the imposed chemoattractant gradient. By minimizing crowding on one side of the channel, this technique also allows a clear demonstration of chemotaxis towards succinate (Supplementary Video 2, Figure 2), which strongly enhances growth. Finally, the increased data available from this technique reveals that the chemotactic bias, β, increases with the magnitude of the chemoattractant gradient $|G|$ (Figure 2h), which is a defining feature of chemotaxis across different biological systems (Rivero et al., 1989).

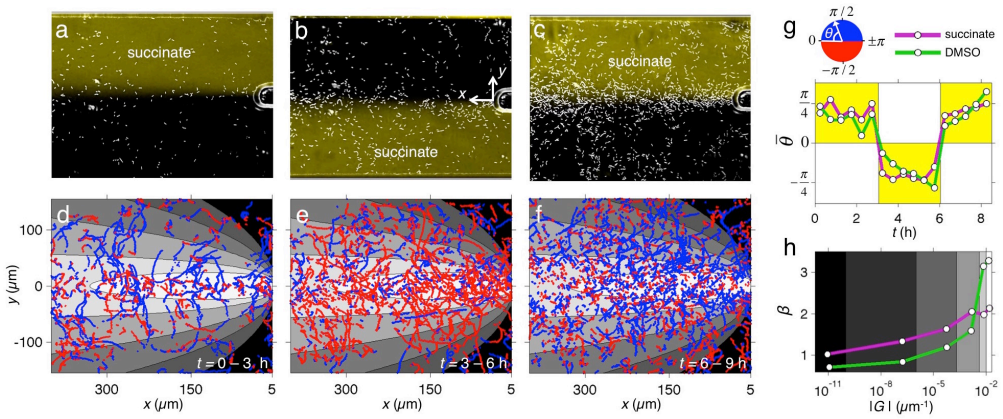

Figure 2: Changing the direction of the chemoattractant gradient elicits a change in the direction of cell motility and reveals the chemotactic response increases with the strength of the gradient. (**a,b,c**) Cells (white spots) were exposed to gradient of succinate (visualized in yellow, C_{max} = 2 mM) whose direction was inverted every three hours. (**d,e,f**) The resulting chemotactic response was measured by calculating the direction of cell movement, θ, over 16 min intervals and segments of trajectories that moved in the $-y$ ($+y$) direction are shown in red (blue). (**g**) The mean movement direction, $\bar{\theta}$, was obtained by averaging θ for all cells (magenta line), revealing that cell motility is maintained in the direction of the instantaneous chemoattractant gradient (yellow regions). (**h**) Combining data from the entire experiment (t = 0 – 9 h) reveals that the chemotactic bias, β, increases with the magnitude of the normalized gradient, $|G| = 1/C_{max}\,|\partial C/\partial y|$ (magenta line). Here β is the number of trajectories moving in the direction of increasing concentration C, divided by the number moving in the direction of decreasing C. Greyscale colors in **d,e,f** show $|G|$ and correspond to the bins used in the analysis presented in **h**. Green lines in **g**,**h** show results of an analogous experiment conducted with a DMSO gradient (C_{max} = 350 mM). In both experiments, the position of chemoattractant was visualized using a dye that does not induce a chemotactic response (Extended Data Figure 2) and $|G|$ was estimated using a mathematical model of diffusion (Supplementary Methods).

What is the genetic basis of the chemotactic response? After attachment, *P. aeruginosa* is well known to use pili-based motility to move during biofilm formation (Klausen et al., 2003; Zhao et al., 2013) and a mutant that cannot generate functional pili (Δ*pilB*) is immobile in our experiments (Figure 3a,c). We next sought the chemosensory system that cells use to perform chemotaxis in our developing biofilms. Chemotaxis in swimming *P. aeruginosa* cells is under the regulation of a Che transduction system homologous to that of *E .coli* (Kato et al., 2008; Sampedro et al., 2014), but this cluster (Che cluster I) is not required for our phenotype (Extended Data Figure 3).

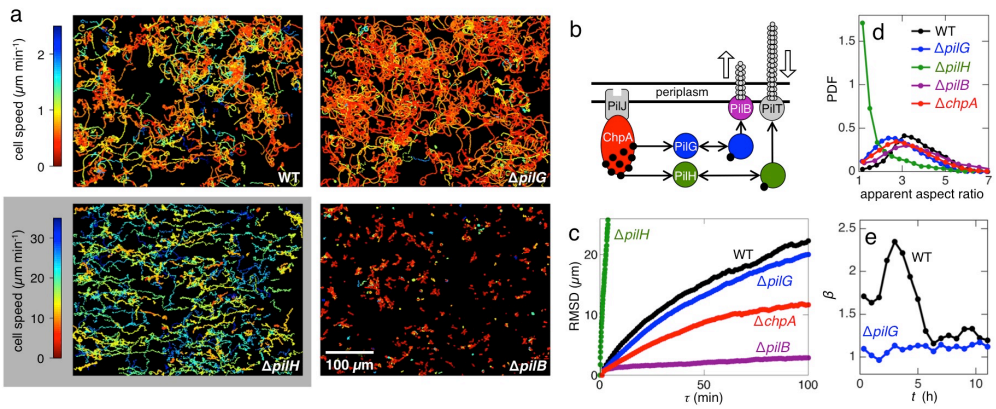

Figure 3: **Twitching chemotaxis in *P. aeruginosa* is mediated by the Chp signal transduction pathway.** (**a**) Trajectories of WT and different Chp mutants in the absence of a chemical gradient where color denotes instantaneous cell speed. (**b**) Simplified diagram of Chp chemosensory system. By homology to the Che system of *E. coli*, it is thought that ChpA drives phosphorylation of two CheY-like response regulator proteins, PilG and PilH, which interact with PilB and PilT to drive pilus extension and retraction, respectively, in a manner similar to how phosphorylated CheY controls flagellar rotation in swimming cells (Bertrand et al., 2010). Black circles denote phosphate groups. (**c**) Root mean squared displacement, *RMSD*, of different strains in the absence of a chemical gradient as a function of time lag, τ (Supplementary Methods). Δ*pilG* cells move similarly to the WT, Δ*pilH* cells move much faster (note separate color bar in **a**), and Δ*pilB* cells lack motility altogether. (**d**) Δ*pilH* cells tend to move with their long axis perpendicular to the surface, leading to an apparent aspect ratio of ≈1 (the cell length divided by cell width, as viewed from below the surface, Supplementary Methods). The remainder of the strains orient themselves parallel to the surface such that their apparent aspect ratio is >1. PDF stands for probability density function. (**e**) Chemotactic bias, β, of Δ*pilG* and its respective WT, measured in an experiment analogous to that in Figure 1d, shows that PilG plays an essential role in twitching chemotaxis. Data used to compose **a**,**c**,**d** for Δ*pilH* cells was collected in the first 15 minutes after inoculation as they move so quickly requiring high frame rate. Otherwise, data was collected over first 10 hours.

Recent work has shown that twitching motility in *P. aeruginosa* is under the regulation of a separate signal-transduction pathway (Che cluster IV) known as the Chp system (Bertrand et al., 2010; Sampedro et al., 2014) (Figure 3b), but to date there is no evidence that this system is involved in chemotaxis. To examine the effects of the Chp system, we first recapitulated the motility phenotypes recently described using agar plates (Bertrand et al., 2010). Specifically, in-frame deletion mutants Δ*pilB,* Δ*chpA* and Δ*pilG* do not form the characteristic twitching rings at the plastic-agar

interface around colonies, while Δ*pilH* cells exhibit an intermediate phenotype by producing rings that are smaller than that of the wild-type (Extended Data Figure 4). However, observing the movement of individual cells in our microfluidic system reveals a very different pattern. We find that Δ*chpA* and Δ*pilG* cells, which were previously diagnosed as incapable of twitching (Bertrand et al., 2010) are in fact both highly motile (Figure 3a,c). Moreover, we find that Δ*pilH* cells, which show reduced twitching rings on agar plates (Extended Data Figure 4), actually move approximately 30 times faster than its wild-type (Figure 3a,c) and tend to orient themselves vertically on the surface (Figure 3d). More formally, the root mean-square displacement (RMSD), a combined measure of both movement speed and the persistence in movement direction (Gibiansky et al., 2010), of the wild-type and Δ*pilG* cells are nearly identical, but show strong differences with that from Δ*chpA* and Δ*pilH* (Figure 3c).

The Chp system then has strong effects on twitching motility in our assay but is it involved in chemotaxis? To answer this question, we focused upon the response regulator PilG, which controls pili extension (Bertrand et al., 2010), as the motility of Δ*pilG* is similar to the wild-type in our microfluidic assay (Figure 3a,c,d, Supplementary Video 3, 4). When exposed to DMSO the movement of wild-type cells is attenuated and this effect is stronger in Δ*pilG* cells (Extended Data Fig. 5). However, Δ*pilG* cells remain highly motile but, importantly, they lack the ability to bias their motility up the DMSO gradient (Figure 3e). This result suggests that the Chp system is not just involved in the biosynthesis of type IV pili but also in the transduction of chemotactic stimuli into directed movement. Accordingly, the inability of Δ*pilG* cells to migrate outwards in the traditional plate-based twitching assay (Extended Data Figure 4) likely results from a deficiency in chemotaxis rather than a deficiency in

motility. Our methods cannot yet assess whether Δ*pilH* cells can chemotax due to their extremely rapid movement and their upright orientation, which makes them tend to align their motility with the flow used to generate the gradient (Figure 3a) (Shen et al., 2012). Nevertheless, it seems likely that cells lacking PilH, the response regulator that controls pili retraction (Bertrand et al., 2010), also have impaired chemotaxis as they move rapidly but make smaller twitching rings than the WT in the agar assay (Extended Data Figure 4).

Chemotaxis in swimming *E. coli* cells is achieved by cells performing straight *runs* interspersed by sharp reorientations (*tumbles*), where tumbles are delayed when moving up a chemoattractant gradient (Berg, 2004; Berg and Brown, 1972). Do twitching bacteria use similar movement strategies in our experiments? While twitching motility gets its name from the jerky motion that cells exhibit over the timescale of minutes (Jin et al., 2011), we find that in chemical gradients cells can maintain a consistent direction for periods longer than an hour (Figure 4a). Moreover, these twitching 'runs' are interspersed by events where a cell reverses by stopping and then moving back in the opposite direction without turning. Even though the motility system is fundamentally different, therefore, these observations suggest that twitching chemotaxis may have some broad similarities to swimming cells. Twitching *P. aeruginosa* cells pull themselves along surfaces with pili that cluster at their poles (Skerker and Berg, 2001), which drives movement parallel to their long axis (Extended Data Figure 6) and allows rapid changes in direction if a cell changes the pole that it is pulling from. To follow this process, we developed an automated algorithm that detects when the cell's movement switches direction such that a cell's leading pole becomes its trailing pole. Importantly, we distinguish these active 'reversals' from changes in

direction that occur passively due to cell division (Figure 4a,b; Supplementary Videos 3,4; Supplementary Methods).

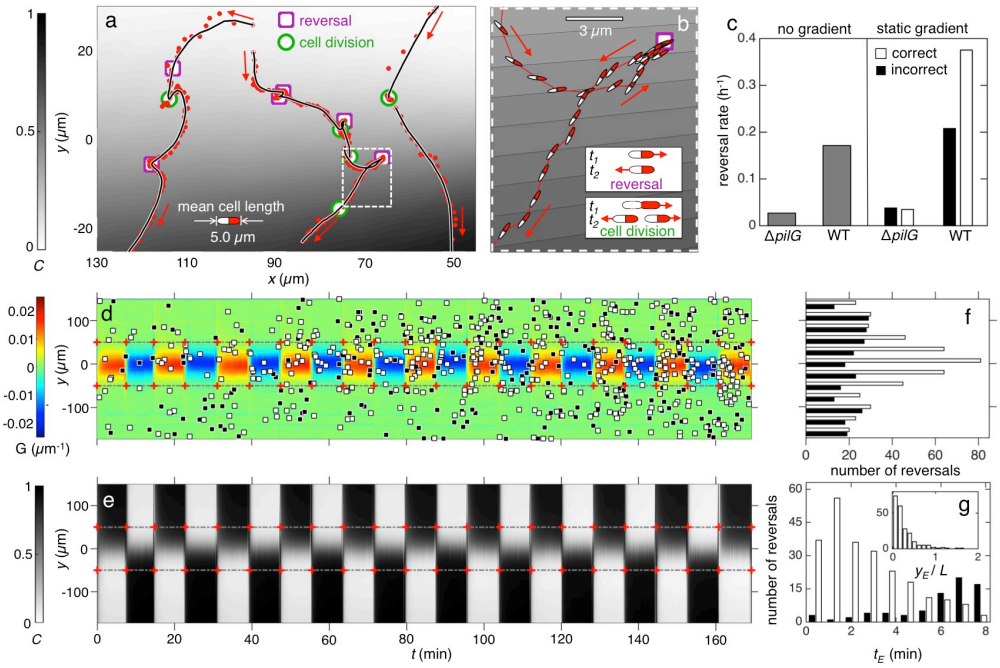

Figure 4: **Cells chemotax by reversing their motility when traveling away from the chemoattractant source.** (**a**) Cells navigate up DMSO gradients by actively performing 'reversals' (magenta squares), though sharp changes in direction can also occur passively during cell division (green circles). Red dots in **a** show positions of cell centroids at one-minute intervals; the black lines show smoothed trajectories, and the average cell length is shown for reference. (**b**) Magnified view of a reversal shows a cell whose movement begins to veer towards decreasing C. The cell quickly performs a reversal sending it back up the DMSO gradient. Ellipses (not drawn to scale) show cell orientation and position in two-minute intervals. Contours show modelled DMSO concentration in C_{max} / 30 increments where C_{max} = 350 mM (Supplementary Methods). (**c**) In both the absence and presence of a DMSO gradient Δ*pilG* actively reverse at a much smaller rate than WT cells. For experiments with a DMSO gradient, we calculated the frequency that cells moving towards smaller C reverse direction (labeled 'correct', white bars) and the frequency that cells moving toward larger C reverse direction (labeled 'incorrect', black bars). While the rate of incorrect reverses in the WT is similar to that in the absence of a gradient (grey bar), correct reversals occur more frequently, suggesting that reversals are deployed as a corrective strategy. (**d-g**). Using a custom microfluidic device (Extended Data Figure 8), we induced reversals by exposing cells to a DMSO gradient that changed direction every eight minutes. Owing to a large flow velocity, C and its gradient $G=1/C_{max}\,\partial C/\partial y$ were nearly constant along our field of view (Supplementary Methods), allowing us to average them along x and present their spatiotemporal variations using kymographs (**d**,**e**). Cell reversals were identified using an automated algorithm and classified as 'correct' (white squares, **d**) or 'incorrect' (black squares, **d**). Both types of reversals increased over time as cell division and attachment increased the number of cells on the surface (**d**). Counting the number of correct and incorrect reversals within equally spaced bins in y, reveals that correct reversals (white bars, **f**) peak along the middle of the device, while the number of incorrect reversals (black bars, **f**) occur more uniformly in y. The reaction

time, t_E, is the time elapsed from the most recent gradient change (red + symbols in **e**,**f**) to the time of a correct reversal. A histogram of t_E for cells in middle 100 μm of the device (dashed grey lines, **d**,**e**) shows that correct reversals peak ≈1 min after the gradient changes direction (**g**). Over this period cells travel a distance y_E in the y direction, which is much smaller than L, the length their bodies span in y (typically y_E/L <<1, **g inset**).

Both Δ*pilG* and wild-type cells were found to actively reverse their direction in both the presence and absence of DMSO gradients. However, Δ*pilG* cells, which do not show chemotaxis, reversed at a much lower rate than wild-type cells in both of these conditions suggesting that the reversals are indeed important for chemotaxis (Figure 4c). This was further supported by detailed analysis of wild-type cells. We find that cells reverse more when moving away from the source of a chemoattractant but keep their basal reversal rate when moving towards the source (Figure 4c). This observation is consistent with a 'pessimistic' chemotactic strategy (Armitage, 1997), and contrasts with the 'optimistic' strategy employed by swimming *E. coli* which chemotax by postponing tumbles when moving towards the chemoattractant source (Berg, 2004; Berg and Brown, 1972). We also find asymmetries in speed: wild-type cells move 25% faster when travelling towards the source as compared to away from it (Extended Data Figure 7). In contrast, Δ*pilG* cells moving towards and away from the chemoattractant source travel at approximately the same rate (Extended Data Figure 7). Taken together our data suggest that PilG is a response regulator that influences both reversal rate and speed of twitching cells in chemical gradients.

Swimming *P. aeruginosa* cells navigate chemical gradients by selectively turning their flagella in the opposite direction, which sharply changes their direction of movement (Porter et al., 2011). In contrast, our experiments suggest that biofilm bacteria climb chemical gradients by regulating when they switch directions by pulling themselves using pili attached to the previously trailing pole. To examine the dynamics

of this process, we experimentally triggered reversals using a purpose-built microfluidic device that allows us to continuously track cells as they respond to DMSO gradient that changes direction every eight minutes (Figure 4d-g; Extended Data Figures 8, 9 and 10). While direct observation suggests that twitching *P. aeruginosa* cells can reverse their movement in response to the alternating gradient (Supplementary Video 5), we quantified their response by categorizing all reversal events as 'correct' or 'incorrect'. Correct reversals occurred in cells moving away from the chemoattractant source and incorrect reversals occurred in cells moving towards the source (Figure 4d,e, Supplementary Video 6).

Correct reversals peak in the middle of the device where cells experience the strongest spatial chemoattractant gradients, whereas incorrect reversals occur more uniformly across the width of the device (Figure 4f). This observation is again consistent with a pessimistic chemotactic response and suggests that cells experiencing stronger concentration gradients are likely to deploy reversals when their motility is directed away from the source of a chemoattractant. In addition, we find that wild-type cells actively increase their speed after performing correct reversals but not after performing incorrect reversals (Extended Data Figure 9). Most striking though is that correct reversals in the middle of the device peak approximately one minute after the gradient changes direction (Figure 4g). This means that the majority of these cells can sense the gradient has changed direction and respond before moving 1/5 the length of their bodies (Figure 4g, inset). A corollary of this is that these cells experience a five-fold larger change in chemoattractant concentration across their length than they experience over time due to their movement relative to the gradient. Therefore, while attached cells may sense changes in concentration over time like swimming cells (Berg, 2004; Wadhams and Armitage, 2004), there is the intriguing possibility that

twitching cells instead directly measure spatial gradients across the length of their bodies.

Bacteria commonly live in biofilms where multiple strains and species meet and interact (Nadell et al., 2009). These cells strongly alter their environment by secreting a wide range of compounds and metabolizing others to create a diverse and changing set of chemical gradients (Stewart and Franklin, 2008). These gradients can be very steep, stable, and important for the fitness of cells that lie in different positions within a community (Kim et al., 2014). This suggests that single-cell chemotaxis within biofilms, like swimming chemotaxis (Adler, 1966), can carry significant evolutionary benefits. Moreover, the combination of steep chemical gradients and slow movement within biofilms means that cells have the potential to perform chemotaxis on much finer spatial scales than swimming cells. We find that twitching bacteria can respond within a fraction of their body length and actively position themselves in gradients that occur on a scale of tens of microns. Our work reveals the hidden potential for single cells to navigate chemical gradients by twitching chemotaxis. This directed movement may prove fundamental to both the biology of biofilms and how we manipulate them.

5. Bacterial chemotaxis towards antibiotics results in extreme phenotypic resistance

Summary	86
Introduction	87
Results	89
Discussion	103
Experimental Procedures	106

Summary

Antibiotic resistance poses a major threat to public health. While the vast majority of antibiotic research focuses on homogeneous cultures, bacteria commonly live in surfaced-attached communities where they are exposed to steep chemical gradients. Here we study the behavior of the pathogen *Pseudomonas aeruginosa* in spatial gradients of antibiotics by tracking thousands of individual cells as they colonize the surface in developing biofilms. Surprisingly, these experiments reveal that cells use twitching chemotaxis to move towards higher concentrations of antibiotics. While antibiotic gradients trigger sharp variations in cell density across the surface, our data suggest that chemotaxis is a direct response to antibiotics and not just driven by secondary *de novo* gradients in nutrients or secreted compounds. Moreover, within 20 hours, migrating cells reach and withstand antibiotic concentrations one thousand times higher than expected from their MIC (minimal inhibitory concentration). We find no evidence for genetic resistance as responding cells lose resistance when transferred back to a homogeneous distribution of antibiotics. Instead, physiological resistance appears key as chemotaxis towards antibiotics is prevented with chemical inhibition of

efflux pumps. We document here what seems a fundamentally new phenotype of bacteria that is likely critical for their survival and how they affect us.

Introduction

The ability of bacteria to resist antibiotic treatment is a growing public concern. While bacteria are commonly studied in shaking culture, a key component of their resistance to antibiotics comes from the ability to form surface-associated communities, often known as biofilms (Lopez et al., 2010). Compared to those in the planktonic state, cells within biofilms are often highly resistant to antibiotics and this occurs via a diversity of mechanisms, including reduced growth rate, hampered antibiotic diffusion, and stress responses (Ciofu and Tolker-Nielsen, 2011; Hoiby et al., 2010; Stewart, 2002; Stewart et al., 2015; Storz et al., 2011). While typically less appreciated, the sociobiology of biofilms is likely important to understand their antibiotic resistance as in nature biofilm bacteria typically occur at high density leading to intense ecological competition between different strains and species that often use an arsenal of antibiotics and other toxins against one another (Basler et al., 2013; Basler and Mekalanos, 2012; Fiegna and Velicer, 2005; Mitri and Foster, 2013; Nadell et al., 2009). Accordingly, there is then a clear evolutionary incentive to develop resistance mechanisms as a response to such ecological competition.

In addition to the ability of biofilms to confer resistance, sub-lethal concentrations of antibiotics also induce biofilm formation in a large and diverse set of species (Elliott et al., 2010; Haddadin et al., 2010; Hoffman et al., 2005; Kaplan, 2011; Kaplan et al., 2012; Kumar and Ting, 2013; Linares et al., 2006; Wang et al., 2010). The striking uniformity of the biofilm response to antibiotics across the bacterial phylogeny is suggestive of a common evolutionary pressure to detect the damage from

antibiotics and respond adaptively (Cornforth and Foster, 2013). While the responses of biofilms to antibiotics have been intensively studied, these phenotypes are typically assessed using single antibiotic concentrations. However, cells in biofilms commonly experience strong chemical gradients owing to attenuated diffusion and the high density of cells that actively consume and secrete compounds (Stewart, 2002; Stewart and Franklin, 2008; Stewart et al., 2015). Chemical gradients can be extremely important for the evolutionary fitness of cells (Kim et al., 2014) and there is growing evidence that they are important for understanding biofilm phenotypes. This includes the recent observation that biofilm cells can detect and respond to gradients of nutrients and other compounds by twitching chemotaxis (Oliveira et al., in review), or that antibiotic gradients drive biofilm formation itself (Oliveira et al., 2015).

The pathogen *Pseudomonas aeruginosa* is highly motile during biofilm formation and is able to navigate chemical gradients via twitching motility and the Chp chemosenory system (Oliveira et al., in review). Twitching motility is performed using pili, grappling hook-like appendices that are extended and then retracted to pull the attached cell along the surface. By governing both their speed and the frequency at which they reverse the direction of their motility, cells actively position themselves in favored locations within developing biofilms via twitching chemotaxis (Oliveira et al., in review). In addition, *P. aeruginosa* biofilms are known to be remarkably resilient to antibiotic treatment (Drenkard and Ausubel, 2002; Mah et al., 2003; Nickel et al., 1985; Stewart et al., 2015). Motivated by these observations we sought to understand how twitching bacteria move in antibiotic gradients. While chemotaxis in biofilms has only recently been documented, there is a large literature on swimming chemotaxis, which shows that cells will commonly move towards beneficial compounds and away from toxic compounds (Berg, 2004; Wadhams and Armitage, 2004). Therefore, we

hypothesized that motile biofilm cells that encounter antibiotic gradients would potentially be repelled and, thereby, better able to resist antibiotic attack. Surprisingly, our single cell assay revealed the opposite behavior. We find that rather than being repelled, twitching cells actively bias their motility towards increasing concentrations of antibiotics. While unexpected, this behavior brings with it an important outcome: as individual cells move along the gradient they acquire extreme levels of antibiotic resistance within a few hours.

Results

Biofilm bacteria move towards antibiotics via twitching chemotaxis. We used microfluidic devices and automated cell tracking to quantify the movement of *P. aeruginosa* cells as they are exposed to well-defined spatial gradients of antibiotics in developing biofilms (Figure 1). While research on biofilms and their antibiotic resistance mostly focus on the mature stages of these bacterial groups, here we focus on the early stages of biofilm formation so that we can isolate the behavior of individual cells and map this to the antibiotic concentrations they experience. However, surface motility is common throughout biofilm development (Klausen et al., 2003), including in mature stages where it has been linked to antibiotic resistance (Haagensen et al., 2007).

Our initial focus was on the antibiotic ciprofloxacin, which is widely used to treat *P. aeruginosa* infections but often leads to high levels of resistance (Breidenstein et al., 2008; Lister et al., 2009). We first determined the minimal inhibitory concentration (hereafter MIC) of our *P. aeruginosa* strain (PAO1) to ciprofloxacin in shaking cultures, which agrees with the published MIC for our strain (0.01 $\mu g\ ml^{-1}$ Figure S1).

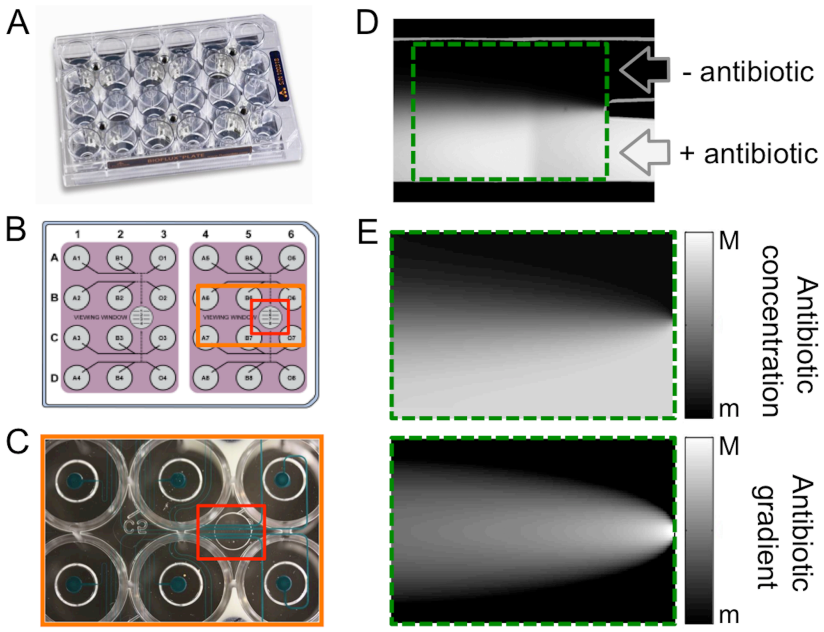

Figure 1. Microfluidic system that generates stable and well-defined chemical gradients via flow control. (**A**) Photograph of a 24 wells BioFlux plate (version 'Invasion'), which can be used to generate chemical gradients via pneumatic pressure. (**B**) Schematic diagram showing 8 independent channels connected by triplets of wells (two inlets and one outlet). Parallel flow streams from the two inlets mix in the main chamber and liquid flows out via the outlet. (**C**) Close-up of two microfluidic channels as viewed from beneath the plate. (**D**) Image of a double-inlet channel. In our setup, growth medium flows through both inlets but one also contains the test antibiotic, which generates a gradient of antibiotic in the main chamber. A fluorescent dye has been added in this particular experiment (white) to illustrate the gradient created. Arrows denote the direction of flow. (**E**) Measuring the antibiotic gradient. From the normalized concentration of fluorescein taken with confocal microscopy, we simulate the distribution of antibiotic using an analytical model of molecular diffusion, which is then differentiated to obtain the normalized antibiotic gradient (Experimental Procedures). 'M' and 'm' denote max and min, respectively. Photographs (A-C) are courtesy of Fluxion Biosciences.

We then exposed surface-attached cells to an antibiotic gradient where the maximum concentration was ten times higher than the MIC of the strain (Figure 2 A,B, Experimental Procedures). Surprisingly, after ten hours of unbiased movement, we observe that twitching cells bias their movement towards increasing concentrations of ciprofloxacin (Figure 2 B,C,D, Movie 1). The chemotactic bias, β, defined as ratio of number of cells moving up the gradient by the number of cells moving down the gradient, peaks after approximately 20 hours, and then decays as the surface becomes

crowded with cells (Movie 1) and tracking becomes difficult (Experimental Procedures). In contrast, the movement of cells in a control without antibiotic is not biased overtime ($\beta \approx 1$, Figure 2C). Importantly, we find that this response is not limited to ciprofloxacin: cells bias their movement up gradients of the antibiotics rifampicin, streptomycin and mitomycin (Figure 2D), which belong to different classes and have different modes of action. In each of these experiments, cells are observed to proliferate at concentrations that are lethal in homogeneous conditions.

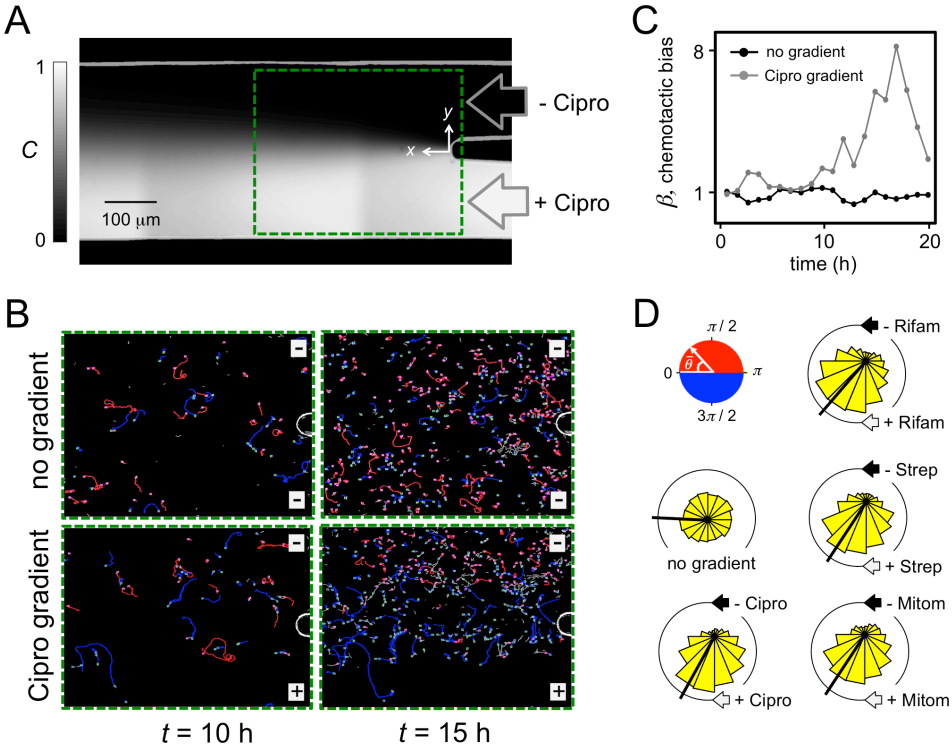

Figure 2. Twitching *P. aeruginosa* cells bias their motility towards increasing concentrations of antibiotics. (**A**) A two-inlet microfluidic device generates a stable chemical gradient of ciprofloxacin via molecular diffusion. Growth medium is continuously injected through both inlets, whilst ciprofloxacin ('Cipro') at a concentration of C_{max} = 1 μg ml^{-1}, corresponding to 10 times the minimum inhibitory concentration in shaken culture (MIC, Figure S1), is injected only through one of the inlets. Here $C = C'/ C_{max}$ where C' is the local concentration of antibiotic which was quantified using fluorescein in a separate cell-free experiment (Experimental Procedures). (**B**) Distribution of cells (white spots) and respective trajectories after 10 and 15 hours of incubation in gradients of ciprofloxacin (bottom) and in control channels (top). Trajectories with net movement toward larger C (i.e. in $-y$) are shown in blue and those with net movement towards smaller C (i.e. in $+y$) are shown in red. Use scale

bar in panel A. (**C**) Time series of the chemotactic bias, β, defined as the number of cells that move in $-y$ divided by the number moving in $+y$, peaks at $t \approx 18$ h in ciprofloxacin gradients. (**D**) Probability density functions of the angle, θ, from each trajectory's origin to final position over the last ten hours of the experiment. Black lines denote the mean of each distribution. 'Rifam' = rifampicin; 'Strep' = streptomycin; 'Mitom' = Mitomycin C.

We find then that twitching cells in antibiotic gradients perform chemotaxis: the ability of directing movement towards, or away from, chemicals (Adler, 1966). Does this biased movement have the same genetic basis as twitching chemotaxis recently reported in DMSO and succinate gradients (Oliveira et al., in review)? From our previous work, we know that the basis for movement in our assay is twitching via type IV pili. However, the ability to bias movement could be under the regulation of a different chemosensory system. We therefore tested if cells lacking the key response regulator PilG, which is homologous to CheY of *Escherichia coli* (Bertrand et al., 2010), could climb antibiotic gradients. Consistent with our earlier report of twitching chemotaxis (Oliveira et al., in review), cells lacking PilG do not bias their movement towards increasing concentrations of ciprofloxacin (Figure 3), despite being highly motile (Figure 3) and having an identical MIC as wild-type cells (Figure S2). Moreover, when we co-culture the mutant with wild-type bacteria in the device, the wild-type cells dominate in the regions of high antibiotic concentration (Figure S3), which is consistent with their differential motility in antibiotic gradients (movie 2).

Nutrient gradients do not explain antibiotic taxis. We find that cells only begin to bias their motility up antibiotic gradients after an initial period of nearly random motility (Figure 2). This delayed response introduces an important complication: there is time for secondary gradients in nutrients and other compounds to build up in the device, which might explain chemotaxis towards antibiotics. In particular, lower antibiotic concentrations tend to allow faster growth while higher antibiotic concentrations

typically promote cell detachment in the first hours of experiment (Movie 1). The result is that the density of cells tends to correlate negatively with the antibiotic concentration (Figures 2,3,4, Movie 1), which has the potential to create both a positive gradient in nutrient concentration and a negative gradient in the diverse set of compounds secreted and released by growing cells.

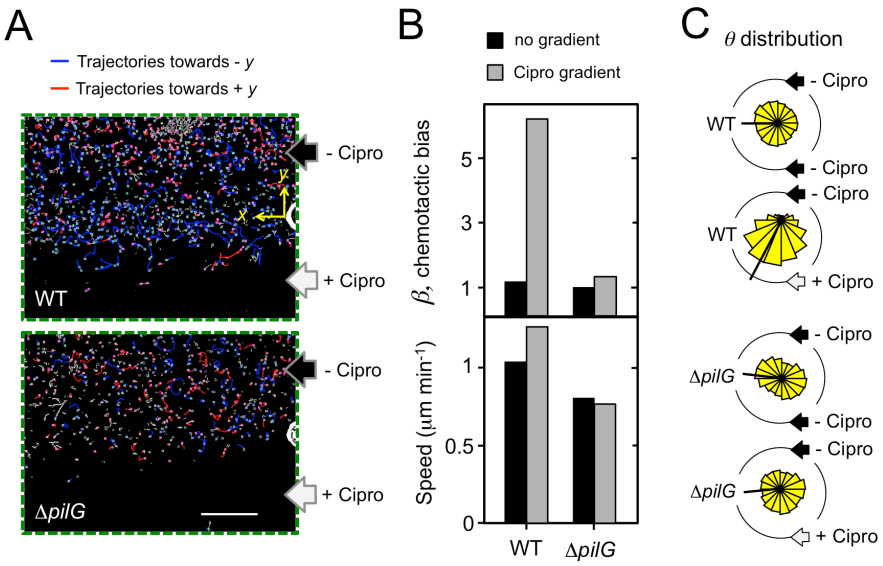

Figure 3. Chemotaxis towards antibiotics is mediated by PilG, a key response regulator of the Chp chemosensory system. (**A**) Distribution of WT cells (top) and Δ*pilG* (bottom), along with the respective trajectories after 20 hours of incubation in ciprofloxacin ('Cipro') gradients with C_{max} = 1 μg ml^{-1}, a concentration 10 times higher than the MIC of the strains (Figure S2). Trajectories with net movement toward larger concentrations of ciprofloxacin (i.e. in –*y*) are shown in blue and those with net movement towards smaller concentrations (i.e. in +*y*) are shown in red. For reference, scale bar is 100 μm as in Figure 1. (**B**) Mean chemotactic bias (top) and mean cell speed (bottom), and (**C**) probability density functions of the angle, θ, from each trajectory's origin to final position, over the last ten hours of the experiments, which run for approximately 20 hours in total. Black lines denote the mean of each distribution. The small black and white arrows in A and C denote the direction of flow.

We focused first on whether emergent nutrient gradients could be responsible for the observed biased movement. Previous work has shown that *P. aeruginosa* exhibit chemotaxis in gradients of succinate (Oliveira et al., in review) and we also find here that cells move up a gradient of tryptone, the growth media used in this study (Figure

4B), which is consistent with published work showing that tryptone drives chemotaxis in swimming *P. aeruginosa* cells (Ferrandez et al., 2002).

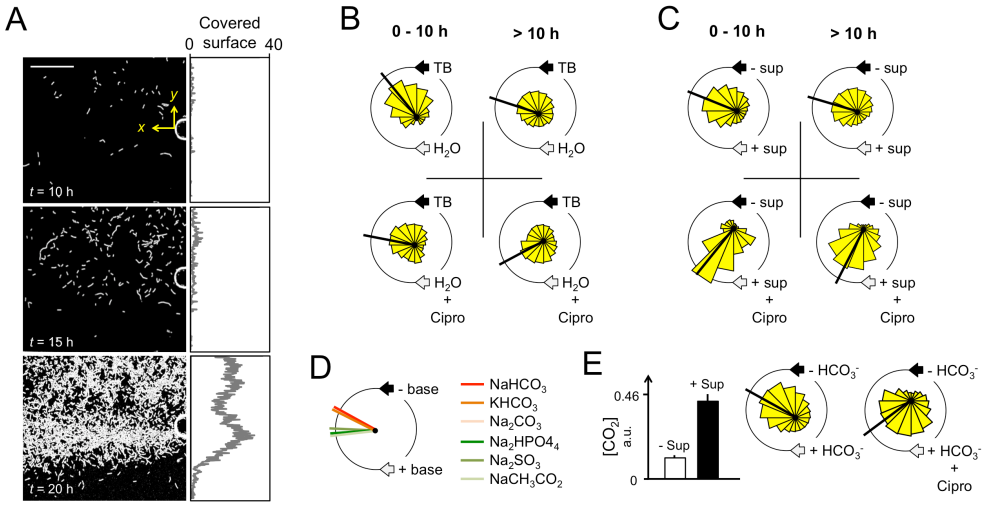

Figure 4. Putative gradients in nutrients or cell secretions do not explain chemotaxis towards antibiotics. (**A**) Development of a gradient in cell density over time in the microfluidic device. Plots show % surface coverage at each horizontal position. The cells (white spots) that persist where antibiotic concentrations are small consume nutrients and secrete compounds that could potentially create secondary, *de novo* gradients that drive cell movement towards antibiotics. Scale bar is 100 μm. (**B**) *P. aeruginosa* chemotax towards increasing concentrations of tryptone broth (TB) as shown by the probability density functions of the angle, θ, of cellular trajectories, where black lines denote the mean of each distribution. The small black and white arrows denote the direction of flow. However, we find that twitching cells move towards increasing concentrations of ciprofloxacin ('Cipro'), even when this means moving away from high nutrient concentration. (**C**) *P. aeruginosa* is repelled by their own stationary-phase cell-free supernatant ('Sup'). However, cells move towards increasing concentrations of ciprofloxacin even when this antibiotic is mixed with cell-free supernatant that alone causes repulsion. (**D**) General pH taxis does not explain the repulsion from cell-free-supernatant. Only weak bases associated with the bicarbonate system drive repulsion as given by the mean θ elicited by each tested chemical (colored lines). Specifically, we considered sodium bicarbonate, potassium bicarbonate, sodium carbonate, sodium phosphate dibasic, sodium sulfite and sodium acetate. In these experiments we injected each base at a concentration of C_{max} = 40 mM, except for sodium carbonate (C_{max} = 10 mM) as 40 mM was toxic and led to cell detachment and reduced motility at high concentrations. (**E**) Stationary-phase cell-free supernatant of PAO1 *P. aeruginosa* ('+ Sup') contains larger concentrations of CO_2/HCO_3^- when compared to fresh growth medium ('- Sup') as predicted from core metabolism. $p < 0.05$ in a *t* test (n = 3). But again, twitching cells move towards increasing concentrations of ciprofloxacin even if by doing so they experience increasing concentrations of bicarbonate as given by the probability density functions of θ (direction of cell movement). Rose plots use the last ten hours of experiment in each condition until the surface gets very crowded with cells, which prevents further analysis of single-cell movement.

To test whether biased movement observed in our experiments with antibiotics could be solely driven by *de novo* gradients in tryptone, we created opposing gradients of tryptone and ciprofloxacin in our microfluidic device. Importantly, our design simulated the strongest possible nutrient gradient in our previous experiments by injecting full strength tryptone through one inlet of the device and ciprofloxacin in water through the other inlet. If cells in our previous experiments are simply moving in response to nutrient gradients, we expect that cells would move away from the antibiotic source. While cells initially move in the direction of increased tryptone, after 10 hours cells exhibit biased movement in the opposite direction, towards increasing concentrations of ciprofloxacin (Figure 4B). Chemotaxis towards nutrients, therefore, is not sufficient to explain the observed movement towards antibiotics (Figures 2,3,4).

Cells move away from cell-free supernatant and bicarbonate. We next explored the possibility that biased movement in antibiotic gradients could be explained by cell secretions which might trigger movement away from regions of higher cell density via negative chemotaxis. To this end, we studied the behavior of twitching cells in gradients of cell-free supernatant, which was obtained from bacteria cultured in the absence of antibiotics (Experimental Procedures, as in Oliveira et al., 2015).

Consistent with the importance of repulsion from areas of high cell density, we find that this supernatant drives negative chemotaxis in twitching cells (Figure 4C). What is driving the repulsion from the cell-free supernatant? We find that the supernatant is mildly alkaline (pH ~ 8), which is consistent with previous observations of *P. aeruginosa* growing in rich medium (Heurlier et al., 2005). This raises the possibility that pH taxis, which is well known in swimming bacteria (Schreiber et al., 2004), is the basis for the observed repulsion. However, we find that the response to

supernatant is not a general response to pH: not all tested bases stimulate repulsion, only weak bases associated with the carbonate system drive negative chemotaxis in our experiments (Figure 4D). Cells could be instead responding to elements of the carbonate system, namely carbon dioxide or the solution-associated ions such as bicarbonate. Repulsion from carbon dioxide has been observed in multiple organisms, from swimming bacteria (Berg, 2004) to worms (Hallem and Sternberg, 2008) and insects (Suh et al., 2004), and it makes sense ecologically as a general cue of overcrowding that drives dispersal, namely in bacterial groups.

As expected from core metabolism, cell-free supernatant from bacterial cultures was found to contain higher concentrations of members of the carbonate system when compared to fresh growth medium (Figures 4E, S4). But is this enough to cause twitching chemotaxis in our developing biofilms? When an equivalent concentration of bicarbonate was injected through one of the inlets of our microfluidic system, we observed a repulsion of twitching bacteria (Figure 4E), which is comparable to that observed with the cell-free supernatant. The supernatant contains a diversity of compounds and we cannot exclude the possibility that additional compounds may drive repulsion or attraction. Nevertheless, our results suggest that bicarbonate plays an important role in how supernatant drives the repulsion of twitching cells.

Movement away from high cell density does not fully explain chemotaxis towards antibiotics. We have observed that twitching cells move away from cell-free supernatant and that a major component of this response is likely to be due to repulsion from members of the carbonate system. However, does this repulsion, which is expected to drive movement away from areas of high cell density, also explain the observed movement towards antibiotics? *A priori*, this does not seem likely as the

movement towards antibiotics is observed when there are relatively few cells in the microfluidic device (Figures 2,3,4). Moreover, this movement towards ciprofloxacin still occurs, if anything at amplified levels, when we combine the antibiotics with cell-free supernatant (Figure 4C, Experimental Procedures), or bicarbonate at the experimentally measured levels present in supernatant (Figures 4E,S4). These results then suggest that chemotaxis towards antibiotics dominates any potential negative chemotaxis away from cell secretions that emerge overtime in developing biofilms.

We performed two additional experiments to evaluate the potential for cells to move towards antibiotics independently of the effects of the gradient in cell density. Firstly, we reasoned that if changes in cell density across the device are driving the response, we should be able to increase the response if we increase the gradient in cell density. We, therefore, compared the response to antibiotics starting with two initial cell densities where the higher density created a stronger gradient in cell density across the device (Figure 5A). This revealed that, if anything, stronger gradients in cell density are associated with decreased chemotactic bias, which again suggests that members of the bicarbonate system - or another secretion linked to cell density - are not the dominant source of taxis towards antibiotics.

Secondly, we exposed bacteria to ciprofloxacin gradients as in our standard assay for 15 hours when a cell gradient is established (Figure 4A). Then we changed the ciprofloxacin-containing inlet with either: (i) new ciprofloxacin (control) or (ii) growth media without antibiotic. This change has a quick and strong effect: we see a clear drop in the chemotactic bias when we remove the antibiotic (Figure 5B). While nutrients, bicarbonate and other factors may influence the movement we observe, therefore, our data suggest that cells are actively responding to the antibiotic.

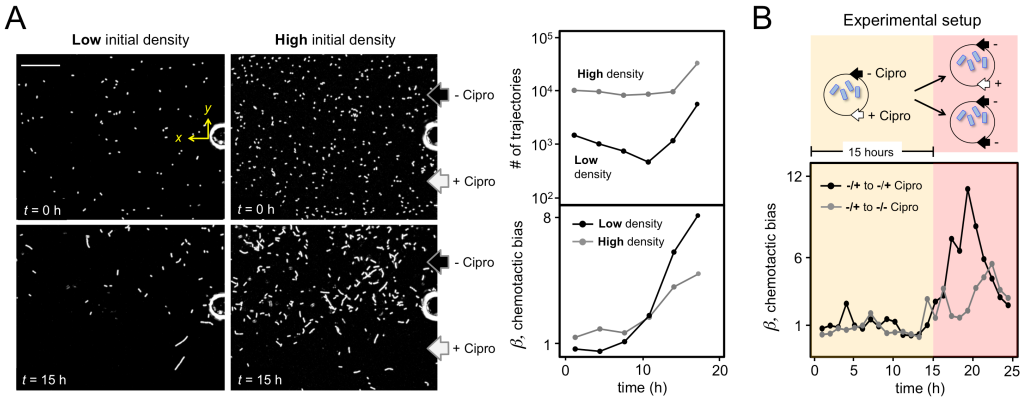

Figure 5. Movement towards antibiotics results from antibiotic action. (**A**) Starting experiments with high cell density does not drive a stronger or faster chemotaxis in antibiotic gradients. Figures show cell density at t = 0 h and t = 15 h, confirming that in the treatment 'High initial density' one finds more attached cells in the device (white spots), which is consistent with the high number of cells being tracked overtime (top-right plot, in log scale). However, this increasing number of cells in the device does not cause an equivalent increase in the chemotactic bias, β (bottom-right plot). If anything β is smaller after 10 hours, which is consistent with cells being repelled by each other as we show with cell-free supernatant. The black and white arrows on the images denote the direction of flow. Scale bar is 100 μm. (**B**) Removing ciprofloxacin after 15 hours of experiment reduces the chemotactic bias. Here we started two parallel experiments where we flowed C_{max} = 1 μg ml^{-1} of ciprofloxacin ('Cipro') for the first 15 hours. After this time point we added new media to each well: in the control experiment we generated identical antibiotic gradient by injecting 1 μg ml^{-1} of ciprofloxacin through one of the inlets as before (black line), while in the other experiment we injected antibiotic-free growth medium (TB) in both inlet wells (grey line). The consequence of removing the antibiotic from the system after 15 hours is clear: we find reduced chemotactic bias when compared to the antibiotic-containing experiment. The small arrows in the guiding diagram denote the direction of flow, while the blue objects represent moving cells.

Chemotaxis occurs towards cell-free media of competing genotypes. Does the observed migration towards clinical antibiotics have its origins in the natural ecology of *P. aeruginosa*? We recently found that the widely reported induction of biofilm formation by clinical antibiotics can be recapitulated in *P. aeruginosa* using cell-free supernatant isolated from strong competitors (Oliveira et al., 2015). However, this effect is only observed when the supernatant is toxic to the focal strain, which is consistent with the hypothesis of competition sensing: an evolved ability to detect and respond to harmful competing strains and their antibiotic arsenal (Cornforth and

Foster, 2013). Accordingly, in the presence of clinical antibiotics bacteria misfire and respond as if the attack is coming from competitors (Oliveira et al., 2015).

We therefore asked whether cells respond to a gradient of cell-free supernatant isolated from a different *P. aeruginosa* strain will elicit similar chemotaxis to that observed with clinical antibiotics. Consistent with the earlier results on biofilm formation (Oliveira et al., 2015), we find that there is a comparable chemotactic response to clinical antibiotics, but that this occurs only when the cell-free supernatant is toxic to the test strain (Figure 6 A,B). More generally, these data also suggest that there is a link between cell damage and taxis towards antibiotics. To confirm this prediction we studied the chemotactic behavior of a streptomycin resistant strain of *P. aeruginosa* in antibiotic gradients. This strain carries a plasmid that codes for an aminoglycoside-3"-adenylyltransferase, which inactivates streptomycin. Importantly, streptomycin resistant cells fail to migrate in our streptomycin assay but retain the ability to migrate towards ciprofloxacin to which they are not resistant (Figure 6 C,D).

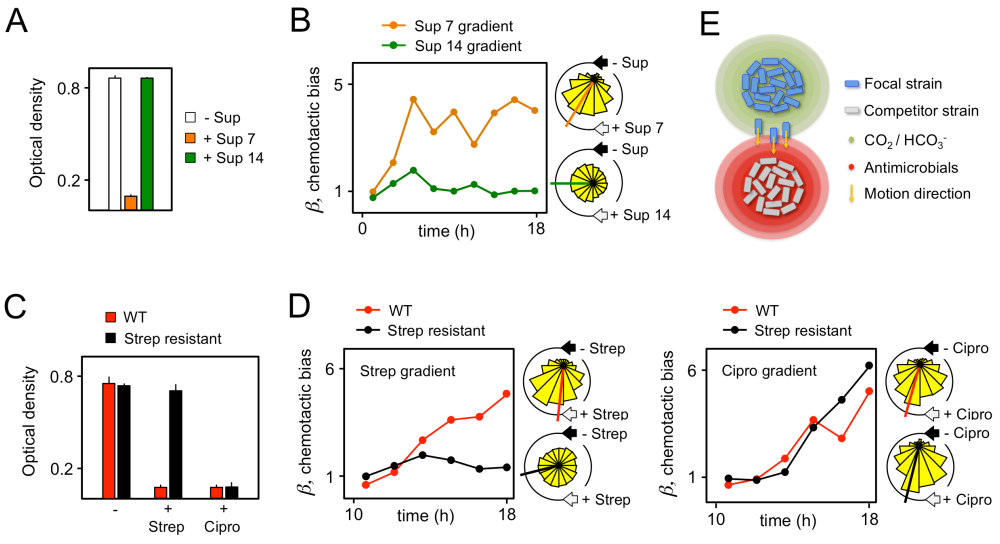

Figure 6. Twitching cells display chemotaxis towards compounds that induce damage, suggesting this response evolved to facilitate attacks on toxin-producing competitors. (**A-B**) show optical density of shaking cultures after 24 hours (**A**), time series of chemotactic bias

and probability density functions of cellular orientation during taxis (**B**) of PAO1 cells experiencing cell-free supernatant from competitor strain 7 or from competitor strain 14 (PA14). Only the supernatant that inhibits growth triggers chemotaxis towards it. The probability density functions of θ for each case were based on the first 18 hours, as we show for the chemotactic bias, β. (**C**) Optical density of shaking cultures after 24 hours of wild-type PAO1 and a strain carrying an aminoglycoside-3''-adenylyltransferase, which inactivates streptomycin, growing in the absence of antibiotics ('-'), in the presence of 8 $\mu g\,ml^{-1}$ of streptomycin ('+ Strep') or in the presence of 1 $\mu g\,ml^{-1}$ of ciprofloxacin ('+ Cipro'). Error bars in A and C are SE of mean, from eight independent replicates. (**D**) Time series of chemotactic bias and probability density functions of θ, direction of cell movement, where C_{max} = 8 $\mu g\,ml^{-1}$ for streptomycin gradients and C_{max} = 1 $\mu g\,ml^{-1}$ for ciprofloxacin gradients. The chemotactic bias remained $\approx$1 in all treatments for t < 10 h, and thus only t >10 h is shown. The distributions of θ are based on t from 10 h to 18 h as it is shown for β. (**E**) Ecological model for chemotaxis towards antibiotics. Bacteria at the edge of a developing biofilm use chemotaxis to spread out. CO_2/HCO_3^- may work as cues that inform on population density acting as repellents. Antibiotics or other toxic compounds ('antimicrobials') may work as cues that inform on the presence of competing genotypes and stimulate a counter-attack via directed motility towards the antimicrobial-producing source.

Taken in whole, our results then suggest a model where cells move away from their own genotype due negative chemotaxis driven by CO_2 directly or carbonate-associated compounds such as bicarbonate, and move towards harmful competing genotypes as a response to antibiosis. While moving away from CO_2 has a clear ecological rationale, it correlates positively with cell density and thus informs on cellular crowding, it is possible that the movement towards antibiotics is a maladaptive response driven by their adverse effects on cells. Nevertheless, considered the ecological context of warring genotypes within a biofilm (Cornforth and Foster, 2013; Nadell et al., 2009), the movement towards antibiotics may also be part of a general strategy to attack and invade the territory of neighboring genotypes that present a threat (Figure 6E). Such aggressive strategies have a precedent in the animal world, particularly in the social insects well known for their territoriality behaviors, where workers will actively seek out and attack neighboring colonies and other harmful species (Holldobler, 1979).

Antibiotic taxis is associated with extreme tolerance to antibiotics. Our data shows that migrating bacteria can invade and grow in regions with several times the antibiotic concentration that they can tolerate in the absence of gradients. We next probed the limits of this ability by testing whether cells could also climb gradients where the concentration of antibiotics injected are 100 and 1000 times the one they can resist in shaking culture (Figure S1). Despite the extreme concentrations, we see that cells still navigate up these antibiotic gradients where they remain highly motile and actively dividing (Figure 7A, Movie 3). Moreover, propidium iodide staining shows that most of these cells have intact membranes (Figure 7B) and addition of a the commonly used redox dye CTC (5-cyano-2,3-ditolyl tetrazolim chloride) shows, as expected, that migrating cells are metabolically active (Figure S5).

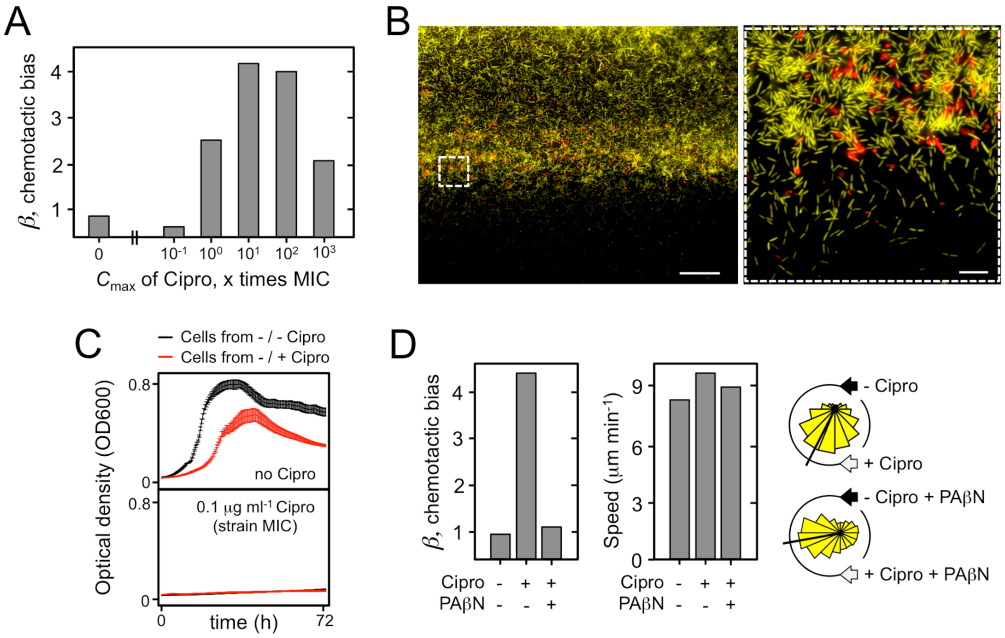

Figure 7. Chemotaxis towards antibiotics is associated with the development of extreme phenotypic resistance. (**A**) Mean chemotactic bias (from t = 10 h to t = 20 h) for increasing C_{max} of ciprofloxacin ('Cipro') injected in dual-inlet microfluidics (here shown as multiples of MIC). *P. aeruginosa* move up ciprofloxacin gradients even when C_{max} = 1000 times the MIC of the strain. (**B**) Propidium iodide staining (red), reveals that only a few (*yfp*-labeled) cells at ~100 μg ml^{-1} have compromised membranes after 24 hours into the experiment. Scale bar on

the left is 50 μm and on the right (zoom in) is 10 μm. (**C**) Cells from channels with C_{max} = 100 μg ml^{-1} of ciprofloxacin do not have increased MIC in well-mixed cultures. After removing cells growing in microfluidic devices we grew them in shaking culture, with and without ciprofloxacin (Experiment procedures), and find that the resistance of cells growing in antibiotic gradients is short-lived. We plot means of eight replicates with respective SE error bars taken every 30 min. (**D**) Effect of the efflux pump inhibitor PAβN on the chemotactic bias and the orientation of cell trajectories in ciprofloxacin gradients. We show the mean chemotactic bias, velocity magnitude (cell speed, here shown as multiples of 0.1 μm ml^{-1}) and probability density functions of θ, over the last ten hours of each experiment. Black lines denote means of each θ distribution, and small arrows denote the direction of flow. C_{max} of ciprofloxacin injected is 10 μg ml^{-1}. '+' ('–') denotes presence (absence) of ciprofloxacin or PAβN. PAβN drastically reduces chemotaxis towards ciprofloxacin while marginally affecting the speed of moving bacteria.

How do the cells achieve such extreme levels of antibiotic resistance? One possibility is genetic resistance, which has been shown to rapidly evolve when swimming bacteria are exposed to antibiotic gradients (Zhang et al., 2011). However, our experiments involve much lower population sizes, and we also observe that a large proportion of the population is able to migrate towards potentially lethal doses of antibiotics and survive (Figures 2, 3, 4, 5, 7, Movies 1, 2, 3). Given that typical mutation rates are extremely low (Drake et al., 1998), it is unlikely that genetic changes could explain the emergence of resistance in our system. However, to test for genetic resistance we allowed *P. aeruginosa* to respond to a gradient with maximum concentration of 1000 times their MIC, and then collected cells from the device after 24 hours (Experimental Procedures). In parallel, we also collected cells from an experiment without antibiotics, which worked as a control. We then grew these collected cells in shaking culture with and without antibiotics. Our data show that cells do not grow at this strain's previously measured MIC (Figures 7C, S1), suggesting that widespread evolution of genetic resistance is not responsible for the observed tolerance to antibiotics as this is short-lived. In comparison, both treatments yielded cells that grew in the absence of antibiotics (Figure 7C).

Our data suggest that the migrating cells achieve a temporary tolerance to antibiotic stress. Such 'adaptive' resistance is commonly mediated by the regulation of porins and efflux pumps, which either limit the transport of antibiotics into the cell or actively pump them out (Fernandez and Hancock, 2012). A key feature of adaptive resistance is that it can be rapidly lost if conditions change as we find with our short-lived tolerance (Figure 7C). In addition, adaptive resistance is most easily achieved when cells are subjected to gradual increases in antibiotic concentration over time (Motta et al., 2015). This leads to a model where the migrating cells in our experiments slowly and systematically modulate their adaptive resistance mechanisms as they move up the antibiotic gradient. To evaluate this model, we exposed cells to phenylalanine-arginine β-naphthylamide, PAβN, a well-studied and broad-spectrum efflux pump inhibitor (Renau et al., 1999). While twitching cells remain highly motile in the presence of PAβN, this inhibitor prevents cells from migrating towards increasing concentrations of the antibiotic (Figure 7D). Importantly, this pump inhibitor does not inhibit the ability of cells to respond to other chemoeffectors such as cell-free supernatant from the responder strain and bicarbonate (Figure S6). These results are again consistent with chemotaxis caused by antibiotic action rather than by secondary gradients resulting from cell secretions.

In sum, our data suggest that a spatial gradient of antibiotics allows twitching bacteria to experience gradual increases in antibiotic concentration and adjust their physiology accordingly, which results in extremely high antibiotic tolerance.

Discussion

A large body of work has dissected how swimming bacteria are able to move towards chemicals, particularly nutrients (Berg, 2004; Wadhams and Armitage, 2004). In

addition, recent work has revealed that surface-attached bacteria are also capable of directed movement towards nutrients and other compounds via twitching chemotaxis (Oliveira et al., in review). Motivated by this, and the fact that swimming bacteria use chemotaxis to avoid toxic compounds (Ohga et al., 1993; Tso and Adler, 1974), we studied how twitching cells respond to antibiotics in developing biofilms with the expectation that cells would be repelled by them, and that could contribute to the well-known antibiotic resistance of *P. aruginosa* biofilms (Drenkard and Ausubel, 2002; Mah et al., 2003; Nickel et al., 1985; Stewart et al., 2015). However, studying the behavior of single cells in defined antibiotic gradients shows that the opposite occurs. We find that *P. aeruginosa* actively move towards high concentrations of antibiotics via twitching chemotaxis, resulting in extreme resistance within a few hours.

The rapid emergence of resistance has recently been documented in swimming *E. coli* in a complex microfluidic device containing 1200 interconnected wells, which created spatial gradients of antibiotics (Zhang et al., 2011). While chemotaxis towards antibiotics was not shown, resistance did emerge on comparable timescales and at comparable levels to that observed here. However, resistance was attributed to a series of mutations arising at the front of the very large population sizes contained in the device. In this respect, our findings are quite different as we observe resistance arising in small migrating populations without any evidence for genetic resistance. Interestingly, the authors note that the critical locations of the device, which they call the 'Goldilocks environments', are those where the antibiotic gradient is the sharpest (Zhang et al., 2011). Our system based on two-inlet microfluidic channels represents a simplified version of those conditions with the advantage of allowing the analysis of single-cell behavior together with fine characterization of the antibiotic gradients that

responding individuals experience. Perhaps there too chemotaxis towards antibiotics is important for the emergence of resistance as we find in our system (Figure S3).

More generally, an association between motility and antibiotic resistance has been reported in multiple and diverse species, including *P. aeruginosa* (Butler et al., 2010; Hol et al., 2015; Kim et al., 2003; Lai et al., 2009; Overhage et al., 2008). However, the level of resistance observed in these studies was moderate relative to that observed here. Moreover, resistance was not linked to chemotaxis but rather to a general shift in physiological state upon swarming (Kim et al., 2003) or, simply, high cell density (Butler et al., 2010; Hol et al., 2015). By contrast, we observe that single cells can migrate up antibiotic gradients at low cell density. Importantly, when co-cultured wild-type cells with a chemotaxis null mutant, the latter achieves much lower cell density in the regions of high antibiotic concentration despite having the same MIC in homogeneous conditions (Figures S2,S3). While swarming cells may well have intrinsically high resistance, our data suggest that the chemotaxis towards antibiotics we find here allows cells to more rapidly and effectively invade regions of high antibiotics concentration (Figure S3).

Cleary there are many compounds that can affect chemotaxis in our experiments, including nutrients and cell secretions, but our data suggest that cells are actively responding to antibiotics (Figures 4, 5). Moreover, it appears important that the antibiotics are actually damaging because resistant strains do not show appreciable response (Figure 6). What then could be the mechanism underlying this chemotactic response to damaging antibiotics? Recent work has suggested that bacteria may use stress responses not only to deal with stress, but also as a means to detect antibiotic attack from other strains (Cornforth and Foster, 2013). A particularly promising candidate for damage detection is oxidative stress, which can be generated by cell

damaging agents from competing microbes (Dong et al., 2015), and also by multiple clinical antibiotics (Dwyer et al., 2014; Foti et al., 2012; Kohanski et al., 2007; Kohanski et al., 2008; Lobritz et al., 2015). However, it remains unclear, if and how, such general stress responses could lead to directed movement in a manner at all comparable to the canonical chemotaxis seen in swimming bacteria.

Our observations are also intriguing at the evolutionary level. Why would bacteria evolve to move towards antibiotics at all? One model is that movement away from compounds like carbon dioxide or bicarbonate and towards antibiotics will enable a strain to seek out and populate a competing strain's territory (Figure 6E). Given that antibiotic stress often leads to a kickback response via antibiotic production in targeted bacteria (Cornforth and Foster, 2013), it is also possible that the chemotaxis towards antibiotics we document here is an attack response if moving cells are indeed producing their own warfare arsenal as they move along. Whatever the mechanistic and evolutionary basis of this phenotype, it is clear that migration towards antibiotics - *antibiotic taxis* - is associated with incredibly high levels of resistance in the pathogen *P. aeruginosa*. The ability to control movement, therefore, may be fundamental to antibiotic resistance in bacteria, a theme that is also emerging in cancer treatment where drug gradients and cell motility within these gradients drive resistance to chemotherapy (Lambert et al., 2011; Wu et al., 2013).

Experimental Procedures

Strains, Media and Culture Conditions. The main strain used throughout this work is a wild-type *P. aeruginosa* PAO1 from the Kolter collection, ZK2019 (O'Toole and Kolter, 1998). The *P. aeruginosa* strains used as competing strains of PAO1, the supernatant of which we study in Figure 6, are also from the Kolter collection and have

been published elsewhere (Oliveira et al., 2015). They include the natural isolate strain 7 (ZK3098), and the clinical isolate PA14 (ZK2466). To specifically study the functional role of the response regulator PilG on twitching chemotaxis towards antibiotics we used a strain with an in-frame deletion mutation in *pilG*, which has been published and described previously (Bertrand et al., 2010). This strain is used in Figures 3 (main text), S2 and S3 (supplemental information) where it is compared with the respective wild-type. The streptomycin resistant strain, which bears the plasmid pRms149 coding an aminoglycoside-3"-adenylyltransferase, was a gift from the MacLean lab.

All strains were grown overnight in LB (37°C, 250 rpm) from frozen stocks and sub-cultured on the day of the experiment to obtain cells in exponential phase. These were then diluted to an optical density of 0.25 (at 600 nm) in the growth medium used in our microfluidic-based experiments, tryptone broth (TB, 10 g Bacto tryptone per 1 L water). To find the minimal concentration of each antibiotic that inhibits growth in homogeneous cultures we used the same growth medium but supplemented with the appropriate concentration of antibiotic (from Sigma Chemical Company). Exponential phase cells from overnight cultures were inoculated in flat-bottomed 96-well plates (Nunc) in 200 μl of TB at the starting optical density (at 600 nm) of 0.05, and allowed to grow for 20 hours at 22ºC, shaking, inside a plate reader (Tecan, Infinite M200 Pro). Readings were taken every 30 minutes. MIC was defined as the minimum concentration of antibiotic that prevents detectable growth after 20 hours. We confirmed that these concentrations prevent cell growth within microfluidic channels where cells experience a single and constant antibiotic concentration (below).

Study of cell secretions. To test the effect of self-produced diffusible substances on twitching chemotaxis we followed previously published protocol (Oliveira et al., 2015). Exponential phase cells were inoculated in 6-well plates in 4 ml of tryptone broth (TB) at starting optical density of 0.25 (at 600 nm). Given the high innoculum size to match our microfluidic experiments, before inoculating the exponential phase cells grown in LB, these were washed twice with fresh TB. Cultures in these 6-well plates were allowed to grow at 22 ºC for 20 hours under static conditions, which are commonly used to study *P. aeruginosa* biofilms (Oliveira et al., 2015). Cultures were then spun down at 3000g for 10 min and filtrated using 0.22 μm filters (Millipore). We quantified carbonate / carbon dioxide in samples using the HACH LANGE cuvette tests (LCK388). Briefly, this measurement is based on a reaction that converts all carbonates and dissolved carbon dioxide in test samples into gaseous carbon dioxide, which passes through a membrane into the indicator cuvette upon heating (1 h of incubation, 95°C). The change of color of the indicator (thymol blue sodium salt, which changes from yellow at pH ≈ 6 to blue at pH ≈ 7.6) is then photometrically evaluated (at 435 nm). We made a calibration curve with increasing concentrations of $NaHCO_3$, which allows us to match the concentration of carbon dioxide and associated ions of the carbonate system present in the supernatant of stationary-phase cultures of *P. aeruginosa* with a defined concentration of bicarbonate (Figures 4, S4).

Cell staining and blocking of the efflux system. When required, cell damage was assessed with propidium iodide (Sigma Chemical Company) at the final concentration of 3 $\mu l\ ml^{-1}$ following standard protocols (Webb et al., 2003). To assess actively respiring bacteria we used the redox probe 5-cyano-2,3-ditolyl tetrazolim chloride, CTC (Sigma Chemical Company), at a final concentration of 2 mM following

(Rodriguez et al., 1992). CTC is water soluble and nonfluorescent in its oxidized state but becomes insoluble and red-fluorescent when reduced by a functional electron transport chain, being used to report on highly metabolically active bacteria (Sherr et al., 1999), with the caveat it is destructive given it precipitates inside cells upon reduction. In both cases, microfluidic experiments were stopped after 24 hours, then the medium on each well was removed, followed by the addition of fresh antibiotic-free media in both inlet wells supplemented with the appropriate dye and finally flow resumption (4 μl h^{-1}, as specified below). Propidium iodide-stained and CTC-stained cells were visualized using epifluorescence microscopy with DsRed-based filters in separate experiments.

To chemically block the activity of efflux pumps from twitching bacteria, we used a broad-spectrum inhibitor Phenylalanine-arginine β-naphthylamide, PAβN (Sigma Chemical Company), at a final concentration of 5 μg ml^{-1}, which was added in both inlet wells at the beginning of each experiment. Consequently, cells experienced a constant and homogeneous concentration of the inhibitor PAβN over time. Higher concentrations of PAβN are often used (Lomovskaya et al., 2001; Renau et al., 1999), but we found that these affect cell growth in antibiotic-free shaking cultures, and that 5 μg ml^{-1} is the minimum concentration that does not substantially affect growth while still preventing chemotaxis towards antibiotics (Figures 7D, S6).

Microfluidic experiments. We used the commercially available Bioflux 200 system (Fluxion Biosciences) for all microfluidic experiments, which were imaged using a Zeiss Axio Observer inverted microscope with a Zeiss 20X Plan Apochromat objective, Zeiss AxioCam MRm camera, and a Zeiss Definite Focus system. We followed closely our previously published experimental protocol (Oliveira et al., in

review). Briefly, exponential phase cells were introduced in dual-inlet glass bottomed microfluidic channels (version 'Invasion') and allowed to attach to the surface in the absence of flow. After flushing out the planktonic and weakly adhered cells from the test section, we kept the flow rate constant at 4 μl h^{-1} and imaged cells at a rate of 1 frame min^{-1}. Stable antibiotic gradients are generated in the test section of the microfluidic channels via molecular diffusion by injecting growth medium through both inlets and the test antibiotic just through one of them (Figure 1). When we inject MIC or above MIC antibiotic concentrations through both inlets we find no growth in the channels. Moreover, most cells detach in the first few hours under these conditions, which is consistent with their inability to tolerate these antibiotic concentrations.

To determine if cells moving in lethal antibiotic gradients had increased antibiotic resistance in shaking cultures (Figure 7) we proceded as follows. Firstly we removed all the liquid in the outlet wells and cleaned them with 70% ethanol as bacteria growing there experienced constant concentrations of antibiotics throughout the experiment, which could affect the emergence of genetic resistance, and we were interested to address the resistance of twitching cells that moved towards antibiotics and remained attached at the end of the experiment. After ethanol we cleaned the outlet wells with fresh growth medium (tryptone broth, TB) to prevent any ethanol-related death of the cells that were going to be flushed out next. Secondly, we injected 200 μl of fresh TB at the rate of 800 μl h^{-1} through both inlets, aiming to detach cells from the surface of the microfluidic channels, until all liquid has passed to the outlet wells and air bubbles generate in the channels. Finally, we injected another set of 200 μl of fresh TB throughout both inlets that pushed the bubbles out the channel to the outlet, bringing the remaining attached cells with them. This stock (800 μl in total per channel) was diluted 1 to 20 in tryptone broth with increasing concentration of

ciprofloxacin (1, 10, and 100 times the MIC), and from these we inoculated eight replicates of 200 μl in flat-bottomed 96-well plates. In Figure 7 we show bacterial growth in the antibiotic-free control and in 0.1 μg ml^{-1} of ciprofloxacin (MIC) only, as for increasing ciprofloxacin concentrations we found the same absence of growth. Growth and measurements of optical density proceeded as described above.

Characterization of antibiotic gradients and image analysis. The concentration field of antibiotics in the microfluidic devices was mapped using a fluorescent dye (fluorescein) in cell-free channels. Imaging was conducted using the microscopy setup described above except with a Zeiss EC Plan Neofluar 10X objective, a Zeiss LSM 700 scanning laser confocal unit to measure fluorescent intensity, and a Zeiss LSM T-PMT unit to simultaneously visualize the channel geometry. We recorded *z*-stacks of images at multiple, overlapping positions along the length of the device and the maximum fluorescent intensity in *z* was used to obtain the relative fluorescein concentration at each *x,y* position as previously described (Oliveira et al., in review).

To correlate cell movement with the antibiotic distribution and gradient we used a mathematical model (one dimensional, time dependent diffusion equation, fully described in Oliveira et al., in review) to simulate molecular diffusion in the *y* direction, and then obtained the gradient of the concentration field by simple differentiation in that dimension. In the analysis of the chemotactic behavior we only considered cells moving in the middle third of the gradient, where the gradient is the steepest (Figure 1), because that reduces artifacts from cell clustering on regions with lower concentrations of antibiotics, and from reduced motility and detachment on regions with very high concentrations, namely during the first hours of experiment.

All images were processed using the open source software Fiji (Schindelin et al., 2012) and its associated plugins, and all tracking data was exported from Fiji to Matlab (Mathworks) for subsequent analysis as described previously (Oliveira et al., in review). Specifically, for our calculation of chemotactic bias (β), defined as the number of cells moving up the gradient divided by the number of cells moving down the gradient, we used the net displacement of moving cells over the length of their trajectory instead of instantaneous direction given the jerky nature of twitching motility (Jin et al., 2011). In addition, we excluded non-motile cells, cell clusters, and cells that do not exhibit appreciable movement from their origin as specified before (Oliveira et al., in review). All rose plots presented derived from the calculation of the angle, θ, from each trajectory's origin to its terminus, which represents the direction of cell movement. The resulting distribution of angles was fitted with a Kernel smoothing function ('ksdensity' in Matlab, Mathworks) to obtain the probability density function of θ for each test condition. For all conditions tested, the data shown are based on thousands of individual trajectories.

6. Discussion and Conclusion

Each of my data chapters has a specific section with detailed discussion and conclusions. In this final chapter I simply summarize the key findings of each of these chapters along with providing some general remarks and main conclusions that have emerged from my work. Additionally, I provide further clarifications, discuss caveats and suggest how to move forward from here.

Chapter 2: Evolutionary limits to cooperation in microbial communities

- Cooperative cross-feeding *between* microbial genotypes is likely uncommon in natural microbial systems as it requires intermediate levels of genetic mixing. At high mixing, genotypes that do not invest in the production of costly secretions are favored as they avoid the burden of secretion production and have access to all secretions they need. At low mixing, autonomous genotypes that produce all secretions will be favored, as despite growing slowly due to the costs of secretion production, they do not rely on other genotypes to grow. Under these conditions, cross-feeders will not often meet the complementing parties and thus cannot grow.
- The costs of secretion production are also important for the evolution of cooperative exchanges in microbial communities: for secretions with low cost, autonomous genotypes will often dominate as there will not be enough incentive to drop a particular secretion and rely on others for the secretions.
- Between-genotype cooperative cross-feeding in microbes is associated with reduced group productivity. We find this outcome in systems where cells have a fixed strategy (i.e. unchanging investment in secretion production), but also in

systems where cells can modulate the investment on cooperation over evolutionary time. Instead of increasing their investment into secretion production to compensate for their low productivity, cross-feeders evolve to invest less in each secretion than full secretors.

- The population dynamics we find suggests that cooperative exchanges among microbial genotypes are more associated with exploitation and cheating dynamics than with canonical cooperation where individuals evolve to help others. One can call it 'exploitative cooperation', which captures the evolutionary tension between cooperation and conflict in microbial groups.
- Accounting for features that often pervade microbial ecology and affect the degree of genetic mixing, such as spatiogenetic structuring[2], emphasizes that the evolution of fitness-promoting secretion exchanges between genotypes is likely to be uncommon. Canonical spatial structure and social insulation (effect of passive genotypes that do not use or produce secretions) limit cooperative cross-feeding as they reduce the probability of interactions between individuals that can complement each other. Instead, spatiogenetic structuring tends to promote autonomous genotypes that do not rely on others to grow and prosper.

Chapter 3: Biofilm formation as a response to ecological competition

- Mixing natural isolates of *Pseudomonas aeruginosa* reliably drives biofilm formation. Instead of a cooperative enterprise between strains, however, we find that competitive exclusion is common in co-cultures.
- We obtain mixing-induced biofilm formation using both classical microtiter dish assays based on crystal violet staining and state-of-the-art microfluidic

[2] Spatiogenetic structuring can be defined as the assortment of individuals by their genotype in space.

chambers where biofilms growing under flow are directly imaged. This biofilm response is not an idiosyncrasy of growth medium as we find similar mixing-induced biofilm formation across multiple environments and growth conditions.

- Biochemical and molecular genetic assays revel that narrow-spectrum antibiotics produced by competitor genotypes are cues for biofilm formation. In particular, we find that pyocins are important drivers of mixing-induced biofilm formation and that this response is associated with cell damage.
- Similar biofilm response is obtained with sub-lethal concentrations of clinical antibiotics: susceptible bacteria form biofilms in response to antibiotics as diverse as pyocins from competitors that disrupt membranes, but also commercial antibiotics that damage DNA, inhibit protein synthesis or transcription. Such generality then suggests that mixing-induced biofilm formation is expected to be common between any two strains or species that can harm each other via antibiotic stress.
- Antibiotic gradients robustly induce biofilm formation in *P. aeruginosa*. We provide direct evidence for increasing surface attachment under some conditions. However, given we could not find increased attachment across all treatments, we suggest that reduced detachment and growth induction may contribute to the biofilm accumulation we find upon strain mixing.
- More generally, our data suggest that the widespread and clinically-relevant phenotype of antibiotic-induced biofilm formation may have its natural origins in the ability to detect and respond to evolutionary competition – competition sensing. By doing so, our data also caution against the recent claims of antibiotics as cooperative signals that coordinate microbial communities and contribute to their homeostasis.

Chapter 4: Single-cell twitching chemotaxis during biofilm formation

- Attached *P. aeruginosa* use pili-based motility (twitching) and the Chp chemosensory system to move up increasing concentrations of canonical chemoeffectors within developing biofilms.
- Behaviorally, individual bacteria reverse the direction of motion more frequently when moving away from the chemoattractant source, and move faster when conversely moving towards the source. Genetically, cells use the response regulator PilG, homologue of *Escherichia coli*'s CheY, to control both reversal rate and speed during twitching chemotaxis.
- The chemotactic response of attached *P. aeruginosa* increases with the strength of the chemical gradient, which is a defining feature of chemotaxis across biological systems.
- Biofilm cells are able to quickly adjust the direction of motion when we change the direction of the chemical gradient. Such corrective maneuvers are achieved with unprecedented spatial resolution: moving cells can respond within a small fraction of their body length and actively position themselves in gradients that occur on a scale of tens of microns. These surprising findings reveal 'submicron chemotaxis in bacteria. Our results for attached cells are consistent with spatial sensing, which contrasts with the behavior of swimming cells that employ temporal sensing instead.
- We argue that the ability to detect and respond to chemical gradients via twitching chemotaxis is likely to help cells to position themselves and compete within biofilms where diverse and often steep chemical gradients emerge from cell metabolism and reaction-diffusion processes.

Chapter 5: Bacterial chemotaxis towards antibiotics results in extreme phenotypic resistance.

- *P. aeruginosa* use twitching chemotaxis to move towards increasing concentrations of antibiotics during biofilm formation. Similar behavior is observed for antibiotics from different classes and modes of action.
- Consistent with twitching chemotaxis towards canonical chemoeffectors, bacterial cells lacking the response regulator PilG cannot bias movement towards increasing concentrations of antibiotics.
- Our data is consistent with antibiotic-induced chemotaxis as the directed movement towards antibiotics we document is unlikely just a response to *de novo* nutrient gradients or exudates from surrounding cells that emerge overtime as a consequence of cell gradients in the microfluidic devices.
- *P. aeruginosa* move towards cell-free supernatant from strong competitor strains, which is associated with cell damage as given by robust growth lags in shaking culture. Cell-free supernatant from poor competitors that does not inhibit growth also does not drive cell movement towards it. As for antibiotic-induced biofilm formation, these findings are consistent with the idea of competition-sensing and the ability to detect and respond to biotic stress from competitor strains and species. Accordingly, bacteria do not move towards clinical antibiotics to which are resistant while retaining the ability to move towards antibiotics to which are susceptible.
- Endogenously produced CO_2/bicarbonate works as a repellent within developing biofilms of *P. aeruginosa*. Altogether, our findings suggest an ecological model where biofilm cells can use CO_2/bicarbonate to disperse

and in parallel antimicrobials from neighboring colonies of competing strains to attack. The latter behavior resembles what we find in social insects where workers seek and attack harmful species.

- Movement towards increasing concentrations of antibiotics brings with it the emergence of extreme resistance. *P. aeruginosa* can reach and withstand regions with antibiotic concentrations one thousand times higher than expected from their MIC (minimal inhibitory concentration) within a few hours.
- The resistance we find is consistent with phenotypic rather than genetic resistance because it is short-lived. When we put twitching cells back to homogenous concentrations of antibiotics we find identical susceptibility profile as cells that did not experience antibiotics before.
- Consistent with a response based on physiological regulation and the so-called 'adaptive' resistance, blocking the efflux pumps of moving cells prevents twitching chemotaxis towards antibiotics.
- Our findings suggest that spatial gradients of antibiotics allow twitching bacteria to experience gradual increases in antibiotic concentration and adjust their physiology accordingly. The result is the emergence of tolerance to extremely high concentrations of antibiotics.

Clarifications, caveats and future work

Words of wisdom from Alan Turing: '*We can only see a short distance ahead, but we can see plenty there that needs to be done.*' (Turing, 1950).

On the genetic diversity of microbial communities

My thesis is centered on the study of interactions among microbial genotypes and how these cellular interactions explain form and function of natural communities. However, most of my work is based on a much more limited genetic diversity than expected in natural microbial communities. In particular, in natural settings, including infections (Murray et al., 2014), it is not only strains that mix but also a diversity of *species*. How would a greater genetic diversity affect my conclusions?

My mathematical modeling is general and broadly applicable across any phylogenetic scale and niche overlap. The key limit on the evolution of cooperative exchange between genotypes is whether a cell can find a complementary partner to exchange with, and this limit is only accentuated within diverse and complex communities as explained in Chapter 2. A wide diversity of additional species and strains will most likely prevent interactions between complementary partners through social insulation.

What about biofilm formation as a response to ecological competition? My work has studied this phenotype based upon intra-specific genetic diversity. Competition within a species is expected to be stronger, on average, than between species because of increased ecological overlap within species as Darwin himself emphasized: '*each variety or species* […] will *press hardest on its nearest kindred*' (Darwin, 1859). This notion suggests that the link between genetic diversity and competition-induced

biofilm formation is likely to be the clearest within species as we studied here. While it is possible that genotypic mixing involving different species may lead to biofilm formation via cooperation, the cause of increased biofilm formation in our studies was antibiotic warfare and this is common between strains as well as between species in natural communities (Cordero et al., 2012b; Hibbing et al., 2010; Vetsigian et al., 2011). Moreover, the biofilm response to sub-lethal concentrations of antibiotics is well known from a wide range of species (Kaplan, 2011). Collectively, these data suggest that competition-induced biofilm formation will likely be seen in genetically diverse communities.

On the alternative actions of antibiotics

Antibiotics have traditionally been viewed as weapons that microbes use to inhibit or even kill one another (Hibbing et al., 2010). Indeed what attracted the attention of Fleming to his 'mold juice', afterwards called penicillin, was its ability to inhibit the growth of susceptible bacteria surrounding penicillin-producing fungi (Figure 1B, Chapter 1). However, there is an increasing number of works claiming that antibiotics are used as cooperative signals that coordinate the homeostasis of natural microbial communities (Davies et al., 2006; Fajardo and Martinez, 2008; Kaplan, 2011; Linares et al., 2006; Yim et al., 2007). This hypothesis stems from the observation that under sub-lethal doses, antibiotics often trigger important phenotypes such as increased gene expression, antibiotic resistance, biofilm formation, conjugative transfer, bacterial virulence or quorum-sensing (Andersson and Hughes, 2014), which seem to benefit the target cell. To be categorized as a signal, however, both sender and receiver individuals need to benefit from the interaction (Maynard Smith and Harper, 2003). How could pore-forming molecules such as pyocins evolve to help instead of harm? Or even

DNA-damaging agents or other compounds that block transcription or translation? And why would antibiotics that evolve to help lead to increased antibiotic production and resistance in susceptible individuals (Cornforth and Foster, 2013)?

It is not clear then how natural selection would work under this alternative model for antibiotic action, and indeed such hypothesis has been viewed as having little evolutionary merit (Ratcliff and Denison, 2011). Very recent work strongly suggests that antibiotics from coexisting Streptomycetes are weapons used in competition between genotypes, and shows that cells can regulate antibiotic production as a facultative response to cues from competitors (Abrudan et al., 2015). My own theoretical work also cautions against the idea that genotypes will often evolve to help via cooperative exchanges (Chapter 2). That logic can be applied to any costly secretion, including communication via chemical signaling (Ratcliff and Denison, 2011). Moreover, the harmful effects of antibiotics are typically clear. For example, pyocins are used to kill closely-related competitor genotypes and the fitness benefits of such production are well-established (Heo et al., 2007; Heo et al., 2005).

Instead of being cooperative signals, antibiotics can be used as cues that indicate the rising threat of competitors. Another possibility is that they work as manipulation compounds instead (Bernier and Surette, 2013; Ratcliff and Denison, 2011). However, the former cue model seems the most plausible for the systems I studied here. Firstly, I observed that strains increase their biofilm formation in response to antibiotics, which is consistent with a response that helps strains to defend themselves in a biofilm. Put simply, the 'benefit' here seems to go to the responder and not to the producer. Secondly, for antibiotic-induced chemotaxis, most responding cells remain viable and increase their resistance as they move up the gradient. This allows the responding genotype to better establish itself upstream in the region with high antibiotic

concentration and potentially from there launch a counter attack. In sum, my data appear most consistent with antibiotics as cues for defense and attack but additional dedicated experiments are required, namely to assess the fitness costs and benefits of the phenotypes I have studied here.

On competition-sensing and the idea of sensing harmfulness

The competition-sensing hypothesis had major influence on my conceptual understanding of microbial communities. The idea is simple and elegant, suggesting that microbes can sense competitors via stress responses that directly detect and respond to harmfulness (Cornforth and Foster, 2013). The argument is particularly compelling when we note that the major stress responses that sense nutrient stress or cell damage, which directly detect biotic harmfulness, also regulate antibiotic production, while stress responses associated with heat or osmotic stress (abiotic stress) typically do not (Cornforth and Foster, 2013). Why would cells produce their own toxins when exposed to antibiotics and other biotic stresses? Discerning the evolutionary function of phenotypes is not always trivial (Gould and Lewontin, 1979), but for antibiotics, particularly those that have narrow spectrum activity such as bacteriocins, it is likely they evolved to influence a biotic target (most likely to inhibit or kill as discussed in the previous section on the alternative actions of antibiotics).

I have used the competition-sensing hypothesis throughout my thesis and, as it predicts, I find a clear association between major bacterial phenotypes (biofilm formation and chemotaxis) and compounds that cause cell damage. In particular, I observe that bacteria display antibiotic-induced biofilm formation (Chapter 3) and what seems antibiotic-induced chemotaxis (Chapter 5) but, importantly, this is only observed when cells are susceptible to the antibiotic. While one can speculate based on

my results (next), one limitation of my work is that I do not provide evidence of the sensing mechanism for any of these phenotypes. Instead, arguably my biggest insight was the realization that we can learn about the evolutionary ecology of microbial communities studying the responses to clinical antibiotics, which has been largely missed in the literature. And the inverse is true as well: by studying microbial interactions, and how they evolve, we may gain insight into phenotypes of major public concern such as biofilm formation or the emergence of antibiotic resistance.

Detecting and responding to antibiotics

What is the mechanistic basis for the common responses that myself and others have observed to a wide range of antibiotics? An interesting observation by Collins and colleagues links the action of many antibiotics to oxidative stress, which is associated, at least partially, with increases in cellular respiration (Dwyer et al., 2014; Kohanski et al., 2010b; Kohanski et al., 2007; Kohanski et al., 2008; Lobritz et al., 2015). These observations led to a model for bacterial death induced by (bactericidal) antibiotics, which was based on the deleterious effects of accumulating reactive oxygen species (ROS) that themselves mostly result from increased activity of the electron transport chain and the TCA cycle upon antibiotic exposure (Kohanski et al., 2007; Kohanski et al., 2008), and are associated with increases in oxygen consumption (Dwyer et al., 2014; Lobritz et al., 2015). Clearly, the reality of microbial death is more complex than this initial model (Dwyer et al., 2015; Imlay, 2015), but nevertheless these are very interesting observations for this discussion. Antibiotic target inhibition often leads to the acceleration of cellular respiration. Why?

The simplest rational for such antibiotic-induced oxygen consumption is that it is a maladaptive byproduct of antibiotic action. By virtue of being under stress, target

cells may aberrantly increase their metabolism, which contributes to antibiotic lethality. However, social evolution provides an alternative model for this intriguing response to antibiotics. There is the possibility that this response is adaptive, or at least it can work as a cue for the presence of competitors.

We should note that oxygen is often a critical nutrient for many bacteria and what Collins and collaborators reported was effectively an increase in the rate of consumption of an important nutrient. This is consistent with an increase in metabolic rate as a response to harmfulness and, as I have been arguing throughout this thesis, such harmfulness often indicates evolutionary competition in nature. A critical point, however, is that in natural communities the antibiotic source will often be a competitor genotype and thus the concentration of antibiotic is not constant overtime as often assumed in antibiotic research. Providing the responder strain can increase in frequency relative to antibiotic-producing strains (for example by depriving them from a critical nutrient such as oxygen, or by using endogenously-produced ROS to boost their own aggressiveness), antibiotic-induced oxygen consumption could indeed be a social adaptation. In accordance with this logic, it was recently shown that lethal attacks from competing genotypes drive ROS formation in target cells (Dong et al., 2015), and it was suggested that ROS can be used as a cue for the onset of antagonist bacterial interactions (Dong et al., 2015; Ho et al., 2013). Clearly, we need more mechanistic insight on what drives the acceleration of oxygen consumption under antibiotic stress, and a detailed analysis of the fitness gains and costs of such phenotype. Finding a putative response regulator that controls antibiotic-induced aerobic respiration would be a strong evidence for claiming this phenotype as an adaptation, but we presently lack that supporting observation.

I have recently been working on another intriguing phenotype, potentially related to this antibiotic-induced acceleration of aerobic metabolism. Using the same natural isolates of *P. aeruginosa* that I studied in Chapter 3, I found that mixing strains leads to what seems increased production of pyoverdine, the main iron-quencher of this species (Appendix). These preliminary data are interesting as siderophore production has commonly been associated with cooperation between cells in the sociomicrobiology literature (Nadell et al., 2009; West et al., 2007a; West et al., 2006), and the data suggests that mixing strong competitors leads to siderophore production. Importantly, what drives this mixing effect is antibiotic competition similarly to the mixing-induced biofilm formation I studied in Chapter 3. And consistent with this, sub-lethal concentrations of clinical antibiotics also seem to drive siderophore production (Appendix). One could speculate that, as for antibiotic-induced oxygen consumption, this phenotype may represent a competitive response based on overexploitation as indeed iron is another critical nutrient for bacterial growth. The idea is that cells may actively increase their basal metabolism and resource exploitation upon antibiotic stress as a way to prevent the putative antibiotic producer from growing. But as I discussed above, it will be necessary to better understand the sensing mechanism leading to this phenotype to fully appreciate its evolutionary basis.

Competition Sensing via indirect damage

What if bacteria sense indirect competition via damage done to their surrounding cells? In an exciting new work, Mougous and colleagues show that cell lysis of *P. aeruginosa*, which in their system is driven by T6SS attacks from competitor species, triggers a response in the remaining kin cells that fight back with their own T6SS and other antimicrobial compounds (LeRoux et al, 2015). Put differently, responding cells

there are sensing indirect damage done to their neighbors instead of direct damage. Rather than being mutually exclusive, however, sensing competition via direct and indirect damage seems at present complementary processes and it will be interesting to study the relative importance of the two in the phenotypes I studied. In particular, do bacteria form biofilms or produce siderophores in response to cell lysis? If yes, can the mixing-induced effects I reported here be explained by antibiotic-induced cell lysis (indirect damage model) instead, or in combination to, a response based on direct competition (direct damage model)? And what about chemotaxis, do twitching bacteria regulate their motion in response to cell lysis? As relevant as these questions there is another that should be addressed: if bacteria are not responding to antibiotics directly, what are cells sensing exactly? What do they have on them (or in them) that drive the response to T6SS attack and might be important to explain the phenotypes I studied?

Whatever the sensing model, and the specific compound(s) that bacteria are detecting and responding to, my main point here is simple. We may miss fundamental biology of microbes if we just study them in monocultures, and that is particularly pertinent when it comes to antibiotic research, which is often centered on single genetic backgrounds and how they respond to single antibiotic concentrations. The richness of behaviors that myself and others have been reporting is a clear indication that the study of microbial interactions is important and should be built upon.

General remarks and future work

Most cell biology rests on the study of pure cultures, often in shaking flasks. There are obviously good reasons to average over populations and indeed from these studies we got a wealth of data on the biochemical and molecular genetics of many important cell

traits. But in nature cell groups often contain genetically distinct populations and nowhere this notion is more appropriate than in the microbial world in which a myriad of strains meet and interact, often strongly. As I hope my work conveys, we may miss important biology if we do not understand microbial interactions and how they evolve.

The data presented here support the idea that evolutionary competition governs the dynamics of non-clonal groups, which agrees with the 'genotypic view' of social interactions in microbial communities: within-genotype cooperation is common but between-genotype cooperation is rare (Mitri and Foster, 2013). I built on this idea by clarifying that a critical determinant for cooperation among genotypes is the degree of genetic mixing. Moreover, even when this mixing is appropriate, I did not find true cooperation among genotypes where individuals evolve to help, but instead competition and wasteful behavior where individuals evolve to exploit each other.

My empirical studies of microbial groups support the idea of 'competition-sensing', which suggests that microbes can use antibiotic stress as a cue for detecting and responding to evolutionary competition (Cornforth and Foster, 2013). I built on this idea by showing that important microbial phenotypes such as biofilm formation and motility control via chemotaxis are indeed modulated upon antibiotic stress and most likely represent a response with natural origins in competition-sensing. But I found something else that is more difficult to understand from present knowledge. Why do bacteria migrate towards antibiotics?

Understanding the genetic basis of *antibiotic taxis*, how it affects the emergence of genetic resistance, and how we can manipulate this behavior to our own advantage, are exciting new directions for antibiotic research. Detailed understanding of this perplexing phenotype can prove critical to our ability to ameliorate the alarming

menace of bacterial antibiotic resistance. Moreover, this discovery hit home how far I am from understanding how bacteria 'think' and play their evolutionary games.

This all being said, I can only add that it is fascinating, and indeed a privilege, to think about and study how bacteria seem to combine luck and skill in their microscopic 'tangled banks' that Darwin never saw, in which very many strains and species meet together and interact, sometimes perhaps through generous cooperation but most likely through harsh competition. Whatever the strategy they play, it is clear that their social abilities are critical for their survival and therefore, as predicted, 'have been, and are being, evolved'. Only by appreciating such sociality, namely the evolutionary competition that pervades natural groups, we will fully understand microbes, their complex communities and, by extension, how and why they affect us as they do.

7. Bibliography

Abrudan, M.I., Smakman, F., Grimbergen A.J., Westhoff, S., Miller, E.L., van Wezel, G.P., Rozen, D.E. (2015). Socially mediated induction and suppression of antibiosis during bacterial coexistence. *PNAS*. Early edition, Epub ahead of print.

Achtman, M., and Wagner, M. (2008). Microbial diversity and the genetic nature of microbial species. *Nat Rev Microbiol 6*, 431-440.

Adler, J. (1966). Chemotaxis in Bacteria. *Science 153*, 708-716.

Adler, J., Hazelbauer, G.L., and Dahl, M.M. (1973). Chemotaxis toward sugars in *Escherichia coli*. *J Bacteriol 115*, 824-847.

Ahmed, T., and Stocker, R. (2008). Experimental verification of the behavioral foundation of bacterial transport parameters using microfluidics. *Biophys J 95*, 4481-4493.

Allen, G.E., and Dytham, C. (2009). An efficient method for stochastic simulation of biological populations in continuous time. *Biosystems 98*, 37-42.

Andersson, D.I., and Hughes, D. (2014). Microbiological effects of sublethal levels of antibiotics. *Nat Rev Microbiol 12*, 465-478.

Andersson, S., Rajarao, G.K., Land, C.J., and Dalhammar, G. (2008). Biofilm formation and interactions of bacterial strains found in wastewater treatment systems. *Fems Microbiol Lett 283*, 83-90.

Armitage, J.P. (1997). Behavioural responses of bacteria to light and oxygen. *Archives Microbiol 168*, 249-261.

Baldan, R., Cigana, C., Testa, F., Bianconi, I., De Simone, M., Pellin, D., Di Serio, C., Bragonzi, A., and Cirillo, D.M. (2014). Adaptation of *Pseudomonas aeruginosa* in cystic fibrosis airways influences virulence of *Staphylococcus aureus* in vitro and murine models of co-infection. *PloS one 9*, e89614.

Basler, M., Ho, B.T., and Mekalanos, J.J. (2013). Tit-for-Tat: Type VI secretion system counterattack during bacterial cell-cell Interactions. *Cell 152*, 884-894.

Basler, M., and Mekalanos, J.J. (2012). Type 6 Secretion dynamics within and between bacterial cells. *Science 337*, 815-815.

Baumgartner, L.K., Spear, J.R., Buckley, D.H., Pace, N.R., Reid, R.P., Dupraz, C., and Visscher, P.T. (2009). Microbial diversity in modern marine stromatolites, Highborne Cay, Bahamas. *Environ Microbiol 11*, 2710-2719.

Beloin, C., and Ghigo, J.M. (2005). Finding gene-expression patterns in bacterial biofilms. *Trends Microbiol 13*, 16-19.

Benoit, M.R., Conant, C.G., Ionescu-Zanetti, C., Schwartz, M., and Matin, A. (2010). New device for high-throughput viability screening of flow biofilms. *Appl Environ Microbiol 76*, 4136-4142.

Berg, H.C. (2004). *E. coli in motion* (New York: Springer).

Berg, H.C., and Brown, D.A. (1972). Chemotaxis in *Escherichia coli* analyzed by 3-dimensional tracking. *Nature 239*, 500-504.

Bernier, S.P., and Surette, M.G. (2013). Concentration-dependent activity of antibiotics in natural environments. *Front Microbiol 4*, 20.

Bertrand, J.J., West, J.T., and Engel, J.N. (2010). Genetic analysis of the regulation of Type IV pilus function by the Chp chemosensory system of *Pseudomonas aeruginosa*. *J Bacteriol 192*, 994-1010.

Bodey, G.P., Bolivar, R., Fainstein, V., and Jadeja, L. (1983). Infections Caused by *Pseudomonas aeruginosa*. *Rev Infect Dis 5*, 279-313.

Breidenstein, E.B.M., Khaira, B.K., Wiegand, I., Overhage, J., and Hancock, R.E.W. (2008). Complex ciprofloxacin resistome revealed by screening a *Pseudomonas aeruginosa* mutant library for altered susceptibility. *Antimicrob Agents Chemother 52*, 4486-4491.

Brown, S.P., and Johnstone, R.A. (2001). Cooperation in the dark: signalling and collective action in quorum-sensing bacteria. *P Roy Soc B-Biol Sci 268*, 961-965.

Buckling, A., Harrison, F., Vos, M., Brockhurst, M.A., Gardner, A., West, S.A., and Griffin, A. (2007). Siderophore-mediated cooperation and virulence in *Pseudomonas aeruginosa*. *Fems Microbiol Ecol 62*, 135-141.

Bull, J.J., and Harcombe, W.R. (2009). Population dynamics constrain the cooperative evolution of cross-feeding. *PLoS one 4*, e4115.

Burmolle, M., Ren, D.W., Bjarnsholt, T., and Sorensen, S.J. (2014). Interactions in multispecies biofilms: do they actually matter? *Trends Microbiol 22*, 84-91.

Burmolle, M., Webb, J.S., Rao, D., Hansen, L.H., Sorensen, S.J., and Kjelleberg, S. (2006). Enhanced biofilm formation and increased resistance to antimicrobial agents and bacterial invasion are caused by synergistic interactions in multispecies biofilms. *Appl Environ Microbiol 72*, 3916-3923.

Burns, J.L., Gibson, R.L., McNamara, S., Yim, D., Emerson, J., Rosenfeld, M., Hiatt, P., McCoy, K., Castile, R., Smith, A.L.*, et al.* (2001). Longitudinal assessment of *Pseudomonas aeruginosa* in young children with cystic fibrosis. *J Infect Dis 183*, 444-452.

Burrows, L.L. (2012). *Pseudomonas aeruginosa* Twitching motility: Type IV pili in action. *Annu Rev Microbiol 66*, 493-520.

Butler, M.T., Wang, Q.F., and Harshey, R.M. (2010). Cell density and mobility protect swarming bacteria against antibiotics. *PNAS 107*, 3776-3781.

Callaway, T.R., Edrington, T.S., Anderson, R.C., Harvey, R.B., Genovese, K.J., Kennedy, C.N., Venn, D.W., and Nisbet, D.J. (2008). Probiotics, prebiotics and competitive exclusion for prophylaxis against bacterial disease. *Anim Health Res Rev 9*, 217-225.

Chandler, J.R., Heilmann, S., Mittler, J.E., and Greenberg, E.P. (2012). Acyl-homoserine lactone-dependent eavesdropping promotes competition in a laboratory co-culture model. *ISME J 6*, 2219-2228.

Chuang, J.S., Rivoire, O., and Leibler, S. (2009). Simpson's paradox in a synthetic microbial system. *Science 323*, 272-275.

Ciofu, O., and Tolker-Nielsen, T. (2011). Antibiotic tolerance and resistance in biofilms. In: Bjarnsholt, T., Moser, C., Jensen, P.O., Hoiby, N., editors. *Biofilm Infections*. Berlim, Germany: Springer. pp. 215-229.

Cordero, O.X., Ventouras, L.A., DeLong, E.F., and Polz, M.F. (2012a). Public good dynamics drive evolution of iron acquisition strategies in natural bacterioplankton populations. *PNAS 109*, 20059-20064.

Cordero, O.X., Wildschutte, H., Kirkup, B., Proehl, S., Ngo, L., Hussain, F., Le Roux, F., Mincer, T., and Polz, M.F. (2012b). Ecological populations of bacteria act as socially cohesive units of antibiotic production and resistance. *Science 337*, 1228-1231.

Cornforth, D.M., and Foster, K.R. (2013). Competition sensing: the social side of bacterial stress responses. *Nat Rev Microbiol 11*, 285-293.

Costerton, J.W. (1995). Overview of microbial biofilms. *J Ind Microbiol 15*, 137-140.

Costerton, J.W. (2007). *The biofilm primer* (Berlin ; New York: Springer).

Costerton, J.W., Lewandowski, Z., Caldwell, D.E., Korber, D.R., and Lappin-Scott, H.M. (1995). Microbial biofilms. *Annu Rev Microbiol 49*, 711-745.

Cowles, K.N., and Gitai, Z. (2010). Surface association and the MreB cytoskeleton regulate pilus production, localization and function in *Pseudomonas aeruginosa*. *Mol Microbiol 76*, 1411-1426.

Crank, J. (1975). *The mathematics of diffusion*, 2nd edn (Oxford: Clarendon Press).

Cremer, J., Melbinger, A., and Frey, E. (2012). Growth dynamics and the evolution of cooperation in microbial populations. *Sci Rep 2*, 281.

Crespi, B.J. (2001). The evolution of social behavior in microorganisms. *Trends Ecol Evol 16*, 178-183.

D'Onofrio, A., Crawford, J.M., Stewart, E.J., Witt, K., Gavrish, E., Epstein, S., Clardy, J., and Lewis, K. (2010). Siderophores from neighboring organisms promote the growth of uncultured bacteria. *Chem Biol 17*, 254-264.

Darwin, C. (1859). *On the origin of species by means of natural selection* (London,: J. Murray).

Datta, M.S., Korolev, K.S., Cvijovic, I., Dudley, C., and Gore, J. (2013). Range expansion promotes cooperation in an experimental microbial metapopulation. *PNAS 110*, 7354-7359.

Davies, J., Spiegelman, G.B., and Yim, G. (2006). The world of subinhibitory antibiotic concentrations. *Curr Opin Microbiol 9*, 445-453.

De Mazancourt, C., Loreau, M., and Dieckmann, U. (2005). Understanding mutualism when there is adaptation to the partner. *J Ecol 93*, 305-314.

Diggle, S.P., Griffin, A.S., Campbell, G.S., and West, S.A. (2007). Cooperation and conflict in quorum-sensing bacterial populations. *Nature 450*, 411-414.

Dobell, C. (1960). *Antony van Leeuwenhoek and his "little animals": being some account of the father of protozoology and bacteriology and his multifarious discoveries in these disciplines* (New York: Dover).

Dong, T.G., Dong, S., Catalano, C., Moore, R., Liang, X., and Mekalanos, J.J. (2015). Generation of reactive oxygen species by lethal attacks from competing microbes. *PNAS 112*, 2181-2186.

Drake, J.W., Charlesworth, B., Charlesworth, D., and Crow, J.F. (1998). Rates of spontaneous mutation. *Genetics 148*, 1667-1686.

Drenkard, E., and Ausubel, F.M. (2002). Pseudomonas biofilm formation and antibiotic resistance are linked to phenotypic variation. *Nature 416*, 740-743.

Drescher, K., Nadell, C.D., Stone, H.A., Wingreen, N.S., and Bassler, B.L. (2014). Solutions to the public goods dilemma in bacterial biofilms. *Curr Biol 24*, 50-55.

Dwyer, D.J., Belenky, P.A., Yang, J.H., MacDonald, I.C., Martell, J.D., Takahashi, N., Chan, C.T., Lobritz, M.A., Braff, D., Schwarz, E.G.*, et al.* (2014). Antibiotics induce redox-related physiological alterations as part of their lethality. *PNAS 111*, E2100-2109.

Dwyer, D.J., Collins, J.J., and Walker, G.C. (2015). Unraveling the physiological complexities of antibiotic lethality. *Annu Rev Pharmacol 55*, 313-332.

Dwyer, D.J., Kohanski, M.A., Hayete, B., and Collins, J.J. (2007). Gyrase inhibitors induce an oxidative damage cellular death pathway in *Escherichia coli*. *Mol Syst Biol 3*, 91.

Elias, S., and Banin, E. (2012). Multi-species biofilms: living with friendly neighbors. *FEMS Microbiol Rev 36*,990-1004.

Elliott, D., Burns, J.L., and Hoffman, L.R. (2010). Exploratory study of the prevalence and clinical significance of tobramycin-mediated biofilm induction in *Pseudomonas aeruginosa* isolates from cystic fibrosis patients. *Antimicrob Agents Chemother 54*, 3024-3026.

Ernebjerg, M., and Kishony, R. (2012). Distinct growth strategies of soil bacteria as revealed by large-scale colony tracking. *Appl Environm Microbiol 78*, 1345-1352.

Estrela, S., Trisos, C.H., and Brown, S.P. (2012). From metabolism to ecology: cross-feeding interactions shape the balance between polymicrobial conflict and mutualism. *Am Nat 180*, 566-576.

Ezraty, B., Vergnes, A., Banzhaf, M., Duverger, Y., Huguenot, A., Brochado, A.R., Su, S.Y., Espinosa, L., Loiseau, L., Py, B.*, et al.* (2013). Fe-S cluster biosynthesis controls uptake of aminoglycosides in a ROS-less death pathway. *Science 340*, 1583-1587.

Fajardo, A., and Martinez, J.L. (2008). Antibiotics as signals that trigger specific bacterial responses. *Curr Opin Microbiol 11*, 161-167.

Fennell, D.E., and Gossett, J.M. (1998). Modeling the production of and competition for hydrogen in a dechlorinating culture. *Environ Sci Technol 32*, 2450-2460.

Fernandez, L., and Hancock, R.E.W. (2012). Adaptive and mutational resistance: role of porins and efflux pumps in drug resistance. *Clin Microbiol Rev 25*, 661-681.

Ferrandez, A., Hawkins, A.C., Summerfield, D.T., and Harwood, C.S. (2002). Cluster II che genes from *Pseudomonas aeruginosa* are required for an optimal chemotactic response. *J Bacteriol 184*, 4374-4383.

Fiegna, F., and Velicer, G.J. (2005). Exploitative and hierarchical antagonism in a cooperative bacterium. *PLoS Biol 3*, 1980-1987.

Filkins, L.M., Graber, J.A., Olson, D.G., Dolben, E.L., Lynd, L.R., Bhuju, S., and O'Toole, G.A. (2015). Coculture of *Staphylococcus aureus* with *Pseudomonas aeruginosa* drives *S. aureus* towards fermentative metabolism and reduced viability in a cystic fibrosis model. *J Bacteriol 197*, 2252-2264.

Folkesson, A., Jelsbak, L., Yang, L., Johansen, H.K., Ciofu, O., Hoiby, N., and Molin, S. (2012). Adaptation of *Pseudomonas aeruginosa* to the cystic fibrosis airway: an evolutionary perspective. *Nat Rev Microbiol 10*, 841-851.

Foster, K.R. (2004). Diminishing returns in social evolution: the not-so-tragic commons. *J Evol Biol 17*, 1058-1072.

Foster, K.R. (2005). Biomedicine - Hamiltonian medicine: Why the social lives of pathogens matter. *Science 308*, 1269-1270.

Foster, K.R., and Bell, T. (2012). Competition, not cooperation, dominates interactions among culturable microbial species. *Curr Biol 22*, 1845-1850.

Foster, K.R., and Wenseleers, T. (2006). A general model for the evolution of mutualisms. *J Evol Biol 19*, 1283-1293.

Foti, J.J., Devadoss, B., Winkler, J.A., Collins, J.J., and Walker, G.C. (2012). Oxidation of the guanine nucleotide pool underlies cell death by bactericidal antibiotics. *Science 336*, 315-319.

Frank, S.A. (1994). Genetics of mutualism: the evolution of altruism between species. *J Theor Biol 170*, 393-400.

Frank, S.A. (2010). Microbial secretor-cheater dynamics. *Philo Trans R Soc Lond B Biol Sci 365*, 2515-2522.

Freilich, S., Zarecki, R., Eilam, O., Segal, E.S., Henry, C.S., Kupiec, M., Gophna, U., Sharan, R., and Ruppin, E. (2011). Competitive and cooperative metabolic interactions in bacterial communities. *Nat Commun 2*, 589.

Fulcher, N.B., Holliday, P.M., Klem, E., Cann, M.J., and Wolfgang, M.C. (2010). The *Pseudomonas aeruginosa* Chp chemosensory system regulates intracellular cAMP levels by modulating adenylate cyclase activity. *Mol Microbiol 76*, 889-904.

Gans, J., Wolinsky, M., and Dunbar, J. (2005). Computational improvements reveal great bacterial diversity and high metal toxicity in soil. *Science 309*, 1387-1390.

Gareau, M.G., Sherman, P.M., and Walker, W.A. (2010). Probiotics and the gut microbiota in intestinal health and disease. *Nat Rev Gastroenterol Hepatol 7*, 503-514.

Ghysels, B., Dieu, B.T.M., Beatson, S.A., Pirnay, J.P., Ochsner, U.A., Vasil, M.L., and Cornelis, P. (2004). FpvB, an alternative type I ferripyoverdine receptor of *Pseudomonas aeruginosa*. *Microbiology 150*, 1671-1680.

Gibiansky, M.L., Conrad, J.C., Jin, F., Gordon, V.D., Motto, D.A., Mathewson, M.A., Stopka, W.G., Zelasko, D.C., Shrout, J.D., and Wong, G.C.L. (2010). Bacteria use Type IV pili to walk upright and detach from surfaces. *Science 330*, 197-U150.

Gillespie, D.T. (1977). Exact stochastic simulation of coupled chemical-reactions. *J Phys Chem 81*, 2340-2361.

Goh, E.B., Yim, G., Tsui, W., McClure, J., Surette, M.G., and Davies, J. (2002). Transcriptional modulation of bacterial gene expression by subinhibitory concentrations of antibiotics. *PNAS 99*, 17025-17030.

Gore, J., Youk, H., and Van Oudenaarden, A. (2009). Snowdrift game dynamics and facultative cheating in yeast. *Nature 459*, 253-256.

Gould, S.J., and Lewontin, R.C. (1979). Spandrels of San-Marco and the Panglossian Paradigm - a critique of the adaptationist program. *Proc R Soc Ser B-Bio 205*, 581-598.

Griffin, A.S., West, S.A., and Buckling, A. (2004). Cooperation and competition in pathogenic bacteria. *Nature 430*, 1024-1027.

Haagensen, J.A.J., Klausen, M., Ernst, R.K., Miller, S.I., Folkesson, A., Tolker-Nielsen, T., and Molin, S. (2007). Differentiation and distribution of colistin- and sodium dodecyl sulfate-tolerant cells in *Pseudomonas aeruginosa* biofilms. *J Bacteriol 189*, 28-37.

Haddadin, R.N.S., Saleh, S., Al-Adham, I.S.I., Buultjens, T.E.J., and Collier, P.J. (2010). The effect of subminimal inhibitory concentrations of antibiotics on virulence factors expressed by *Staphylococcus aureus* biofilms. *J Appl Microbiol 108*, 1281-1291.

Hall-Stoodley, L., Costerton, J.W., and Stoodley, P. (2004). Bacterial biofilms: From the natural environment to infectious diseases. *Nat Rev Microbiol 2*, 95-108.

Hallatschek, O., Hersen, P., Ramanathan, S., and Nelson, D.R. (2007). Genetic drift at expanding frontiers promotes gene segregation. *PNAS 104*, 19926-19930.

Hallem, E.A., and Sternberg, P.W. (2008). Acute carbon dioxide avoidance in *Caenorhabditis elegans*. *PNAS 105*, 8038-8043.

Hamilton, W.D. (1964a). Genetical Evolution of Social Behaviour I. *J Theor Biol 7*, 1-16.

Hamilton, W.D. (1964b). Genetical Evolution of Social Behaviour II. *J Theor Biol 7*, 17-52.

Hamilton, W.D. (1975). Innate social aptitudes of man: An approach from evolutionary genetics. *Biosocial Anthropology*, Ed Fox R (Malaby Press, London).

Harcombe, W. (2010). Novel cooperation experimentally evolved between species. *Evolution 64*, 2166-2172.

Harmsen, M., Yang, L.A., Pamp, S.J., and Tolker-Nielsen, T. (2010). An update on *Pseudomonas aeruginosa* biofilm formation, tolerance, and dispersal. *FEMS Immunol Med Microbiol 59*, 253-268.

Haubert, K., Drier, T., and Beebe, D. (2006). PDMS bonding by means of a portable, low-cost corona system. *Lab Chip 6*, 1548-1549.

Heo, Y.J., Chung, I.Y., Choi, K.B., and Cho, Y.H. (2007). R-Type pyocin is required for competitive growth advantage between *Pseudomonas aeruginosa* strains. *J Microbiol Biotechn 17*, 180-185.

Heo, Y.J., Ko, K.S., Song, J.H., and Cho, Y.H. (2005). Profiling pyocins and competitive growth advantages of various *Pseudomonas aeruginosa* strains. *J Microbiol Biotechn 15*, 1368-1376.

Heurlier, K., Denervaud, V., Haenni, M., Guy, L., Krishnapillai, V., and Haas, D. (2005). Quorum-sensing-negative (lasR) mutants of *Pseudomonas aeruginosa* avoid cell lysis and death. *J Bacteriol 187*, 4875-4883.

Hibbing, M.E., Fuqua, C., Parsek, M.R., and Peterson, S.B. (2010). Bacterial competition: surviving and thriving in the microbial jungle. *Nat Rev Microbiol 8*, 15-25.

Hillesland, K.L., and Stahl, D.A. (2010). Rapid evolution of stability and productivity at the origin of a microbial mutualism. *PNAS 107*, 2124-2129.

Ho, B.T., Basler, M., and Mekalanos, J.J. (2013). Type 6 Secretion System-mediated immunity to Type 4 Secretion System-mediated gene transfer. *Science 342*, 250-253.

Hoffman, L.R., D'Argenio, D.A., MacCoss, M.J., Zhang, Z.Y., Jones, R.A., and Miller, S.I. (2005). Aminoglycoside antibiotics induce bacterial biofilm formation. *Nature 436*, 1171-1175.

Hoiby, N., Bjarnsholt, T., Givskov, M., Molin, S., and Ciofu, O. (2010). Antibiotic resistance of bacterial biofilms. *Int J Antimicrob Ag 35*, 322-332.

Hol, F.J., Hubert, B., Dekker, C., and Keymer, J.E. (2015). Density-dependent adaptive resistance allows swimming bacteria to colonize an antibiotic gradient. *ISME J*, Epub ahead of print.

Holldobler, B. (1979). Territoriality in Ants. *P Am Philos Soc 123*, 211-218.

Imlay, J.A. (2013). The molecular mechanisms and physiological consequences of oxidative stress: lessons from a model bacterium. *Nat Rev Microbiol 11*, 443-454.

Imlay, J.A. (2015). Diagnosing oxidative stress in bacteria: not as easy as you might think. *Curr Opin Microbiol 24*, 124-131.

Inglis, R.F., Gardner, A., Cornelis, P., and Buckling, A. (2009). Spite and virulence in the bacterium *Pseudomonas aeruginosa*. *PNAS 106*, 5703-5707.

Jaqaman, K., Loerke, D., Mettlen, M., Kuwata, H., Grinstein, S., Schmid, S.L., and Danuser, G. (2008). Robust single-particle tracking in live-cell time-lapse sequences. *Nat Methods 5*, 695-702.

Jin, F., Conrad, J.C., Gibiansky, M.L., and Wong, G.C.L. (2011). Bacteria use Type-IV pili to slingshot on surfaces. *PNAS 108*, 12617-12622.

Jiricny, N., Diggle, S.P., West, S.A., Evans, B.A., Ballantyne, G., Ross-Gillespie, A., and Griffin, A.S. (2010). Fitness correlates with the extent of cheating in a bacterium. *J Evol Biol 23*, 738-747.

Julou, T., Mora, T., Guillon, L., Croquette, V., Schalk, I.J., Bensimon, D., and Desprat, N. (2013). Cell-cell contacts confine public goods diffusion inside *Pseudomonas aeruginosa* clonal microcolonies. *PNAS 110*, 12577-12582.

Kaeberlein, T., Lewis, K., and Epstein, S.S. (2002). Isolating "uncultivable" microorganisms in pure culture in a simulated natural environment. *Science 296*, 1127-1129.

Kaiser, D. (2003). Coupling cell movement to multicellular development in myxobacteria. *Nat Rev Microbiol 1*, 45-54.

Kamada, N., Chen, G.Y., Inohara, N., and Nunez, G. (2013). Control of pathogens and pathobionts by the gut microbiota. *Nat Immunol 14*, 685-690.

Kaplan, J.B. (2011). Antibiotic-induced biofilm formation. *Int J Artif Organs 34*, 737-751.

Kaplan, J.B., Izano, E.A., Gopal, P., Karwacki, M.T., Kim, S., Bose, J.L., Bayles, K.W., and Horswill, A.R. (2012). Low levels of beta-lactam antibiotics induce extracellular DNA release and biofilm formation in *Staphylococcus aureus*. *mBio 3*, e00198-00112.

Karatan, E., and Watnick, P. (2009). Signals, regulatory networks, and materials that build and break bacterial biofilms. *Microbiol Mol Biol* R *73*, 310-347.

Kato, J., Kim, H.E., Takiguchi, N., Kuroda, A., and Ohtake, H. (2008). *Pseudomonas aeruginosa* as a model microorganism for investigation of chemotactic behaviors in ecosystem. *J Biosci Bioeng 106*, 1-7.

Kearns, D.B., and Shimkets, L.J. (1998). Chemotaxis in a gliding bacterium. *PNAS 95*, 11957-11962.

Keller, L., and Surette, M.G. (2006). Communication in bacteria: an ecological and evolutionary perspective. *Nat Rev Microbiol 4*, 249-258.

Keren, I. (2013). Killing by bactericidal antibiotics does not depend on reactive oxygen species. *Science 340*, 1404-1404.

Kiewitz, C., and Tummler, B. (2000). Sequence diversity of *Pseudomonas aeruginosa*: Impact on population structure and genome evolution. *J Bacteriol 182*, 3125-3135.

Kim, W., Killam, T., Sood, V., and Surette, M.G. (2003). Swarm-cell differentiation in *Salmonella enterica serovar typhimurium* results in elevated resistance to multiple antibiotics. *J Bacteriol 185*, 3111-3117.

Kim, W., Racimo, F., Schluter, J., Levy, S.B., and Foster, K.R. (2014). Importance of positioning for microbial evolution. *PNAS 111*, E1639-E1647.

Klausen, M., Heydorn, A., Ragas, P., Lambertsen, L., Aaes-Jorgensen, A., Molin, S., and Tolker-Nielsen, T. (2003). Biofilm formation by *Pseudomonas aeruginosa* wild type, flagella and Type IV pili mutants. *Mol Microbiol 48*, 1511-1524.

Klitgord, N., and Segre, D. (2011). Ecosystems biology of microbial metabolism. *Curr Opin Biotech 22*, 541-546.

Kohanski, M.A., DePristo, M.A., and Collins, J.J. (2010a). Sublethal antibiotic treatment leads to multidrug resistance via radical-induced mutagenesis. *Mol Cell 37*, 311-320.

Kohanski, M.A., Dwyer, D.J., and Collins, J.J. (2010b). How antibiotics kill bacteria: from targets to networks. *Nat Rev Microbiol 8*, 423-435.

Kohanski, M.A., Dwyer, D.J., Hayete, B., Lawrence, C.A., and Collins, J.J. (2007). A common mechanism of cellular death induced by bactericidal antibiotics. *Cell 130*, 797-810.

Kohanski, M.A., Dwyer, D.J., Wierzbowski, J., Cottarel, G., and Collins, J.J. (2008). Mistranslation of membrane proteins and two-component system activation trigger antibiotic-mediated cell death. *Cell 135*, 679-690.

Kohler, T., Donner, V., and van Delden, C. (2010). Lipopolysaccharide as shield and receptor for R-pyocin-mediated killing in *Pseudomonas aeruginosa*. *J Bacteriol 192*, 1921-1928.

Kolter, R., and Greenberg, E.P. (2006). Microbial sciences - The superficial life of microbes. *Nature 441*, 300-302.

Korgaonkar, A., Trivedi, U., Rumbaugh, K.P., and Whiteley, M. (2013). Community surveillance enhances *Pseudomonas aeruginosa* virulence during polymicrobial infection. *PNAS 110*, 1059-1064.

Korgaonkar, A.K., and Whiteley, M. (2011). *Pseudomonas aeruginosa* enhances production of an antimicrobial in response to N-Acetylglucosamine and peptidoglycan. *J Bacteriol 193*, 909-917.

Kreikenbohm, R., and Bohl, E. (1986). A Mathematical-model of syntrophic cocultures in the chemostat. *FEMS Microbiol Ecol 38*, 131-140.

Kumar, A., and Ting, Y.P. (2013). Effect of sub-inhibitory antibacterial stress on bacterial surface properties and biofilm formation. *Colloid Surf B Biointerfaces 111*, 747-754.

Kummerli, R., and Brown, S.P. (2010). Molecular and regulatory properties of a public good shape the evolution of cooperation. *PNAS 107*, 18921-18926.

Lai, S., Tremblay, J., and Deziel, E. (2009). Swarming motility: a multicellular behaviour conferring antimicrobial resistance. *Environ Microbiol 11*, 126-136.

Lambert, G., Estevez-Salmeron, L., Oh, S., Liao, D., Emerson, B.M., Tlsty, T.D., and Austin, R.H. (2011). An analogy between the evolution of drug resistance in bacterial communities and malignant tissues. *Nat Rev Cancer 11*, 375-382.

Lambertsen, L., Sternberg, C., and Molin, S. (2004). Mini-Tn7 transposons for site-specific tagging of bacteria with fluorescent proteins. *Environ Microbiol 6*, 726-732.

Lamont, I.L., Beare, P.A., Ochsner, U., Vasil, A.I., and Vasil, M.L. (2002). Siderophore-mediated signaling regulates virulence factor production in *Pseudomonas aeruginosa*. *PNAS 99*, 7072-7077.

Lee, K.W.K., Periasamy, S., Mukherjee, M., Xie, C., Kjelleberg, S., and Rice, S.A. (2014). Biofilm development and enhanced stress resistance of a model, mixed-species community biofilm. *ISME J 8*, 894-907.

LeRoux, M. et al. (2015). Kin cell lysis is a danger signal that activates antibacterial pathways of *Pseudomonas aeruginosa*. *eLife* 4:05701.

Liberati, N.T., Urbach, J.M., Miyata, S., Lee, D.G., Drenkard, E., Wu, G., Villanueva, J., Wei, T., and Ausubel, F.M. (2006). An ordered, nonredundant library of *Pseudomonas aeruginosa* strain PA14 transposon insertion mutants. *PNAS 103*, 19931-19931.

Linares, J.F., Gustafsson, I., Baquero, F., and Martinez, J.L. (2006). Antibiotics as intermicrobial signaling agents instead of weapons. *PNAS 103*, 19484-19489.

Lister, P.D., Wolter, D.J., and Hanson, N.D. (2009). Antibacterial-resistant *Pseudomonas aeruginosa*: clinical impact and complex regulation of chromosomally encoded resistance mechanisms. *Clin Microbiol Rev 22*, 582-610.

Little, A.E.F., Robinson, C.J., Peterson, S.B., Raffa, K.E., and Handelsman, J. (2008). Rules of engagement: interspecies interactions that regulate microbial communities. *Annu Rev Microbiol 62*, 375-401.

Liu, Y.Y., and Imlay, J.A. (2013). Cell death from antibiotics without the involvement of reactive oxygen species. *Science 339*, 1210-1213.

Lobritz, M.A., Belenky, P., Porter, C.B.M., Gutierrez, A., Yang, J.H., Schwarz, E.G., Dwyer, D.J., Khalil, A.S., and Collins, J.J. (2015). Antibiotic efficacy is linked to bacterial cellular respiration. *PNAS 112*, 8173-8180.

Lomovskaya, O., Warren, M.S., Lee, A., Galazzo, J., Fronko, R., Lee, M., Blais, J., Cho, D., Chamberland, S., Renau, T.*, et al.* (2001). Identification and characterization of inhibitors of multidrug resistance efflux pumps in *Pseudomonas aeruginosa*: Novel agents for combination therapy. *Antimicrob Agents Chemother 45*, 105-116.

Lopez, D., Vlamakis, H., and Kolter, R. (2010). Biofilms. *Csh Perspect Biol 2*.

Lozupone, C.A., and Knight, R. (2007). Global patterns in bacterial diversity. *PNAS 104*, 11436-11440.

MacLean, R.C., and Gudelj, I. (2006). Resource competition and social conflict in experimental populations of yeast. *Nature 441*, 498-501.

Mah, T.F., Pitts, B., Pellock, B., Walker, G.C., Stewart, P.S., and O'Toole, G.A. (2003). A genetic basis for *Pseudomonas aeruginosa* biofilm antibiotic resistance. *Nature 426*, 306-310.

Mahenthiralingam, E., Campbell, M.E., Foster, J., Lam, J.S., and Speert, D.P. (1996). Random amplified polymorphic DNA typing of *Pseudomonas aeruginosa* isolates recovered from patients with cystic fibrosis. *J Clin Microbiol 34*, 1129-1135.

Martiny, J.B.H., Bohannan, B.J.M., Brown, J.H., Colwell, R.K., Fuhrman, J.A., Green, J.L., Horner-Devine, M.C., Kane, M., Krumins, J.A., Kuske, C.R.*, et al.* (2006). Microbial biogeography: putting microorganisms on the map. *Nat Rev Microbiol 4*, 102-112.

Masduki, A., Nakamura, J., Ohga, T., Umezaki, R., Kato, J., and Ohtake, H. (1995). Isolation and characterization of chemotaxis mutants and genes of *Pseudomonas aeruginosa. J Bacteriol 177*, 948-952.

Mashburn, L.M., Jett, A.M., Akins, D.R., and Whiteley, M. (2005). *Staphylococcus aureus* serves as an iron source for *Pseudomonas aeruginosa* during in vivo coculture. *J Bacteriol 187*, 554-566.

May, R.M., and McLean, A.R. (2007). *Theoretical ecology: principles and applications*, 3rd edn (Oxford ; New York: Oxford University Press).

Maynard Smith, J., and Harper, D. (2003). *Animal signals* (Oxford: Oxford University Press).

Mee, M.T., Collins, J.J., Church, G.M., and Wang, H.H. (2014). Syntrophic exchange in synthetic microbial communities. *PNAS 111*, E2149-E2156.

Michel-Briand, Y., and Baysse, C. (2002). The pyocins of *Pseudomonas aeruginosa*. *Biochimie 84*, 499-510.

Migliore, L., Rotini, A., and Thaller, M.C. (2013). Low doses of tetracycline trigger the *E. Coli* growth: a case of hormetic response. *Dose-Response 11*, 550-557.

Mitri, S., and Foster, K.R. (2013). The genotypic view of social interactions in microbial communities. *Annu Rev Genet 47*, 247-273.

Mitri, S., Xavier, J.B., and Foster, K.R. (2011). Social evolution in multispecies biofilms. *PNAS 108*, 10839-10846.

Moller, S., Sternberg, C., Andersen, J.B., Christensen, B.B., Ramos, J.L., Givskov, M., and Molin, S. (1998). In situ gene expression in mixed-culture biofilms: Evidence of metabolic interactions between community members. *App Environ Microbiol 64*, 721-732.

Momeni, B., Waite, A.J., and Shou, W. (2013). Spatial self-organization favors heterotypic cooperation over cheating. *eLife 2*, e00960.

Monds, R.D., and O'Toole, G.A. (2009). The developmental model of microbial biofilms: ten years of a paradigm up for review. *Trends Microbiol 17*, 73-87.

Morris, J.J., Johnson, Z.I., Szul, M.J., Keller, M., and Zinser, E.R. (2011). Dependence of the cyanobacterium Prochlorococcus on hydrogen peroxide scavenging microbes for growth at the ocean's surface. *PLoS one 6*, e16805.

Morris, J.J., Lenski, R.E., and Zinser, E.R. (2012). The Black Queen Hypothesis: evolution of dependencies through adaptive gene loss. *mBio 3*, e00036-12.

Motta, S.S., Cluzel, P., and Aldana, M. (2015). Adaptive resistance in bacteria requires epigenetic inheritance, genetic noise, and cost of efflux pumps. *PLoS one 10*, e0118464.

Moulton, R.C., and Montie, T.C. (1979). Chemotaxis by *Pseudomonas aeruginosa*. *J Bacteriol 137*, 274-280.

Murray, J.L., Connell, J.L., Stacy, A., Turner, K.H., and Whiteley, M. (2014). Mechanisms of synergy in polymicrobial infections. *J Microbiol 52*, 188-199.

Nadell, C.D., and Bassler, B.L. (2011). A fitness trade-off between local competition and dispersal in *Vibrio cholerae* biofilms. *PNAS 108*, 14181-14185.

Nadell, C.D., Foster, K.R., and Xavier, J.B. (2010). Emergence of spatial structure in cell groups and the evolution of cooperation. *PLoS Comp Biol 6*, e1000716.

Nadell, C.D., Xavier, J.B., and Foster, K.R. (2009). The sociobiology of biofilms. *FEMS Microbiol Rev 33*, 206-224.

Nickel, J.C., Wright, J.B., Ruseska, I., Marrie, T.J., Whitfield, C., and Costerton, J.W. (1985). Antibiotic resistance of *Pseudomonas aeruginosa* colonizing a urinary catheter in vitro. *Eur J Clin Microbiol 4*, 213-218.

Nogueira, T., Rankin, D.J., Touchon, M., Taddei, F., Brown, S.P., and Rocha, E.P. (2009). Horizontal gene transfer of the secretome drives the evolution of bacterial cooperation and virulence. *Curr Biol 19*, 1683-1691.

Nowak, M.A., and May, R.M. (1992). Coexistence and competition in HIV infections. *J Theor Biol 159*, 329-342.

O'malley, M.A. (2009). What did Darwin say about microbes, and how did microbiology respond? *Trends Microbiol 17*, 341-347.

O'Toole, G.A., and Kolter, R. (1998). Flagellar and twitching motility are necessary for *Pseudomonas aeruginosa* biofilm development. *Mol Microbiol 30*, 295-304.

Ohga, T., Masduki, A., Kato, J., and Ohtake, H. (1993). Chemotaxis away from thiocyanic and isothiocyanic esters in *Pseudomonas aeruginosa*. *FEMS Microbiol Lett 113*, 63-66.

Oliveira, N.M., Durham, W.M., Foster, K.R. Single-cell twitching chemotaxis during biofilm formation. In review.

Oliveira, N.M., Martinez-Garcia, E., Xavier, J., Durham, W.M., Kolter, R., Kim, W., Foster, K.R. (2015). Biofilm formation as a response to ecological competition. *PLoS Biol* 13(7):e1002191.

Oliveira, N.M., Niehus, R., and Foster, K.R. (2014). Evolutionary limits to cooperation in microbial communities. *PNAS 111*, 17941-17946.

Overhage, J., Bains, M., Brazas, M.D., and Hancock, R.E.W. (2008). Swarming of *Pseudomonas aeruginosa* is a complex adaptation leading to increased production of virulence factors and antibiotic resistance. *J Bacteriol 190*, 2671-2679.

Pande, S., Merker, H., Bohl, K., Reichelt, M., Schuster, S., de Figueiredo, L.F., Kaleta, C., and Kost, C. (2013). Fitness and stability of obligate cross-feeding interactions that emerge upon gene loss in bacteria. *ISME J 8*, 953-962.

Papke, R.T., and Gogarten, J.P. (2012). How Bacterial Lineages Emerge. *Science 336*, 45-46.

Penterman, J., Nguyen, D., Anderson, E., Staudinger, B.J., Greenberg, E.P., Lam, J.S., and Singh, P.K. (2014a). Rapid evolution of culture-impaired bacteria during adaptation to biofilm growth. *Cell Rep 6*, 293-300.

Penterman, J., Singh, P.K., and Walker, G.C. (2014b). Biological cost of pyocin production during the SOS response in *Pseudomonas aeruginosa*. *J Bacteriol 196*, 3351-3359.

Pernet, E., Guillemot, L., Burgel, P.R., Martin, C., Lambeau, G., Sermet-Gaudelus, I., Sands, D., Leduc, D., Morand, P.C., Jeammet, L.*, et al.* (2014). *Pseudomonas*

aeruginosa eradicates *Staphylococcus aureus* by manipulating the host immunity. *Nat Commun 5*, 5105.

Porter, S.L., Wadhams, G.H., and Armitage, J.P. (2011). Signal processing in complex chemotaxis pathways. *Nat Rev Microbiol 9*, 153-165.

Qi, Q., Preston, G.M., and MacLean, R.C. (2014). Linking system-wide impacts of RNA polymerase mutations to the fitness cost of rifampin resistance in *Pseudomonas aeruginosa*. *mBio 5*, e01562-14

Rainey, P.B., and Rainey, K. (2003). Evolution of cooperation and conflict in experimental bacterial populations. *Nature 425*, 72-74.

Rankin, D.J., Rocha, E.P.C., and Brown, S.P. (2011). What traits are carried on mobile genetic elements, and why? *Heredity 106*, 1-10.

Ratcliff, W.C., and Denison, R.F. (2011). Alternative actions for antibiotics. *Science 332*, 547-548.

Raymond, B., West, S.A., Griffin, A.S., and Bonsall, M.B. (2012). The dynamics of cooperative bacterial virulence in the field. *Science 337*, 85-88.

Ren, D., Madsen, J.S., de la Cruz-Perera, C.I., Bergmark, L., Sorensen, S.J., and Burmolle, M. (2014a). High-throughput screening of multispecies biofilm formation and quantitative PCR-based assessment of individual species proportions, useful for exploring interspecific bacterial interactions. *Microb Ecol 68*, 146-154.

Ren, D., Madsen, J.S., Sorensen, S.J., and Burmolle, M. (2014b). High prevalence of biofilm synergy among bacterial soil isolates in cocultures indicates bacterial interspecific cooperation. *ISME J* 9, 81-89.

Renau, T.E., Leger, R., Flamme, E.M., Sangalang, J., She, M.W., Yen, R., Gannon, C.L., Griffith, D., Chamberland, S., Lomovskaya, O.*, et al.* (1999). Inhibitors of efflux pumps in *Pseudomonas aeruginosa* potentiate the activity of the fluoroquinolone antibacterial levofloxacin. *J Med Chem 42*, 4928-4931.

Renders, N., Verbrugh, H., and Van Belkum, A. (2001). Dynamics of bacterial colonisation in the respiratory tract of patients with cystic fibrosis. *Infect Genet Evol 1*, 29-39.

Riley, M.A., and Wertz, J.E. (2002). Bacteriocins: evolution, ecology, and application. *Annu Rev Microbiol 56*, 117-137.

Rivero, M.A., Tranquillo, R.T., Buettner, H.M., and Lauffenburger, D.A. (1989). Transport models for chemotactic cell-populations based on individual cell behavior. *Chem Eng Sci 44*, 2881-2897.

Robeson, M.S., King, A.J., Freeman, K.R., Birky, C.W., Martin, A.P., and Schmidt, S.K. (2011). Soil rotifer communities are extremely diverse globally but spatially autocorrelated locally. *PNAS 108*, 4406-4410.

Rodriguez, G.G., Phipps, D., Ishiguro, K., and Ridgway, H.F. (1992). Use of a fluorescent redox probe for direct visualization of actively respiring bacteria. *Appl Environ Microbiol 58*, 1801-1808.

Roesch, L.F., Fulthorpe, R.R., Riva, A., Casella, G., Hadwin, A.K., Kent, A.D., Daroub, S.H., Camargo, F.A., Farmerie, W.G., and Triplett, E.W. (2007). Pyrosequencing enumerates and contrasts soil microbial diversity. *ISME J 1*, 283-290.

Rojo, F. (2010). Carbon catabolite repression in Pseudomonas: optimizing metabolic versatility and interactions with the environment. *FEMS Microbil Rev 34*, 658-684.

Romling, U., Kjelleberg, S., Normark, S., Nyman, L., Uhlin, B.E., and Akerlund, B. (2014). Microbial biofilm formation: a need to act. *J Int Med* 276, 98-110.

Rumbaugh, K.P., Diggle, S.P., Watters, C.M., Ross-Gillespie, A., Griffin, A.S., and West, S.A. (2009). Quorum sensing and the social evolution of bacterial virulence. *Curr Biol 19*, 341-345.

Sachs, J.L., and Hollowell, A.C. (2012). The origins of cooperative bacterial communities. *mBio 3*, e00099-12.

Sachs, J.L., Mueller, U.G., Wilcox, T.P., and Bull, J.J. (2004). The evolution of cooperation. *Q Rev Biol 79*, 135-160.

Saeidi, N., Wong, C.K., Lo, T.M., Nguyen, H.X., Ling, H., Leong, S.S.J., Poh, C.L., and Chang, M.W. (2011). Engineering microbes to sense and eradicate *Pseudomonas aeruginosa*, a human pathogen. *Mol Syst Biol 7*, 521.

Sampedro, I., Parales, R.E., Krell, T., and Hill, J.E. (2014). Pseudomonas chemotaxis. *FEMS Microbiol Rev 39*, 17-46.

Sandoz, K.M., Mitzimberg, S.M., and Schuster, M. (2007). Social cheating in *Pseudomonas aeruginosa* quorum sensing. *PNAS 104*, 15876-15881.

Santelli, C.M., Orcutt, B.N., Banning, E., Bach, W., Moyer, C.L., Sogin, M.L., Staudigel, H., and Edwards, K.J. (2008). Abundance and diversity of microbial life in ocean crust. *Nature 453*, 653-657.

Savoia, D., and Zucca, M. (2007). Clinical and environmental Burkholderia strains: Biofilm production and intracellular survival. *Curr Microbiol 54*, 440-444.

Saxer, G., Doebeli, M., and Travisano, M. (2009). Spatial structure leads to ecological breakdown and loss of diversity. *P Roy Soc B-Biol Sci 276*, 2065-2070.

Schindelin, J., Arganda-Carreras, I., Frise, E., Kaynig, V., Longair, M., Pietzsch, T., Preibisch, S., Rueden, C., Saalfeld, S., Schmid, B*., et al.* (2012). Fiji: an open-source platform for biological-image analysis. *Nat Methods 9*, 676-682.

Schink, B. (2002). Synergistic interactions in the microbial world. *Anton Leeuw Int J G 81*, 257-261.

Schreiber, S., Konradt, M., Groll, C., Scheid, P., Hanauer, G., Werling, H.O., Josenhans, C., and Suerbaum, S. (2004). The spatial orientation of *Helicobacter pylori* in the gastric mucus. *PNAS 101*, 5024-5029.

Semmler, A.B.T., Whitchurch, C.B., and Mattick, J.S. (1999). A re-examination of twitching motility in *Pseudomonas aeruginosa*. *Microbiology 145*, 2863-2873.

Seymour, J.R., Marcos, and Stocker, R. (2009). Resource patch formation and exploitation throughout the marine microbial food web. *Am Nat 173*, E15-E29.

Shen, Y., Siryaporn, A., Lecuyer, S., Gitai, Z., and Stone, H.A. (2012). Flow directs surface-attached bacteria to twitch upstream. *Biophys J 103*, 146-151.

Sherr, B.F., del Giorgio, P., and Sherr, E.B. (1999). Estimating abundance and single-cell characteristics of respiring bacteria via the redox dye CTC. *Aquat Microb Ecol 18*, 117-131.

Shi, W.Y., Kohler, T., and Zusman, D.R. (1993). Chemotaxis plays a role in the social-behavior of *Myxococcus xanthus*. *Mol Microbiol 9*, 601-611.

Shi, W.Y., Ngok, F.K., and Zusman, D.R. (1996). Cell density regulates cellular reversal frequency in *Myxococcus xanthus*. *PNAS 93*, 4142-4146.

Shou, W.Y., Ram, S., and Vilar, J.M.G. (2007). Synthetic cooperation in engineered yeast populations. *PNAS 104*, 1877-1882.

Skerker, J.M., and Berg, H.C. (2001). Direct observation of extension and retraction of Type IV pili. *PNAS 98*, 6901-6904.

Sogin, M.L., Morrison, H.G., Huber, J.A., Mark Welch, D., Huse, S.M., Neal, P.R., Arrieta, J.M., and Herndl, G.J. (2006). Microbial diversity in the deep sea and the underexplored "rare biosphere". *PNAS 103*, 12115-12120.

Stewart, P.S. (2002). Mechanisms of antibiotic resistance in bacterial biofilms. *Int J Med Microbiol 292*, 107-113.

Stewart, P.S., and Franklin, M.J. (2008). Physiological heterogeneity in biofilms. *Nat Rev Microbiol 6*, 199-210.

Stewart, P.S., Franklin, M.J., Williamson, K.S., Folsom, J.P., Boegli, L., and James, G.A. (2015). Contribution of stress responses to antibiotic tolerance in *Pseudomonas aeruginosa* biofilms. *Antimicrob Agents Chemother 59*, 3838-3847.

Storz, G., Hengge, R., and American Society for Microbiology. (2011). *Bacterial stress responses*, 2nd edn (Washington, DC: ASM Press).

Stover, C.K., Pham, X.Q., Erwin, A.L., Mizoguchi, S.D., Warrener, P., Hickey, M.J., Brinkman, F.S.L., Hufnagle, W.O., Kowalik, D.J., Lagrou, M.*, et al.* (2000). Complete genome sequence of *Pseudomonas aeruginosa* PAO1, an opportunistic pathogen. *Nature 406*, 959-964.

Suh, G.S.B., Wong, A.M., Hergarden, A.C., Wang, J.W., Simon, A.F., Benzer, S., Axel, R., and Anderson, D.J. (2004). A single population of olfactory sensory neurons mediates an innate avoidance behaviour in Drosophila. *Nature 431*, 854-859.

Taylor, R.G., and Welch, R.D. (2008). Chemotaxis as an emergent property of a swarm. *J Bacteriol 190*, 6811-6816.

Traxler, M., F., Watrous, J.D., Alexandrov, T., Dorrestein, P.C., and Kolter, R. (2013). Interspecies interactions stimulate diversification of the *Streptomyces coelicolor* secreted metabolome. *mBio 4*, e00459.

Tseng, B.S., Zhang, W., Harrison, J.J., Quach, T.P., Song, J.L., Penterman, J., Singh, P.K., Chopp, D.L., Packman, A.I., and Parsek, M.R. (2013). The extracellular matrix protects *Pseudomonas aeruginosa* biofilms by limiting the penetration of tobramycin. *Environ Microbiol 15*, 2865-2878.

Tso, W.W., and Adler, J. (1974). Negative Chemotaxis in *Escherichia coli*. *J Bacteriol 118*, 560-576.

Tsui, W.H.W., Yim, G., Wang, H.H.M., McClure, J.E., Surette, M.G., and Davies, J. (2004). Dual effects of MLS antibiotics: Transcriptional modulation and interactions on the ribosome. *Chem Biol*, 1307-1316.

Turing, A.M. (1950). Computer Machinery and Intelligence. MIND – *Q Rev Psych Phil 59* 433-460.

Van Dyken, J.D., Muller, M.J., Mack, K.M., and Desai, M.M. (2013). Spatial population expansion promotes the evolution of cooperation in an experimental Prisoner's Dilemma. *Curr Biol 23*, 919-923.

Varma, A., and Chincholkar, S.B. (2007). *Microbial siderophores* (Berlin ; New York: Springer).

Vetsigian, K., Jajoo, R., and Kishony, R. (2011). Structure and evolution of Streptomyces interaction networks in soil and in silico. *PLoS Biol 9*, e1001184.

Visca, P., Imperi, F., and Lamont, I.L. (2007). Pyoverdine siderophores: from biogenesis to biosignificance. *Trends Microbiol 15*, 22-30.

Visser, A.W., and Kiorboe, T. (2006). Plankton motility patterns and encounter rates. *Oecologia 148*, 538-546.

Wadhams, G.H., and Armitage, J.P. (2004). Making sense of it all: Bacterial chemotaxis. *Nat Rev Mol Cell Bio 5*, 1024-1037.

Waite, R.D., and Curtis, M.A. (2009). *Pseudomonas aeruginosa* PAO1 pyocin production affects population dynamics within mixed-culture biofilms. *J Bacteriol 191*, 1349-1354.

Wang, M.Z., Schaefer, A.L., Dandekar, A.A., and Greenberg, E.P. (2015). Quorum sensing and policing of *Pseudomonas aeruginosa* social cheaters. *PNAS 112*, 2187-2191.

Wang, Q., Sun, F.J., Liu, Y., Xiong, L.R., Xie, L.L., and Xia, P.Y. (2010). Enhancement of biofilm formation by subinhibitory concentrations of macrolides in icaADBC-positive and -negative clinical isolates of *Staphylococcus epidermidis*. *Antimicrob Agents Chemother 54*, 2707-2711.

Wanner, G., Vogl, K., and Overmann, J. (2008). Ultrastructural characterization of the prokaryotic symbiosis in "Chlorochromatium aggregatum". *J Bacteriol 190*, 3721-3730.

Webb, J.S., Thompson, L.S., James, S., Charlton, T., Tolker-Nielsen, T., Koch, B., Givskov, M., and Kjelleberg, S. (2003). Cell death in *Pseudomonas aeruginosa* biofilm development. *J Bacteriol 185*, 4585-4592.

West, S.A., and Buckling, A. (2003). Cooperation, virulence and siderophore production in bacterial parasites. *Proc Biol Sci 270*, 37-44.

West, S.A., Diggle, S.P., Buckling, A., Gardner, A., and Griffins, A.S. (2007a). The social lives of microbes. *Annu Rev Ecol Evol S 38*, 53-77.

West, S.A., Griffin, A.S., and Gardner, A. (2007b). Social semantics: altruism, cooperation, mutualism, strong reciprocity and group selection. *J Evol Biol 20*, 415-432.

West, S.A., Griffin, A.S., Gardner, A., and Diggle, S.P. (2006). Social evolution theory for microorganisms. *Nat Rev Microbiol 4*, 597-607.

Wintermute, E.H., and Silver, P.A. (2010). Emergent cooperation in microbial metabolism. *Mol Syst Biol 6*, 407.

Wu, A., Loutherback, K., Lambert, G., Estevez-Salmeron, L., Tlsty, T.D., Austin, R.H., and Sturm, J.C. (2013). Cell motility and drug gradients in the emergence of resistance to chemotherapy. *PNAS 110*, 16103-16108.

Xavier, J.B., Kim, W., and Foster, K.R. (2011). A molecular mechanism that stabilizes cooperative secretions in *Pseudomonas aeruginosa. Mol Microbiol 79*, 166-179.

Yim, G., Wang, H.M.H., and Davies, J. (2007). Antibiotics as signalling molecules. *Philos T R Soc B 362*, 1195-1200.

Yooseph, S., Sutton, G., Rusch, D.B., Halpern, A.L., Williamson, S.J., Remington, K., Eisen, J.A., Heidelberg, K.B., Manning, G., Li, W.Z.*, et al.* (2007). The sorcerer II

global ocean sampling expedition: Expanding the universe of protein families. *PLoS Biol 5*, 432-466.

Zelezniak, A., Andrejev, S., Ponomarova, O., Mende, D.R., Bork, P., and Patil, K.R. (2015). Metabolic dependencies drive species co-occurrence in diverse microbial communities. *PNAS 112*, 6449-6454.

Zhang, Q.C., Lambert, G., Liao, D., Kim, H., Robin, K., Tung, C.K., Pourmand, N., and Austin, R.H. (2011). Acceleration of emergence of bacterial antibiotic resistance in connected microenvironments. *Science 333*, 1764-1767.

Zhang, Y., Ducret, A., Shaevitz, J., and Mignot, T. (2012). From individual cell motility to collective behaviors: insights from a prokaryote, *Myxococcus xanthus*. *FEMS Microbiol Rev 36*, 149-164.

Zhao, K., Tseng, B.S., Beckerman, B., Jin, F., Gibiansky, M.L., Harrison, J.J., Luijten, E., Parsek, M.R., and Wong, G.C.L. (2013). Psl trails guide exploration and microcolony formation in *Pseudomonas aeruginosa* biofilms. *Nature 497*, 388-391.

8. Appendix

Supplementary materials of Chapter 2	149
Supplementary materials of Chapter 3	161
Supplementary materials of Chapter 4	170
Supplementary materials of Chapter 5	191
Antibiosis drives exploitative competition[3]	197
Published work	202

Supplementary materials of Chapter 2

SI Materials and Methods

Here, we present an extended version of the methods used in the paper.

Ordinary differential equation models with fixed investment into secretion. There is a large literature on the evolution of single microbial secretions - often known as studies of cheaters and cooperators - that includes both theory (Brown and Johnstone, 2001; Cremer et al., 2012; Frank, 2010; West and Buckling, 2003) and empirical tests (Chuang et al., 2009; Diggle et al., 2007; Griffin et al., 2004; Rumbaugh et al., 2009). Our goal here is to build directly upon this work. We, therefore, base our models on two recent and detailed studies of single secretions (Chuang et al., 2009; Cremer et al., 2012). These studies assume that cells land in patches stochastically, such that the number of cells across patches follows a Poisson distribution (Poisson-based seeding, Figure S9). Such seeding is based on the realistic assumption that the number of cells

[3] Preliminary data.

per patch is not deterministic and the same across patches but random. Earlier models used simpler demographies, but this does not affect our conclusions (Figure S9), such that our model also recapitulates the predictions of other studies of single secretions (Frank, 2010; West and Buckling, 2003).

We model the population dynamics of microbial genotypes growing in a well-mixed environment using systems of ordinary differential equations (ODEs). Each system is composed by 2^s equations, where *s* is number of traits (secretions) in a given model and each equation represents the population dynamics of a given microbial genotype in each subpopulation. The total number of genotypes in each model is, thus, captured by binary combinatorics; each genotype is labeled by a binary string, where one and zero mean production or nonproduction of a certain trait, respectively. Here we explain the two-trait model but the framework is equivalent for the one-trait, three-trait and four-trait cases presented in the main text. For a system of two cooperative traits, the four genotypes, [1,1], [1,0], [0,1] and [0,0], grow according to the following general form:

$$\frac{dg_i}{dt} = (r - (i + j) \cdot c) \cdot g_{ij} \cdot \left(1 - \frac{\sum g}{K}\right)$$

where g_{ij} represents the density of individuals of genotype [i,j] in each subpopulation, $[(\mathrm{i},\mathrm{j}) \in \{1,0\}^s]$, and *s* being the number of traits. Specifically for the two-trait model, one has the following system of four ODEs:

$$\begin{cases} \frac{dg_{11}}{dt} = (r - (1+1)\cdot c)\cdot g_{11}\cdot\left(1 - \frac{g_{11}+g_{10}+g_{01}+g_{00}}{K}\right) \\ \frac{dg_{10}}{dt} = (r - (1+0)\cdot c)\cdot g_{10}\cdot\left(1 - \frac{g_{11}+g_{10}+g_{01}+g_{00}}{K}\right) \\ \frac{dg_{01}}{dt} = (r - (0+1)\cdot c)\cdot g_{01}\cdot\left(1 - \frac{g_{11}+g_{10}+g_{01}+g_{00}}{K}\right) \\ \frac{dg_{00}}{dt} = (r - (0+0)\cdot c)\cdot g_{00}\cdot\left(1 - \frac{g_{11}+g_{10}+g_{01}+g_{00}}{K}\right) \end{cases}$$

where *r* is the intrinsic growth rate (here assumed 1 for simplicity), and *c* the cost of producing each trait. Note that we assume here additive costs for secretion production (given by the summation of the genotype index). We also considered nonlinear costs, both accelerating and decelerating, and these do not qualitatively affect our conclusions (Figure S6). Importantly, *K* (the carrying capacity of the environment) is a function of the traits available (here given by the frequency of producers of each trait) and has the following general form:

$$K = K_{basal} + K_{\max B}\left(\frac{g_{11}+g_{10}}{g_{11}+g_{10}+g_{01}+g_{00}}\cdot\frac{g_{11}+g_{01}}{g_{11}+g_{10}+g_{01}+g_{00}}\right)$$

where K_{basal} and K_{maxB} are constants representing the minimal carrying capacity of the system and the maximum benefit from secretions, respectively (here $K_{basal} = 1$, $K_{maxB} = 100000$). Note that we use multiplicative benefits as we assume that all cooperative traits are essential, which together with K_{basal} being 1 represents the requirement of cells having access to all secretions to be able to grow. However, we also vary the strength of selection by considering increasing values of K_{basal}. Figure S1 shows that increasing K_{basal} reduces the potential for between-genotype cooperation but when it evolves it does so under the same demographic conditions, intermediate values of genetic mixing. Moreover, given it is not fully known how *K* scales with secretions we

additionally implemented an additive version where now we consider additive benefits instead of multiplicative (Figure S8). Again, the evolution of between-genotype cooperation is restricted to intermediate values of genetic mixing. To model the effect of niche overlap on the evolution of between-genotype cooperation we analyzed an extension of the two-trait model presented above, where we considered eight genotypes belonging to two different species. In this case, only genotypes from the same species compete for resources (Figure S4).

We consider a standard lifecycle of microbes (see the work by Cremer and colleagues (Cremer et al., 2012) and references therein for further discussion of the lifecycle): (*i*) formation, where a random number of cells is allocated to each subpopulation (based on a Poisson process with mean n_0), in a set of M subpopulations (here $M = 1000$), and the identity of each cell follows a uniform distribution based on the frequency of each genotype (which we assumed the same for all genotypes at the beginning, *G0*); (*ii*) growth, where genotypes in each group proliferate according to logistic dynamics (until saturation is reached), and (*iii*) merging, where the M groups are merged together and the global genotypic frequencies are updated. After a full cycle of seeding, growth and merging (equivalent to one generation), new patches are seeded according to the re-calculated genotypic frequency. These cycles are repeated for G generations (typically 1000), which is sufficient for genotypic frequencies reaching equilibrium.

ODE models with variable investment into secretion. To model the evolution of investment into secretion production, we implemented two different frameworks, here called discrete and continuous models for the evolution of investment. In the discrete version we simply extended our model described above to allow strains to invest in

three different levels of secretion (0.5, 1, 2). We thus considered the genotypes [0.5,0.5], [1,1], [2,2], [0.5,0], [1,0], [2,0], [0,0.5], [0,1], [0,2] and [0,0], and show that [2,2] evolves under low mixing but [0.5,0] and [0,0.5] will evolve under the conditions favoring cross-feeding. Here, we assume for simplicity that full producers invest the same to both secretions but we find the same qualitative results when we drop this assumption (Figure S5).

In the continuous version, we use the same lifecycle but add a mutation phase, where we allow for mutations that can either increase or decrease the investment into cooperation. The lifecycle is then, (*i*) formation; (*ii*) mutation, where each cell of the subpopulation mutates its parameter *x*, which governs how much a cell invests into its public goods; (*iii*) growth; and (4) merging. In the growth phase, the evolution of each single subpopulation is governed by a set of *z* ordinary differential equations, where *z* is the number of individuals that inhabit each subpopulation after mutation. Each initial cell *z* then proliferates according to the general ODE

$$\frac{dg_{x,ij}}{dt} = (r - (i+j)\cdot x \cdot c)\cdot g_{x,ij}\cdot\left(1 - \frac{\sum g}{K}\right)$$

where $g_{x,ij}$ represents the density of cell type with genotype [i,j] and investment *x*, and *K* is still a function of the secretions available (given by the frequency of secretors), which now incorporates explicitly the evolvable investment *x* of cells:

$$K = K_{basal} + K_{\max B}\left(\frac{x\cdot g_{11} + x\cdot g_{10}}{g_{11}+g_{10}+g_{01}+g_{00}}\cdot\frac{x\cdot g_{11} + x\cdot g_{01}}{g_{11}+g_{10}+g_{01}+g_{00}}\right)$$

Thus, the genotypes are now effectively $x \cdot g_{ij}$, not g_{ij} as before. For example, if $x = 2$, [1,1] will behave as a genotype [2,2] as we assume for simplicity that full producers will evolve the same level of investment for both traits.

Individual-based model. We used an individual-based model to examine the effects of spatial structure on our predictions. In particular we ask if between-genotype cooperation can evolve if secreted traits have limited diffusion, which may be common on surfaces (Julou et al., 2013). To capture the effect of diffusion we use spatial simulations that consider 2D lattices with periodic boundaries. Cells can only divide into empty spaces of their closest neighborhood (eight spaces around the focal individual), and the effect of a public good is limited to a neighborhood of a certain size around the producer cell. This spatial version is based upon the same assumptions as the previous model for homogenous environments and it uses an adaptation of the Gillespie algorithm for simulating population dynamics in continuous time (Allen and Dytham, 2009). Although exactly equivalent to the Direct Method by Gillespie (Gillespie, 1977), this alternative is computationally more efficient and can easily handle large populations of individuals with individual properties according to rules for cellular growth. At each sampled time step, a focal individual is selected with uniform probability, and a cell division event is then realized with a probability directly proportional to its growth rate, which depends on population density and the presence of public goods, following logistic kinetics. The stochasticity of cell division adds extra variance to the final genotypic composition of the simulated patches when compared to the deterministic growth in the ODE version. Thus, the results of the individual-based model and the ODE model are not always identical for identical parameter values with cooperation typically emerging more easily in the individual

based model. Nevertheless, we can use the individual-based model to specifically evaluate the effects of spatial structure by comparing a high diffusion case, where between-genotype cooperation emerges, with a low diffusion case (here given by a neighborhood of 24 cells from the source).

We implemented the standard three-step lifecycle as for the deterministic version. First, a number of M separate lattices are seeded according to the initial genotypic frequencies. Second, each subgroup develops separately with cell growth being spatially simulated. Third, the subgroups are merged to update the genotypic frequencies, which are used for the following seeding step. Importantly, we let the yield of a focal subgroup depend on the presence of traits (secretions) in this group, with the consequence that subgroups with more producers will have higher final yield. Although in the ODE model K changed continuously with the number of producers, in the individual-based model K remained constant for the duration of the growth phase, but then, we weighted subgroups according to the proportion of producers present at the end of the simulation before the merging step. This implementation captures the dependence of subgroup yield upon the proportion of producers in a group in a manageable way, but it differs from the ODE model. This different implementation of secretion-dependent carrying capacity could potentially affect comparisons between the two model frameworks. However, as discussed above, we only directly compare the cases of global and local diffusion within the individual-based model framework.

SI Figures

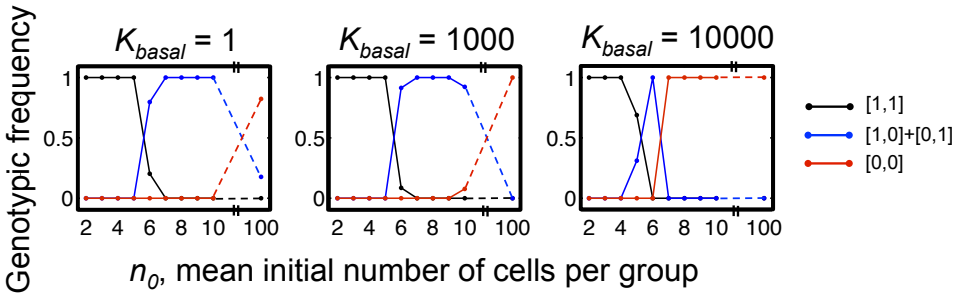

Figure S1: Effect of basal fitness on the evolution of between-genotype cooperation in microbial communities. Our main models assume that secreted traits are essential for growth, which means that groups without secretions will not grow. Here we vary K_{basal} (carrying capacity without secretions) from 1 to 10000 (up to 10% of the maximum benefit from secretions (K_{maxB}), see SI Methods and Materials). The only effect is to reduce the scope for between-genotype cooperation, which further suggests that cooperation among microbial genotypes is limited. Results from the two-trait model (ODE version) with the cost (c) at 5% of growth rate are shown.

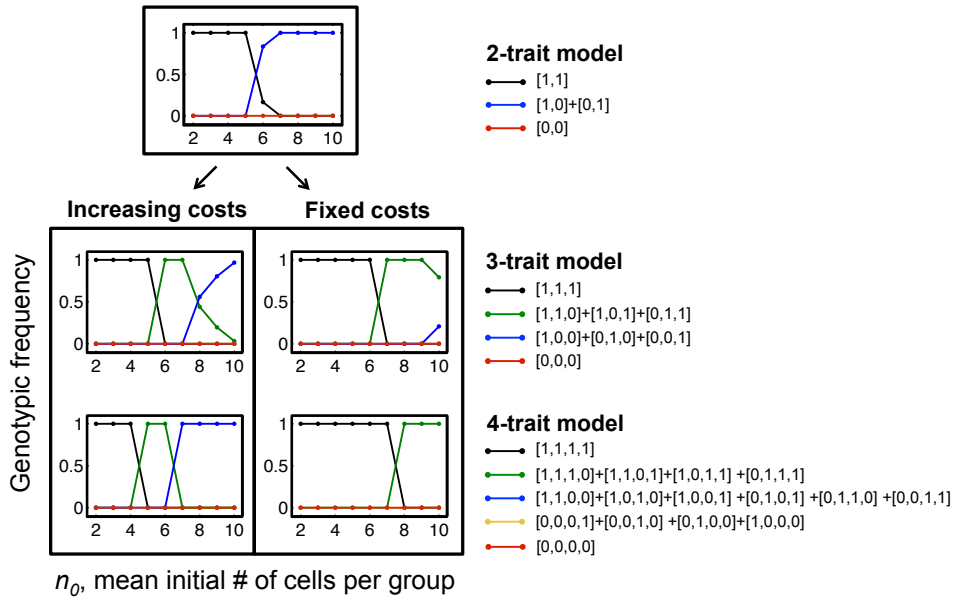

Figure S2: Effect of increasing number of traits on the evolution of cross-feeding. (*Lower Left*) Systems that rely on four secretions select more for cooperative cross-feeding than those relying on three only. This results from the increasing cost of adding another secretion to a genotype that produces all traits. (*Lower Right*) If total costs are fixed (here 10% of maximum growth rate), then adding another secretion reduces the prevalence of cross-feeding.

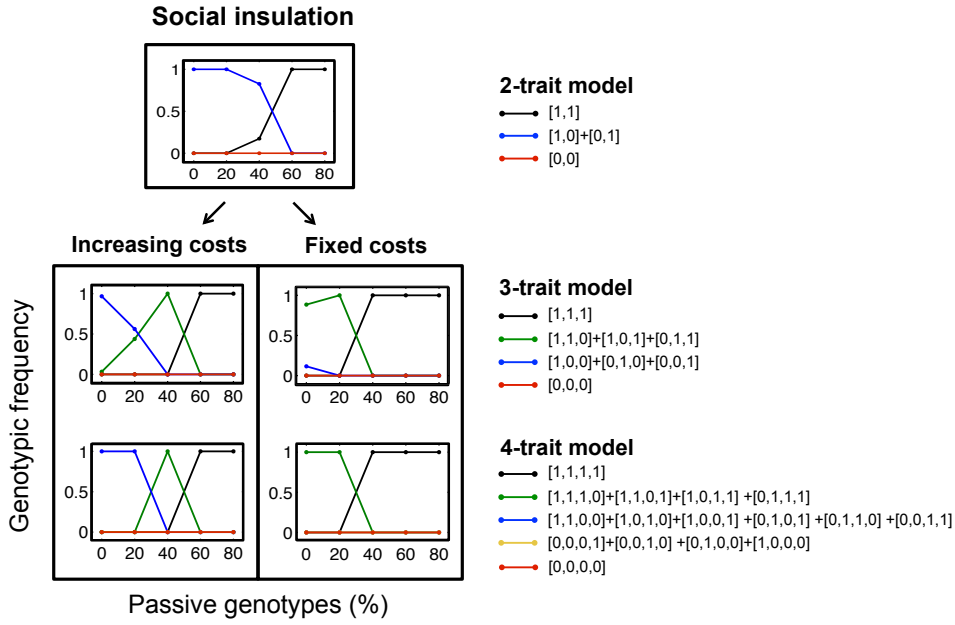

Figure S3: Social insulation in systems with increasing number of traits. The introduction of passive genotypes has the same effect on the evolution of cooperative cross-feeding in systems relying on two, three and four traits: a high percentage of passive genotypes prevents between-genotype cooperation. (*Lower Right*) Holding the total cost of all secretions constant shows that social insulation is particularly problematic for system with many secretions. Here, we fixed total costs at 10% of maximum growth rate and genetic mixing at $n_0 = 10$, which promote cross-feeding in the absence of passive genotypes.

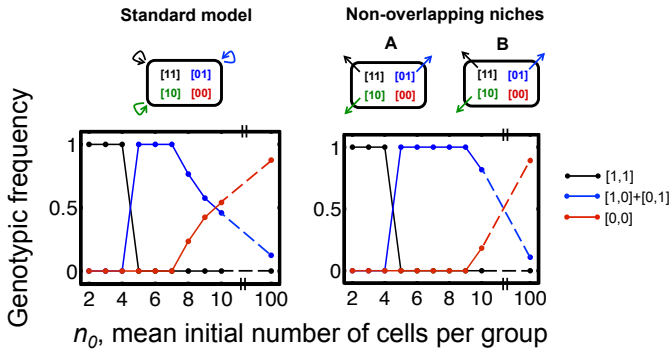

Figure S4: Evolution of cooperation between genotypes without overlapping niches. For the nonoverlapping case, we consider two species of bacteria (species A and B) that do not compete for the same resources. Each species is composed by the same four genotypes considered in the standard model. Importantly, secretions can be used by any genotype regardless of the species. However, to allow natural selection to differentiate between the species, we also assume asymmetric costs: species A is more efficient on secretion 1 than species B, but less efficient on secretion 2. As for the standard model, cooperative cross-

feeding between A and B is possible at intermediate levels of genotypic mixing only. However, the scope for cooperation is now improved, because cross-feeders do not compete for the same resources. For both cases, we considered well-mixed conditions and high secretion cost (here c = 10% of maximum growth rate per secretion).

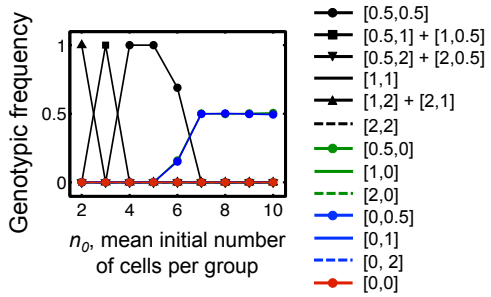

Figure S5: Independent evolution of investment into secretion production. In the main text (Figure 4) we show the results of a discrete model where the producers of both traits invest the same amount in each secretion. That is, we considered only genotypes [0.5,0.5], [1,1] and [2,2] in the full secretors. Here, we show that identical results are obtained when full producers can invest differentially in each trait: high investment is selected at low mixing while increasing mixing selects for reducing investment.

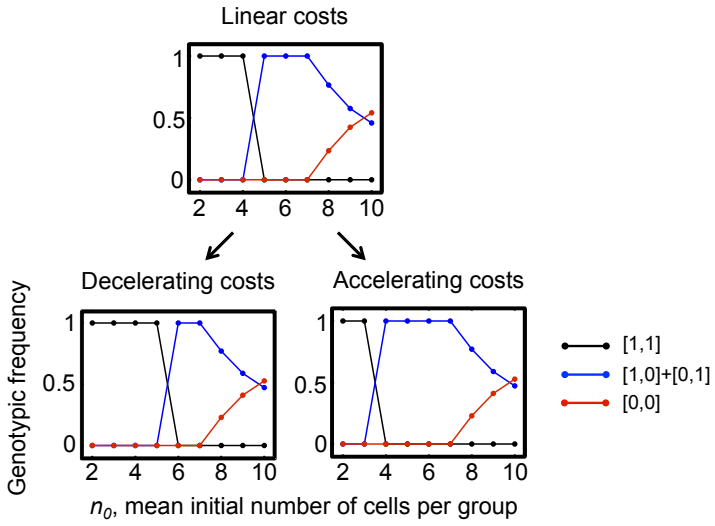

Figure S6: Effect of non-linear costs on the evolution of between-genotype cooperation. Our models assume that genotypes that invest in more than one trait experience a linear increase in costs. For example, if one sets c = 0.1, then [1,1] will reduce its growth rate by 20% whereas genotypes that produce only 1, [1,0] and [0,1], reduce by 10%. Here, we considered the effect of non-linear decelerating (left) and accelerating costs (right). Specifically, [1,1] now invests 15% (*Lower Left*) and 30%, (*Lower Right*), while the investment is the same for cross-feeders.

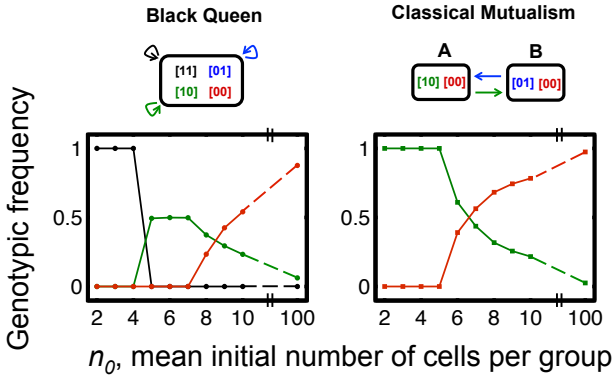

Figure S7: Evolution of genotypic cooperation in our model (Black Queen-like) compared to a classical mutualism model. We modeled classical mutualism by considering two species of bacteria (species A and B) that do not compete for the same resources and possess unique traits (one secretion each) that can only be used by the partner species for growth. That is, there is no [1,1] genotype but just a single-trait producer and respective cheater genotype within each species. For both cases, we considered well-mixed conditions and high secretion cost (c = 10% of maximum growth rate per secretion). The potential for genotypic cooperation is higher under canonical mutualistic interactions (here given by a wider region of genotypic mixing under which cooperative partners dominate the population). The within-species frequencies of [1,0] and [0,1] in both plots overlap, as expected, and therefore, only one of the two colors is seen in the plot.

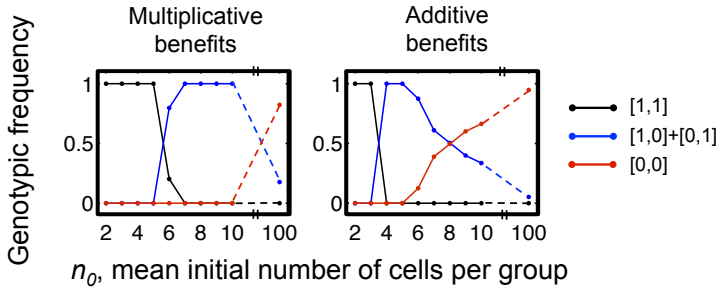

Figure S8: Effect of the functional form of benefits on the evolution of between-genotype cooperation in microbial communities. Qualitative conclusions are robust to both multiplicative and additive benefits to secretions. Our main models assume that the benefits of multiple secretions combine multiplicatively to set population carrying capacity (K). For example, for two traits, K is proportional to the product of the amount of secretion 1 and secretion 2 in each subpopulation. Here, this scenario is compared to a case where K scales as the sum of the amounts of two secretions. Results are shown from the two-trait model (ODE version) with the cost (c) at 5% of maximum growth rate, where the two fitness functions are for multiplicative benefits:

$$K = K_{basal} + K_{\max B}\left(\frac{g_{11}+g_{10}}{g_{11}+g_{10}+g_{01}+g_{00}} \cdot \frac{g_{11}+g_{01}}{g_{11}+g_{10}+g_{01}+g_{00}}\right)$$

and for additive benefits:

$$K = K_{basal} + K_{\max B}\left(\frac{g_{11}+g_{10}}{g_{11}+g_{10}+g_{01}+g_{00}} + \frac{g_{11}+g_{01}}{g_{11}+g_{10}+g_{01}+g_{00}}\right)/2.$$

As before K_{basal} and K_{maxB} are the minimal carrying capacity of the system and the maximum benefit from secretions, respectively, and g_{ij} the density of individuals of genotype [i,j] in each subpopulation.

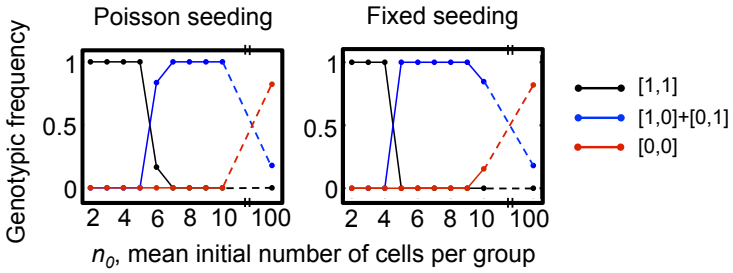

Figure S9: Effect of type of seeding on the evolution of cooperative cross-feeding. We find the same qualitative behavior for (*Left*) Poisson-based seeding, where a random number of cells are initially introduced in each group, and (*Right*) fixed seeding, where we introduce the same number of cells in all groups. However, there are some quantitative differences, because fixing the number of cells introduced per group reduces the variance between groups. This reduction in variance between groups affects the potential for Simpson's Paradox and thus, the evolution of cooperation, both within and between genotypes. Costs per trait were set at 5% of maximum growth rate.

Supplementary materials of Chapter 3

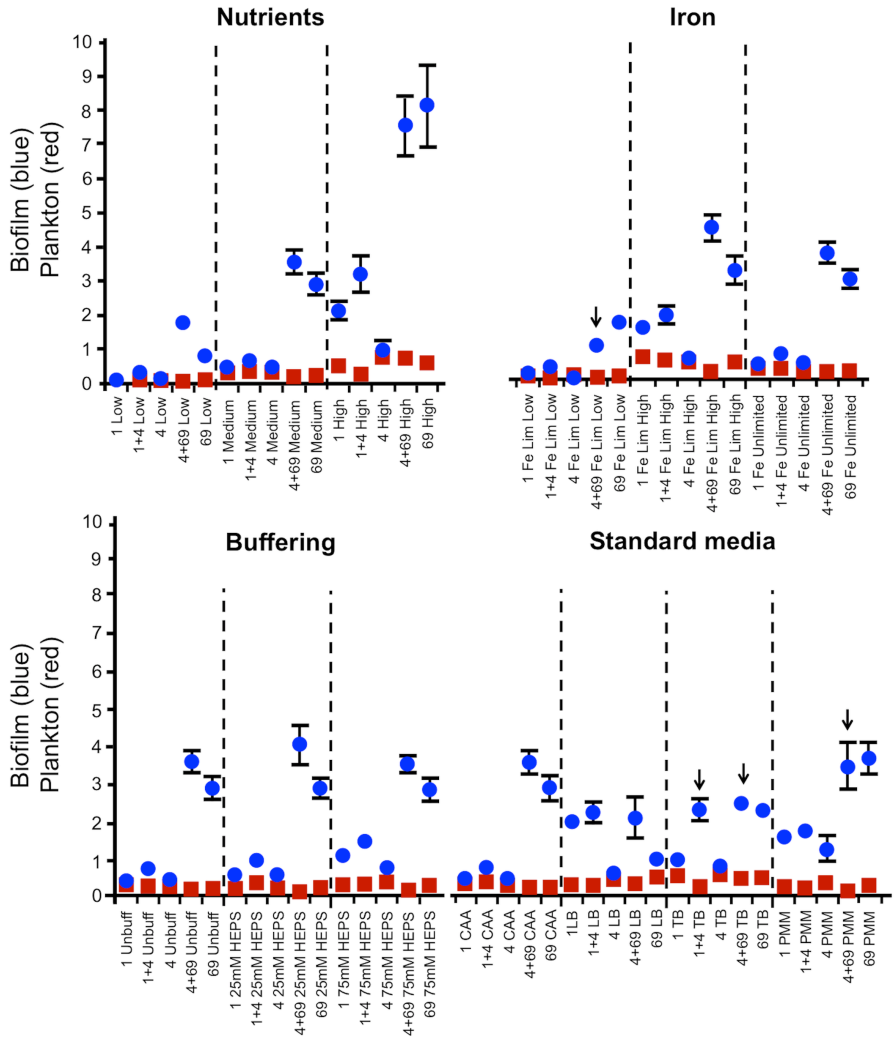

Figure S1. The biofilm response is observed across multiple environmental conditions. Biofilm formation in single-strain and mixed-strain cultures is shown across a range of conditions. We compared biofilm formation across (i) three nutrient concentrations with casamino acids (CAA) media: 0.1% CAA (low), 0.5% CAA (medium), 2.5% CAA (high); (ii) three iron levels with casamino acids media (100 mg apotransferin + 1 µM FeCl, 100mg apotransferin + 5 µM FeCl, no added apotransferin or FeCl); (iii) three buffering levels with casamino acids media (Unbuffered, 25 mM HEPES, 75mM HEPES); and (iv) four standard media including Luria broth (LB), tryptone broth (TB), *Pseudomonas* minimal medium (PMM), and casamino acid (CAA) medium. Note that the CAA standard media treatment is replotted in each quadrant for comparison, where it represents medium nutrients, unlimited iron, no buffering, and CAA, respectively. In most cases, strain 4 is outcompeted and represents <5% of the planktonic cells after 24 h. A few exceptions are marked with an arrow

where strain 4 is >5% frequency in the planktonic cells. Most notably, the 4 + 69 mixtures marked with an arrow have strain 4 at >90% of planktonic cells, showing how the outcome of competition is strongly influenced by the environment, while the biofilm response is much less so. Error bars indicate the 95% confidence intervals of the mean.

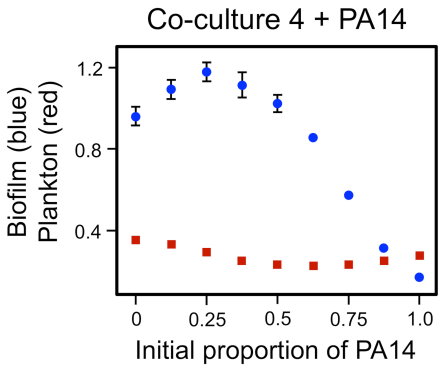

Figure S2. Dose-dependent effect of strain mixing on the biofilm response of strains 4 and PA14. Error bars are 95% confidence intervals of the mean.

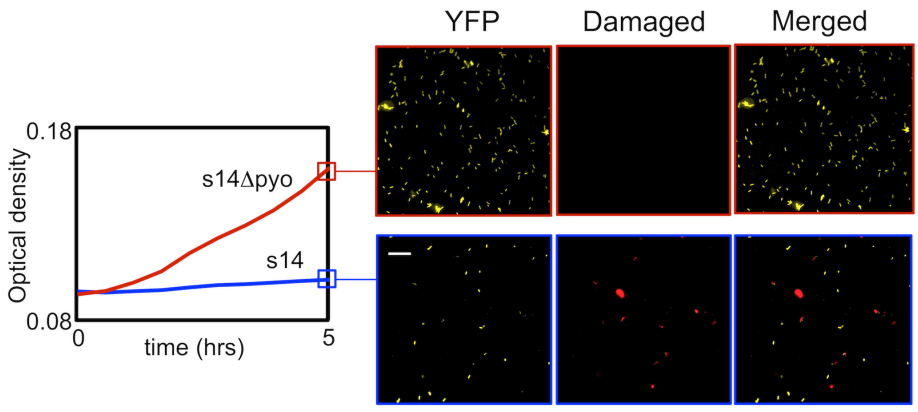

Figure S3. Pyocin-induced cell damage in shaking culture. Cell-free supernatant from wild-type PA14 inhibits the growth of strain 4, as shown in Figure 3. The observed growth lag (left-hand plot) is driven by pyocins, the narrow spectrum antibiotics of *P. aeruginosa*, and is associated with cell damage (right hand images). After 5 h of growth in the presence of 25% of PA14 cell free supernatant with pyocins ('s14') or without ('s14Δpyo') we stained cultures of strain 4 with propidium iodide, and imaged cells using epifluorescence microscopy (see Table S3 for details of PA14 strains). The responder genotype (strain 4) is tagged with a fluorescent protein (YFP), and damaged cells are seen in red. The growth curves on the left are means of eight independent replicates and images on the right are representative images of cell damage in the cultures at the end of the growth period (large red blob is an out-of-focus damaged cell).

Images from each fluorescent channel were collected and processed using the same settings to ensure consistency. Scale bar is 20 μm.

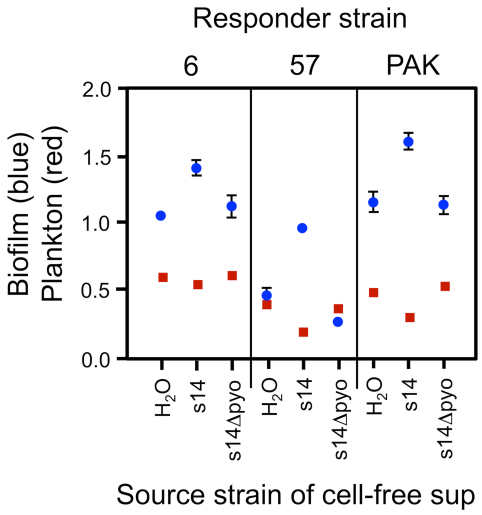

Figure S4. Pyocin-induced biofilm formation in additional strains of *P. aeruginosa.* Shown are the effects of cell-free culture supernatants from PA14 ('s14') and the pyocin-null mutant ('s14Δpyo') on two natural isolates from Figure 1C. Pyocin-induced biofilm formation is also observed in PAK, a strain known to be susceptible to pyocins from PA14. Error bars are 95% confidence intervals of the mean.

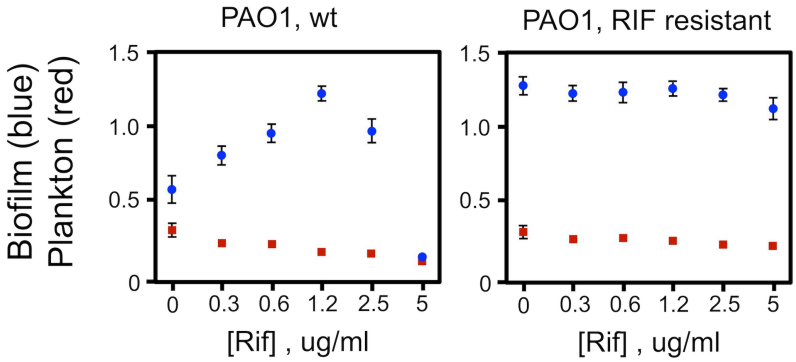

Figure S5. Effect of antibiotic resistance on antibiotic-induced biofilm formation. Strain PAO1 exhibits a rifampicin-induced biofilm response, but its rifampicin resistant mutant does not. Error bars are 95% confidence intervals of the mean.

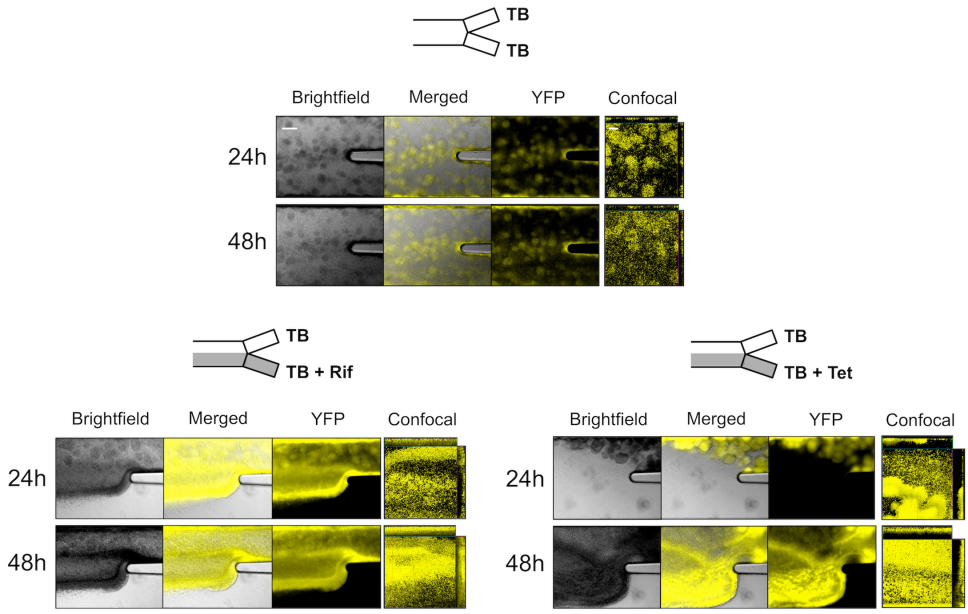

Figure S6. Different classes of clinical antibiotics promote biofilm formation in flow cells. Gradients of rifampicin (Rif) and tetracycline (Tet) drive biofilm accumulation in strain 4 as one finds with gradients of ciprofloxacin (Figure 6). The effect is particularly clear after 48 h of incubation when the biofilm increase is such that blocks the flow. For each treatment we show representative epifluorence microscopy images captured with 10X lens (scale bar is 100 µm for 'Brightfield', 'YFP', and 'Merged'), as well as representative confocal images captured with 40X lens (scale bar is 30 µm). Epifluorence images were collected and processed using the same settings to ensure consistency. Confocal images show that the increase in the YFP signal with antibiotic gradients is explained by an increase in both cell density and volume of the biofilm.

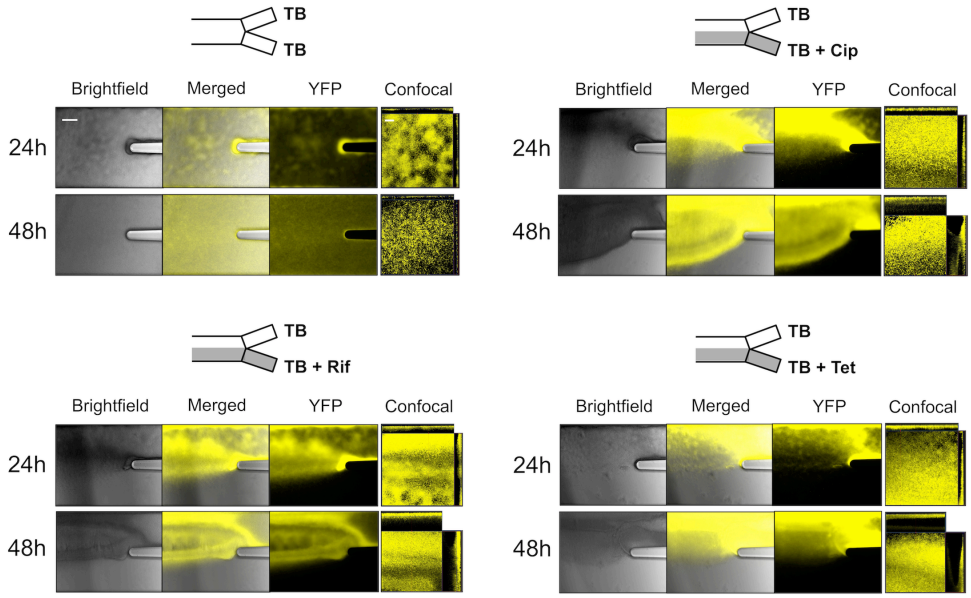

Figure S7. Antibiotics promote biofilm formation in flow cells in a second strain background (strain 69). Gradients of ciprofloxacin (Cip), rifampicin (Rif), and tetracycline (Tet) drive biofilm accumulation. The effect is particularly clear after 48 h of incubation when the biofilm increase is such that it can block the flow. For each treatment we show representative epifluorence microscopy images captured with 10X lens (scale bar, 100 μm for 'Brightfield', 'YFP, and 'Merged'), as well as representative confocal images captured with 40X lens (scale bar is 30 μm). Confocal images show that the increase in the YFP signal with antibiotic gradients is explained by an increase in both cell density and volume of the biofilm.

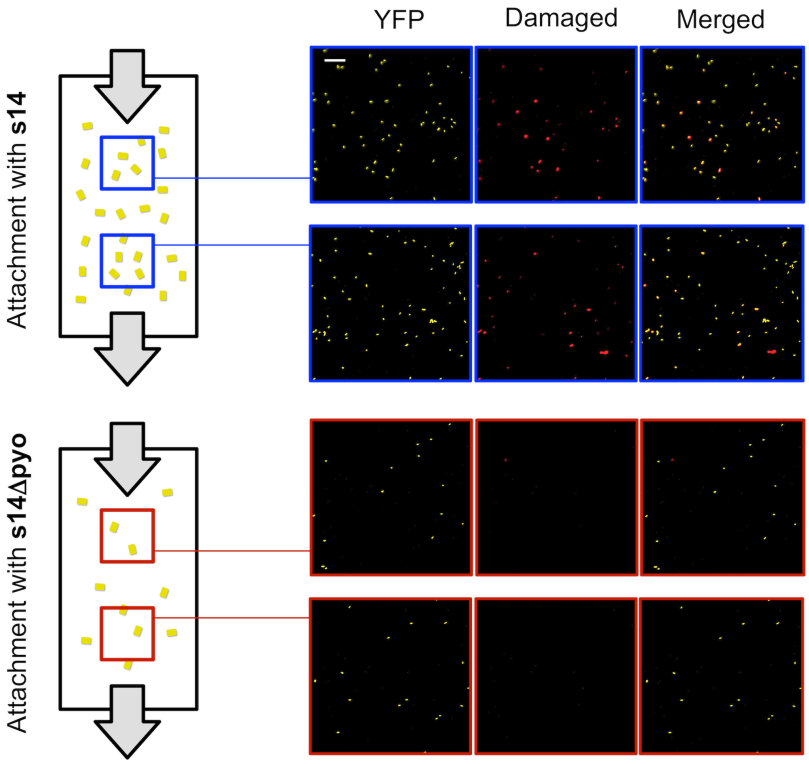

Figure S8. Pyocins from competitor genotypes drive both attachment and cell damage in *P. aeruginosa*. Cell-free supernatant from wild-type PA14 ('s14') promotes surface attachment of strain 4 when compared to supernatant from the respective pyocin-null genotype ('s14Δpyo') as observed by two representative regions of each channel. Following the attachment phase we stained *yfp*-labeled cells with propidium iodide to test for cell damage (red). Images from each fluorescent channel were collected and processed using the same settings to ensure consistency. Scale bar is 20 μm. Experiments were repeated on different days to validate results.

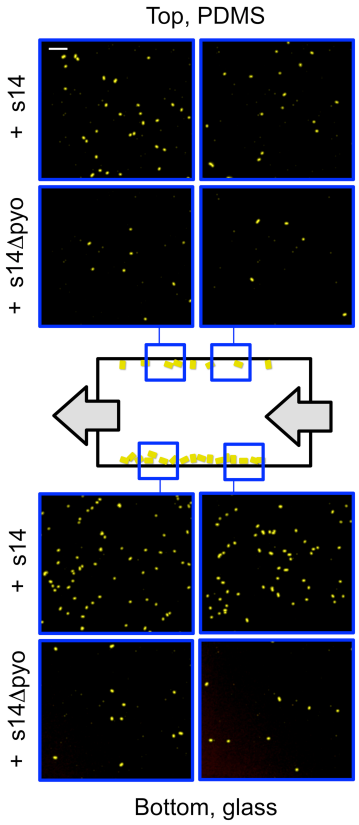

Figure S9. Pyocin-induced attachment occurs on the top and bottom of the microfluidic device. Specifically, we see increased cellular attachment of YFP-labeled strain 4 in the presence of pyocin-containing cell-free supernatant from WT PA14 ('s14') on both the bottom (glass) and top (PDMS) of channels, when compared to supernatant from the respective pyocin-null genotype ('s14Δpyo'). $p < 0.05$ in unpaired t tests at 5% significance. We show two representative images of each condition. Scale bar is 20 μm.

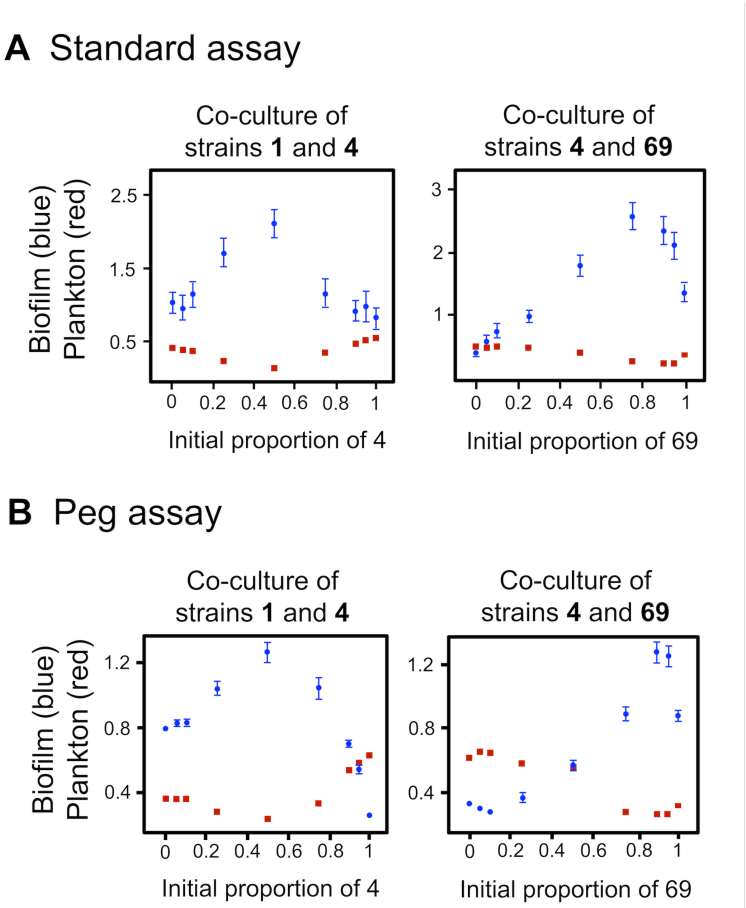

Figure S10. Comparison of standard assays (A) and peg assays (B) on mixing-induced biofilm formation. In standard assays, the biofilms measured are those attached to the edge of the wells in microtiter plates. In peg assays, the biofilms measured are those attached to pegs inserted into the wells. Here we show dose-dependent effects of strain mixing on the biofilm response of strains 1 and 4 (left) and 4 and 69 (right). Increased biofilm due to strain mixing is seen in both assays. Error bars are 95% confidence intervals of the mean.

Table S1. Natural isolates of *Pseudomonas aeruginosa* used in this study.

Strains #	Source	Origin	ZK #
1	**Wound**	**PAO1**	**ZK2019**
2	Wound	PA14	ZK2466
3	Oil contaminated water	Colombia	ZK3094
4	**Oil contaminated water**	**Colombia**	**ZK3095**
5	Oil contaminated water	Colombia	ZK3096
6	Oil contaminated water	Colombia	ZK3097
7	**Soil**	**Colombia**	**ZK3098**
8	Bone	Colombia	ZK3099
13	Catheter	Colombia	ZK3104
14	Amputation	Colombia	ZK3105
15	Catheter	Colombia	ZK3106
18	Soil	Colombia	ZK3091
19	**CF patient**	**Seattle, USA**	**ZK2870**
20	Water	Boston, USA	ZK3566
45	CF patient	Boston, USA	ZK45
50	Stool	Boston, USA	ZK50
52	Water	Boston, USA	ZK3572
55	Water	Boston, USA	ZK3575
57	Soil	Boston, USA	ZK3577
69	**Trachea**	**Boston, USA**	**ZK69**
77	Catheter	Boston, USA	ZK77
80	CF patient (mucoid)	Boston, USA	ZK80

All strains come from the Kolter lab collection as specified by the ZK # designation (strains in bold were subjected to detailed analysis).

Table S2. Tryptic peptide fragments identified by mass spectrometry found by Protein Mass Spectrometry with homology to pyocin proteins.

Homologue	Protein sequence
PA14 8070 (R pyocin)	MSFFHGVTVTNVDIGARTIALPASSVIGLCDVFTPGAQASAKPNVP VLLTSKKDAAAAFGIGSSIYLACEAIYNRAQAVIVAVGVEAAETPEAQ ASAVIGGVSAAGERTGLQALLDGKSRFNAQPRLLVAPGHSAQQAV ATAMDGLAEKLRAIAILDGPNSTDEAAVAYAKNFGSKRLFMVDPGV QVWDSATNAARKAPASAYAAGLFAWTDAEYGFWSSPSNKEIKGIT GTSRPVEFLDGDETCRANLLNNANIATIIRDDGYRLWGNRTLSSDS KWAFVTRVRTMDLVMDAILAGHKWAVDRGITKTYVKDVTEGLRAF MRDLKNQGAVINFEVYADPDLNSASQLAQGKVYWNIRFTDVPPAE NPNFRVEVTDQWLTEVLDVA
PA14 8090 (R pyocin)	MIPQTLTNTNLFIDGVSFAGDVPSLTLPKLAVKTEQYRAGGMDAPV SIDMGLEAMEAKFSTNGARREALNFFGLADQSAFNGVFRGSFKG QKGASVPVVATLRGLLKEVDPGDWKAGEKAEFKYAVAVSYYKLEV DGREVYEIDPVNGVRAINGVDQLAGMRNDLGL
PA14 8210 (F pyocin)	MSILTQGTQIYALVPPVSGTGAATVLEIEGVTSFNPGGNPADQIEDP CLSDTSRKYKKGLRTPGQATLGINADPRLASHVRLFQLSEKDGETS VKWAIGWSDGIDVKPTVSTEGDDFVLPPARTWFTFEGYVSDFPFD FASNTLVATQATIQRSGAGKWTPKSA

Amino acid sequences of the three pyocin homologs recovered from fraction C9. Individual peptides that were identified are indicated in yellow and green denotes the second of two adjoining fragments

Table S3. Additional strains used in this study.

Strains	Relevant characteristic	Lab / reference
PA14	• Wild type (parental strain)	Penterman
Δpyo	• Endogenous *prtR* replaced with *prtR*^{S153A}, producing constitutively active repressor	Penterman, (S1)
ΔRpyo	• R pyocin transposon mutant insertion, PA14_08070, ID 56201	Ausubel, (S2)
ΔFpyo	• F pyocin transposon mutant insertion, PA14_08300, ID 28328	Ausubel, (S2)
PAO1	• Wild type (parental strain)	MacLean
Δ*rpoB*	• Rifampicin resistant mutant with point mutation C1736T in *rpoB*	MacLean, (S3)
PAK	• Wild type	Lam / van Delden

S1: Penterman J, Singh PK, Walker GC. Biological Cost of Pyocin Production during the SOS Response in Pseudomonas aeruginosa. Journal of bacteriology. 2014;196(18):3351-9.

S2: Liberati NT, Urbach JM, Miyata S, Lee DG, Drenkard E, Wu G, et al. An ordered, nonredundant library of Pseudomonas aeruginosa strain PA14 transposon insertion mutants. Proceedings of the National Academy of Sciences of the United States of America. 2006;103(8):2833–8.

S3: Qi Q, Preston GM, MacLean RC. Linking System-Wide Impacts of RNA Polymerase Mutations to the Fitness Cost of Rifampin Resistance in Pseudomonas aeruginosa. mBio. 2014;5(6).

Supplementary materials of Chapter 4

Supplementary Methods

Bacterial strains and culturing. Our experiments use wild-type *P. aeruginosa* PAO1 (Kolter collection, ZK2019 (O'Toole and Kolter, 1998)) as working model for twitching chemotaxis (Figures 1, 2 and Extended Data Figures 2, 6). To study the functional role of the Chp chemosensory system we used in-frame deletion mutants of *pilB*, *chpA, pilG*, and *pilH*, along with their respective wild-type, which have all been published and described elsewhere (Bertrand et al., 2010). These strains are used in Figures 3 and 4 (main text), and in Extended Data Figures 4, 5, 7, 9 and 10. The Δ*cheY1* mutant strain shown in Extended Data Figure 3 was a gift from the group of Caroline Harwood. All strains were grown overnight in LB (37°C, 250 rpm) from frozen stocks and sub-cultured to obtain cells in exponential phase. These were then diluted to an optical density of 0.25 (at 600 nm) in tryptone broth (TB, 10 g Bacto tryptone per 1 L water), the media used in our microfluidic-based experiments.

Subsurface twitching assay. We followed standard protocols previously described (Bertrand et al., 2010; Semmler et al., 1999). Briefly, strains were grown overnight in LB (37°C, 250 rpm) from frozen stocks and spotted on 1.5% LB agar, which were incubated at 37°C under static conditions for 24 hours. Using cells isolated from a single colony, we stab-inoculated Petri dishes filled with 1% agar (LB or TB) with a needle to deposit bacteria at the interface between the agar and the underlying plastic dish. After 48 hours of incubation at 37°C the dishes were photographed with a DSLR camera (EOS 30D, Canon). The software Fiji (Schindelin et al., 2012) was used to

enhance the contrast (over the whole image) to make the relatively faint twitching rings on the bottom of the plate more visible.

Microfluidic experiments. Two different microfluidic setups were used in this study. We used the commercially available Bioflux 200 system (Fluxion Biosciences) for all microfluidic experiments except the alternating gradient experiments presented in Figure 4d-g and Extended Data Figures 9 and 10, which used a custom designed microfluidic device (Extended Data Figure 8). All microfluidic experiments were conducted at 22°C. We imaged microfluidic experiments using a Zeiss Axio Observer inverted microscope with a Zeiss 20X Plan Apochromat objective, Zeiss AxioCam MRm camera, and a Zeiss Definite Focus system.

Experiments using Bioflux microfluidic devices. Dual inlet Bioflux microfluidic channels were primed with tryptone broth (TB) medium as previously described (Benoit et al., 2010). Exponential phase cells were then introduced (in TB, at the final optical density of 0.25, A_{600}) and allowed to attach to the surface for 20 min in the absence of flow. Planktonic and weakly adhered cells were then flushed from the test section by applying a flow rate of 40 μl h^{-1} for 10 min. The flow rate was then reduced to 4 μl h^{-1} at $t = 0$, which was maintained for the reminder of the experiment. Cells were imaged at a rate of 1 frame min^{-1}, with the exception of the Δ*pilH* mutant (Figure 3), which was imaged at 12 frames min^{-1} given their very fast motility. The test sections of all Bioflux channels were 350 μm wide and 75 μm deep, but they came in two slightly different designs (Extended Data Figure 1). Studies with fluorescein dye showed the different geometries of these designs upstream of the test section caused

them to generate slightly different chemical distributions (Extended Data Figure 1a,d). We accounted for these differences in the model of diffusion that simulates the distribution of chemoattractant in these devices (see Extended Data Figure 1b,c,e,f, and section below).

The experiments in Figure 2 were conducted using the Bioflux 'Invasion' channels (Extended Data Figure 1). To continuously track the location of the chemoattractant in these experiments, we mixed the solution containing DMSO or succinate with Chicago Sky Blue 6B dye (3% by volume of saturated stock solution, Sigma Aldrich). Both dye and cells were visualized simultaneously within the same image. We confirmed in a separate experiment that the dye did not induce a chemotactic response (Extended Data Figure 2). Every 3 hours we reversed the direction of the chemoattractant gradient by manually replacing the fluid in the reservoirs that were connected to each inlet. While this process took approximately five minutes, it required the removal of the microfluidic system from the microscope and thus it was not possible to continuously image cells as the chemoattractant gradient changed direction. To quantify reversals in cells responding to a change in the chemoattraction direction (Figure 4d,e,f,g) it was required the development of a custom microfluidic device (Extended Data Figure 8) that did not have this limitation.

Alternating gradient experiment using custom microfluidic device. To observe cells as they respond to a chemoattractant gradient that alternates in direction, we designed a microfluidic device with four inlet ports (Extended Data Figure 8). Molds with this design were fabricated from SU-8 on a silicon wafer (FlowJEM, Toronto, Canada). Microfluidic channels were cast using PDMS (Sylgard 184, Dow Corning) and holes

for tubing were punched using a Harris Unicore 1.5 mm biopsy tool (Agar Scientific). Cured PDMS was bonded to glass coverslips (50 mm by 75 mm, No. 1 thickness, Agar Scientific) with a corona treater (BD-20AC, Electro-Technic Products) using previously described techniques (Haubert et al., 2006). Tygon microbore tubing (0.06 inch outside diameter) was used to plumb both the inlets and outlets of the device. The outlet was connected to a single 10 ml syringe (Becton Dickinson) mounted on a syringe pump (PhD Ultra, Harvard Apparatus) that generated flow through the device via suction. The test section of the device is 600 μm wide and 75 μm deep.

After the system was primed with TB, exponential phase cells (WT or Δ*pilG*) were drawn into the device at 100 μl min^{-1} using the pair of inlets marked 'A' in Extended Data Figure 8. After cells reached the test section, tubes connected to all four inlets were clamped with hemostats for 20 mins to allow cells to attach to surfaces in the absence of flow. Next, the tubing connected to the inlets were inserted to reservoirs containing either TB or 350 mM DMSO and Chicago Sky Blue 6B dye dissolved in TB. We then pulled fluid through the device at 100 μl min^{-1} to both remove planktonic cells and allow the chemoattractant to reach test section of the device. The flow was then reduced to 5 μl min^{-1} for the remainder of the experiment. We then clamped the tubes connected to one pair of inlets, which exposed cells to a DMSO gradient. Next, we changed the direction of the gradient approximately every eight minutes by sequentially unclamping and clamping the tubes connected to the inlets marked 'A' and 'B' in Extended Data Figure 8. Our analysis began at $t = 0$, when we first changed the direction of the gradient. Dye and cells were imaged simultaneously every four seconds at $x = 2.5$ mm (Extended Data Figure 8). While the distribution of dye was analyzed in each frame, cells were tracked in every other frame (i.e. every eight seconds) owing to computational constraints.

Characterization of concentration field in Bioflux devices using fluorescein and mathematical modeling. The distribution of chemoattractant, C, within the Bioflux devices was mapped using fluorescein, a fluorescent dye whose diffusion coefficient, D, approximates that of the low molecular weight compounds used in this study. Fluorescein was observed to strongly affect biofilm development, so we conducted separate experiments without cells to resolve the distribution of C and mapped this back onto experiments with cells.

Imaging was conducted using the microscopy setup noted above except with a Zeiss EC Plan Neofluar 10X objective, a Zeiss LSM 700 scanning laser confocal unit to measure fluorescent intensity, and a Zeiss LSM T-PMT unit to simultaneously visualize the channel geometry. We recorded z-stacks of images at multiple, overlapping positions along the length of the device and the maximum fluorescent intensity in z was used to obtain the relative fluorescein concentration at each x,y position. Slight variations in C occurred along x because thermally induced fluctuations in z led to differences in the maximum measured fluorescent intensity between adjacent images (Extended Data Figure 1a,d). To correlate cell movement with the chemoattractant distribution we used a mathematical model to calculate C within the Bioflux devices. More specifically, we used a one dimensional, time dependent diffusion equation to simulate molecular diffusion in the y direction and then used the mean flow velocity in the device to transform time into distance along x. We consider a one-dimensional domain with impermeable, no-flux boundaries at $y = -L/2$ and $y = L/2$. At $t = 0$ two regions of constant concentration are initialized: $C = C_{max}$ in the region $-L/2 < y < h - L/2$ and $C = 0$ in the region $h - L/2 < y < L/2$. Subject

to these initial and boundary conditions, the solution of the one dimensional diffusion equation is given by (Crank, 1975):

$$C = C_{max}\left\{\frac{h}{L} + \frac{2}{\pi}\sum_{n=1}^{\infty}\frac{1}{n}\sin\frac{n\pi h}{L}\exp(-Dn^2\pi^2 t/L^2)\cos\frac{n\pi(y+L/2)}{L}\right\}.$$

This time dependent solution was transformed, assuming constant advection speed, to distance along the device via the substitution $t = x\,U^{-1}$, where $U = 42$ μm s^{-1} is the mean flow velocity, $L = 350$ μm is the channel width, and $D = 10^2$ μm^2 s^{-1}. This approach assumes uniform flow and that the distribution of chemoattractant is constant over the depth of the device. For modeling the Bioflux 'Invasion' plates, which are symmetric about $y = 0$, we used $h = L/2 = 175$ μm, which yielded a distribution of C that closely matched that obtained experimentally using fluorescein dye (Extended Data Figure 1d,e,f). For modeling the Bioflux 'WPM' plates, which have a slight asymmetry upstream of the test section, we used $h = 160$ μm and introduced an offset in y to directly match position of the $C = 0.5$ isocontour in the fluorescein experiment (Extended Data Figure 1a,b,c). This concentration field was used exclusively for presentation purposes (Figure 1b), but not for any quantitative analyses.

Modeling the chemical environment in the alternating gradient experiment. In the alternating gradient experiment, we used a larger flow velocity ($U = 1.85$ mm s^{-1}) to minimize the variation in chemical stimuli along the x direction of the device. The characteristic width of the gradient generated by diffusion can be approximated as $L \approx \sqrt{2Dx/U}$ and we imaged at $x = 2.5$ mm (Extended Data Figure 8), yielding $L \approx 20$ – 50 μm for $D = 10^2$–10^3 μm^2 s^{-1}, which is in the range experimentally observed with the dye (Figure 4d). Our field of view spans 0.45 mm in the x dimension: the formula

above, predicts that the width of the gradient increases by ≈10% from the upstream to the downstream edge of our field of view. Thus, within our field of view, cells at the same *y* position experience nearly the same chemical environment regardless of their position in *x.* This small amount of variation allows us to average *C* along *x* to present its spatiotemporal variation as a kymograph (Figure 4d,e) and pool cell behavior along *x* (Figure 4f,g).

***Image analysis and cell tracking*.** All images were processed using the open source software Fiji (Schindelin et al., 2012) and its associated plugins. After correcting the time series of images for thermally-induced drift of the microscope stage (using the Image Stabilizer plug in) and enhancing the contrast of cells (using background subtraction and noise reduction functions), we tracked the movement of cells through space and time using TrackMate plug in (Jaqaman et al., 2008). To distinguish solitary cells from those residing within groups, we calculated the mean image intensity within a 3 μm radius from the centroid each detected cell. Cells in close proximity to other cells (e.g. those within a cluster) yielded larger mean intensities than solitary cells, which allowed us to exclude the former prior to running the tracking algorithm. To quantify cell length and cell orientation we fitted each cell with an ellipse at every time point, a functionality that is accessible by running Trackmate via a Python script (this feature is not available in the Graphical User Interface). All tracking data was exported from Fiji to Matlab (Mathworks) for subsequent analysis.

Experiments where dye gradients and cells were visualized simultaneously within the same image (Figure 2, Figure 4d-g, and Extended Data Figures 9,10), required additional processing. To isolate cells, we removed the variable intensity

background by normalizing the local contrast with Fiji's Integral Image Filter plugin. To isolate the dye, we removed cells from the image using Fiji's Rolling Ball Background Subtraction function.

Calculation of chemotactic bias, β. The strength of the chemotactic response, β, was quantified by dividing number of cells moving up the gradient by the number of cells moving down the gradient as a function of time. While analogous metrics have been used to quantify chemotaxis in swimming bacteria (Ahmed and Stocker, 2008), twitching cells exhibit jerky, unsteady movement (Jin et al., 2011), such that the instantaneous direction of a cell's movement is not representative of the direction of its transport over longer timescales. Thus, in our calculation of β we defined the direction of movement using a cell's net displacement over the length of its trajectory (with the exception of Figure 2, see below). In addition, we excluded non-motile cells and cells that do not exhibit appreciable movement from their origin. This was accomplished by calculating the net to gross displacement ratio (NGDR), which is defined as the straight line distance between the start and end points of a trajectory divided by the total distance traveled along the path of the trajectory (Seymour et al., 2009). Trajectories with NGDR<0.15 were excluded from our calculation. This threshold was chosen based on visual inspection to exclude cells with convoluted paths that do not show significant movement in any direction (trajectories with NGDR<0.15 are shown in Supplementary Video 1). All measurements of β were obtained by analyzing cells within two adjacent fields view of the microscope (with the exception of Figure 2, see below), which spanned the full channel width in y and approximately from $x = -0.05$ to 0.85 mm.

The rose plots in Figure 1b,c were obtained by calculating the angle, θ, from each trajectory's origin to its terminus. The resulting angles were weighted by the trajectory length, binned within 12 equally spaced bins around the unit circle, and normalized to obtain the probability density function. As cell crowding significantly restricted cell movement at later time points, this analysis considered only trajectories collected from $t = 0$ to 5 h.

In Figure 2, we quantified how cells respond to changes in the direction of the gradient. To capture changes in motility that occur mid-trajectory, we subdivided trajectories into segments 16 minutes long and used these to calculate β (Figure 2g) and the mean θ (Figure 2h). This segment length is long enough to capture the overall direction of cell movement (smoothing over the frequent, rapid changes in movement direction that are characteristic of twitching motility), whilst being short enough capture the response of cells to the changing gradient with reasonable temporal resolution (Figure 2g). The normalized gradient, G, at each point along the trajectory was calculated via bilinear interpolation from the mathematical model of diffusion (Extended Data Figure 1f) and was averaged to obtain the mean G for each segment. In these experiments cells were imaged in only one field of view, which spanned the full channel width in y and approximately from $x = -0.05$ to 0.43 mm.

Calculation of the apparent aspect ratio. To quantify the orientation of cells relative to the surface, we calculated cell length divided by the cell width to obtain its aspect ratio as viewed from below the surface. *P. aeruginosa* cells have an elongated cylindrical shape, such that when cells are oriented perpendicular to the surface they have an apparent aspect ratio of one, whereas cells oriented parallel to the surface yield an

aspect ratio greater than one. The apparent aspect ratio of each cell was calculated over time and data from all trajectories were pooled to obtain the probability density function for each strain (Figure 3d).

Calculation of root mean squared displacement. The root mean square displacement (*RMSD*) measures how far cells venture from their initial position as a function of time, allowing us to objectively compare motility between different strains (Figure 3c), and in different chemical environments (Extended Data Figure 5). The *RMSD* is given by

$$RMSD(\tau) = \sqrt{\langle (x(\tau) - x_O)^2 + (y(\tau) - y_O)^2 \rangle},$$

where τ is the time lag, $[x_o, y_o]$ is a cell's initial position, and angled brackets denote averaging. When plotted on a log-log plot (Extended Data Figure 5b), the $RMSD(\tau)$ of twitching cells exhibits a slope of approximately one for small τ, denoting ballistic motion, and transitions into a slope of ½ for larger τ, which corresponds to diffusive motion. Similar observations have been made for the motility of a diverse range of microorganisms (Visser and Kiorboe, 2006).

Reversal detection. While the reversals in *M. xanthus* have been comprehensively studied (Zhang et al., 2012), reversals in twitching *P. aeruginosa* have largely escaped mention in the literature (see Semmler and colleagues (Semmler et al., 1999) for an exception). One possible reason for this is that the latter occur much more infrequently: while *M. xanthus* cells reverse once every several minutes (Kearns and Shimkets, 1998; Shi et al., 1996), we find that on average *P. aeruginosa* cells reverse once every

few hours (Figure 4c). Reversals in *M. xanthus* are typically enumerated manually by direct observation (Kearns and Shimkets, 1998; Shi et al., 1996), but quantifying the relatively infrequent reversals exhibited by *P. aeruginosa*, necessitated the development of an automated algorithm to detect reversal events among a large number of cell trajectories.

Cells tend to move along their long axis (Extended Data Figure 6) by pulling themselves along using pili that extend from their leading pole (Cowles and Gitai, 2010; Skerker and Berg, 2001). A reversal occurs when a cell stops and moves back in the other direction without turning. Under idealized conditions then a reversal occurs when a cell's body orientation, ϕ, remains constant, but its movement direction, θ, changes by $\pm\pi$ such that the leading pole becomes its trailing pole (Extended Data Figure 6). However, in practice both the unsteady, jerky movement of twitching motility and cell division (Figure 4a, b) can generate events that a basic algorithm would misdiagnose as a reversal. Since 'true' reversals are readily observed by eye (Supplementary Videos 3, 4, 5, 6), our approach was to develop an algorithm that agrees with what one would obtain by direct observation. To achieve this, we developed a system of filters to discriminate true reversals from spurious events and adjusted parameters of these filters using direct observation as a benchmark. Importantly, we used exactly the same method to analyze each experiment, allowing us to objectively compare the reversal rate in different strains and in different chemical environments.

To detect reversals in the static gradients, we first smoothed trajectories using a 10 min moving average filter (Figure 4a) to calculate the mean movement direction, θ_M. At each time point along the trajectory we identify the leading pole by determining which of the cell's two poles is most closely aligned with the direction of cell

movement (i.e. we determine whether ϕ or $\phi+\pi$ forms the smallest angle with θ_M). A potential reversal occurs when a cell's leading pole shifts to the opposite side of the cell between subsequent time points. We used the same procedure to identify potential reversals in the alternating gradient experiments, but because reversals were induced more frequently and cells were tracked at a higher temporal resolution (every 8 seconds, as opposed to every minute in the static gradient experiments) we used a 160 second moving average filter to obtain θ_M. After identifying potential reversals, we developed a series of filters to objectively resolve which of these are 'true' reversals and which result from aberrant cell motion. Below we describe each of these filters and the specific cell behavior that they are designed to discriminate. Smoothed cell trajectories were used in each of these calculations.

We exclude potential reversals from:

1. Cells who are sliding sideways, for example, when they are pushed by flow. These cells have motility that is not aligned with the cell's long axis before and after the reversal. We measure the cosine of the angle between the direction of the leading pole and the direction of cell motility and reversals are excluded if this is smaller than 0.55.
2. Cells who are upright and only attached by one pole to the surface (whose mean apparent aspect ratio is smaller than 1.4 either before or after the reversal).
3. Cells who are non-motile (speed is smaller than 0.08 $\mu m\ min^{-1}$ either before or after the reversal).
4. Cells who are rapidly pivoting about their point of attachment with the surface (whose bodies rotate more than $\pi/8$ radians between subsequent time points).

5. Cells that are jiggling back and forth on the surface. We do this by excluding cells that have experienced another potential reversal in the preceding or following 5 min in the static gradient experiments (2.4 min in the alternating gradient experiments).
6. Cells undergoing division. Cell division events were detected by measuring the change in cell length over time. We exclude potential reversals in trajectories that experience a large reduction in cell length immediately before or after a reversal. Apparent reversals arising from cell division are marked in Supplementary Videos 3 and 4.

Calculation of reversal rate. To estimate the reversal rate, we divided the total number of reversals in an experiment by the cumulative time of all trajectories. In the calculation of the latter, we omitted the trajectories of weakly motile cells that are incapable of generating reversals (owing to our specification of a minimum cell speed, see previous section). This ensures consistency when comparing the reversal rate across experiments that may have different fractions of weakly motile cells.

In experiments with a static DMSO gradient (Figure 4c) we separately measured the reversal rate of cells that are initially traveling down the gradient (white bars) and cells initially traveling up the gradient (black bars). The rate of 'correct' reversals was calculated by dividing the total number of correct reversals by the cumulative time that trajectories moved down the gradient. Conversely, the rate of 'incorrect' reversals was calculated by dividing the total number of incorrect reversals by the cumulative time that trajectories moved up the gradient. In both calculations, the cumulative time was adjusted using the cell speed consideration noted in the previous paragraph.

Extended Data Figures

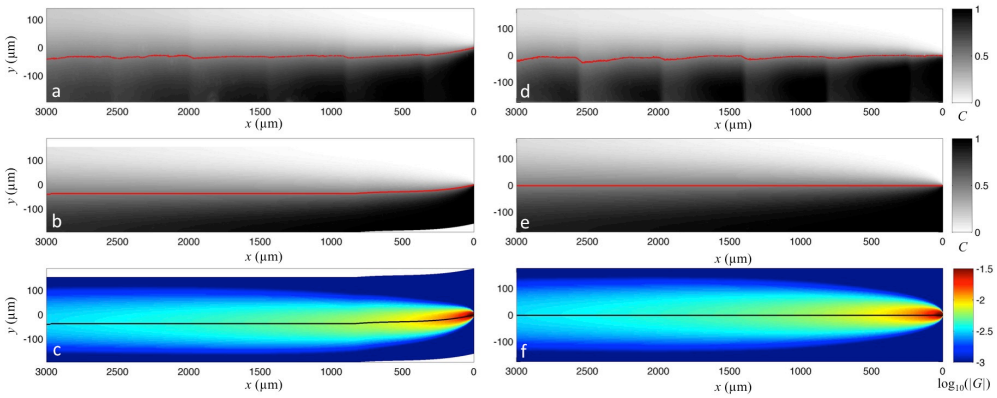

Extended Data Figure 1: A mathematical model accurately predicts the distribution of chemoattractant in two Bioflux microfluidic devices. The 'WPM' channels (**a**, **b**, **c**) and 'Invasion' channels (**d**, **e**, **f**) generate slightly different chemoattractant distributions owing to the different geometry of their inlets. In experiments without bacteria, we measured the normalized concentration, C, of fluorescein in each channel design using confocal microscopy (**a**, **d**, Supplemental Methods). This distribution was simulated using an analytical model of molecular diffusion (**b**, **e**), which was then differentiated to obtain, G, the normalized chemoattractant gradient (**c**, **f**, Supplemental Methods). The $C = 0.5$ contour is marked with red line in the upper two rows and a black line in the lower row. The WPM channels generate a chemoattractant distribution slightly asymmetric about $y = 0$, which was accounted for in the model by matching the $C = 0.5$ contour from the empirical measurement (red line in **a**, Supplemental Methods). Note the different scales in x and y.

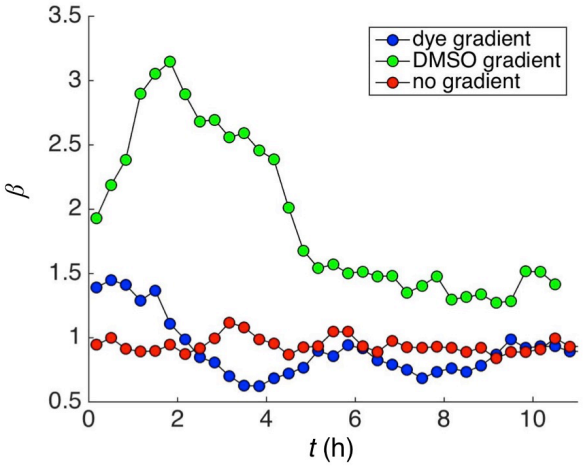

Extended Data Figure 2: Cells do not exhibit appreciable chemotaxis to Chicago Blue dye. The chemotactic bias, β, of cells in a gradient of dye (blue line) lacks the strong response observed in a gradient of DMSO (green line) and more closely resembles that of a gradient-free control (red line). We used this dye in alternating gradient experiments to track the distribution of chemoattractant within the microfluidic device.

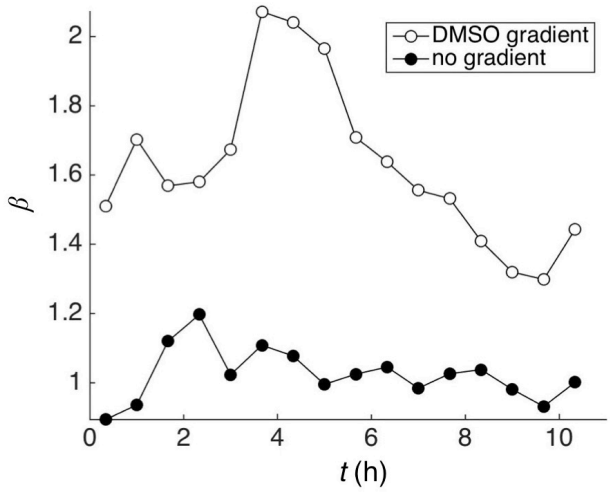

Extended Data Figure 3: The response regulator CheY1 is not required for twitching chemotaxis. *cheY1*-null cells exposed to a gradient of DMSO (line with white circles) exhibit a chemotactic bias, β, larger than they exhibit in the absence of chemical gradients (line with black circles), indicating that they are strongly chemotactic. CheY1 mediates chemotaxis in swimming *P. aeruginosa* cells (Kato et al., 2008; Masduki et al., 1995; Sampedro et al., 2014).

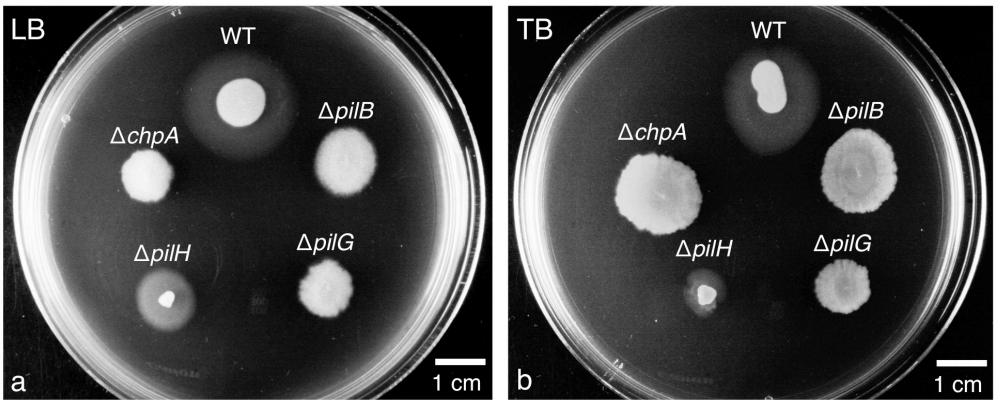

Extended Data Figure 4: The behavior of Chp chemosensory mutants in agar-based 'stab' assays. Twitching motility in this assay is detected by the formation of the so-called *twitching rings* (faint rings that form around colonies), which form at the bottom of plates, between the plastic and the agar. In-frame deletions of *pilB*, *chpA* and *pilG* prevent twitching rings while *pilH*-null cells form smaller twitching rings than the respective WT. We recapitulate the data published previously using plates containing Luria broth (LB, **a**) (Bertrand et al., 2010; Fulcher et al., 2010) and also study twitching motility in plates containing tryptone broth (TB, **b**) as this is the growth medium used in our microfluidic experiments. Plates were imaged after 48 hours of incubation.

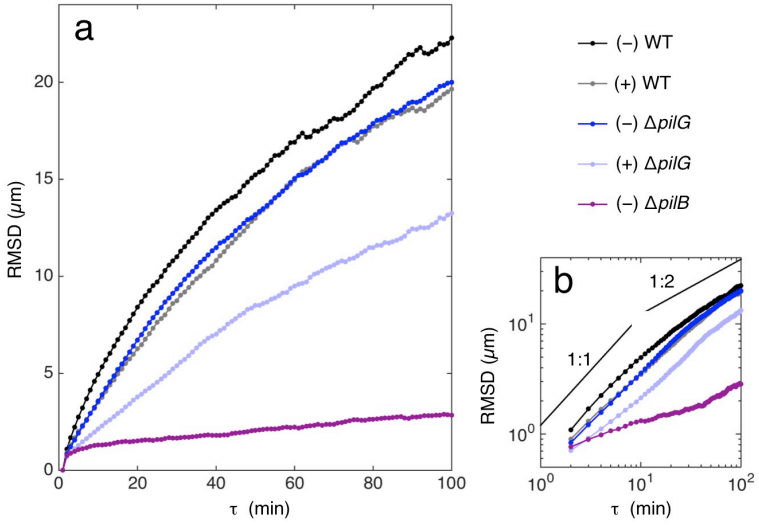

Extended Data Figure 5: Both wild-type and Δ*pilG* cells exhibit reduced motility in the presence of DMSO. The root mean square displacement, *RMSD*, of twitching cells in the absence (−) and presence (+) of DMSO reveals the latter venture a shorter distance from their origin over a time lag, τ. Data for the nonmotile Δ*pilB* strain is shown for comparison. Here the *RMSD* is plotted as function of τ on linear (**a**) and logarithmic (**b**) axes. The line with a 1:1

slope in (**b**) corresponds to ballistic movement, whilst the 1:2 slope corresponds to diffusive movement (Supplemental Methods). All experiments were performed in the absence of gradients, in either TB (−) or TB supplemented with 350 mM DMSO (+).

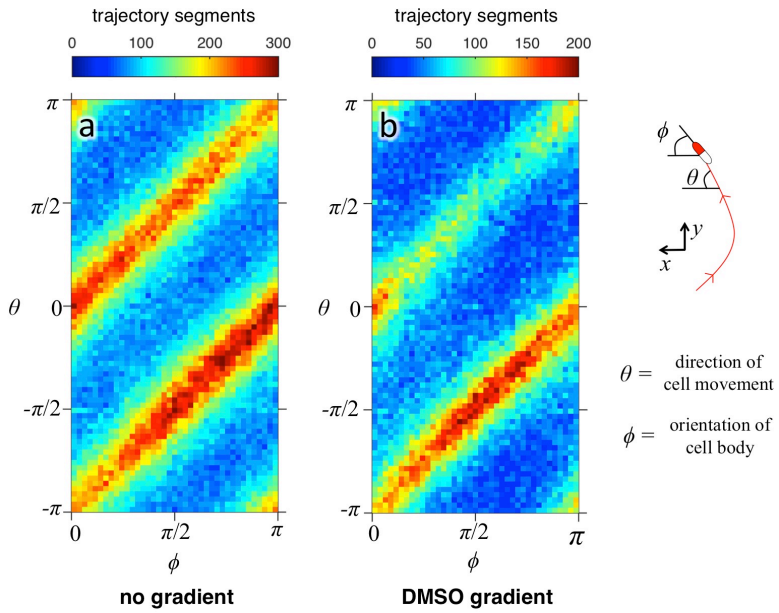

Extended Data Figure 6: Twitching cells tend to move along their long axis both in the absence (a) and presence (b) of a DMSO gradient. The orientation of the cell body, ϕ, and the direction of cell motility, θ, were calculated at each time point along the trajectories (Supplemental Methods). Each pair of angles was used to generate a histogram that shows their relative frequency in ϕ - θ space. While the orientation of a cell body, which lacks polarity, can be fully specified by its angle in the half plane, $\phi = [0, \pi]$, cell motility can occur in any direction on the unit circle, $\theta = [-\pi, \pi]$. When a cell undergoes a 'reversal', ϕ remains constant, but θ shifts by $\pm\pi$. Strong clustering in (**a**) along the lines $\phi = \theta$ and $\phi = \theta - \pi$ reveals that in the absence of a gradient cells tend to move along their long axis, likely owing to fact that the pili, with which cells pull themselves along a surfaces, cluster at their poles (Cowles and Gitai, 2010; Skerker and Berg, 2001). A similar distribution is observed in a gradient of DMSO (**b**), but cells preferentially move along their long axis in the direction of increasing DMSO concentration.

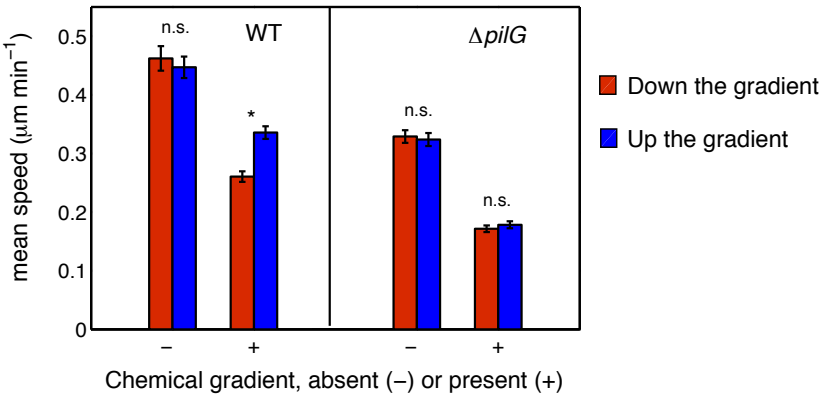

Extended Data Figure 7: Wild-type cells traveling towards the DMSO source ('up gradient') move approximately 25% faster than cells moving away from the DMSO source ('down gradient'), but this asymmetry in speed is absent in Δ*pilG* cells and in gradient-free controls. (+) denotes data from experiments with a DMSO gradient, whereas (−) denotes data from control experiments which use pure tryptone broth (TB). For each experiment, we smoothed trajectories with a 10 min moving average filter and calculated the speed and direction of cell movement at each point along these smoothed trajectories. The resultant measurements of cell speed were pooled by whether they were recorded as the cell moved in the $-y$ or $+y$ direction, which correlates to 'Up the gradient' and 'Down the gradient' respectively. In the gradient-free controls, 'Up the gradient' and 'Down the gradient' correspond to cell speed in the same y direction as experiments with a DMSO gradient (Figure 1). 'n.s.' denote non-significant differences in speed while '*' denote a p-value < 0.05, according to Wilcoxon rank tests at a significance of 5%. Error bars are standard errors of means.

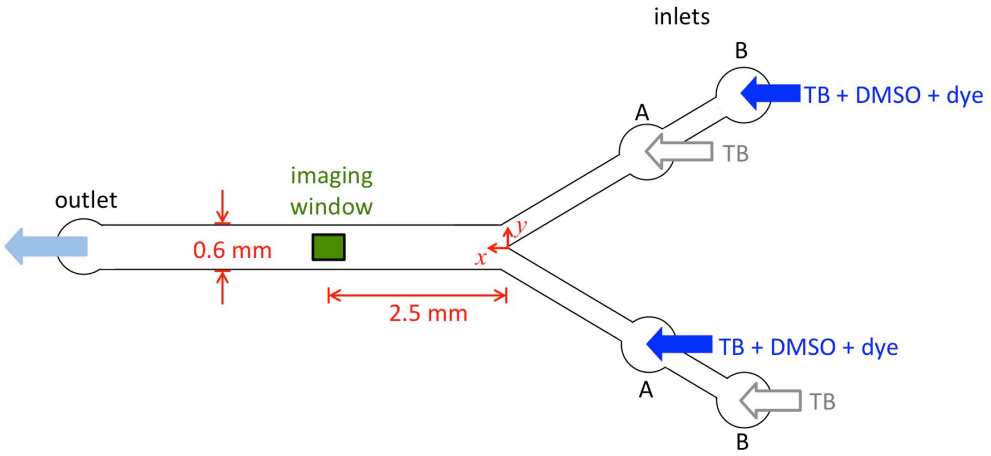

Extended Data Figure 8: A schematic of the microfluidic device used to rapidly alternate the direction of a chemoattractant gradient. The four inlets of the device were connected to reservoirs containing either TB mixed with 350 mM DMSO and Chicago blue dye or pure TB. Fluid was continuously withdrawn from the outlet and the pairs of inlets marked 'A' and 'B' were sequentially clamped (Supplemental Methods) such that fluid is pulled from only one pair

of inlets at a time. Moving the clamps to the opposite pair changes the direction of the chemoattractant gradient in the imaging window (green box). The channel is 75 μm deep.

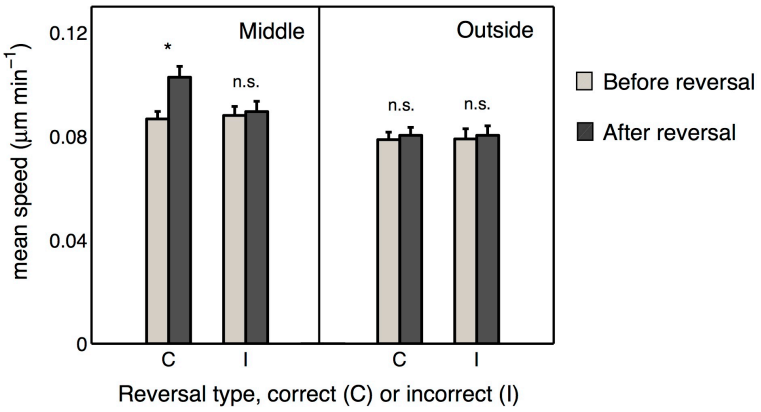

Extended Data Figure 9: Cells move faster after responding to a change in the direction of a chemoattractant gradient. We calculated the mean speed of individual cells before (light grey bars) and after (dark grey bars) they performed reversals (Supplemental Methods), and pooled these according to whether they occurred in the 'Middle' of the device (the region between the dashed lines in Figure 4d,e), where spatial gradients are strongest, or on the 'Outside' edges of the device (the region outside the dashed lines in Figure 4d,e), where spatial gradients were relatively weak. Correct reversals occur in cells initially moving away from a chemoattractant source, and incorrect reversals occur in cells initially moving towards a chemoattractant source. Cells increase their speed after performing correct reversals in the middle of the channel, where they are induced at a higher rate (Figure 4f). These asymmetries are not found in the outside region or for incorrect reversals. 'n.s.' denote non-significant differences in speed while '*' denotes a p-value < 0.05, according to paired-sample t tests at a significance of 5%. Error bars are standard errors of means.

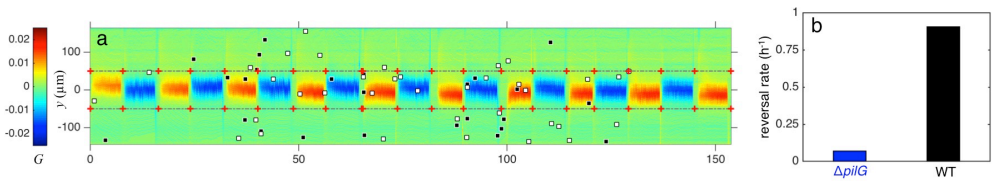

Extended Data Figure 10: Cells lacking the response regulator PilG rarely reverse direction in the alternating gradient experiment. (**a**) When Δ*pilG* cells were exposed chemoattractant conditions analogous to that shown in Figure 4d, reversals (black and white boxes) occurred relatively infrequently when compared to the wild-type, which is consistent with the behavior of swimming Δ*cheY1* cells (CheY1 being homologue of PilG) that rarely reverse their swimming direction and lack the ability of flagella-based chemotaxis (Masduki et al., 1995). Data in **a** are presented in the same manner as Figure 4d of the main text (the x axis in μm as for the y axis). (**b**) The reversal rate of Δ*pilG* and wild-type cells in the alternating gradient was quantified by dividing the total number of reversals (correct and incorrect) by the total time of trajectories (Supplemental Methods), revealing that reversals occurred 13 times more frequently in the WT than in Δ*pilG*.

Supplementary Videos

Supplementary Video 1: Surface attached cells display chemotaxis in a static gradient of DMSO. Cells with red trajectories are traveling towards higher concentrations of DMSO, cells with cyan trajectories are traveling towards lower concentrations of DMSO, and cells with yellow trajectories display little net movement in any direction. The latter are distinguished by measurements of the 'Net to Gross Displacement Ratio' (NGDR<0.15; Supplementary Methods).

Filename: OliveiraDurhamFosterVideo1.mov

Supplementary Video 2: Surface attached cells bias their motility to track gradients of succinate. Dye is used to visualize the distribution of succinate (Supplementary Methods), which here has been processed to appear yellow. We alternate the direction of the gradient every three hours and cells respond by biasing their movement such that they consistently move towards larger concentrations of succinate.

Filename: OliveiraDurhamFosterVideo2.mov

Supplementary Video 3: Wild-type cells perform reversals in the absence of chemical gradients. By definition, a reversal occurs when a cell stops and moves back in the other direction without turning. This can be captured when the cell's leading pole, the end of the cell that is pointing in the direction of movement (small green circles), shifts to the opposite side of the cell. Cells performing 'true' reversals are marked with yellow rings, reversals associated with cell division are marked with cyan rings, and reversals that occur too close to the end of the trajectories to ascertain their origin are shown with magenta rings (Supplementary Methods). Cells whose motility is being actively monitored for reversals are marked with a small red dot.

Filename: OliveiraDurhamFosterVideo3.mov

Supplementary Video 4: Cells lacking the response regulator PilG, homologue of CheY of *Escherichia coli*, reverse less frequently than wild type cells. Here we analyze the movement of Δ*pilG* cells that are exposed to the same conditions as shown in Supplementary Video 3 and we use the same notation to mark the reversals. Compared to the wild type, Δ*pilG* cells perform true reversals (thick yellow rings) less frequently (Figure 4c).

Filename: OliveiraDurhamFosterVideo4.mov

Supplementary Video 5: Cells reverse to track a DMSO gradient that rapidly changes direction. We visualized the DMSO gradient, which changes direction every eight minutes, using dye (shown here in red, Supplementary Methods). The two cells highlighted here reverse direction to keep their motility directed towards larger concentrations of DMSO. All reversals are marked with yellow rings and the leading poles of cells are denoted with small green circles. Yellow lines show cell trajectories.

Filename: OliveiraDurhamFosterVideo5.mov

Supplementary Video 6: Cells exposed to a rapidly alternating DMSO gradient reverse more frequently in the middle of the device, where spatial gradients of chemoattractant are the largest. Dye is used to visualize the instantaneous distribution of DMSO, which here has been processed to appear red. Correct reversals (white rings) occur in cells whose leading pole (small green circles) is initially directed down the DMSO gradient, whereas incorrect reversals (light blue rings) occur in cells whose leading pole is initially directed up the DMSO gradient. Cells whose motility is being actively monitored for reversals are marked with a small blue circle.

Filename: OliveiraDurhamFosterVideo6.mov

Supplementary materials of Chapter 5

Supplementary Figures

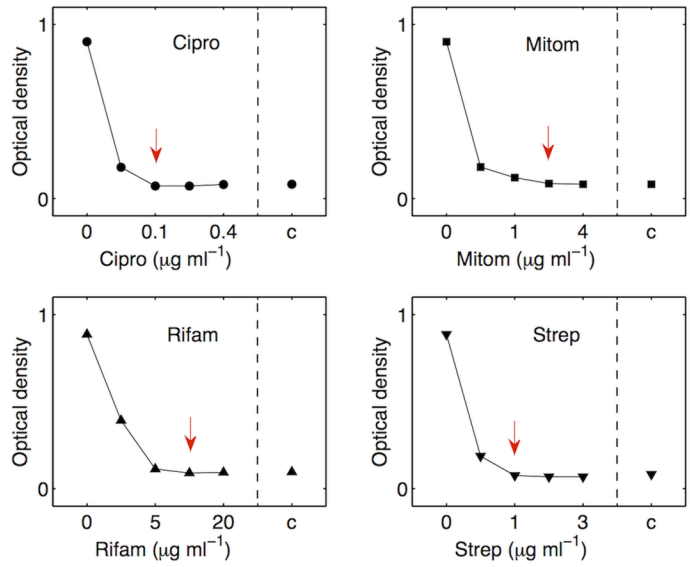

Figure S1. Growth effects of increasing concentrations of antibiotics in shaking culture of *P. aeruginosa* to determine the respective MIC of the strain. Red arrow denotes the minimal inhibitory concentration (MIC) for each antibiotic, which is defined as the minimum concentration of antibiotic that prevents detectable growth in shaking culture after 20 hours when compared to cell-free controls. 'Cipro' = ciprofloxacin, 'Mitom' = Mitomycin C, 'Rifam' = Rifampicin, 'Strep' = Streptomycin and 'c' denotes cell-free controls (fresh tryptone broth). Error bars representing SE of 8 independent replicates are too small to see and fall within each data point shown.

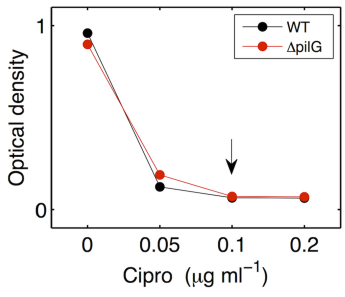

Figure S2. Cells lacking the key response regulator for twitching chemotaxis, PilG, and respective wild-type have identical MIC for ciprofloxacin. Data points are means of 8 independent replicates showing the mean optical density of shaking cultures after 20 hours of growth for increasing concentrations of ciprofloxacin, 'Cipro'. Error bars representing SE are too small to see and fall within each circle. Arrow denotes MIC.

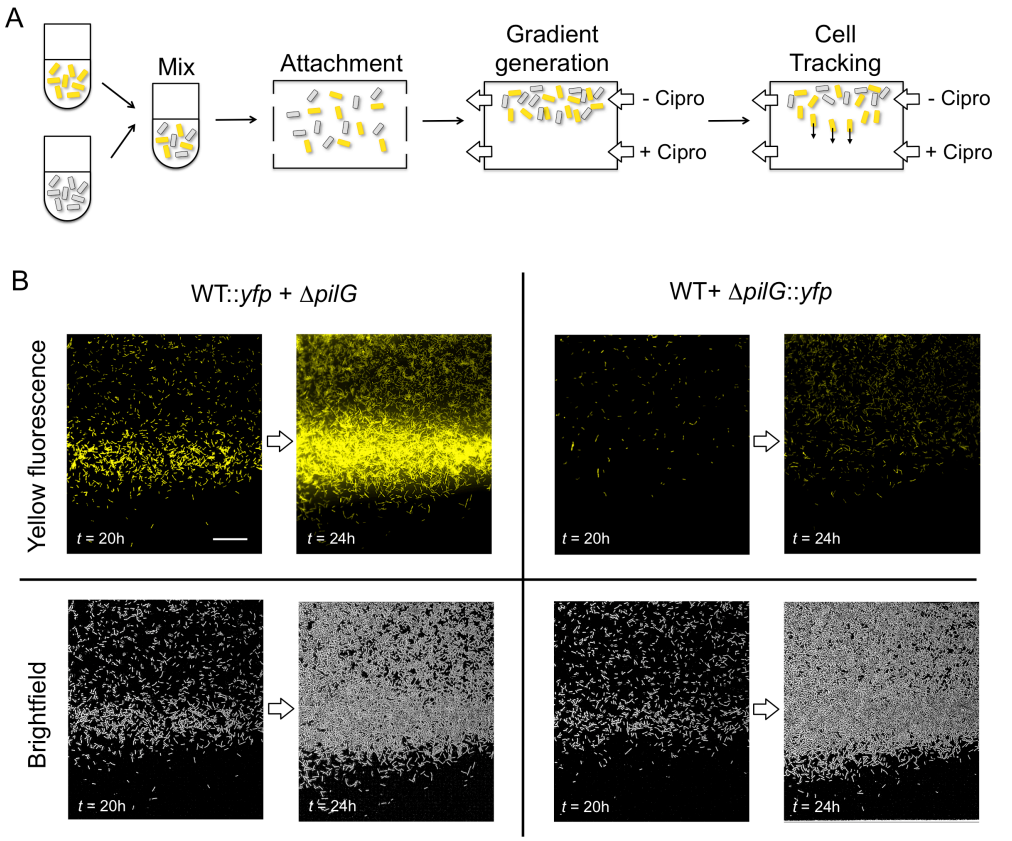

Figure S3. Mixing wild-type *P. aeruginosa* together with cells lacking the response regulator PilG shows that chemotaxis towards antibiotics allows cells to more rapidly and effectively invade regions of high ciprofloxacin concentration. (**A**) Schematic of the experimental design, which involves mixing genotypes from overnight cultures at 1:1 ratio, initial attachment in the absence of flow, generation of antibiotic gradient (here 'Cipro' denotes ciprofloxacin, which was injected at C_{max} = 1 μg ml^{-1}) and finally imaging after competition between strains and tracking of cell movement. White arrows represent the direction of flow and small black arrows on cells in the last step denote direction of cell movement. (**B**) Epifluorescence micrographs and brightfield images show the developing biofilms after 20 h and 24 h. We considered two mixing scenarios: *yfp*-labeled WT cells mixed with non-labeled Δ*pilG* cells (left), and non-labeled WT cells mixed with *yfp*-labeled Δ*pilG* cells (right). Both show the same pattern: accumulation of WT cells at theoretically lethal concentrations of ciprofloxacin, which results from twitching chemotaxis. Scale bar is 50 μm. All images were taken upstream, where the two flow streams meet and the antibiotic gradient is the steepest (Figure 1). Δ*pilG* and respective wild-type were chromosomally tagged with constitutively-expressed yellow fluorescent proteins using the mini-*Tn*7 system (Lambertsen et al., 2004). Identical image collection and processing settings were used in all images. Brightfield images were edited as follows: background was removed and changed to black, and cells (white spots) were changed to white for contrast purposes.

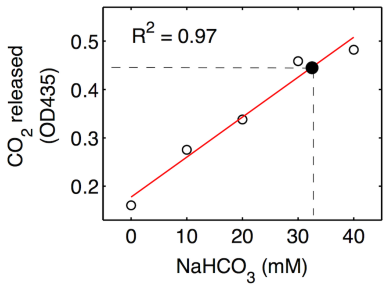

Figure S4. Assessing carbon dioxide in the cell-free supernatant from standing cultures of *P. aeruginosa*. Open circles show CO_2 content in tryptone broth with increasing concentrations of sodium bicarbonate, $NaHCO_3$, and the red line is a linear fit to the data ($R^2 = 0.97$). The black circle represents the mean CO_2 content of 3 independent replicates of cell-free supernatant from 20-hours grown cultures of *P. aeruginosa*. CO_2 content of samples was obtained using the HACH LANGE cuvette tests as explained in the section 'Experimental Procedures'. These measurements are based on a reaction that converts all carbonates and dissolved carbon dioxide in test samples into gaseous carbon dioxide. This released CO_2 changes the color of the indicator thymol blue sodium salt and can be quantified photometrically using the absorbance of the solution at 435 nm.

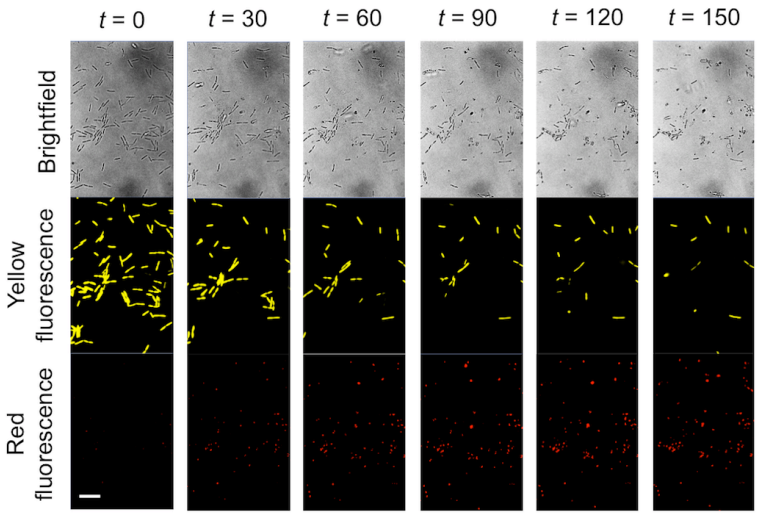

Figure S5. Cells experiencing theoretically lethal concentrations of ciprofloxacin, remain metabolically active. We show the reduction of the redox dye 5-cyano-2,3-ditolyl tetrazolim chloride, CTC, by cells experiencing ~100 μg ml^{-1} of ciprofloxacin (MIC = 0.1 μg ml^{-1}) after 24 hours of an experiment where the concentration of ciprofloxacin injected corresponds to C_{max} = 100 μg ml^{-1}. CTC is water-soluble and non-fluorescent in its oxidized state but becomes insoluble and fluoresces in red when reduced (CTC-formazan) by a functional electron transport chain. Once injected through both inlet wells of the microfluidic channel (diluted in fresh growth medium), and after a period of 20 min of incubation, we imaged CTC reduction every 30 min. Note that overtime (*t* in minutes) the red signal increases, indicative of CTC-formazan accumulation, and the yellow signal decays as upon reduction CTC precipitates, which leads to the death and burst of the respiring cell. Scale bar is 5 μm. Epifluorescence

micrographs were collected and processed using the same settings overtime to ensure consistency. The two black spots at the top and bottom of each (non-edited) brightfield image are crud present on the outside of the glass bottomed channel.

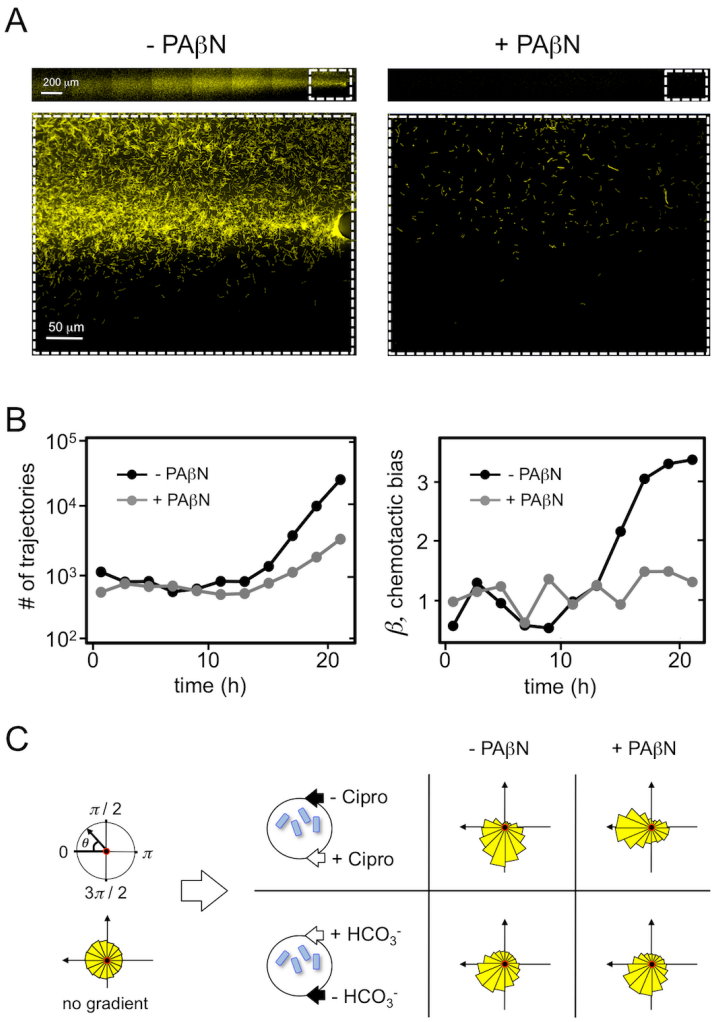

Figure S6. Effect of the efflux pump inhibitor PAβN on twitching chemotaxis in developing biofilms. (**A**) Adding PAβN reduces biofilm accumulation (*yfp*-labelled cells) in ciprofloxacin gradients, which is consistent with the model of phenotypic resistance we discussed in the main text. We show composed tiles made by eight consecutive sections of the channels (top), with blow-ups of the upstream regions where the flow streams meet and the antibiotic gradient is the steepest (bottom), after 24 hours of growth. '- PAβN' denotes PAβN-free control, where C_{max} = 100 μg ml^{-1} of ciprofloxacin (corresponding to 1000 times the MIC of the strain), while in '+ PAβN' we complemented the PAβN-free control by adding 5 μg ml^{-1} of PAβN in the media being injected through both inlets of the device. Cells in the device thus experience uniform concentration of PAβN. Identical image collection and processing settings were used in both conditions. (**B**) Time series of number of trajectories (log scale) and chemotactic bias with and without PAβN. Consistent with the reduced number of cells in the

device shown in panel (A), the number of trajectories being tracked in the presence of the pump inhibitor PAβN is smaller compared to the PAβN-free control, namely after ten hours of experiment (left panel). Importantly, we find a sharp increase in the chemotactic bias overtime in the PAβN-free control, but this pattern is absent in the presence of PAβN (right panel). (**C**) The addition of PAβN does not prevent chemotaxis away from bicarbonate. Similar behavior is obtained when PAβN is added to cell-free supernatant of the responding genotype (data not shown). Rose plots show the probability density functions of θ, the angle of cell trajectories from their beginning to their terminus in antibiotic gradients (top) and bicarbonate gradients (bottom), with (+) and without (-) the pump inhibitor, PAβN. We used the last ten hours of each experiment (from t = 10 h to t = 20 h), before the system became too crowded, which prevents cell tracking and further analysis. Note that in the absence of PAβN twitching cells move towards ciprofloxacin, which is prevented by the addition of PAβN. However, in both '- PAβN' and '+ PAβN' we find that cells move away from bicarbonate. We injected through one of the inlets (more specifically, top inlet in the diagram) C_{max} = 30 mM of bicarbonate in both cases, which closely matches the expected concentration of carbon dioxide and carbonate-associated ions present in the cell-free supernatant of the test strain (see Figure S4). For guidance, we show the distribution of θ in TB-only controls (left) along with basic diagrams of the chemical gradient created in each condition, where blue objects denote moving cells and small arrows denote flow direction.

Supplementary Videos

Supplementary Video 1: Surface attached *Pseudomonas aeruginosa* cells display chemotaxis in a static gradient of ciprofloxacin. Cells with blue trajectories are traveling towards higher concentrations of ciprofloxacin, while cells with red trajectories are traveling towards lower concentrations of ciprofloxacin. The concentration of antibiotic injected in this experiment, C_{max}, is 10 times the MIC of the strain (0.1 μg ml^{-1}).

Filename: OliveiraDurhamFoster_AntibioticTaxis_Video1.mov

Supplementary Video 2: Chemotaxis allows bacteria to rapidly and effectively invade regions of high antibiotics concentration. The video shows the result of mixing *yfp*-labeled wild-type cells with non-labeled Δ*pilG* cells that lack the response regulator of twitching chemotaxis, PilG, at 1:1 ratio in spatial gradients of ciprofloxacin where C_{max} = 1 μg ml^{-1}, which is 10 times the MIC of the strains.

Filename: OliveiraDurhamFoster_AntibioticTaxis_Video2.mov

Supplementary Video 3: Twitching bacteria move towards antibiotic concentrations one thousand times higher than their MIC. Cells with blue trajectories are traveling towards higher concentrations of ciprofloxacin, while cells with red trajectories are traveling towards lower concentrations of ciprofloxacin. The concentration of ciprofloxacin injected in this experiment is 1000 times the MIC of the strain, C_{max} = 100 μg ml^{-1}.

Filename: OliveiraDurhamFoster_AntibioticTaxis_Video3.mov

Antibiosis drives exploitative competition

In this section of the appendix I briefly present preliminary data on the effect of mixing strains of *Pseudomonas aeruginosa* on the production of pyoverdine (iron-scavenging agent). Pyoverdine production has been the focus of intense research namely because it is an important virulence factor of *P. aeruginosa*, and can even regulate the production of other virulence factors (Lamont et al., 2002; Visca et al., 2007).

In the sociomicrobiology literature, siderophores such as pyoverdine have been studied as public goods as indeed these are fitness-promoting secretions that are costly to produce and may benefit other non-producer cells (Griffin et al., 2004). Accordingly the consensus in the field is that they evolve to help other cells of the same genotype and siderophore production became a classical example of cooperation in bacteria (Nadell et al., 2009; West et al., 2007a; West et al., 2006). But in natural populations where multiple strains and species meet and mix together, it is not clear how such mixing affects siderophore production. Motivated by this lack of knowledge on the effect of strain competition on the classical example of microbial cooperation, we have recently been studying the effect of mixing natural isolates of *P. aeruginosa* on pyoverdine production and, as for biofilm formation, preliminary data suggest that mixing strains drives the production of these siderophores (Figure 1). Specifically, we considered pairwise mixtures of the main set of strains studied in Chapter 3 (strains 1, 4, 7 and 69), and found a higher pyoverdine index in co-cultures (Figure 1A).

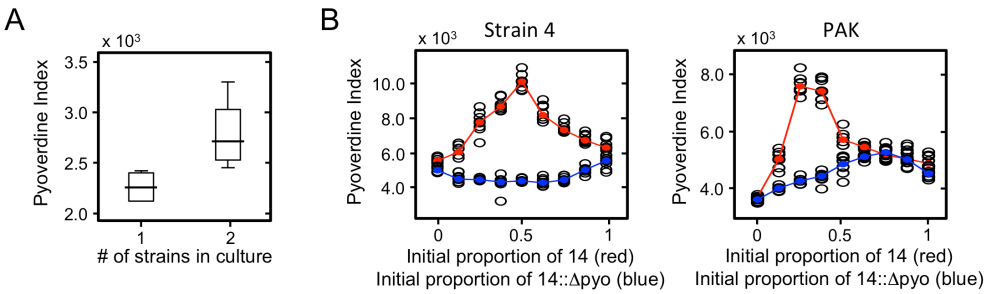

Figure 1. Mixing different natural isolates of *P. aeruginosa* induces pyoverdine production. (**A**) The pyoverdine index (pyoverdine per cell density) is significantly higher in cultures with two strains compared to monocultures ($p < 0.05$ in a Wilcoxon-signed rank test). The box plots show means of eight independent replicates of four different *P. aeruginosa* strains (1, 4, 7 and 69, see Chapter 3 and respective supporting material for details on these strains), and the respective pair-wise mixtures. We used the same growth conditions and dilutions as for the biofilm study in Chapter 3 with two main differences: instead of static cultures, which promote biofilm growth, we considered well-mixed conditions, and instead of tryptone broth (TB) we used CAA medium (5 g casamino acids, 1.18 g $K_2HPO_4.3H_2O$, 0.25 g $MgSO_4.7H_2O$ per liter) as pyoverdine production in TB is small. The absorbance at 600 nm was used as a proxy for cell density (A_{600}) and for pyoverdine production we followed standard protocols (Jiricny et al., 2010). Specifically, we considered the relative fluorescence units (RFU) of cultures at an excitation wavelength of 400 nm and an emission wavelength of 460 nm using a SpectraMax M2 fluorimeter after 20 h of incubation. (**B**) Mixing increases pyoverdine production in two pairwise combinations of strains (4 + 14 and PAK + 14) in which the initial proportion of each strain was varied. Importantly, when we mix strain 4 or strain PAK with mutants of strain PA14 ('14') that do not produce pyocins ('14::Δpyo'), we do not find mixing-induced pyoverdine production, suggesting that antibiotic competition is an important driver of siderophore production in co-cultures. White circles denote the pyoverdine index of eight independent replicates for each condition, while the red (blue) circles show medians of cultures with PA14 WT (pyocin-null) strains. These pairs of strains were chosen based on the results of Chapter 3 where we show that strains 4 and PAK are susceptible to pyocins from strain PA14 and robustly respond to these antibiotics via biofilm formation.

While siderophores are unequivocally cooperative traits (Griffin et al., 2004), their primary function is to scavenge iron, a critical growth resource for microbes (Varma and Chincholkar, 2007). Siderophore production is thus consistent with both cooperation and exploitation. But which are the drivers of mixing-induced pyoverdine production in our experiments? Understanding this phenotype is important to know if siderophores are being produced to help or to exploit. Consistent with what we found for mixing-induced biofilm formation, mixing-induced siderophore production is dose

dependent (Figure 1B) and, importantly, it is a response to antibiotic competition (Figures 1B and 2A).

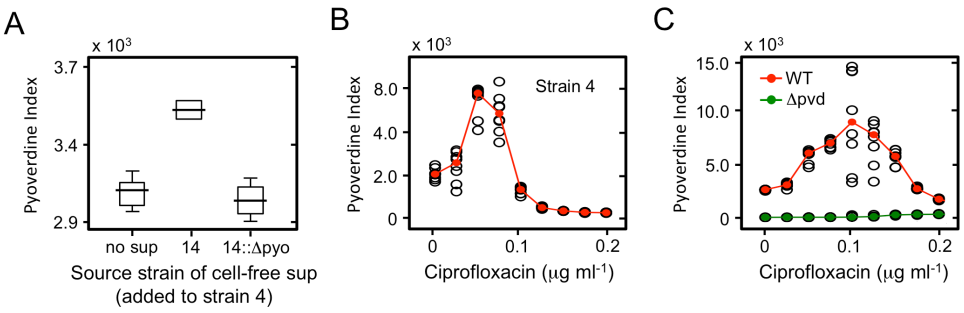

Figure 2. Antibiosis drives pyoverdine production in *P. aeruginosa*. (**A**) Supplementing cell free-supernatant from strain PA14 ('14') to cultures of strain 4, which is susceptible to pyocins produced by PA14 (Chapter 3), leads to in an increase in the pyoverdine index (RFU / A_{600}). As for antibiotic-induced biofilm formation, cell-free supernatant from a pyocin-null mutant strain ('14::Δpyo') does not elicit enhanced pyoverdine production in the focal strain 4. Identical results were obtained with PAK as test strain (data not shown). The box plots show means of eight independent replicates, and 'no sup' shows the basal pyoverdine index of the strain in the absence of cell-free supernatant from competitors after 20 h of incubation. (**B**) Sub-lethal concentrations of the antibiotic ciprofloxacin also drive pyoverdine production in strain 4 as it happens for antibiotic-induced biofilm formation (Chapter 3). (**C**) As expected, the pyoverdine index of mutant cells that do not produce pyoverdine (here 'Δpvd') is not affected by increasing concentrations of antibiotics. This pyoverdine-negative strain is a deletion mutant derived from PAO1 and defective for the pyoverdine synthetase gene *pvdD* (Ghysels et al., 2004). Both WT and Δpvd strains were gifts from the West lab. White circles show the pyoverdine index of eight independent replicates for each condition, while the red (green) circles show medians of cultures with PAO1 WT (pyoverdine-null) as responder strain.

What is the evolutionary basis of these effects of strain mixing on pyoverdine production? Given that siderophore production is a form of resource exploitation, one can speculate that the phenotype we document here is a response to interference competition. The idea is that upon antibiotic stress target cells respond by up-regulating their metabolism and the scavenging of important resources such as iron. As in our study of biofilm formation (Chapter 3), the pyoverdine response presented here would be consistent with the idea of competition sensing. However, it is not clear at present how this strategy would preferentially benefit the producer strain, unless it evolved in the context of biofilm growth where cells can better control the environment

with secreted products such as siderophores that favor their genotype over others given the hampered diffusion typical of surface-associated communities (Julou et al., 2013).

Alternatively, and as discussed for antibiotic-induced oxygen consumption (see Chapter 6), the effect of antibiosis on the pyoverdine production reported here may simply reflect a non-adaptive byproduct of antibiotic action. Clearly one needs more mechanistic understanding about the system. In particular, are target bacteria up-regulating pyoverdine production or simply lysing upon antibiotic stress and releasing their siderophores in the medium? If up-regulation is indeed observed, which is the response regulator controlling it? Our most recent data show that cells lacking *gacA* have an ameliorated response, suggesting that the protein GacA is an interesting candidate to consider regarding the regulation of the mixing-induced response reported here. More generally, is siderophore production in our ecology a strategy aimed to prevent antibiotic-producing competitors from growing or simply results from antibiotic-induced imbalances in the iron homeostasis of target cells that need to be compensated? Under which demographies and spatiogenetic structuring will exploitative competition evolve as a response to antibiosis? The combination of careful ecoevolutionary modeling, with the empirical study of how strain mixing affects cell groups, will hopefully clarify these questions.

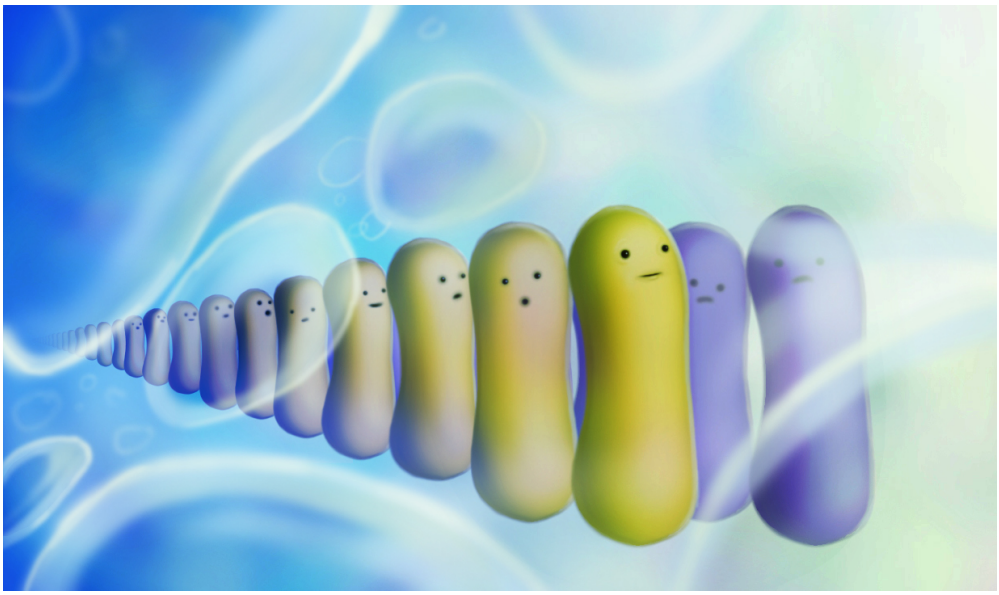

Bacteria marching towards antibiotics. Natural selection for competition sensing or something else? Future will tell. Cartoon credit: Raimundo Pousada.

Evolutionary limits to cooperation in microbial communities

Nuno M. Oliveira, Rene Niehus, and Kevin R. Foster[1]

Department of Zoology, University of Oxford, Oxford OX1 3PS, United Kingdom; and Oxford Centre for Integrative Systems Biology, University of Oxford, Oxford OX1 3QU, United Kingdom

Edited by W. Ford Doolittle, Dalhousie University, Halifax, Nova Scotia, Canada, and approved November 7, 2014 (received for review July 4, 2014)

Microbes produce many compounds that are costly to a focal cell but promote the survival and reproduction of neighboring cells. This observation has led to the suggestion that microbial strains and species will commonly cooperate by exchanging compounds. Here, we examine this idea with an ecoevolutionary model where microbes make multiple secretions, which can be exchanged among genotypes. We show that cooperation between genotypes only evolves under specific demographic regimes characterized by intermediate genetic mixing. The key constraint on cooperative exchanges is a loss of autonomy: strains become reliant on complementary genotypes that may not be reliably encountered. Moreover, the form of cooperation that we observe arises through mutual exploitation that is related to cheating and "Black Queen" evolution for a single secretion. A major corollary is that the evolution of cooperative exchanges reduces community productivity relative to an autonomous strain that makes everything it needs. This prediction finds support in recent work from synthetic communities. Overall, our work suggests that natural selection will often limit cooperative exchanges in microbial communities and that, when exchanges do occur, they can be an inefficient solution to group living.

Black Queen evolution | cooperation/exploitation | ecoevolutionary model | genetic mixing | microbial communities

> 'Benefit-of-the-species' arguments ... provide for the reader an escape from inner conflict, exacting nothing emotionally beyond what most of us learn to accept in childhood, that most forms of life exploit and prey on one another.
>
> Hamilton, 1975 (1)

Microbes typically live in dense communities containing many strains and species. These genetically diverse societies are widespread and central to how microbes affect us, including examples such as the gut microbiome, polymicrobial infections, and communities vital to bioremediation and nutrient cycling (2, 3). In these collectives, ecological interactions are thought to be both common and strong given that cell density is typically high and that microbes possess many phenotypes that influence the reproduction and survival of surrounding cells (4, 5). Such social traits include many secretions, such as extracellular enzymes and scavenging molecules (4–6), and other beneficial "leaky" traits, such as detoxification agents (7) or amino acids (8, 9).

A central explanation for cooperative phenotypes in microbes is that they function to help cells of the same genotype (10, 11), which is backed up by a growing body of theory and experiments (12–18). However, it is also clear that, in nature, microbes commonly interact with many different genotypes (both different strains and species) in complex ecological networks (19–21). Do these different microbial genotypes cooperate with one another? Understanding this question is central to building models of microbial communities and how they will respond to both environmental and anthropogenic perturbations (22).

Studies involving genetically engineered (8, 9, 23, 24) and/or artificially selected communities (23, 25, 26) emphasize how easily cooperation between genotypes can be achieved in the laboratory. Additionally, there are a growing number of suggestions that cooperation should commonly evolve between microbial strains and species (27–30). This view contrasts with empirical surveys of natural bacterial communities, which suggest that competitive interactions predominate over cooperative interactions (31). However, it has also been suggested that cooperation between different genotypes may explain the unculturability of many species in the laboratory when in monoculture (32–34). If correct, studies with culturable species could underestimate cooperativity in microbial communities.

The potential for cooperation between different microbial genotypes then remains unclear. Indeed, we even lack clear predictions of what to expect. There is a need for general theory on cooperation between microbial genotypes. One microbial interaction that has been explored theoretically is syntrophy, where one species produces a toxic waste product that another species consumes (35–38). Syntrophy is likely to be ecologically important and under some conditions (36), can benefit both species. However, syntrophic species need not pay energetic costs to interact: one species is producing waste, and the other species is feeding. Such byproduct cooperation can, therefore, readily evolve but is fundamentally different to the exchange of costly secretions (39, 40). Other models have analyzed when costly cooperation between species is expected in microbes and other organisms (35, 39, 41). However, these models assume that there is no opportunity for one partner to express the beneficial trait of the other. Although this constraint will sometimes occur, there is considerable functional overlap in the cooperative traits of microbial species (7). In addition, the potential for horizontal gene transfer in microbes means that there is a broad scope for a focal strain to pick up the phenotypes of co-occurring strains and species (42–44).

Significance

Microbes form dense and diverse communities that affect every aspect of our lives. Microbial communities are often viewed as cooperative networks with species working together toward a common goal. Here, we critically evaluate this view using an ecoevolutionary model. We show that cooperating with other species can be a poor evolutionary strategy, because it renders a cell dependent on species that may not be nearby. Moreover, when cooperative exchanges do evolve, they are inefficient and reduce the productivity of the community. Evolution by natural selection then limits the potential for productive cooperation between microbial species. We argue that understanding these limits and how to overcome them will be key to engineering microbial communities for our own ends.

Author contributions: N.M.O. and K.R.F. designed research; N.M.O. and R.N. performed research; N.M.O. and R.N. contributed new reagents/analytic tools; N.M.O. and K.R.F. analyzed data; and N.M.O., R.N., and K.R.F. wrote the paper.

The authors declare no conflict of interest.

This article is a PNAS Direct Submission.

Freely available online through the PNAS open access option.

[1]To whom correspondence should be addressed. Email: kevin.foster@zoo.ox.ac.uk.

This article contains supporting information online at www.pnas.org/lookup/suppl/doi:10.1073/pnas.1412673111/-/DCSupplemental.

Here, we examine the potential for microbial cooperation between different strains and species. We base our work on the well-established models of within-genotype microbial cooperation for a single public good (12, 18, 45–47) so that the relationship to previous work is clear (*SI Materials and Methods*). We add one key feature to these models: we allow cells to invest in multiple distinct cooperative secretions, such that there is the potential for different genotypes to exchange secretions with one another. Our analysis shows that the degree of genetic mixing defines the potential for cooperation both within and between genotypes. Low mixing favors genotypes that produce all secretions, whereas high mixing favors genotypes that do not produce any at all. Only for intermediate levels of genetic mixing do we find between-genotype cooperation, where strains produce a subset of secretions and rely on other genotypes for the complementary traits. Moreover, the form of cooperation that emerges is inefficient and results in a loss of productivity relative to one genotype making all secretions. Natural selection limits both the occurrence and effectiveness of cooperation within microbial communities.

Results and Discussion

Logic of the Model. We are interested in the potential for the evolution of cooperative exchanges in microbial communities. Cooperative phenotypes can be central to growth in microbes (4, 6, 48) in both natural (49–51) and disease (52) settings. These phenotypes are typically costly to produce but provide large shared benefits that increase the yield of all cells in a neighborhood (4–6, 48). To reflect these strong benefits, we focus on secretions that are essential for bacterial growth and set final population yield (*Materials and Methods*), although our conclusions also hold for nonessential secretions (Fig. S1). Whereas our analysis is phrased in terms of secretions, like enzymes that liberate nutrients, it also captures a range of other leaky beneficial traits, such as detoxifying enzymes like catalase (7) or amino acids (8, 9).

Fig. 1 outlines the logic of our ecoevolutionary model. For two secretions, our model has four genotypes: a producer of both traits [1,1], a producer of the first trait [1,0], a producer of the second trait [0,1], and a nonproducer [0,0], where for simplicity, 1 and 0 denote production or no production, respectively, of a given secretion, thus labeling each genotype. Our modeling is intended to capture two related scenarios. The first scenario is a single strain that makes multiple secretions, where loss of function mutations can generate the above trait combinations. The second scenario is where the different genotypes come from a combination of interacting strains and species that have similar ecologies. This latter case has clear potential for complexities that we do not represent, but we can, nevertheless, capture the evolutionary dynamics that would be driven by the focal traits. In addition to extending models of single secretions, our model is intended to formalize the hypothesis that cooperation can arise by different genotypes losing the genes for different secretions (29). This hypothesis was developed from the idea of "Black Queen" evolution (7). Specifically, if many strains all make and use the same leaky trait, some strains can lose the trait and rely on others to grow. For a single trait, Black Queen evolution then has similarities to the evolution of cheating, where a diverse network of species may be involved as either a producer or receiver of a particular trait. When microbes possess multiple leaky traits, it raises the possibility that two genotypes may reciprocally exchange beneficial traits when one loses one trait and one loses another trait (29). Linked to this scenario, a key assumption in our analysis is that it is possible for a cell to make all secretions if favored by natural selection (i.e., in a system relying on two secretions, for example, there is always the possibility of a [1,1] genotype). Although not always the case, this possibility seems likely to be common, because many secretion systems are associated with horizontal gene transfer (42, 44). However, we discuss later the effect of some secretions only being achievable by some genotypes.

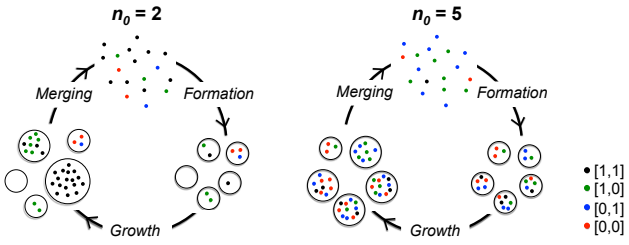

Fig. 1. Ecoevolutionary model of the microbial lifecycle. We considered three cyclically recurrent phases to model the evolutionary dynamics of a microbial population that depends on multiple secretions to grow: (*i*) formation (stochastic seeding of *M* separate subpopulations following a Poisson process with mean n_0), (*ii*) growth (independent evolution of each group following logistic growth, where the carrying capacity of the environment is proportional to the concentration of secretions in the focal group), and (*iii*) merging (*M* groups merge, and the cycle starts again after updating the genotypic frequencies). As an illustrative example, we show the effect of two different n_0 values in a two-trait model of four genotypes ([1,1], [1,0], [0,1], and [0,0], which make both secretions, one secretion, the other secretion, and none, respectively).

Between-Genotype Cooperation Emerges with Intermediate Levels of Genotypic Mixing. We are interested in understanding the effects of natural selection when microbes produce more than one fitness-promoting secretion. In particular, we are interested in whether strains will evolve to exchange secretions. Fig. 2 gives the final (steady-state) frequencies of each of the different secretion genotypes as a function of the degree of genotypic mixing. We include a model of a single secretion, which recapitulates the well-known cooperator–cheater dynamics where limited genotypic mixing (high relatedness) leads to the evolution of secretion, whereas high genotypic mixing (low relatedness) leads to a loss of secretion (15, 16, 18, 45–47). What happens when cells can produce two secretions? At low mixing, the genotype that produces all secretions dominates, and at high mixing, one sees the opposite (the genotype that does not produce any secretions dominates). Interestingly, however, at intermediate levels of genotypic mixing, there is natural selection for partial secretors that produce only a subset of the secretions, such as [1,0], which rely on the complementary strain [0,1] for the other secretion. The emergence of such cross-feeding between partial secreting genotypes represents a simple form of between-genotype cooperation.

Why do complementary genotypes dominate nonsecretors at intermediate genotypic mixing? The answer is in the demographics of the system and the potential for something known as Simpson's Paradox (45, 47). Within any one group, nonsecretors outcompete secretor genotypes because of the costs associated with making the secretions. However, the groups containing more secretors produce more cells in total to seed new groups. Then, at intermediate levels of genetic mixing, complementary genotypes are associated with more productive groups relative to nonsecretors and therefore, can outcompete them. Additionally, because there is a significant amount of mixing, one partial secretor genotype [0,1] will often meet the partner genotype [1,0] within a given group, allowing them to outcompete full secretors [1,1] that grow more slowly to make both traits. Partial secretors compete best against full secretors [1,1] when the costs of secretions are relatively high, because there is a more significant growth advantage from not making a secretion (Fig. 2).

The behavior of the model for two, three, and four secretions is broadly similar (Fig. 2 and Fig. S2). However, adding more secretions to the system increases the scope for cross-feeding genotypes to outcompete other genotypes. A key reason for this is that increasing the number of secretions increases the associated costs, which promotes cross-feeders over full secretors (Fig. 2). The importance of costs is shown by changing the number of secretions

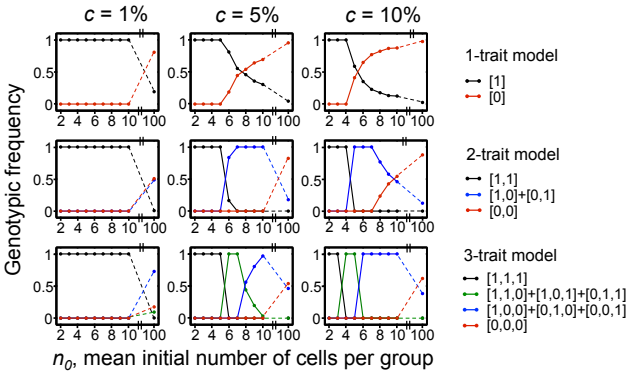

Fig. 2. The evolution of within- and between-genotype cooperation in microbial communities. We show steady-state frequencies of different genotypes as a function of the average number of cells founding each group (n_0) and the cost of each trait (c) in systems that depend on one, two, and three secretions to grow. Genotypes are labeled with one and zero to show whether they invest or not in a given secretion; [1], [1,1], and [1,1,1] have the advantage at low n_0, whereas [0], [0,0], and [0,0,0] have the advantage at high n_0. Cross-feeding genotypes that cooperatively exchange secretions dominate at intermediate values of n_0 (a proxy for mixing among genotypes), particularly for secretions with high cost (c).

in the system while keeping the total cost of all secretions constant (Fig. S2). A general prediction then is that raising the costs of secretions, either through a single secretion that is very costly or the expression of many individually costly secretions, can favor cross-feeders relative to full secretors. As we show below, however, using many secretions also creates problems, because cross-feeders need to reliably find multiple partners to be successful. This dependence on multiple other genotypes makes cross-feeding with many secretions particularly fragile to factors that limit access to other genotypes (Fig. S3).

Our model assumes that all strains compete for the same niche. Although this assumption seems reasonable given the competition observed between strains and species from a common environment (31, 53), the extent of niche overlap will vary between different genotypes. We, therefore, decided to test the importance of complete niche overlap for our conclusions. We did this by modeling two sets of interacting strains. All strains can cooperate with one another, but only within a set do the strains compete. Between sets, there is no resource competition consistent with each set occupying a different niche. Importantly, this model shows the same qualitative behavior as our simpler single-niche model: between-genotype cooperation requires intermediate levels of genotypic mixing to evolve by natural selection (Fig. S4).

In sum, we find that between-genotype cooperation can evolve by natural selection, particularly with high costs to secretions and intermediate levels of mixing of microbial genotypes.

Between-Genotype Cooperation Is Associated with Reduced Group Productivity. The two-way exchanges of secretions that emerge in the model can be viewed in at least two different ways. The first way is cooperation for mutual benefit. Indeed, if two complementary strains or species were examined in a laboratory experiment, one would find that each cannot grow alone but together they grow well, a result that is commonly used to diagnose cooperation or mutualism (31, 54). However, another aspect of the interaction is competitive, where each partial secretor is acting as a cheater on full secretors and its complementary partner. Can one then quantify the impact of this competition? A simple but powerful way to assess the effects of competition is to look at overall group performance, which can be harmed by genotypes investing in competitive traits instead of cooperative traits that benefit the group (55).

Fig. 3 shows the evolved group productivities as a function of founder cell number (the degree of genotypic mixing). The emergence of cross-feeding exchanges with increased genetic mixing is associated with a loss of group productivity—a diagnostic of wasteful competition that is inefficient at the group level. The greater the potential for between-genotype cross-feeding, therefore, the lower the group performance relative to a single strain that makes all secretions. Accordingly, any factor that promotes cross-feeding exchanges, such as increasing the cost or number of secretions, leads to greater losses in group productivity. Why this reduction? The emergence of this type of cross-feeding is associated with a loss of genes for secretion in each partner. This loss means that less of the secretion will accumulate in a cross-feeding group relative to a group of cells that all make all secretions.

The model does not allow strains to modulate the amount of secretion that they make. If allowed, will cross-feeders compensate for their low productivity by increasing their investment in cooperation? We evaluated this in two ways. First, we extended our model to allow strains to invest in three different levels of secretion (0.5, 1, and 2). Second, we developed another model that allows strains to invest any amount in secretions by considering mutations that can change the level of investment (*Materials and Methods*). Rather than increasing group productivity, however, allowing strains to modulate secretion levels only makes things worse for cross-feeders (Fig. 4 and Fig. S5). The evolution of cross-feeding is now associated with even greater losses in group productivity, because cross-feeders evolve to invest less in each secretion than full secretors. In sum, the evolution of cross-feeding cooperation between microbial genotypes is associated with significant levels of competition and mutual exploitation.

The idea that a cooperative interaction between genotypes can arise by exploitation has a precedent in discussions of mutualism and host–parasite evolution (54). There it has been observed that a chronic parasite might produce a factor that a host evolves to depend upon. Under these conditions, removing a parasite can harm a host, although the original basis for the interaction was strongly negative for the host. These situations, like in our system, can be viewed either as competitive or cooperative depending on the comparison taken. Specifically, if an experimenter simply removes a partner, he or she will diagnose the relationship as cooperative. However, this diagnosis will hide the evolutionary history and the fact that the partnership originally evolved through competition and exploitation. This historical effect of competition is not merely a definitional issue; it predicts that the productivity of microbial communities relying on cross-feeding exchanges will be low relative to their full potential.

Constraints on the Evolution of Between-Genotype Cooperation. The evolution of cooperation between genotypes is predicted with relatively high costs to secretions and intermediate levels of

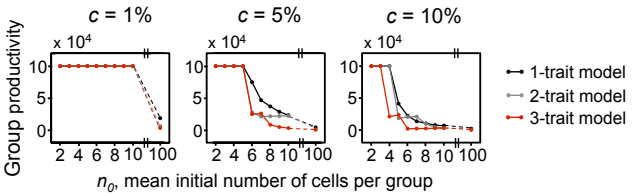

Fig. 3. Evolved average group productivity as a function of founder cell number (n_0). The emergence of cooperative exchanges between genotypes is associated with a loss of group productivity (two- and three-trait models). This loss of productivity occurs for the same reason that cheaters harm group function in single-secretion models (one-trait model). This outcome is particularly clear for secretions with high cost (c) and a high number of traits. Average group productivities were obtained from 1,000 independent subpopulations. SE bars are smaller than the plotting dots and therefore, not shown.

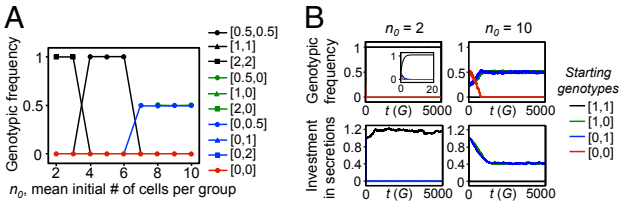

Fig. 4. Evolved investment into secretion production as a function of founder cell number (n_0). Allowing for differential investment in secretion production amplifies the tragedy of the commons, because cross-feeders evolve to invest less in secretions than strains that make all secretions. (*A*) Discrete model. Genotypes that invest two times as much in secretions ([2,2] instead of [1,1]) reach fixation when genetic mixing is low. However, at high mixing, the genotypes that fixate are cross-feeders that invest less in secretions than in the original model ([0.5,0] and [0,0.5] instead of [1,0] and [0,1], respectively). (*B*) Continuous model. If cells continuously tune their investments into secretion production, we find the same patterns, where cross-feeding strains invest less in cooperation than strains that make all secretions. *Upper* shows the genotypic frequencies of systems for low and high mixing, whereas *Lower* shows the mean investment in secretions. *Inset* clarifies that genotypic frequencies are identical at the beginning, but producers of both traits quickly reach fixation. SE bars for steady-state investments are smaller than the plotting lines and therefore, not shown. We set the cost per trait (c) at 5%.

mixing of microbial genotypes. Do these conditions commonly occur in nature? The fitness cost of secretion can be highly variable in strongly regulated traits, such as siderophores, depending on how much a cell makes (56). Nevertheless, estimates of costs of secretions are often low (in the range of a few percent of growth rate or less) (57–59). Low-cost secretions are expected whenever prudent regulation limits secretion to times when it is cheap to do so (59). The effects of costs are also limited when secretions have a private component that benefits a secreting cell more than other cells (60). If low-cost secretions are the norm in nature, then our model suggests that the emergence of between-genotype cooperation will be limited. Potential exceptions to this prediction are if cells use many relatively costly secretions (Fig. 2 and Fig. S2) or indeed, if using multiple secretions is, for some reason, disproportionally costly (Fig. S6).

What about the levels of genetic mixing in microbial communities? This key variable is still poorly understood (6, 22). However, what is clear is that many natural microbial communities display spatial structure, whereby microbes attach to surfaces and each other and grow (16, 61). This structuring will affect genetic mixing and is not accounted for in our model, which assumes that genetic mixing within any one microbial group is perfect. To examine the impacts of spatial structure, we implemented an individual-based version of our two-secretion model, where cells are seeded on a lattice and divide if they have space around them and access to both public goods (*Materials and Methods*). In particular, we focus on parameter ranges that strongly promote cross-feeding pairs in the absence of spatial structure within the group.

We first use the individual-based model to recapitulate the well-mixed model by allowing secretions to diffuse a long distance so that cells have access to all secretions. We then implement a low-diffusion scenario so that secretions only reach a limited range. This simple change has a strong qualitative effect on predictions: now, the genotype that produces both secretions is dominant (Fig. 5*A*). The reason for this effect is intuitive: spatial structure limits the potential for interactions with other genotypes. Cross-feeders are now much less likely to interact with their complementary partner, which means that they will often lack secretions that they need for their growth.

Spatial structure then tends to limit cooperation between microbial genotypes, which is consistent with recent empirical work showing that spatial structure can limit positive interactions between microbial genotypes (26, 62). This effect contrasts with the typical conclusion that spatial structure promotes cooperation (13, 16, 17, 63, 64) by increasing the probability of interacting with the same genotype (10, 11). However, cooperation between genotypes in our multitrait model emerges under the same conditions as cheating in the classical models. Accordingly, we find that spatial structure simultaneously inhibits between-genotype cooperation and promotes within-genotype cooperation.

Another assumption of our model, which is important for genetic mixing, is that all interacting genotypes in the system make use of the secretions. This assumption is likely to be broken, because the extreme diversity associated with natural microbial communities suggests that there will often be many species present that do not use or make the secretions of our focal genotypes (65). In models of a single secretion, it has been shown that such passive genotypes can insulate a focal genotype from interacting with other genotypes that might use its secretions [social insulation (65)]. Fig. 5*B* shows the effect of introducing passive genotypes that do not use the secretions or resources of the focal group. Like the effect of introducing space, the presence of passive genotypes decreases the probability that cross-feeding genotypes interact with their complementary partner, thereby favoring strains that can function effectively in isolation. Put another way, passive genotypes reduce the group size of the focal interacting genotypes, which reduces the effective level of genetic mixing and promotes autonomous genotypes like [1,1].

We saw earlier that a high number of secretions can promote cross-feeding (Fig. 2 and Fig. S2). However, it is important to note that the introduction of passive genotypes has a disproportionately strong effect when cells use a high number of secretions (Fig. S3). With many secretions, each cross-feeder has to find multiple partners, and passive genotypes become more of a problem than when a cell has to find just one partner. In sum, the use of many traits presents cross-feeders with two problems. First, cross-feeding involving many traits is associated with greater reductions in group productivity than with fewer traits; communities become more inefficient (Fig. 3). Second, relying on many traits makes cross-feeding networks fragile in the sense that each cross-feeder will typically require multiple other genotypes nearby to grow (Fig. S3).

Although we expect the effect of passive genotypes to be strong, mechanisms that promote association between complementary strains will improve the prospects of cross-feeding. Candidate mechanisms that promote association include emergent sorting that can occur if two strains grow more in each other's presence than when alone (22, 65, 66), chemotaxis toward partner genotypes, or even direct attachment (67). The importance of such

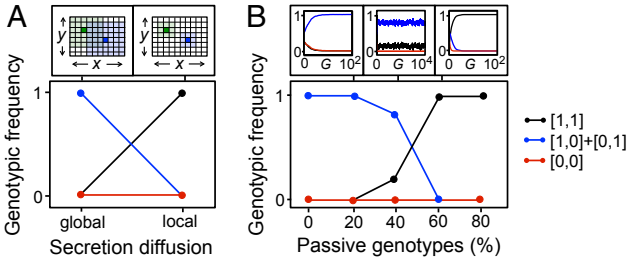

Fig. 5. Effect of spatial structure and social insulation on the evolution of between-genotype cooperation. (*A*) Spatial structure (individual-based model). Space hinders the evolution of between-genotype cooperation with local diffusion of secretions, because genotypes are prevented from interacting. *Upper* shows cartoons to illustrate the diffusibility of secretions. (*B*) Social insulation modeled in well-mixed groups. The presence of passive genotypes, which do not compete with focal genotypes and do not contribute with traits, can prevent the evolution of between-genotype cooperation. *Upper* illustrates temporal dynamics (in generations G) for the three outcomes of the model. The cost per secretion (c) was set at 5%.

assortment processes in nature is not known, but it is an interesting area for future studies.

Conclusions

Our models identify conditions under which different microbial genotypes evolve to exchange fitness-promoting secretions. This outcome might occur through the selective loss of costly but leaky traits through Black Queen dynamics (7, 29). The Black Queen Hypothesis was developed to explain the genome streamlining often seen among free-living organisms (7, 58). It suggests that microbes will lose functions that are costly but can be obtained from other genotypes because of their leaky nature (7). This process leads to the evolution of dependencies among genotypes and potentially interdependent networks of cooperation in microbial communities (29). However, consideration of the costs of secretions and the levels of genetic mixing in natural communities suggests that the evolution of such cooperative networks is not always expected. Instead, our models predict that it may often be beneficial for a microbial genotype to produce all of the secretions that it needs.

Constraints may sometimes prevent a microbe from evolving all of the cooperative traits that it needs (i.e., a [1,1] strain cannot evolve). This scenario makes cooperative exchanges with other genotypes much more likely and corresponds to the typical view of mutualism between species (Fig. S7). However, the widespread potential for horizontal gene transfer (42–44) suggests that the evolution of multiple traits should often be possible. Possessing multiple traits is beneficial in our model, because it removes reliance on other strains that may not be encountered. This benefit of autonomy then has the potential to limit both between-genotype cooperation and the evolution of cheating genotypes (10, 11, 15, 63, 65).

Does the between-genotype cooperation that we see in our model ever evolve in nature? An interesting corollary of the similarity between cheating and between-genotype cooperation in our model (Fig. 2) is that the discovery of one in nature should help to identify conditions that favor the other. A phenotype often associated with both cheating (15) and Black Queen evolution (7) is the production of siderophores, which are secreted iron-scavenging molecules. Studies of marine assemblages suggest that bacterial strains often evolve to not secrete siderophores, while retaining the import proteins to take up siderophores made by other strains and species (32, 49). In addition, siderophores seem particularly amenable to cheating and cross-feeding, because they can be both costly (56) and diffusible (Figs. 2 and 5*A*). Siderophore interactions, therefore, may be unusually prone to the evolution of between-genotype cooperation.

Amino acids are another potential currency for cooperative exchange in microbial communities. Many bacteria lack the ability to make certain amino acids, particularly those that are costly to make (8). This observation raises the possibility that cooperative networks of amino acid exchange occur in microbial communities, which was recently shown for synthetic communities of up to 14 different auxotrophic genotypes of *Escherichia coli* (8). What is critical for our arguments, however, is that the WT *E. coli* that makes all amino acids grows at least 1.5–2 times faster than the cooperating communities. If these networks of amino acid exchange do evolve in nature, therefore, then they are likely to be relatively inefficient.

Cooperation between cells of a single genotype seems common, which is likely explained by the clonal and patchy nature of microbial growth that guarantees frequent association between genetically identical cells within microbial communities (13, 16, 17, 68). Here, we have shown that cooperation between microbial genotypes is expected under different conditions (intermediate levels of genetic mixing), and it remains to be seen how often these conditions arise in nature. Both spatial structure and social insulation can cause problems finding a cooperating partner. Moreover, we show that, even when cooperation does emerge between strains and species, it can be exploitative and wasteful relative to single-genotype cooperation. This prediction has implications for synthetic ecology and our ability to engineer microbial communities for our own ends (8, 22, 69). If cooperative interactions in natural microbial communities are both limited and inefficient, there should be a broad scope for improving community productivity using strategies that promote positive interactions between species. More generally, our work cautions strongly against a view where microbial communities are dominated by networks of species working together in harmony. Competition is likely to be central to many microbial interactions, perhaps even the cooperative ones.

Materials and Methods

Ordinary Differential Equation Models with Fixed Investment into Secretion. We model the population dynamics of microbial genotypes growing in a well-mixed environment using systems of ordinary differential equations (*SI Materials and Methods*). Briefly, each system is composed by 2^s equations, where s is number of secretions in a given model, and each equation represents the population dynamics of a given microbial genotype in each subpopulation. For a system of two cooperative secretions, the four genotypes ([1,1], [1,0], [0,1], and [0,0]) grow according to the following general form:

$$\frac{dg_{ij}}{dt} = (r - (i+j)\cdot c)\cdot g_{ij}\cdot\left(1 - \frac{\sum g}{K}\right),$$

where g_{ij} represents the density of individuals of genotype [i,j] in each subpopulation [$(i,j) \in \{1,0\}^s$], r is the intrinsic growth rate (here assumed to be $r = 1$ for simplicity), and c is the cost of producing each trait. Here, we assume additive costs for secretion production, but we also considered nonlinear costs—both accelerating and decelerating (Fig. S6). K, the carrying capacity of the environment, is a function of the secretions available in each subpopulation (Fig. S8).

We consider a standard lifecycle of microbes [the work by Cremer et al. (45) and references therein further discuss the lifecycle]: (*i*) formation, where a random number of cells is allocated to each subpopulation (based on a Poisson process with mean n_0; Fig. S9) in a set of M subpopulations and the identity of each cell follows a uniform distribution based on the frequency of each genotype; (*ii*) growth, where genotypes in each group proliferate according to logistic dynamics (until saturation is reached); and (*iii*) merging, where the M groups are merged together and the global genotypic frequencies are updated. After a full cycle of seeding, growth, and merging (equivalent to one generation), new patches are seeded according to the recalculated genotypic frequency. These cycles are repeated for G generations until genotypic frequencies reach equilibrium.

Ordinary Differential Equation Models with Variable Investment into Secretion. We implemented two different frameworks that are here called discrete and continuous models for the evolution of investment. In the discrete version, we extended our model described above to allow strains to invest in three different levels of secretion to give genotypes [0.5,0.5], [1,1], [2,2], [0.5,0], [1,0], [2,0], [0,0.5], [0,1], [0,2], and [0,0]. In Fig. 4, full producers invest the same in both secretions, but we find the same qualitative results when we drop this assumption (Fig. S5). The continuous version uses the same lifecycle, but we add a mutation phase, where a mutation can either increase or decrease the investment into cooperation. The lifecycle is then (*i*) formation; (*ii*) mutation, where each cell of the subpopulation mutates its parameter x, which governs how much a cell invests into its public goods; (*iii*) growth; and (*iv*) merging. Each cell type proliferates as before, but we additionally consider its investment in secretions:

$$\frac{dg_{x,ij}}{dt} = (r - (i+j)\cdot x\cdot c)\cdot g_{x,ij}\cdot\left(1 - \frac{\sum g}{K}\right),$$

where $g_{x,ij}$ represents the density of the cell type with genotype [i,j] and investment x. Thus, the genotypes are now effectively $x{\cdot}g_{ij}$ and not g_{ij} as before. For example, if $x = 2$, a strain [1,1] will behave as a genotype [2,2].

Individual-Based Model. We use spatial simulations of 2D lattices with periodic boundaries. Cells can only divide into empty spaces of their closest neighborhood, and the effect of a public good is limited to a neighborhood of a certain size around the producer cell. At each sampled time step, a focal individual is selected with uniform probability, and the cell divides with probability directly proportional to growth rate, which depends on population density and public goods level, following logistic kinetics. As for the deterministic version with fixed investment, cells undergo our standard three-step lifecycle (*SI Materials and Methods*).

EVOLUTION

ACKNOWLEDGMENTS. We thank Steve Frank, Joel Sachs, Jeff Morris, Richard Lenski, Katharine Coyte, Melanie Ghoul, Ashleigh Griffin, Jonas Schluter, Harris Wang, and three anonymous reviewers for helpful comments. We also thank Linus Schumacher and Alex Fletcher for help and advice on the models. This work was funded by European Research Council Grant 242670 and Fundação para a Ciência e Tecnologia Fellowship SFRH-BD-73470-2010.

1. Hamilton WD (1975) Innate social aptitudes of man: An approach from evolutionary genetics. *Biosocial Anthropology*, Ed Fox R (Malaby Press, London).
2. Costerton JW (2007) *The Biofilm Primer* (Springer, Berlin).
3. López D, Vlamakis H, Kolter R (2010) Biofilms. *Cold Spring Harb Perspect Biol* 2(7): a000398.
4. West SA, Diggle SP, Buckling A, Gardner A, Griffins AS (2007) The social lives of microbes. *Annu Rev Ecol Evol Syst* 38:53–77.
5. West SA, Griffin AS, Gardner A, Diggle SP (2006) Social evolution theory for microorganisms. *Nat Rev Microbiol* 4(8):597–607.
6. Nadell CD, Xavier JB, Foster KR (2009) The sociobiology of biofilms. *FEMS Microbiol Rev* 33(1):206–224.
7. Morris JJ, Lenski RE, Zinser ER (2012) The Black Queen Hypothesis: Evolution of dependencies through adaptive gene loss. *MBio* 3(2):e00036-12.
8. Mee MT, Collins JJ, Church GM, Wang HH (2014) Syntrophic exchange in synthetic microbial communities. *Proc Natl Acad Sci USA* 111(20):E2149–E2156.
9. Pande S, et al. (2014) Fitness and stability of obligate cross-feeding interactions that emerge upon gene loss in bacteria. *ISME J* 8(5):953–962.
10. Hamilton WD (1964) The genetical evolution of social behaviour. I. *J Theor Biol* 7(1): 1–16.
11. Hamilton WD (1964) The genetical evolution of social behaviour. II. *J Theor Biol* 7(1): 17–52.
12. Brown SP, Johnstone RA (2001) Cooperation in the dark: Signalling and collective action in quorum-sensing bacteria. *Proc Biol Sci* 268(1470):961–965.
13. Datta MS, Korolev KS, Cvijovic I, Dudley C, Gore J (2013) Range expansion promotes cooperation in an experimental microbial metapopulation. *Proc Natl Acad Sci USA* 110(18):7354–7359.
14. Diggle SP, Griffin AS, Campbell GS, West SA (2007) Cooperation and conflict in quorum-sensing bacterial populations. *Nature* 450(7168):411–414.
15. Griffin AS, West SA, Buckling A (2004) Cooperation and competition in pathogenic bacteria. *Nature* 430(7003):1024–1027.
16. Nadell CD, Foster KR, Xavier JB (2010) Emergence of spatial structure in cell groups and the evolution of cooperation. *PLOS Comput Biol* 6(3):e1000716.
17. Van Dyken JD, Müller MJ, Mack KM, Desai MM (2013) Spatial population expansion promotes the evolution of cooperation in an experimental Prisoner's Dilemma. *Curr Biol* 23(10):919–923.
18. West SA, Buckling A (2003) Cooperation, virulence and siderophore production in bacterial parasites. *Proc Biol Sci* 270(1510):37–44.
19. Gans J, Wolinsky M, Dunbar J (2005) Computational improvements reveal great bacterial diversity and high metal toxicity in soil. *Science* 309(5739):1387–1390.
20. Roesch LF, et al. (2007) Pyrosequencing enumerates and contrasts soil microbial diversity. *ISME J* 1(4):283–290.
21. Santelli CM, et al. (2008) Abundance and diversity of microbial life in ocean crust. *Nature* 453(7195):653–656.
22. Mitri S, Foster KR (2013) The genotypic view of social interactions in microbial communities. *Annu Rev Genet* 47:247–273.
23. Shou W, Ram S, Vilar JMG (2007) Synthetic cooperation in engineered yeast populations. *Proc Natl Acad Sci USA* 104(6):1877–1882.
24. Wintermute EH, Silver PA (2010) Emergent cooperation in microbial metabolism. *Mol Syst Biol* 6:407.
25. Harcombe W (2010) Novel cooperation experimentally evolved between species. *Evolution* 64(7):2166–2172.
26. Hillesland KL, Stahl DA (2010) Rapid evolution of stability and productivity at the origin of a microbial mutualism. *Proc Natl Acad Sci USA* 107(5):2124–2129.
27. Elias S, Banin E (2012) Multi-species biofilms: Living with friendly neighbors. *FEMS Microbiol Rev* 36(5):990–1004.
28. Little AEF, Robinson CJ, Peterson SB, Raffa KF, Handelsman J (2008) Rules of engagement: Interspecies interactions that regulate microbial communities. *Annu Rev Microbiol* 62:375–401.
29. Sachs JL, Hollowell AC (2012) The origins of cooperative bacterial communities. *MBio* 3(3):e00099-12.
30. Schink B (2002) Synergistic interactions in the microbial world. *Antonie van Leeuwenhoek* 81(1-4):257–261.
31. Foster KR, Bell T (2012) Competition, not cooperation, dominates interactions among culturable microbial species. *Curr Biol* 22(19):1845–1850.
32. D'Onofrio A, et al. (2010) Siderophores from neighboring organisms promote the growth of uncultured bacteria. *Chem Biol* 17(3):254–264.
33. Ernebjerg M, Kishony R (2012) Distinct growth strategies of soil bacteria as revealed by large-scale colony tracking. *Appl Environ Microbiol* 78(5):1345–1352.
34. Kaeberlein T, Lewis K, Epstein SS (2002) Isolating "uncultivable" microorganisms in pure culture in a simulated natural environment. *Science* 296(5570):1127–1129.
35. Bull JJ, Harcombe WR (2009) Population dynamics constrain the cooperative evolution of cross-feeding. *PLoS ONE* 4(1):e4115.
36. Estrela S, Trisos CH, Brown SP (2012) From metabolism to ecology: Cross-feeding interactions shape the balance between polymicrobial conflict and mutualism. *Am Nat* 180(5):566–576.
37. Fennell DE, Gossett JM (1998) Modeling the production of and competition for hydrogen in a dechlorinating culture. *Environ Sci Technol* 32(16):2450–2460.
38. Kreikenbohm R, Bohl E (1986) A Mathematical-Model of Syntrophic Cocultures in the Chemostat. *FEMS Microbiol Ecol* 38(3):131–140.
39. Foster KR, Wenseleers T (2006) A general model for the evolution of mutualisms. *J Evol Biol* 19(4):1283–1293.
40. Sachs JL, Mueller UG, Wilcox TP, Bull JJ (2004) The evolution of cooperation. *Q Rev Biol* 79(2):135–160.
41. Frank SA (1994) Genetics of mutualism: The evolution of altruism between species. *J Theor Biol* 170(4):393–400.
42. Nogueira T, et al. (2009) Horizontal gene transfer of the secretome drives the evolution of bacterial cooperation and virulence. *Curr Biol* 19(20):1683–1691.
43. Papke RT, Gogarten JP (2012) Ecology. How bacterial lineages emerge. *Science* 336(6077):45–46.
44. Rankin DJ, Rocha EPC, Brown SP (2011) What traits are carried on mobile genetic elements, and why? *Heredity (Edinb)* 106(1):1–10.
45. Cremer J, Melbinger A, Frey E (2012) Growth dynamics and the evolution of cooperation in microbial populations. *Sci Rep* 2:281.
46. Frank SA (2010) Microbial secretor-cheater dynamics. *Philos Trans R Soc Lond B Biol Sci* 365(1552):2515–2522.
47. Chuang JS, Rivoire O, Leibler S (2009) Simpson's paradox in a synthetic microbial system. *Science* 323(5911):272–275.
48. Crespi BJ (2001) The evolution of social behavior in microorganisms. *Trends Ecol Evol* 16(4):178–183.
49. Cordero OX, Ventouras LA, DeLong EF, Polz MF (2012) Public good dynamics drive evolution of iron acquisition strategies in natural bacterioplankton populations. *Proc Natl Acad Sci USA* 109(49):20059–20064.
50. Cordero OX, et al. (2012) Ecological populations of bacteria act as socially cohesive units of antibiotic production and resistance. *Science* 337(6099):1228–1231.
51. Raymond B, West SA, Griffin AS, Bonsall MB (2012) The dynamics of cooperative bacterial virulence in the field. *Science* 337(6090):85–88.
52. Rumbaugh KP, et al. (2009) Quorum sensing and the social evolution of bacterial virulence. *Curr Biol* 19(4):341–345.
53. Vetsigian K, Jajoo R, Kishony R (2011) Structure and evolution of Streptomyces interaction networks in soil and in silico. *PLoS Biol* 9(10):e1001184.
54. De Mazancourt C, Loreau M, Dieckmann U (2005) Understanding mutualism when there is adaptation to the partner. *J Ecol* 93(2):305–314.
55. Foster KR (2004) Diminishing returns in social evolution: The not-so-tragic commons. *J Evol Biol* 17(5):1058–1072.
56. Jiricny N, et al. (2010) Fitness correlates with the extent of cheating in a bacterium. *J Evol Biol* 23(4):738–747.
57. Drescher K, Nadell CD, Stone HA, Wingreen NS, Bassler BL (2014) Solutions to the public goods dilemma in bacterial biofilms. *Curr Biol* 24(1):50–55.
58. Morris JJ, Johnson ZI, Szul MJ, Keller M, Zinser ER (2011) Dependence of the cyanobacterium *Prochlorococcus* on hydrogen peroxide scavenging microbes for growth at the ocean's surface. *PLoS ONE* 6(2):e16805.
59. Xavier JB, Kim W, Foster KR (2011) A molecular mechanism that stabilizes cooperative secretions in *Pseudomonas aeruginosa*. *Mol Microbiol* 79(1):166–179.
60. Gore J, Youk H, van Oudenaarden A (2009) Snowdrift game dynamics and facultative cheating in yeast. *Nature* 459(7244):253–256.
61. Hallatschek O, Hersen P, Ramanathan S, Nelson DR (2007) Genetic drift at expanding frontiers promotes gene segregation. *Proc Natl Acad Sci USA* 104(50):19926–19930.
62. Saxer G, Doebeli M, Travisano M (2009) Spatial structure leads to ecological breakdown and loss of diversity. *Proc R Soc Lond B Biol Sci* 276(1664):2065–2070.
63. MacLean RC, Gudelj I (2006) Resource competition and social conflict in experimental populations of yeast. *Nature* 441(7092):498–501.
64. Nowak MA, May RM (1992) Coexistence and competition in HIV infections. *J Theor Biol* 159(3):329–342.
65. Mitri S, Xavier JB, Foster KR (2011) Social evolution in multispecies biofilms. *Proc Natl Acad Sci USA* 108(Suppl 2):10839–10846.
66. Momeni B, Waite AJ, Shou W (2013) Spatial self-organization favors heterotypic cooperation over cheating. *eLife* 2:e00960.
67. Wanner G, Vogl K, Overmann J (2008) Ultrastructural characterization of the prokaryotic symbiosis in "Chlorochromatium aggregatum." *J Bacteriol* 190(10):3721–3730.
68. Kim W, Racimo F, Schluter J, Levy SB, Foster KR (2014) Importance of positioning for microbial evolution. *Proc Natl Acad Sci USA* 111(16):E1639–E1647.
69. Klitgord N, Segrè D (2011) Ecosystems biology of microbial metabolism. *Curr Opin Biotechnol* 22(4):541–546.

Supporting Information

Oliveira et al. 10.1073/pnas.1412673111

SI Materials and Methods

Here, we present an extended version of the methods used in the paper.

Ordinary Differential Equation Models with Fixed Investment into Secretion. There is a large literature on the evolution of single microbial secretions—often known as studies of cheaters and cooperators—that includes both theory (1–4) and empirical tests (5–8). Our goal here is to build directly on this work. We, therefore, base our models on two recent and detailed studies of single secretions (3, 7). These studies assume that cells land in patches stochastically, such that the number of cells across patches follows a Poisson distribution (Poisson-based seeding) (Fig. S9). Such seeding is based on the realistic assumption that the number of cells per patch is not deterministic and the same across patches but random. Earlier models used simpler demographics, but this difference does not affect our conclusions (Fig. S9), such that our model also recapitulates the predictions of other studies of single secretions (2, 4).

We model the population dynamics of microbial genotypes growing in a well-mixed environment using systems of ordinary differential equations (ODEs). Each system is composed by 2^s equations, where s is the number of traits (secretions) in a given model, and each equation represents the population dynamics of a given microbial genotype in each subpopulation. The total number of genotypes in each model is, thus, captured by binary combinatorics; each genotype is labeled by a binary string, where one and zero mean production or nonproduction of a certain trait, respectively. Here, we explain the two-trait model, but the framework is equivalent for the one- and three-trait cases presented in the text. For a system of two cooperative traits, the four genotypes ([1,1], [1,0], [0,1], and [0,0]) grow according to the following general form:

$$\frac{dg_{ij}}{dt} = \left(r - (i+j)\cdot c\right)\cdot g_{ij}\cdot\left(1 - \frac{\sum g}{K}\right),$$

where g_{ij} represents the density of individuals of genotype [i,j] in each subpopulation $[(\mathrm{i},\mathrm{j}) \in \{1,0\}^s]$, and s is the number of traits. Specifically for the two-trait model, one has the following system of four ODEs:

$$\begin{cases} \frac{dg_{11}}{dt} = \left(r - (1+1)\cdot c\right)\cdot g_{11}\cdot\left(1 - \frac{g_{11}+g_{10}+g_{01}+g_{00}}{K}\right) \\ \frac{dg_{10}}{dt} = \left(r - (1+0)\cdot c\right)\cdot g_{10}\cdot\left(1 - \frac{g_{11}+g_{10}+g_{01}+g_{00}}{K}\right) \\ \frac{dg_{01}}{dt} = \left(r - (0+1)\cdot c\right)\cdot g_{01}\cdot\left(1 - \frac{g_{11}+g_{10}+g_{01}+g_{00}}{K}\right) \\ \frac{dg_{00}}{dt} = \left(r - (0+0)\cdot c\right)\cdot g_{00}\cdot\left(1 - \frac{g_{11}+g_{10}+g_{01}+g_{00}}{K}\right) \end{cases},$$

where r is the intrinsic growth rate (here assumed to be $r = 1$ for simplicity), and c is the cost of producing each trait. Note that we assume here additive costs for secretion production (given by the summation of the genotype index). We also considered nonlinear costs (both accelerating and decelerating), and these functional forms do not qualitatively affect our conclusions (Fig. S6). Importantly, K (the carrying capacity of the environment) is a function of the traits available (here given by the frequency of producers of each trait) and has the following general form:

$$K = K_{basal} + K_{maxB}\left(\frac{g_{11}+g_{10}}{g_{11}+g_{10}+g_{01}+g_{00}}\cdot\frac{g_{11}+g_{01}}{g_{11}+g_{10}+g_{01}+g_{00}}\right),$$

where K_{basal} and K_{maxB} are constants representing the minimal carrying capacity of the system and the maximum benefit from secretions, respectively (here, $K_{basal} = 1$ and $K_{maxB} = 100{,}000$). Note that we use multiplicative benefits, because we assume that all cooperative traits are essential, which together with $K_{basal} = 1$, represents the requirement of cells having access to all secretions to be able to grow. However, we also vary the strength of selection by considering increasing values of K_{basal}. Fig. S1 shows that increasing K_{basal} reduces the potential for between-genotype cooperation, but when it evolves, it does so under the same demographic conditions and intermediate values of genetic mixing. Moreover, given that it is not fully known how K scales with secretions, we additionally implemented an additive version, where now we consider additive benefits instead of multiplicative benefits (Fig. S8). Again, the evolution of between-genotype cooperation is restricted to intermediate values of genetic mixing. To model the effect of niche overlap on the evolution of between-genotype cooperation, we analyzed an extension of the two-trait model presented above, where we considered eight genotypes belonging to two different species. In this case, only genotypes from to the same species compete for resources (Fig. S4).

We consider a standard lifecycle of microbes [the work by Cremer et al. (3) and references therein further discuss the lifecycle]: (*i*) formation, where a random number of cells is allocated to each subpopulation (based on a Poisson process with mean n_0) in a set of M subpopulations (here, $M = 1{,}000$) and the identity of each cell follows a uniform distribution based on the frequency of each genotype [which we assumed is the same for all genotypes at the beginning (*G0*)]; (*ii*) growth, where genotypes in each group proliferate according to logistic dynamics (until saturation is reached); and (*iii*) merging, where the M groups are merged together and the global genotypic frequencies are updated. After a full cycle of seeding, growth, and merging (equivalent to one generation), new patches are seeded according to the recalculated genotypic frequency. These cycles are repeated for G generations (typically 1,000), which is sufficient for genotypic frequencies reaching equilibrium.

ODE Models with Variable Investment into Secretion. To model the evolution of investment into secretion production, we implemented two different frameworks (here called discrete and continuous models for the evolution of investment). In the discrete version, we simply extended our model described above to allow strains to invest in three different levels of secretion (0.5, 1, and 2). We, thus, considered the genotypes [0.5,0.5], [1,1], [2,2], [0.5,0], [1,0], [2,0], [0,0.5], [0,1], [0,2], and [0,0] and show that [2,2] evolves under low mixing but that [0.5,0] and [0,0.5] will evolve under the conditions favoring cross-feeding. Here, we assume for simplicity that full producers invest the same to both secretions, but we find the same qualitative results when we drop this assumption (Fig. S5).

In the continuous version, we use the same lifecycle but add a mutation phase, where we allow for mutations that can either increase or decrease the investment into cooperation. The lifecycle is then (*i*) formation; (*ii*) mutation, where each cell of the subpopulation mutates its parameter x, which governs how much

a cell invests into its public goods; (*iii*) growth; and (*iv*) merging. In the growth phase, the evolution of each single subpopulation is governed by a set of z ODEs, where z is the number of individuals that inhabit each subpopulation after mutation. Each initial cell z then proliferates according to the general ODE

$$\frac{dg_{x,ij}}{dt} = \left(r - (i+j)\cdot x \cdot c\right)\cdot g_{x,ij}\cdot\left(1 - \frac{\sum g}{K}\right),$$

where $g_{x,ij}$ represents the density of the cell type with genotype [i,j] and investment x, and K is still a function of the secretions available (given by the frequency of secretors), which now incorporates explicitly the evolvable investment x of cells:

$$K = K_{basal} + K_{maxB}\left(\frac{x\cdot g_{11} + x\cdot g_{10}}{g_{11}+g_{10}+g_{01}+g_{00}}\cdot\frac{x\cdot g_{11} + x\cdot g_{01}}{g_{11}+g_{10}+g_{01}+g_{00}}\right).$$

Thus, the genotypes are now effectively $x{\cdot}g_{ij}$ and not g_{ij} as before. For example, if $x = 2$, [1,1] will behave as a genotype [2,2], because we assume for simplicity that full producers will evolve the same level of investment for both traits.

Individual-Based Model. We used an individual-based model to examine the effects of spatial structure on our predictions. In particular, we ask if between-genotype cooperation can evolve if secreted traits have limited diffusion, which may be common on surfaces (9). To capture the effect of diffusion, we use spatial simulations that consider 2D lattices with periodic boundaries. Cells can only divide into empty spaces of their closest neighborhood (eight spaces around the focal individual), and the effect of a public good is limited to a neighborhood of a certain size around the producer cell. This spatial version is based on the same assumptions as the previous model for homogenous environments, and it uses an adaptation of the Gillespie algorithm for simulating population dynamics in continuous time (10). Although exactly equivalent to the Direct Method by Gillespie (11), this alternative is computationally more efficient and can easily handle large populations of individuals with individual properties according to rules for cellular growth. At each sampled time step, a focal individual is selected with uniform probability, and a cell division event is then realized with a probability directly proportional to its growth rate, which depends on population density and the presence of public goods following logistic kinetics. The stochasticity of cell division adds extra variance to the final genotypic composition of the simulated patches compared with the deterministic growth in the ODE version. Thus, the results of the individual-based model and the ODE model are not always identical for identical parameter values, with cooperation typically emerging more easily in the individual-based model. Nevertheless, we can use the individual-based model to specifically evaluate the effects of spatial structure by comparing a high-diffusion case, where between-genotype cooperation emerges, with a low-diffusion case (here given by a neighborhood of 24 cells from the source).

We implemented the standard three-step lifecycle like for the deterministic version. First, a number of M separate lattices is seeded according to the initial genotypic frequencies. Second, each subgroup develops separately, with cell growth being spatially simulated. Third, the subgroups are merged to update the genotypic frequencies, which are used for the following seeding step. Importantly, we let the yield of a focal subgroup depend on the presence of traits (secretions) in this group, with the consequence that subgroups with more producers will have higher final yield. Although in the ODE model K changed continuously with the number of producers, in the individual-based model K remained constant for the duration of the growth phase, but then, we weighted subgroups according to the proportion of producers present at the end of the simulation before the merging step. This implementation captures the dependence of subgroup yield on the proportion of producers in a group in a manageable way, but it differs from the ODE model. This different implementation of secretion-dependent carrying capacity could potentially affect comparisons between the two model frameworks. However, as discussed above, we only directly compare the cases of global and local diffusion within the individual-based model framework.

1. Brown SP, Johnstone RA (2001) Cooperation in the dark: Signalling and collective action in quorum-sensing bacteria. *Proc Biol Sci* 268(1470):961–965.
2. West SA, Buckling A (2003) Cooperation, virulence and siderophore production in bacterial parasites. *Proc R Soc Lond B Biol Sci* 270(1510):37–44.
3. Cremer J, Melbinger A, Frey E (2012) Growth dynamics and the evolution of cooperation in microbial populations. *Sci Rep* 2(2012):281.
4. Frank SA (2010) Microbial secretor-cheater dynamics. *Philos Trans R Soc Lond B Biol Sci* 365(1552):2515–2522.
5. Diggle SP, Griffin AS, Campbell GS, West SA (2007) Cooperation and conflict in quorum-sensing bacterial populations. *Nature* 450(7168):411–414.
6. Griffin AS, West SA, Buckling A (2004) Cooperation and competition in pathogenic bacteria. *Nature* 430(7003):1024–1027.
7. Chuang JS, Rivoire O, Leibler S (2009) Simpson's paradox in a synthetic microbial system. *Science* 323(5911):272–275.
8. Rumbaugh KP, et al. (2009) Quorum sensing and the social evolution of bacterial virulence. *Curr Biol* 19(4):341–345.
9. Julou T, et al. (2013) Cell-cell contacts confine public goods diffusion inside *Pseudomonas aeruginosa* clonal microcolonies. *Proc Natl Acad Sci USA* 110(31):12577–12582.
10. Allen GE, Dytham C (2009) An efficient method for stochastic simulation of biological populations in continuous time. *Biosystems* 98(1):37–42.
11. Gillespie DT (1977) Exact stochastic simulation of coupled chemical reactions. *J Phys Chem* 81:2340–2361.

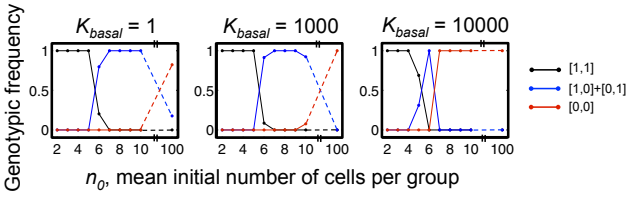

Fig. S1. Effect of basal fitness on the evolution of between-genotype cooperation in microbes. Our main models assume that secreted traits are essential for growth, which means that groups without secretions will not grow. Here, we vary K_{basal} (carrying capacity without secretions) from 1 to 10,000 [up to 10% of the maximum benefit from secretions (K_{maxB})] (*SI Materials and Methods*). The only effect is to reduce the scope for between-genotype cooperation, which further suggests that cooperation among microbial genotypes is limited. Results from the two-trait model (ODE version) with the cost (c) at 5% of growth rate are shown.

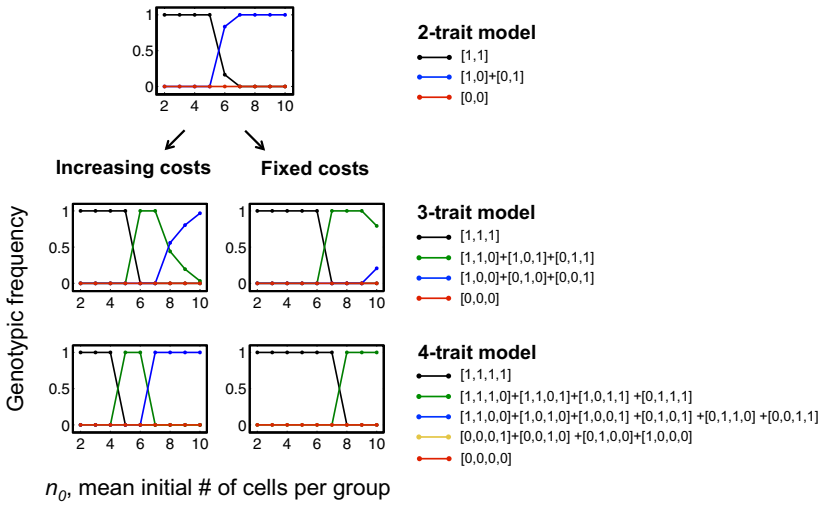

Fig. S2. Effect of increasing the number of traits on the evolution of cross-feeding. (*Lower Left*) Systems that rely on four secretions select more for cooperative cross-feeding than those relying on three secretions only. This results from the increasing cost of adding another secretion to a genotype that produces all traits. (*Lower Right*) If total costs are fixed (here, at 10% of maximum growth rate), then adding another secretion reduces the prevalence of cross-feeding.

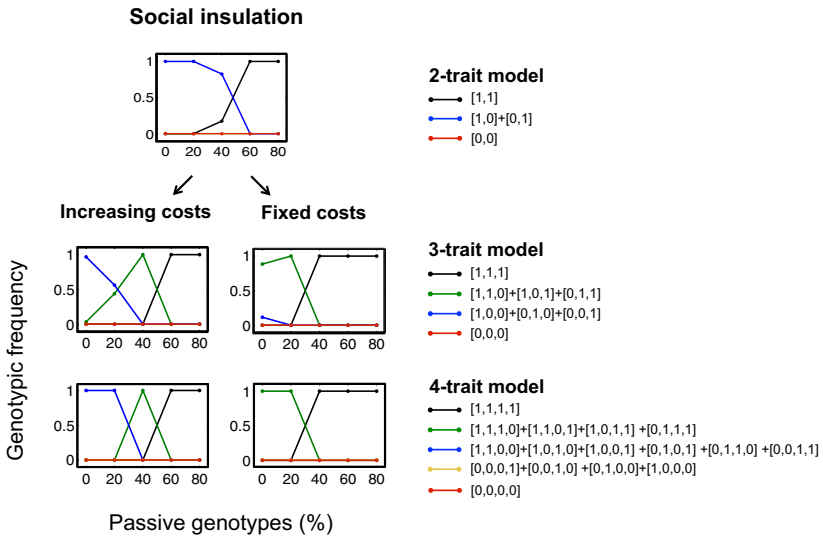

Fig. S3. Social insulation in systems with increasing numbers of traits. The introduction of passive genotypes has the same effect on the evolution of cooperative cross-feeding in systems relying on two, three, and four traits: a high percentage of passive genotypes prevents between-genotype cooperation. (*Lower Right*) Holding the total cost of all secretions constant shows that social insulation is particularly problematic for systems with many secretions. Here, we fixed total costs at 10% of maximum growth rate and genetic mixing at $n_0 = 10$, which promote cross-feeding in the absence of passive genotypes.

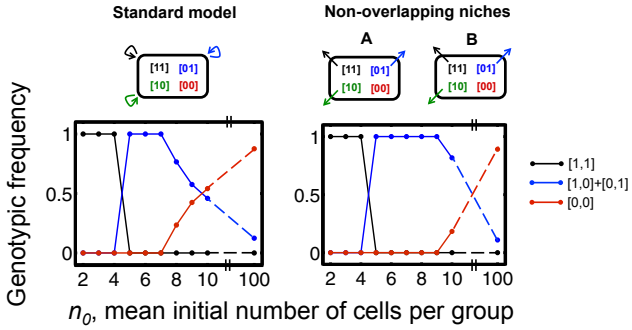

Fig. S4. Evolution of cooperation between genotypes without overlapping niches. For the nonoverlapping case, we consider two species of bacteria (species A and B) that do not compete for the same resources. Each species is composed by the same four genotypes considered in the standard model. Importantly, secretions can be used by any genotype, regardless of the species. However, to allow natural selection to differentiate between the species, we also assume asymmetric costs: species A is more efficient on secretion 1 than species B but less efficient on secretion 2. As for the standard model, cooperative cross-feeding between species A and B is possible at intermediate levels of genotypic mixing only. However, the scope for cooperation is now improved, because cross-feeders do not compete for the same resources. For both cases, we considered well-mixed conditions and high secretion cost (here, c = 10% of maximum growth rate per secretion).

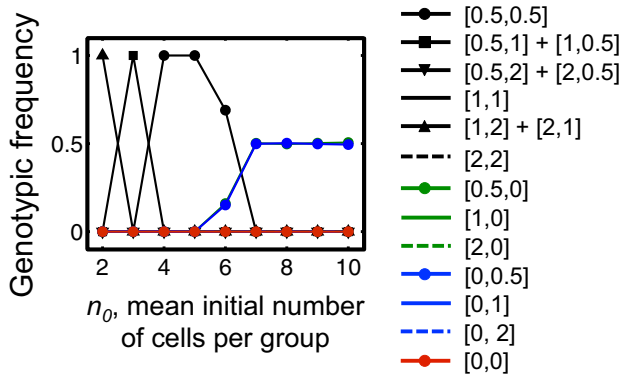

Fig. S5. Independent evolution of investment into secretion production. In the text (Fig. 4), we show the results of a discrete model, where the producers of both traits invest the same amount in each secretion. That is, we considered only genotypes [0.5,0.5], [1,1], and [2,2] in the full secretors. Here, we show that identical results are obtained when full producers can invest differentially in each trait: high investment is selected at low mixing, whereas increasing mixing selects for reducing investment.

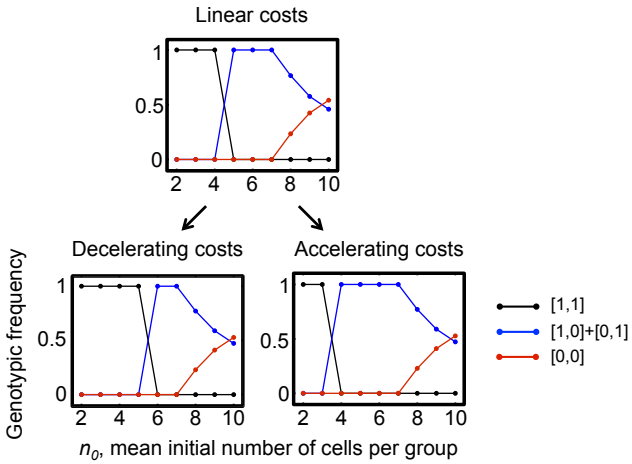

Fig. S6. Effect of nonlinear costs on the evolution of between-genotype cooperation. Our models assume that genotypes that invest in more than one trait experience a linear increase in costs. For example, if one sets c equal to 0.1, then [1,1] will reduce its growth rate by 20%, whereas genotypes that produce only 1, [1,0], and [0,1] reduce by 10%. Here, we considered the effect of nonlinear (*Lower Left*) decelerating and (*Lower Right*) accelerating costs. Specifically, [1,1] now invests (*Lower Left*) 15% and (*Lower Right*) 30%, whereas the investment is the same for cross-feeders.

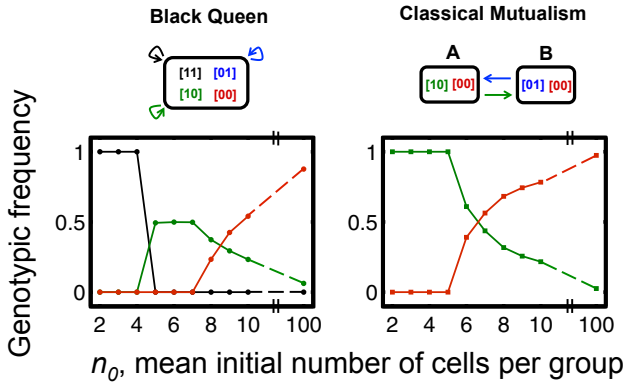

Fig. S7. Evolution of the genotypic cooperation in our model (Black Queen-like) compared with a classical mutualism model. We modeled classical mutualism by considering two species of bacteria (species A and B) that do not compete for the same resources and possess unique traits (one secretion each) that can only be used by the partner species for growth. That is, there is no [1,1] genotype but just a single-trait producer and respective cheater genotype within each species. For both cases, we considered well-mixed conditions and high secretion cost (c = 10% of maximum growth rate per secretion). The potential for genotypic cooperation is higher under canonical mutualistic interactions (here given by a wider region of genotypic mixing, under which cooperative partners dominate the population). The within-species frequencies of [1,0] and [0,1] in both plots overlap, as expected, and therefore, only one of two colors is seen in the plot.

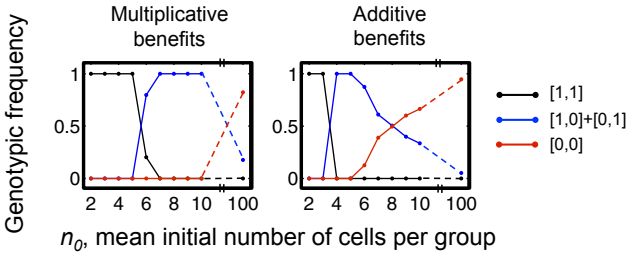

Fig. S8. Effect of the functional form of benefits on the evolution of between-genotype cooperation in microbial communities. Qualitative conclusions are robust to both multiplicative and additive benefits to secretions. Our main models assume that the benefits of multiple secretions combine multiplicatively to set population carrying capacity (K). For example, for two traits, K is proportional to the product of the amount of secretions 1 and 2 in each subpopulation. Here, this scenario is compared with a case where K scales as the sum of the amounts of two secretions. Results are shown from the two-trait model (ODE version) with cost (c) at 5% of the maximum growth rate, where the two fitness functions are, for multiplicative benefits,

$$K = K_{basal} + K_{maxB}\left(\frac{g_{11}+g_{10}}{g_{11}+g_{10}+g_{01}+g_{00}} \cdot \frac{g_{11}+g_{01}}{g_{11}+g_{10}+g_{01}+g_{00}}\right),$$

and for additive benefits,

$$K = K_{basal} + K_{maxB}\left(\frac{g_{11}+g_{10}}{g_{11}+g_{10}+g_{01}+g_{00}} + \frac{g_{11}+g_{01}}{g_{11}+g_{10}+g_{01}+g_{00}}\right)\Big/2.$$

As before, K_{basal} and K_{maxB} are the minimal carrying capacity of the system and the maximum benefit from secretions, respectively, and g_{ij} is the density of individuals of genotype [i,j] in each subpopulation.

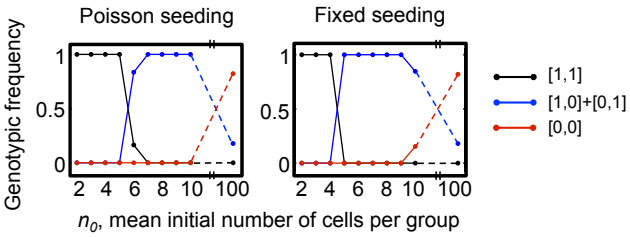

Fig. S9. Effect of the type of seeding on the evolution of cooperative cross-feeding. We find the same qualitative behavior for (*Left*) Poisson-based seeding, where a random number of cells is initially introduced in each group, and (*Right*) fixed seeding, where we introduce the same number of cells in all groups. However, there are some quantitative differences, because fixing the number of cells introduced per group reduces the variance between groups. This reduction in variance between groups affects the potential for Simpson's Paradox and thus, the evolution of cooperation both within and between genotypes. Costs per trait were set at 5% of the maximum growth rate.

PLOS | BIOLOGY

RESEARCH ARTICLE

Biofilm Formation As a Response to Ecological Competition

Nuno M. Oliveira[1,2], Esteban Martinez-Garcia[3,4], Joao Xavier[3,5], William M. Durham[1], Roberto Kolter[6], Wook Kim[1,2,3], Kevin R. Foster[1,2,3]*

1 Department of Zoology, University of Oxford, Oxford, United Kingdom, **2** Oxford Centre for Integrative Systems Biology, University of Oxford, Oxford, United Kingdom, **3** FAS Center for Systems Biology, University of Harvard, Cambridge, Massachusetts, United States of America, **4** Centro Nacional de Biotecnologia-CSIC, Campus de Cantoblanco, Madrid, Spain, **5** Memorial Sloan-Kettering Cancer Center, Computational Biology Program, New York, New York, United States of America, **6** Harvard Medical School, Department of Microbiology and Immunobiology, Boston, Massachusetts, United States of America

* kevin.foster@zoo.ox.ac.uk

CrossMark
click for updates

OPEN ACCESS

Citation: Oliveira NM, Martinez-Garcia E, Xavier J, Durham WM, Kolter R, Kim W, et al. (2015) Biofilm Formation As a Response to Ecological Competition. PLoS Biol 13(7): e1002191. doi:10.1371/journal.pbio.1002191

Academic Editor: Michael T. Laub, Massachusetts Institute of Technology, United States

Received: October 28, 2014

Accepted: May 29, 2015

Published: July 9, 2015

Copyright: © 2015 Oliveria et al. This is an open access article distributed under the terms of the Creative Commons Attribution License, which permits unrestricted use, distribution, and reproduction in any medium, provided the original author and source are credited.

Data Availability Statement: All relevant data are within the paper and its Supporting Information files.

Funding: European Research Council Grant 242670 (KRF), National Institute of Health Grant GM58213 (RK), and Fundação para a Ciência e Tecnologia fellowship SFRH-BD-73470-2010 (NMO). The funders had no role in study design, data collection and analysis, decision to publish, or preparation of the manuscript.

Competing Interests: The authors have declared that no competing interests exist.

Abstract

Bacteria form dense surface-associated communities known as biofilms that are central to their persistence and how they affect us. Biofilm formation is commonly viewed as a cooperative enterprise, where strains and species work together for a common goal. Here we explore an alternative model: biofilm formation is a response to ecological competition. We co-cultured a diverse collection of natural isolates of the opportunistic pathogen *Pseudomonas aeruginosa* and studied the effect on biofilm formation. We show that strain mixing reliably increases biofilm formation compared to unmixed conditions. Importantly, strain mixing leads to strong competition: one strain dominates and largely excludes the other from the biofilm. Furthermore, we show that pyocins, narrow-spectrum antibiotics made by other *P. aeruginosa* strains, can stimulate biofilm formation by increasing the attachment of cells. Side-by-side comparisons using microfluidic assays suggest that the increase in biofilm occurs due to a general response to cellular damage: a comparable biofilm response occurs for pyocins that disrupt membranes as for commercial antibiotics that damage DNA, inhibit protein synthesis or transcription. Our data show that bacteria increase biofilm formation in response to ecological competition that is detected by antibiotic stress. This is inconsistent with the idea that sub-lethal concentrations of antibiotics are cooperative signals that coordinate microbial communities, as is often concluded. Instead, our work is consistent with competition sensing where low-levels of antibiotics are used to detect and respond to the competing genotypes that produce them.

Author Summary

Bacteria often attach to each other and to surfaces and make biofilms. These dense communities occur everywhere, including on us and inside us, where they are central to both health and disease. Biofilm formation is often viewed as the coordinated action of multiple strains that work together in order to prosper and protect each other. In this study, we

Abbreviations: CAA, casamino acid; CFP, cyan fluorescent protein; LB, Luria broth; PMM, Pseudomonas minimal medium; TB, tryptone broth; YFP, yellow fluorescent protein; WT, wild-type.

provide evidence for a very different view: biofilms are formed when bacterial strains compete with one another. We mixed together different strains of the widespread pathogen *Pseudomonas aeruginosa* and found that pairs often make bigger biofilms than either one alone. Rather than working together, however, we show that one strain normally kills the other off and that biofilm formation is actually a response to the damage of antibiotic warfare. Our work helps to explain the widespread observation that treating bacteria with clinical antibiotics can stimulate biofilm formation. When we treat bacteria, they respond as if the attack is coming from a foreign strain that must be outnumbered and outcompeted in a biofilm.

Introduction

While the traditional model for bacterial life was one of cells swimming in liquid, it is now realized that bacteria commonly live in surface-associated communities known as biofilms [1–4]. These groups of bacteria carry significant medical and economic importance that includes a role in chronic diseases, antibiotic tolerance, biofouling, and waste-water treatment [5–7]. The importance of biofilms has led to their intensive study in many species of bacteria. However, this work has revealed that the genetic and biochemical mechanisms underlying biofilm formation are extremely variable across strains and growth conditions [8,9]. This variability has made it difficult to identify common principles of biofilm formation across species.

One property common to the biofilms of many bacterial species, both gram-negative and gram-positive, is that they are induced by sub-lethal concentrations of antibiotics [10–17]. The diversity of the species displaying this response is striking [13] and suggestive of the general principles that so often elude the study of biofilms. This, and the observation that sub-lethal antibiotics induce a range of other physiological changes [18], has led to the hypothesis that antibiotics may not function as killing agents in nature. Instead, it is suggested that antibiotics may function as cooperative signals between species that contribute to the homeostasis of bacterial communities [13,16,19–21]. In parallel, there are a growing number of studies concluding that natural microbial communities are cooperative enterprises in which strains and species work together, both in biofilm formation and metabolism [22–31].

Cooperative phenotypes—such as secreted enzymes or polymers—are important in biofilms for cells of a single genotype [4,32–35]. However, evolutionary theory and ecological experiments caution against the idea that this cooperation will always extend to cells of different genotypes [32,34,36–38]. Competition between strains and species appears to be commonplace and it is not clear how cooperative signaling via antibiotics could widely evolve [39]. An alternative to the idea that sub-lethal antibiotics are cooperative signals between species is that they are cues used by competing species to detect competitors and respond appropriately [39–41]. Under the cue model, antibiotics are not secreted in order to signal to others [42,43], they are secreted to attack but can inadvertently provide information to others at low concentration. The idea that bacteria use antibiotics and other factors as cues of competition is central to the idea of "competition sensing" [41]. This is based on the observation that both nutrient and antibiotic stress, which are associated with ecological competition, often cause bacteria to release their own antibiotics. Bacteria appear to attack back when they are themselves attacked.

If sub-lethal concentrations of antibiotics are cues of competition from other strains, and biofilms are induced by such concentrations, this implies that biofilm formation can be a response to ecological competition from other strains. Here we test this hypothesis by co-culturing natural isolates of the opportunistic pathogen *Pseudomonas aeruginosa* and studying

the effects on biofilm formation. We focus on members of a single species here because these are expected to have the strongest ecological overlap and, therefore, the strongest ecological competition; something first noted by Darwin: "The struggle almost invariably will be most severe between the individuals of the same species, for they frequent the same districts, require the same food, and are exposed to the same dangers" [44]. More concretely, data from the cystic fibrosis lung suggest that different isolates can colonize and, at least temporarily, co-exist in young patients [45–47], which is consistent with different strains meeting. *P. aeruginosa* also forms robust biofilms that have been intensively studied [6,48]. The co-culture of *P. aeruginosa* strains then provides a test case to evaluate the link between ecological competition and biofilm formation. Specifically, if biofilm formation is a response to ecological competition, we expect to observe (i) evidence of competition between strains and (ii) evidence of increased biofilm formation in co-cultures relative to monocultures.

Results and Discussion

Both Clinical Antibiotics and Mixing Strains Promote Biofilm Formation

We begin by recapitulating the known effects of antibiotic stress on bacterial survival and biofilm formation. Fig 1 (panels A, B) shows the effects of antibiotics on *Pseudomonas aeruginosa* where we use optical density as a qualitative indicator of cell number. As expected, increasing the concentration of three widely used clinical antibiotics—ciprofloxacin, rifampicin and tetracycline—monotonically reduces the optical density of shaking cultures. However, as previously shown, this monotonic decrease is not seen when the same concentrations are applied to standing cultures. In standing cultures, the liquid is not agitated and cells can readily attach to the edge of the well and establish biofilms. Under this condition, biofilm formation actually increases for many concentrations of the antibiotics, until the concentrations become so high that toxicity dominates [13].

Applying sub-lethal concentrations of antibiotics then leads to an increase in biofilm formation. Can we understand these widely reported biofilm responses to antibiotics in terms of ecological competition? We tested this by mixing natural isolates of *P. aeruginosa* in standing cultures and studying the impact on biofilm formation. Consistent with the hypothesis that biofilm formation is a response to ecological competition, we find that biofilm formation is increased in mixed cultures compared to pure cultures, both in a broad scale survey that mixed combinations of 22 natural isolates (Fig 1C) and in defined pairwise comparisons in which we show that the strength of the biofilm response depends on the relative proportion of each strain at the start of the co-cultures (Fig 1D).

Competitive Exclusion Is Common in Pairwise Mixtures

The observed biofilm response is consistent with a competitive response. However, an alternative hypothesis is that the strains cooperate with one another to produce more biofilm (see Introduction). In order to better assess whether the strains were cooperating to make more biofilm, we labeled five of our *P. aeruginosa* natural isolates with constitutive fluorescent proteins (cyan fluorescent protein, CFP, and yellow fluorescent protein, YFP) by putting a single copy of the desired fluorescent protein gene at a specific site in the genome [50]. We then set up a round-robin tournament, in which the five strains were mixed in all combinations, and measured biofilm formation, planktonic growth, and the relative frequency of the two strains (Fig 2). This revealed a strong competitive effect with one strain typically dominating after 24 h (median proportion of dominant strain in biofilm = 0.98, Wilcoxon-signed rank test versus 0.5, $n = 10$, $p < 0.01$). Thus, the biofilm response is a manifestation of competition between

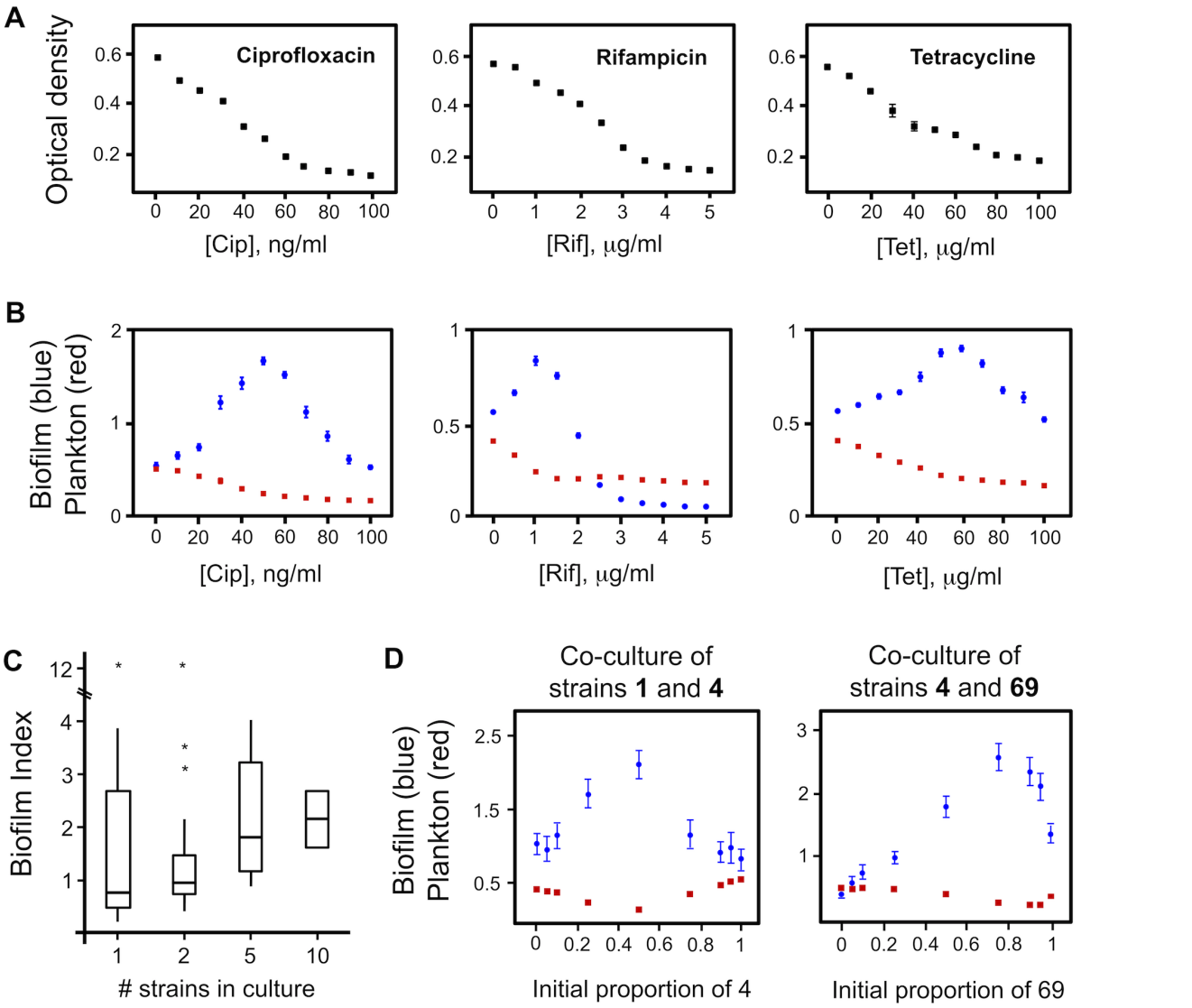

Fig 1. Effect of clinical antibiotics and strain mixing on biofilm formation of *P. aeruginosa*. A) Increasing concentrations of three antibiotics from different classes, ciprofloxacin (Cip), rifampicin (Rif), and tetracycline (Tet), reduce the optical density of strain PAO1 shaking cultures. B) Under static conditions, sub-lethal concentrations of antibiotics induce biofilm formation. C) Mixing different natural isolates of *P. aeruginosa* induces biofilm formation in an assay with increasing numbers of strains. The *y*-axis of box plots represents the biofilm index of each strain and mixtures, which is the ratio of biofilm to planktonic cell density (A_{595}/A_{600}). This measure controls for the large variability in overall growth between the strains and is a way to assess biofilm relative to the amount of planktonic cells [49]. The biofilm index increases with the more strains present (2-tailed Spearman rank correlation, non-normal data, $n = 52$, $\rho = 0.305$, $p = 0.025$). D) Mixing increases biofilm formation in two pairwise combinations of strains (1 + 4 and 4 + 69) in which the initial proportion of each strain was varied. Panels A, B, and D show means and 95% confidence intervals. Error bars are too small to see in some cases, particularly for the planktonic data. Find numerical values in S1 Data.

doi:10.1371/journal.pbio.1002191.g001

strains rather than a cooperative synergy in which both strains benefit from the presence of one another [34].

There are some cases in which biofilm formation in the mixture is less than that expected from the average of the two starting strains (Fig 2). However, accounting for which strain

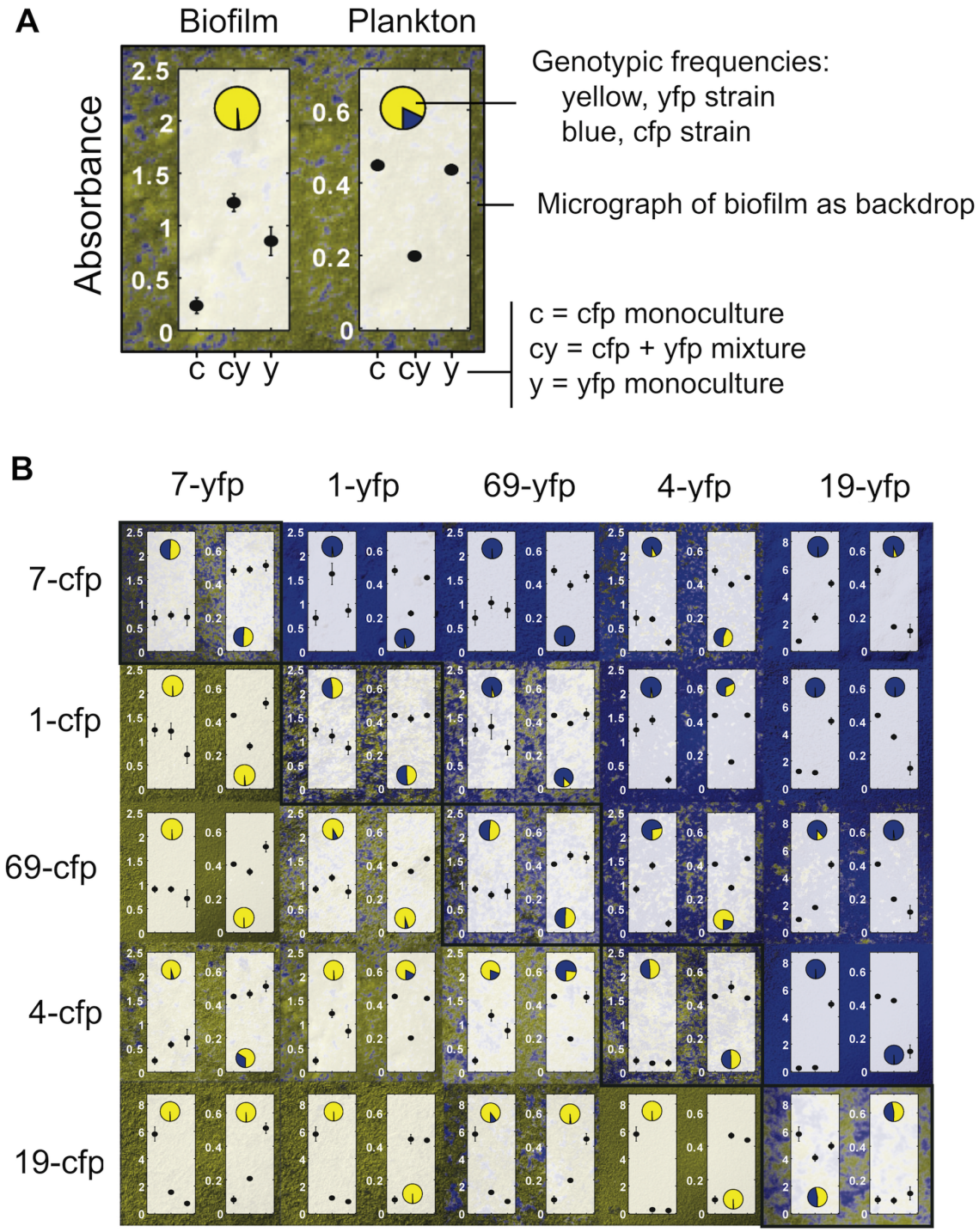

Fig 2. Round-robin tournament among natural isolates of *P. aeruginosa* showing strong competitive effects upon strain mixing. Five isolates were mixed together in all pairwise combinations and data from each mixture are shown in a corresponding panel. A) Example data from strains 4 and 1 illustrating the different measures in a given mixture. In this example, mixing the two strains increases biofilm, decreases planktonic cells, and strain 1 (*yfp*-labeled) strain strongly outcompetes strain 4 (*cfp*-labeled) strain. B) All data from the round-robin tournament. As in panel A, the backdrop to each panel is an

epifluorescence image of the coculture biofilm from a coverslip. All other data shown are from 96-well microtiter experiments. Specifically, the left-hand side graph in each panel shows information about the biofilm. Here, the plotted points show biofilm formation in the crystal violet assay by the *cfp*-labeled strain alone, both strains together, and the *yfp*-labeled strain alone, from left to right. The pie chart on the left shows frequencies of the two strains in the biofilm. The right-hand side of each panel—graph and pie chart—shows the planktonic cell data from the same experiments as the biofilms measurements. *cfp* and *yfp* stand for cyan and yellow fluorescent protein, respectively. Plotted data show means and 95% confidence intervals. Find numerical values in S1 Data.

doi:10.1371/journal.pbio.1002191.g002

actually makes the final biofilm reveals that mixing nearly always causes an increase in biofilm formation by the dominant strain. For example, mixtures of 7 and 19 result in less biofilm than monocultures of strain 19. However, strain 7 eliminates strain 19 in co-cultures, producing more biofilm than it does when alone (Fig 2). More generally, we can calculate the expected biofilm formation from the pure culture data using a weighted average, which weights by the frequencies of the two strains in the biofilm after competition. This reveals that the mixed culture biofilm normally increases relative to the expectation based upon pure cultures (9/10 mixes increase, Wilcoxon signed rank test of expected/observed biofilm against a null of 1, $n = 10$, $p < 0.01$), while the amount of cells in the planktonic phase decreases ($n = 10$, $p < 0.01$). Moreover, the increases in biofilm and decreases in plankton that we observe upon mixing strains are significantly negatively correlated across the different strain mixes (Spearman rank correlation, $n = 10$, $r = -0.782$, $p < 0.01$). This correlation agrees with recent observations on multispecies interactions during biofilm formation [31].

The biofilm response is not an idiosyncrasy of our particular growth medium. S1 Fig shows the effect of varying levels of nutrients, buffering, and soluble iron for two genotype mixtures. Despite the success of strains in pairwise competition being strongly dependent on the environment, the biofilm response is detected across all conditions in at least one of the two strain combinations, but typically in both (S1 Fig).

Pyocins Serve As a Cue for Biofilm Formation

We next focus on the cue that drives the increase in biofilm formation in co-cultures. We first examined whether the biofilm response requires cell–cell contact by growing pairs of strains on either side of a 0.4 μm permeable membrane (Fig 3A). Increased biofilm is observed across the membrane in most cases. In one case, there is a strong inhibitory effect on both biofilm and planktonic growth, which is consistent with the responder strain losing in co-culture (specifically, strain 4 is inhibited and outcompeted by strain 1, Fig 2). We also found that the biofilm response is recapitulated by the addition of cell-free culture supernatant of different strains. We focus on strain 4, which responds robustly to the addition of the supernatant from other strains (Fig 3B). The nature of the response is dose dependent: lower concentrations tend to induce biofilm formation while high concentrations inhibit both planktonic growth and biofilm formation.

In order to identify the active component within the supernatant, we first performed anion exchange chromatography on the supernatant of strain 69 as it generates a robust response in strain 4 (Fig 3B). The active fraction that induced biofilm formation in strain 4 was further separated based on size by gel filtration. A single fraction (C9) appeared to contain the bulk of the active component as it strongly inhibited growth in strain 4, while the two flanking fractions C8 and C10 (i.e., lower concentrations of the effector) induced the biofilm response (Fig 4A). We subjected fraction C9 to protein mass spectrometry (see Methods). Of the proteins identified, three are notable for their known role in microbial interactions: homologs (PA14_8070, PA14_8090, PA14_8210) of the R and F pyocins in *P. aeruginosa* strain PA14 (S1 Table) [51]. Given that PA14 is a well-characterized strain, we next sought to explore how the pyocins of PA14 induce the biofilm response in our natural isolates.

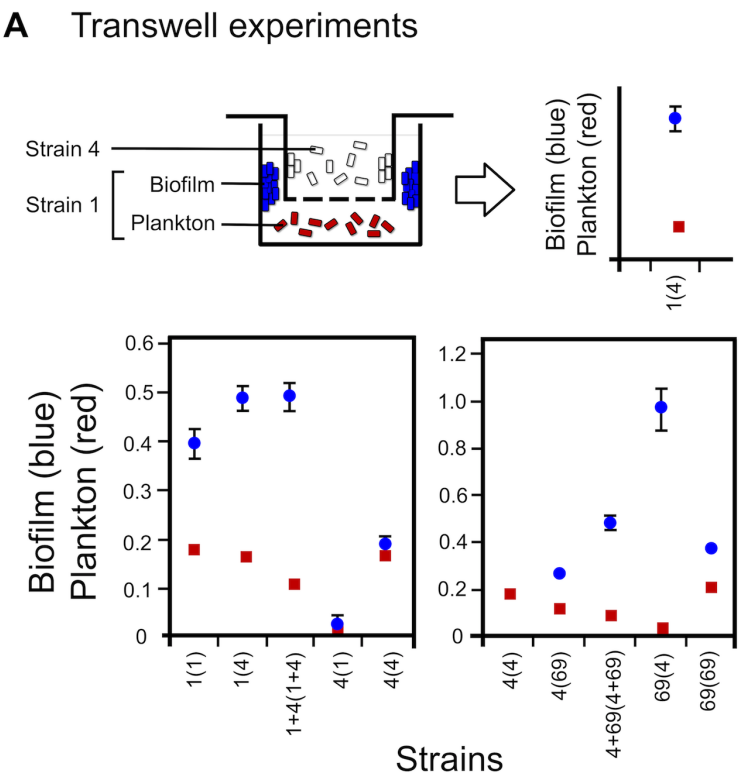

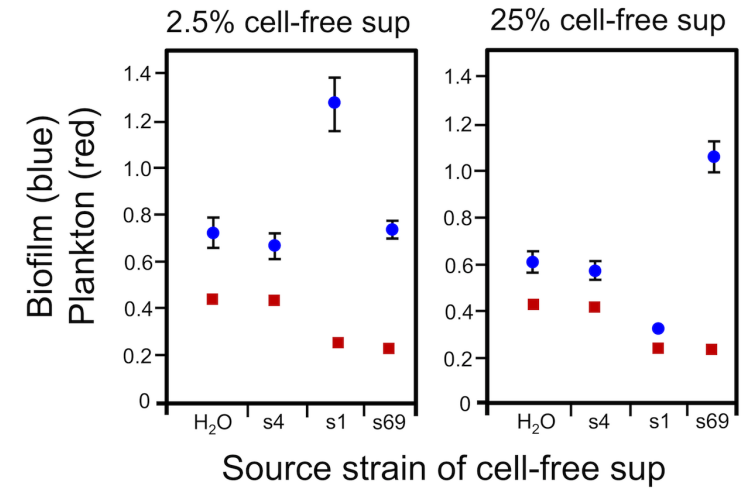

Fig 3. Increased biofilm in co-cultures is not dependent on cellular contact between strains. A) Membrane-separated growth using Transwell plates (see Methods). Top diagram shows experimental design (left) and how results are plotted (right). On the axes, the first number refers to the responder strain for which the data are shown, while the number in parentheses is the inducer strain that is grown above, across the

membrane. B) Increased biofilm due to cell-free culture supernatants. Data are for strain 4 growing in the presence of various supernatants ("H_2O" is water in place of the supernatant, and "s4," "s1," and "s69" indicate the supernatant from strains 4, 1, and 69, respectively). Two concentrations of the supernatant are shown: 2.5% (left) and 25% (right). Data show means and 95% confidence intervals. Find numerical values in S1 Data.

doi:10.1371/journal.pbio.1002191.g003

We first evaluated the effects of cell-free culture supernatant from PA14 on biofilm formation in the five strains from the round robin tournament. Strain 19, which was isolated from a cystic fibrosis infection, is a very poor competitor (Fig 2) and showed no detectable growth in our supernatant assays. It was therefore excluded from further analysis. Among the remaining strains, increased biofilm was observed in only strain 4 (Fig 4B), and we confirmed that direct mixtures of PA14 and strain 4 also lead to increased biofilm formation (S2 Fig). Why is the biofilm response absent in the other three strains? To address this question, we grew the four strains in shaking culture in the presence or absence of the supernatant from PA14 and followed their growth over time. The results obtained show that the strains that do not show the biofilm response to the supernatant of PA14 also are not harmed by it (Fig 4C). This correlation between toxicity and increased biofilm helps explain the lack of response in the three strains. Cell damage appears to be required for the biofilm response.

We next studied the effect of various mutants of pyocin production in PA14 on their ability to damage and induce the biofilm response in strain 4. We focused particularly on a strain of PA14 that has the repressor of pyocins, *prtR*, mutated to a version that is constitutively active (S3 Table) [52]. We added cell-free supernatant of the PA14 *prtR* mutant to strain 4 and compared the effect to the addition of WT PA14 supernatant by propidium iodide staining. Propidium iodide preferentially enters cells with envelope damage (see Methods), and this assay confirmed that the pyocins produced by PA14 cause cell damage to strain 4 (S3 Fig), which agrees with published literature on pyocin-driven lethality [51]. Moreover, additional experiments showed that the pyocins of PA14 are the major effectors of both population growth inhibition (Fig 4C) and the biofilm response of strain 4 (Fig 4D).

Focusing on the biofilm response, the use of mutants that lack only one class of pyocin suggested that F pyocins have some effect on biofilm formation at high concentrations, but it is particularly the R pyocins that strongly stimulate biofilm formation. This is, furthermore, consistent with the importance of cell damage because R pyocins are known to be efficient killers that can contribute significantly to competition among *P. aeruginosa* strains [53,54]. To further explore the potential of cell damage being required for the biofilm response, we screened 12 natural isolates for inhibition by the supernatant of PA14 in shaking culture and found that three strains were inhibited like strain 4. We randomly selected two of the inhibited strains for further study in the biofilm assay. This revealed that both exhibit a biofilm response comparable to that of strain 4 and, again, the response occurs in a pyocin-dependent manner (S3 Fig). We also tested the response of the strain PAK under the same conditions. This serves as a good control case since PAK is known to be inhibited by the pyocins produced by PA14 [53]. Again, we find evidence of pyocin-driven biofilm formation (S4 Fig).

These data further support the idea that pyocin-driven damage under these conditions is sufficient to drive the biofilm response. We note, however, that this does not exclude the possibility that there are additional mechanisms by which *P. aeruginosa* strains damage and induce biofilm in other susceptible strains. Indeed, the link between pyocin-based cell damage and the biofilm response is consistent with experiments using clinical antibiotics, in which antibiotic resistance mutants require higher concentrations of antibiotics to elicit the biofilm response [10]. To confirm this effect in our assays, we tested a rifampicin resistant mutant of PAO1, with defined mutations in *rpoB* [55] and found that it does not respond to the same

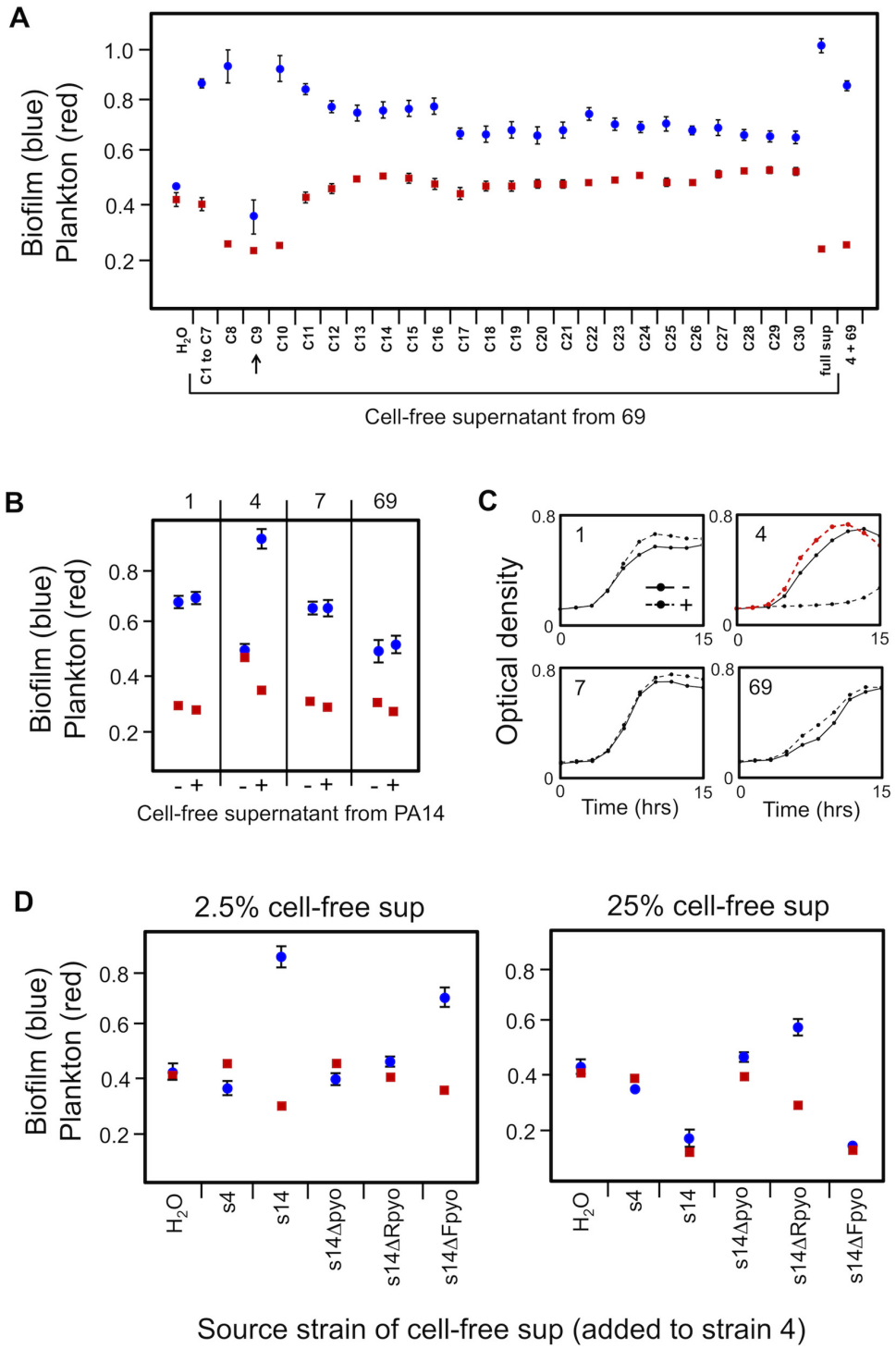

Fig 4. Pyocins are drivers of biofilm formation in co-cultures. A) Size-based separation of the cell-free culture supernatant from strain 69 isolates fractions that induce biofilm formation at low concentrations and growth inhibition at high concentrations. Adding the unfractionated supernatant ("full sup") induces biofilm in strain 4, which is comparable to direct mixtures of strains 4 and 69 (here labeled as "4 + 69"). Mass spectrometry analysis of fraction C9

(arrow) identified three proteins that are homologous to R and F pyocins in strain PA14. Compared to manufacturer size standards for the column, fraction C9 is expected to be >600 kDa. B) Cell-free culture supernatant at 2.5% in tryptone broth from PA14 ("+") causes increased biofilm formation in strain 4 relative to tryptone broth with the same amount of water added ("-"), but this effect is not seen for strains 1, 7, or 69. C) The supernatant from PA14 is toxic to only strain 4, causing a strong population growth lag. This suggests that some degree of cell damage is needed for the biofilm response. Supernatant from a PA14 pyocin-null mutant (PA14 *prtR*^{S153A}) does not cause any growth lag in strain 4 (red curve), confirming that the toxicity to strain 4 is driven by pyocins. D) R pyocins, and F pyocins to a lesser degree, drive the biofilm response in strain 4. At 2.5%, the supernatant from both PA14 ("s14") and F-pyocin-null mutant ("s14ΔFpyo") elicit a strong biofilm response in strain 4, which is largely removed by mutating either a master regulator of pyocins ("s14Δpyo") or R pyocins ("s14ΔRpyo") in PA14 (left panel). At a higher concentration (25%), supernatant that contains R pyocins is strongly toxic to strain 4, and R pyocin free supernatant now induces biofilm formation, which is consistent with the effects of other pyocins. Data from biofilm assays are means and 95% confidence intervals. Growth curves are means of eight replicates. Find numerical values in S1 Data.

doi:10.1371/journal.pbio.1002191.g004

concentrations of rifampicin that trigger the biofilm responses in the wild type (S5 Fig). In sum, we see comparable effects on biofilm formation from diverse forms of cell damage. This suggests that cell damage from a diverse range of bacteria interactions, both between strains and between species, has the potential to promote biofilm formation.

The Biofilm Response Is Observed in Microfluidic Experiments

Our experiments so far have utilized the crystal violet microtiter dish assay of standing cultures [48]. Although this experimental approach is widely used to quantify biofilm responses to antibiotics [13], it comes with two notable limitations. Firstly, indirect proxies are used to estimate biofilm formation (crystal violet staining) and planktonic cell numbers (optical density). Secondly, the presence of a large planktonic population in the standing culture means that the planktonic cells can affect the biofilm, and vice versa, in an undefined manner throughout the experiment. We therefore sought to recapitulate our results in a more defined assay using flow cells and direct imaging of the biofilms (Fig 5A).

We begin by studying one of our focal combinations, strain 1 (PAO1) and strain 4. As we find in the standing culture assay (Figs 1D and 2B), PAO1 dominates strain 4 and largely excludes it from the biofilm after 24 h (Fig 5B). Moreover, we observe an increase in the volume of biofilm formed by PAO1. Our observations in the less-defined crystal violet assays, therefore, are recapitulated in flow cell biofilms: strain-mixing results in a single strain dominating and an increase in biofilm formation. Do we also observe this biofilm response in strain 4, which was the focus of detailed analyses in the previous section? In order to study this, we needed to create a condition where strain 4 is not eliminated from the biofilm. Preliminary tests with our two focal mixtures (1 + 4, 4 + 69, Fig 1D) revealed that strain 4 will persist with strain 69, if it is over-represented at inoculation. We, therefore, tested strain 4 mixed with strain 69 in the flow cells at a 3:1 initial ratio. Under these conditions, strain 4 dominates the biofilms and largely excludes strain 69 and, most importantly, we see a clear increase in biofilm formation in strain 4 here when compared to its single-strain counterpart (Fig 5C).

Experiments using flow cells have a separate attachment phase at the beginning of the experiment to seed the surface with bacteria (see Methods). Counting attached cells after the attachment phase revealed that strain 4 attaches more in the presence of strain 69 but strain 1 does not attach more in the presence of strain 4 (Fig 5). Both initial attachment and subsequent biofilm accumulation, then, contribute to the response to strain mixing but while we always see increased biofilm formation, we do not always see an initial difference in attachment (also see next section). In sum, the flow cell experiments provide validation from a second assay that *P. aeruginosa* strains increase biofilm formation in response to the presence of competing strains.

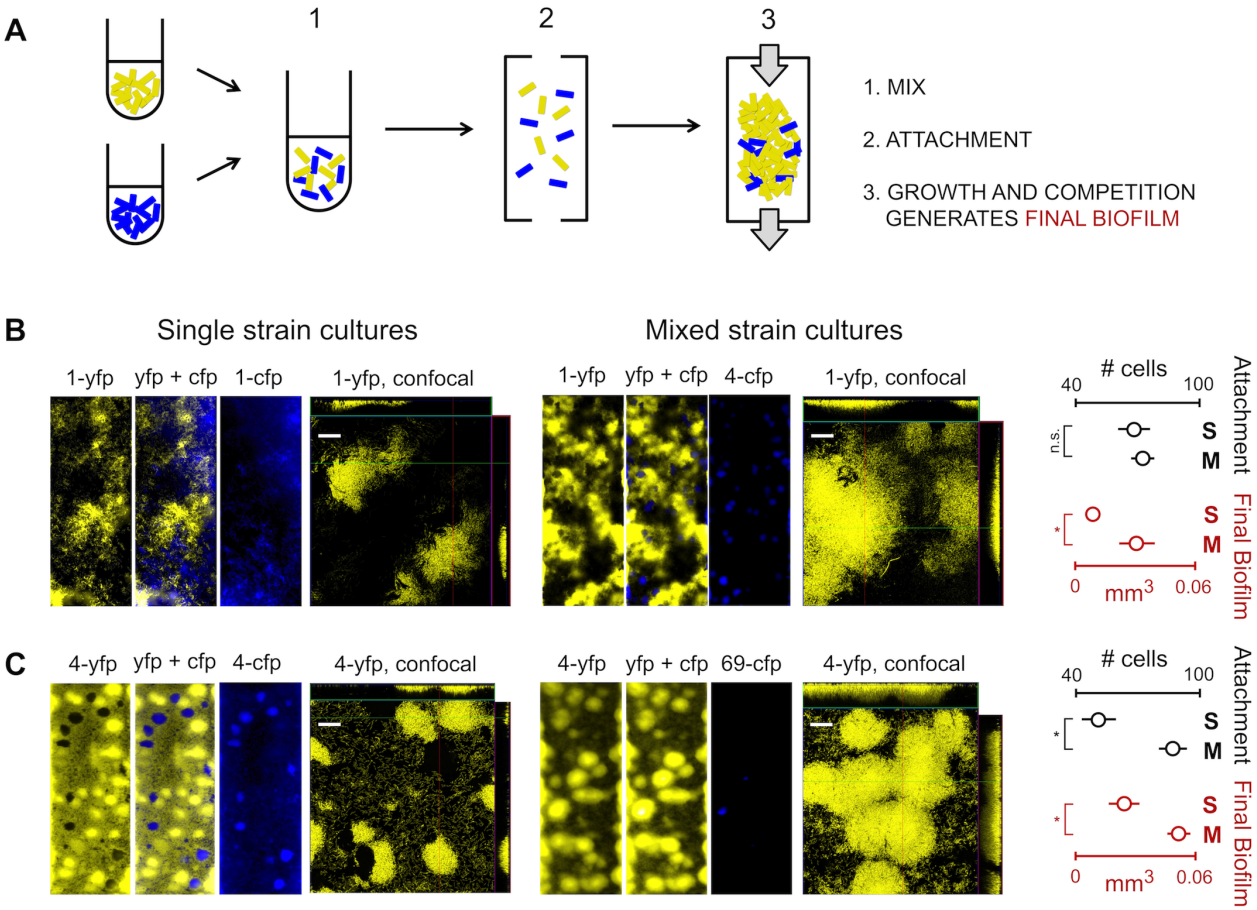

Fig 5. Strain mixing induces biofilm formation in *P. aeruginosa* in flow cells. A) Schematic of the experimental design, which involves mixing genotypes, initial attachment in the absence of flow, and finally, growth and competition under constant flow. Grey arrows represent the flow of nutrient media (tryptone broth). B) PAO1 biofilm compared to a mixed biofilm of PAO1 (strain 1) and strain 4. Within each image panel are three representative 10x epifluorescence micrographs of the flow cell channel showing the individual and merged YFP and CFP signals, and one 40x confocal image (scale bar is 30 μm) showing only the numerically-dominant *yfp* strain (autofluorescence in the CFP channel leads to a poor confocal signal). The charts at the far right show the initial attachment and final volume of biofilm of strain 1-*yfp* in single strain cultures (S) where 1-*yfp* is mixed with 1-*cfp* and in mixed strain cultures (M) where 1-*yfp* is mixed with 4-*cfp*. In both mixed and single cultures, the two differently-colored strains were initially mixed at a 1:1 ratio, *yfp*:*cfp*. Strain 1-*yfp* shows increased biofilm accumulation when mixed with 4, but cellular attachment is identical between single strain and mixed strain cultures. C) Strain 4 biofilm compared to a mixed biofilm of strain 4 and strain 69. In both mixed and single strain conditions, two differently-colored strains were initially mixed at a 3:1 ratio, *yfp*:*cfp*. Strain 4-*yfp* attaches more and makes more biofilm when mixed with 69. Error bars are 95% confidence intervals of the mean from six replicates, which combines data from two different days. *, $p < 0.05$ and n.s., not significant in a *t* test. Find numerical values in S1 Data.

doi:10.1371/journal.pbio.1002191.g005

Antibiotic Gradients As Drivers of Biofilm Formation

Our data suggest that bacteriocins produced by natural isolates of *P. aeruginosa* act as a cue that drives biofilm formation. This raises the possibility that the widely reported biofilm responses to clinical antibiotics [10–17] also have their origins in responses to ecological competition from strains and species. But does the addition of antibiotics, or cell-free culture supernatant from competitors, also result in increased biofilm formation in a microfluidic device?

Experiments with a single concentration of antibiotic revealed that the addition of cell-free culture supernatant or clinical antibiotics commonly results in cell detachment at the initial stage of the experiment. This is consistent with the effects of supernatants and antibiotics in

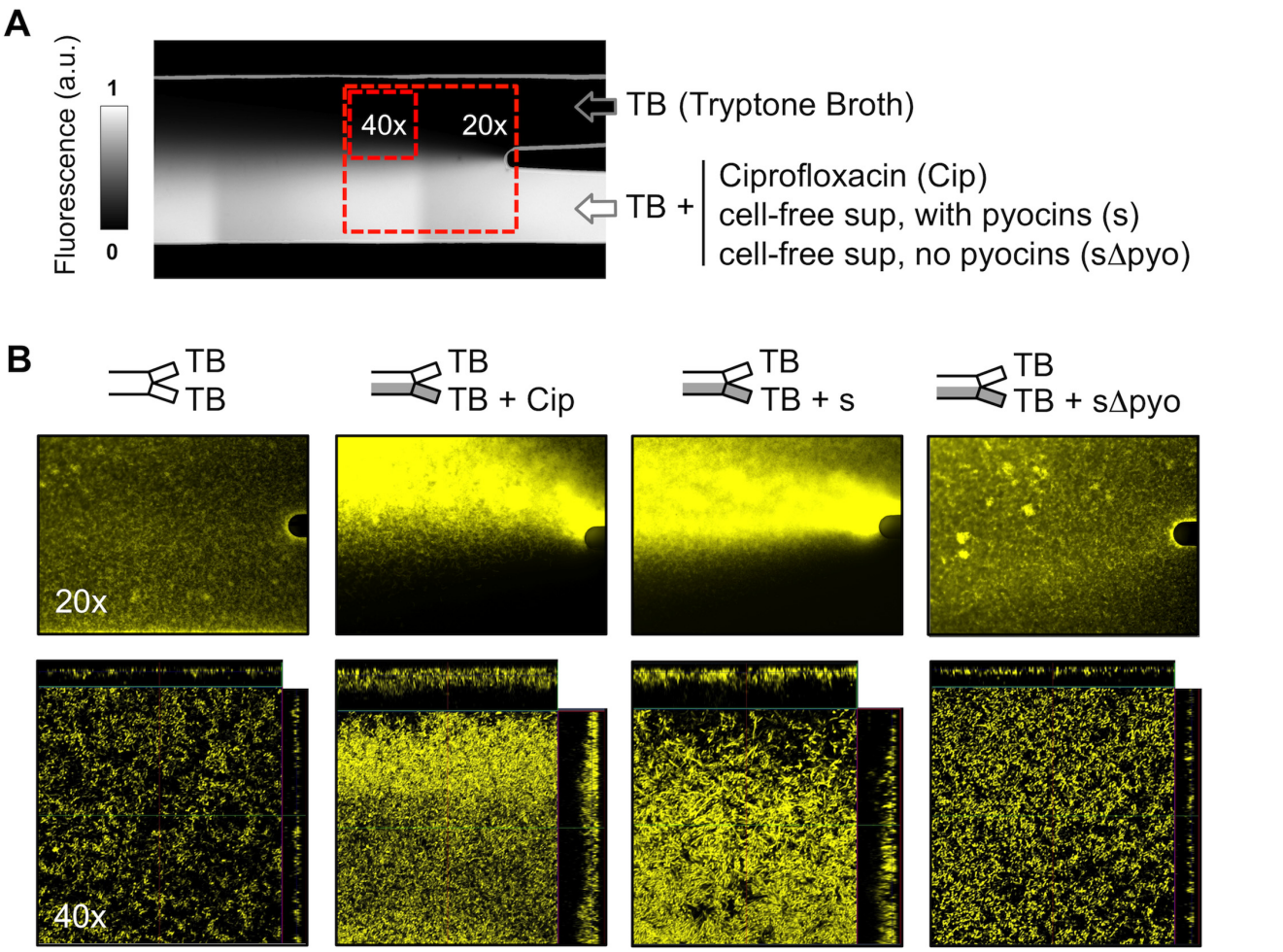

Fig 6. Antibiotic gradients drive biofilm formation. A) Image of the double inlet flow cell. Growth medium flows through both inlets but one also contains the test compound, which generates a gradient of the compound in the main chamber. Arrows indicate the direction of the flow. A fluorescent dye (fluorescein) has been added in this particular example (white) to illustrate the gradient created, but this is not present in the experiments in which we study the response of cells to antibiotics and cell-free supernatant (a.u., arbitrary units). B) Images corresponding to the red boxes shown in panel A, captured using a 20x objective (epifluorescence microscopy) and a 40x objective (confocal microscopy), respectively. 20x images are 350 μm by 450 μm, and 40x are 182 μm by 182 μm. Identical image collection and processing settings were used in all images to illustrate that ciprofloxacin ("Cip") and cell-free culture supernatant from strain PA14 ("s") both enhance the yellow signal when compared to controls at 20x magnification ("sΔpyo" is cell-free supernatant from the pyocin-null mutant and "TB" is tryptone broth, the standard medium). The confocal microscopy shows that the increase in the YFP signal in the epifluorescence images is explained by an increase in both cell density and volume of the biofilm.

doi:10.1371/journal.pbio.1002191.g006

the crystal violet assay being strongly concentration dependent, whereby lower concentrations cause the biofilm response and higher concentrations cause growth inhibition (Fig 3). We, therefore, developed a more robust method to study the effects of cell-free supernatant and antibiotics on biofilms in microfluidic devices. We moved to use microfluidic platforms with two inlet channels in which only one of the two inlets contains the antibiotics (Fig 6A).

The goal of this experimental approach was to create a gradient inside the main chamber with a wide range of antibiotic concentrations, from sub-lethal to lethal (see Methods). Our protocol always allows some parts of the chamber to contain negligible amounts of the antibiotic, which ensures that not all cells detach when antibiotics are flowed through. Importantly,

the cells will experience a wide range of concentrations of antibiotic in a single experiment, and we can directly observe how they respond. Under these conditions, we observe a large increase in biofilm formation upon the addition of multiple classes of antibiotics in multiple strain backgrounds (Figs 6, S6 and S7). Our data show that antibiotics do indeed promote biofilm formation in flow cells. In addition, they support the value of studying gradients for understanding cellular responses to stress. Such gradients are common in biofilms [56,57], but their effects can be missed by static culture assays.

We next asked whether pyocins are also capable of promoting biofilm formation in our dual inlet experiment. In support of this, we find that flowing the cell-free culture supernatant of PA14 over strain 4 results in increased biofilm formation, but not when we use the supernatant of the pyocin null-mutant (Fig 6). What drives the increase in biofilm? Increased biofilm accumulation could occur through stronger attachment and better retention of cells throughout the experiment, or through the acceleration of cell division. In order to test the impact of pyocins on attachment, we allowed strain 4 cells to attach in the presence of cell free supernatant of PA14 and compared this to the effect of cell free supernatant of the PA14 pyocin null-mutant (S8 Fig). This shows that pyocins do indeed lead to increased attachment. This phenotype is not simply sedimentation of damaged cells. We flush unattached cells out before imaging and, importantly, we see increased attachment in the presence of pyocins both on the bottom and the top of the channel (S9 Fig). Moreover, propidium iodide staining shows that, concurrently, there is increased cell damage from the supernatant of PA14 than with the supernatant of the pyocin null mutant (S8 Fig), consistent with what we found for shaking culture (S3 Fig). We see, therefore, that pyocins from competitors both cause cell damage (S3 and S8 Figs) and an increase in biofilm formation (Figs 6, S4, S8 and S9).

The attachment experiments (S8 and S9 Figs) suggest that the biofilm response may occur via an increased propensity for cells to attach, and subsequently persist, in the biofilm. An increased rate of cell division could also contribute to the biofilm response in some or all strains. Direct assessments of cell division in three-dimensional biofilms is challenging and was not possible with our current methods. However, there is evidence from *Escherichia coli* that sub-lethal levels of antibiotics can increase growth rate [58]. More generally, there is evidence for widespread transcriptional and metabolic changes in response to antibiotics [16,59–66], which have recently been the focus of intense debate [62,67–70] but still lack evolutionary explanation. If these changes are also involved in the responses to other bacterial strains and species, it would suggest that many of the physiological and metabolic changes seen upon antibiotic use have their natural origins in competition sensing [41] and the ecology of the species concerned.

Conclusions

Biofilms are central to microbiology. Despite this, we still understand relatively little about the drivers of biofilm formation in a natural context. Our data suggest that a major factor in biofilm formation in nature is ecological competition with other strains. We have shown that co-culturing strains of *P. aeruginosa* often leads to increased biofilm (Figs 1, 2 and 5). We have also shown that this increase in *P. aeruginosa* should not be interpreted as a cooperative interaction between strains. Mixing pairs of strains shows that one of the two strains is largely eliminated during the process of biofilm formation (Figs 2 and 5). Moreover, our data suggest that biofilm formation is stimulated as a response to cell damage caused by other strains: cell-free supernatant of one strain only induces biofilms in another strain when it can also causes cell damage (Figs 4, S3 and S8).

In pairwise mixtures of natural isolates, we have shown that one driver of the biofilm response are R and F pyocins, the narrow-spectrum antibiotics produced by *P. aeruginosa*. We, therefore, expect that pyocin-mediated competition will often be an inducer of biofilm formation in *P. aeruginosa*. However, our work also emphasizes that the biofilm responses to clinical antibiotics are highly comparable to those seen with pyocins. The different sets of antibiotics studied here have very different modes of action, including inhibition of DNA replication (ciprofloxacin), transcription (rifampicin), or translation (tetracycline) and, in the case of R and F pyocins, disruption of membrane potentials. The responses we observe, therefore, are very general and suggest that any toxin made by one *P. aeruginosa* strain has the potential to induce biofilm formation in another. Is there a common mechanism linking the diverse forms of cell damage to the biofilm response? Bacteria have a number of stress responses that are triggered by cell damage, which have been proposed as candidates for sensing the presence of competing strains [41]. Perhaps most notably, this includes the responses to oxidative stress, which is associated with the action of clinical antibiotics and diverse damaging agents from competing microbes [59,62,68,71,72].

What is the evolutionary basis of *P. aeruginosa* strains increasing biofilm formation in response to ecological competition? Mechanistically, our experiments suggest that the biofilm response is caused, at least in part, by an increase in surface-attachment in the presence of other strains. Whether a biofilm response is caused by differential attachment or another mechanism, the key effect is to increase the frequency of the responder relative to competing genotypes. We hypothesize that the evolutionary advantage of this increase in frequency is that it allows strains to better defend against and attack other genotypes. Biofilms are known to promote resistance to a wide range of stressors, including R pyocins [73]. In addition, competitive ability in a biofilm is expected to be linked to the relative density of each strain. At high density, cells can better control the environment with secreted products that favor their genotype over others [4,74]. Dominating a biofilm early, then, is likely to enable a genotype to dominate in the long term. In this model, the well-known biofilm responses to antibiotics [10–17] have their roots in natural selection to detect competing genotypes and respond in a manner that maximized the ability to defend and attack [39,41].

The fact that antibiotics are known to induce biofilm formation in diverse species suggests that ecological competition may increase biofilm formation in many microbial communities in which many strains and species meet. Consistent with this prediction, recent work on assemblage of multiple species, including known antibiotic producers, found that strain mixing increases biofilm formation [26,30,31], although it was interpreted there as cooperation between species. Understanding the effects of ecological competition on biofilm formation also has implications for health and disease. An important new idea in the treatment of disease is that we can harness ecological competition between microbes to our advantage [75,76]. Probiotic supplements for the gut are already an important industry [77], and a major goal of synthetic biology is to arm benign bacteria with the antibiotics they need to combat disease-causing strains [78]. We must be cautious, then, that this escalation of ecological competition does not result in the outcomes that we observe here: a more abundant pathogen.

Methods

Strains

A total of 22 strains of *Pseudomonas aeruginosa* were used, including both clinical and environmental isolates from the Kolter strain collection (S2 Table). A subset of these strains was subject to detailed analyses, including the well-studied clinical strain PAO1 (here referred to as strain 1), and strains 4, 7, 19, and 69. These five strains were chromosomally tagged with

constitutively-expressed fluorescent tags (*cfp* or *yfp*) using the mini-*Tn7* system [50]. The pyocin-null $prtR^{S153A}$ (constructed as in [52]), producing constitutively active repressor, and its parental strain PA14 were kindly provided by Jon Penterman. The R and F pyocin mutants are from the PA14 Non-Redundant Transposon Insertion Mutant Set [79]. We found no differences in our assays between the two sources of PA14 strains and only show the data from the Penterman source in the figures. Other strains are described in S3 Table.

Static Biofilm Assays

These assays were based on standard protocols [48]. Briefly, cells from overnight cultures of *P. aeruginosa* were sub-cultured and from these, exponential phase cells were inoculated in peg-lidded 96-well plates (Nunc, conical bottom) in 100 μl tryptone broth (10 g Bacto triptone per 1 l water) at starting optical density of 0.0025 (A_{600}), and allowed to grow at 22°C. After 24 h, 50 μl of medium was removed and the optical density at A_{600} was measured to estimate the density of planktonic cells. Pegs were then washed, stained with 0.1% crystal violet, washed again, and then the remaining stain was dissolved with 200 μl of 33% acetic acid. Finally, the optical density at A_{595} was measured and used as a proxy for biofilm formation. For direct strain-mixing experiments (Figs 1C, 1D and 2), we used plates without pegs because this allows cells to be more easily removed and sampled from the biofilms when required (see below). The only substantive difference is that the biofilm on the edge of the well is assessed using crystal violet rather than the biofilm on a peg. We confirmed that the two assays give very similar results (S10 Fig). While the experiments presented in the main text were done in tryptone broth, the biofilm response was also investigated in other standard bacterial growth media, including Luria broth (LB), *Pseudomonas* minimal medium (PMM) and casamino acid (CAA) medium, along with different concentrations of iron or buffer, which did not have qualitative effects in the cellular responses to mixing (S1 Fig).

Antibiotics

Three antibiotics belonging to different structural families, namely ciprofloxacin, rifampicin, and tetracycline, were chosen to recapitulate the effect of sub-inhibitory concentrations of antibiotics on biofilm formation of *P. aeruginosa* [13]. Stock solutions of each antibiotic (obtained from Sigma Chemical Company) were stored at -20°C and diluted to the desired concentration on the day of each experiment. All antibiotics experiments used tryptone broth as the growth medium. Biofilm formation and growth in shaking culture were assayed as detailed in the sections "Static Biofilm Assays" (above) and "Growth Curves" (below), respectively. For the dual-flow microfluidic experiments (Fig 6) we used 10x the concentration that inhibited growth in shaking culture, as shown in Fig 1. These are 1 μg/mL for ciprofloxacin, 50 μg/mL for rifampicin, and 1,000 μg/mL for tetracycline.

Strain Mixing Experiments

The initial survey of how strain mixing affects biofilm formation was based on 22 strains of *P. aeruginosa*. Biofilm formation after 24 h was evaluated in 22 single strains, 22 pair-wise combinations, eight combinations of five strains, and two of ten strains. Strains were evenly mixed based upon the optical density of stationary phase cultures. The strain combinations in the mixtures were chosen to ensure a near-even representation of the strains across the mixtures. Each strain occurred twice in the pairs, twice in the mixtures of fives (with one strain appearing only once), and once in a mixture of ten (with one strain excluded). Sixteen replicates were performed in each experiment for each strain or mixture, to give a total of 432 biofilm assays in each experiment. All treatments were performed on two different days.

The second set of experiments mixed five fluorescently-labeled strains in all combinations. We assessed biofilm formation and planktonic cell density in 96 well plates after 24 h. Samples of planktonic cells and biofilm cells were taken from each treatment to record the frequency of the two strains using fluorescence microscopy. The biofilm sample was taken by vigorously shaking the washed plates in phosphate buffer for one hour (experiments revealed that this treatment gives identical frequency estimates as shaking with 500 μm glass beads and removing the whole biofilm). In addition, direct images of the biofilms were taken by growing strains in 2 ml of media containing 25 x 25 mm^2 glass coverslips in 6-well plates under conditions otherwise identical to the 96-well plate assay. The bacteria form a biofilm on the coverslip slightly below the air-water interface, which is then visualized by fluorescent microscopy (Fig 2).

All experiments were repeated twice on different days. Comparison of these data with the pair-wise mixtures in the first experiments (above) confirmed that the mixing responses were not affected by fluorescent labeling. All methods were the same as before with the addition that we diluted overnight cultures of each strain and grew them for 2 h to obtain exponential phase cells to inoculate the biofilm assays (Fig 2). This did not affect biofilm formation, but it helped reduce variability in the strain frequency in the mixtures. For the two large-scale strain-mixing experiments (Figs 1C and 2), we present data that is the combination of the two repeats from different days as variability between days was relatively high.

Microfluidic Biofilm Assays

Biofilm formation was also monitored under laminar flow conditions using the BioFlux 200 system (Fluxion Biosciences, South San Francisco, CA, United States). Experiments were performed essentially as described elsewhere [80]. First, microfluidic channels (350 μm x 75 μm x 4.89 mm for width, height, and length, respectively) were primed with growth media, here tryptone broth, to prevent air bubbles from entering the channels on subsequent loading steps, and just after, inoculated with cells at the exponential phase. The concentration of these cultures was adjusted so that the optical density at 600 nm in tryptone broth was 0.25. Then, after the attachment period without flow (20 min at 22°C), fresh medium was pumped from inlet wells through the channels to outlet, firstly with a flow rate of 40 μl/h for 20 min to flush out planktonic cells, and then with a constant flow rate of 4 μl/h until the end of the experiments (24 or 48 h). To address the effect of pyocins on cellular attachment we allowed cells to attach in the channels for 20 min with tryptone broth made with 10% cell-free supernatant, either from strain PA14 WT or a mutant that has the repressor of pyocins, *prtR*, mutated to a version that is constitutively active (S3 Table). We then flushed out planktonic cells, as explained above, and imaged to assess attachment.

For consistency, we used only one plate type for all microfluidic experiments, the "Invasion" plate of Fluxion Biosciences that has two parallel inlets and one outlet (Fig 6). When studying co-cultures, the two inlets contained the same medium, and when studying the effect of antibiotic gradients we added the required concentration of the antibiotic (or cell-free culture supernatant) to one of the inlets only, thus creating a gradient of the compound being tested in the main chamber. Each experiment was repeated twice, on different days, and the images of biofilms taken come from the middle of the channels, where the channels are the flattest, when accessing the effects of strain mixing. In all treatments, images were taken at the same distance from the respective inlets. When accessing the effect of antibiotics or cell-free supernatant we imaged directly downstream of the inlets, as shown in Fig 6, where the gradient is the steepest.

Study of Diffusible Substances

To access the effects of diffusible substances in the biofilm response, two sets of experiments were performed. Firstly, we used 96-well Transwell plates (Corning) with two different inlays separated by a 0.4 μm pore size membrane. In these experiments, the strain in the bottom of the well was inoculated at an optical density of 0.0025 (A_{600}) in 75 μl of media. This bottom strain was the tester strain in which biofilm formation was analyzed. The top strain was the inducer and was inoculated at a higher density of 0.1 (A_{600}) with 50 μl media. These revealed cell-to-cell contact is not strictly necessary for the biofilm response (Fig 3A). To investigate this further, we studied responses of strains to cell-free supernatants from other strains. The supernatant of the strains were obtained as follows. Exponential phase cells of all strains were inoculated in 6-well plates in 4 ml of tryptone broth at starting optical density of 0.025 (A_{600}), and allowed to grow at 22°C for 21 h. Cultures were then spun down (3,000 g during 10 min) and filtrated using 0.22 μm filters (Millipore). The spent media assay followed the same methods for the biofilm assay, except that exponential phase cells of the responder strain were inoculated in media containing (2.5/25%) cell-free culture supernatant from itself or others.

Fractionation of the cell free supernatant was performed by GE 1 ml resource Q anion exchange chromatography (buffer A: 50 mM Tris-HCl [pH 7.5], 2% glycerol, 2 mM β-mercaptoethanol; buffer B: buffer A + 1 M NaCl) followed by GE Superdex 200 10/300 GL gel filtration in SEC buffer. The active fraction, as determined by the crystal violet assay (Fig 4), was subject to mass spectrometry by the FAS Center for Systems Biology Core Facilities, Harvard University, US. Briefly, the sample was reduced, carboxyamidomethylated and digested with trypsin. Peptide sequence analysis of each digestion mixture was then performed by microcapillary reversed phase high-performance liquid chromatography coupled with nanoelectrospray tandem mass spectrometry (μLC-MS/MS) on an LTQ-Orbitrap mass spectrometer (Thermo-Fisher Scientific, San Jose, CA, US).

Growth Curves

Exponential phase cells from overnight cultures were inoculated in flat-bottomed 96-well plates (Nunc) in 200 μl of tryptone broth at the starting optical density (A_{600}) of 0.0025, as for the biofilm assays, and allowed to grow at 22°C, shaking, inside a plate reader (Tecan, Infinite M200 Pro). Test treatments were supplemented with 25% of cell-free supernatant from PA14, the respective pyocin-null, or distilled water (control). The optical density at A_{600} was measured automatically every 500 s. When required, cell damage was assessed by staining shaking cultures or attached cells in a microfluidic device with propidium iodide (at the final concentration of 3 μl/ml)[81]. Propidium iodide-stained cells were visualized using epifluorescence microscopy with DsRed-based filters.

Fluorescence and Confocal Microscopy

Images of BioFlux biofilms were obtained using a Zeiss confocal laser scanning microscope (LSM 700), a digital camera (AxioCam MRm), and the associated Zen 2011 software (blue or black edition, for fluorescence or confocal microscopy, respectively). Objectives used were 10x, 20x, or 40x, as specified in the figure legends.

Image Analysis

A MATLAB (MathWorks) script was used to determine the number of attached cells on the surface of microfluidics, along with the volume of biofilms after 24 h and 48 h of incubation.

The volume calculation uses the area of fluorescence signal of biofilms in each confocal slice, which is then summed across the slices in *z*-plane.

Supporting Information

S1 Data. Excel file containing the data for Figs 1A–1D, 2A, 2B, 3A, 3B, 4A–4D, 5B–5C, S1, S2, S3, S4, S5 and S10.
(XLSX)

S1 Fig. The biofilm response is observed across multiple environmental conditions. Biofilm formation in single-strain and mixed-strain cultures is shown across a range of conditions. We compared biofilm formation across (i) three nutrient concentrations with casamino acids (CAA) media: 0.1% CAA (low), 0.5% CAA (medium), 2.5% CAA (high); (ii) three iron levels with casamino acids media (100 mg apotransferin + 1 μM FeCl, 100mg apotransferin + 5 μM FeCl, no added apotransferin or FeCl); (iii) three buffering levels with casamino acids media (Unbuffered, 25 mM HEPES, 75mM HEPES); and (iv) four standard media including Luria broth (LB), tryptone broth (TB), *Pseudomonas* minimal medium (PMM), and casamino acid (CAA) medium. Note that the CAA standard media treatment is replotted in each quadrant for comparison, where it represents medium nutrients, unlimited iron, no buffering, and CAA, respectively. In most cases, strain 4 is outcompeted and represents <5% of the planktonic cells after 24 h. A few exceptions are marked with an arrow where strain 4 is >5% frequency in the planktonic cells. Most notably, the 4 + 69 mixtures marked with an arrow have strain 4 at >90% of planktonic cells, showing how the outcome of competition is strongly influenced by the environment, while the biofilm response is much less so. Error bars indicate the 95% confidence intervals of the mean. Find numerical values in S1 Data.
(TIFF)

S2 Fig. Dose-dependent effect of strain mixing on the biofilm response of strains 4 and PA14. Error bars are 95% confidence intervals of the mean. Find numerical values in S1 Data.
(TIFF)

S3 Fig. Pyocin-induced cell damage in shaking culture. Cell-free supernatant from wild-type (WT) PA14 inhibits the growth of strain 4, as shown in Fig 3. The observed growth lag (left-hand plots) is driven by pyocins, the narrow spectrum antibiotics of *P. aeruginosa*, and is associated with cell damage (right hand images). After 5 h of growth in the presence of 25% of PA14 cell free supernatant with pyocins ("s14") or without ("s14Δpyo") we stained cultures of strain 4 with propidium iodide, and imaged cells using epifluorescence microscopy (see S3 Table for details of PA14 strains). The responder genotype (strain 4) is tagged with a fluorescent protein (YFP), and damaged cells are seen in red. The growth curves on the left are means of eight independent replicates and images on the right are representative images of cell damage in the cultures at the end of the growth period (large red blob is an out-of-focus damaged cell). Images from each fluorescent channel were collected and processed using the same settings to ensure consistency. Scale bar is 20 μm. Find numerical values in S1 Data.
(TIFF)

S4 Fig. Pyocin-induced biofilm formation in additional strains of *P. aeruginosa*. Shown are the effects of cell-free culture supernatants from PA14 and the pyocin-null mutant (14Δpyo) on two natural isolates from Fig 1C. Pyocin-induced biofilm formation is also observed in PAK, a strain known to be susceptible to pyocins from PA14. Error bars are 95% confidence intervals of the mean. Find numerical values in S1 Data.
(TIFF)

S5 Fig. Effect of antibiotic resistance on antibiotic-induced biofilm formation. Strain PAO1 exhibits a rifampicin-induced biofilm response, but its rifampicin resistant mutant does not. Error bars are 95% confidence intervals of the mean. Find numerical values in S1 Data.
(TIFF)

S6 Fig. Different classes of clinical antibiotics promote biofilm formation in flow cells. Gradients of rifampicin (Rif) and tetracycline (Tet) drive biofilm accumulation in strain 4 as one finds with gradients of ciprofloxacin (Fig 6). The effect is particularly clear after 48 h of incubation when the biofilm increase is such that blocks the flow. For each treatment we show representative epifluorence microscopy images captured with 10x lens (scale bar is 100 μm for "Brightfield," "YFP," and "Merged"), as well as representative confocal images captured with 40x lens (scale bar is 30 μm). Epifluorence images were collected and processed using the same settings to ensure consistency. Confocal images show that the increase in the YFP signal with antibiotic gradients is explained by an increase in both cell density and volume of the biofilm.
(TIFF)

S7 Fig. Antibiotics promote biofilm formation in flow cells in a second strain background (strain 69). Gradients of ciprofloxacin (Cip), rifampicin (Rif), and tetracycline (Tet) drive biofilm accumulation. The effect is particularly clear after 48 h of incubation when the biofilm increase is such that it can block the flow. For each treatment we show representative epifluorence microscopy images captured with 10x lens (scale bar, 100 μm for "Brightfield," "YFP," and "Merged"), as well as representative confocal images captured with 40x lens (scale bar is 30 μm). Confocal images show that the increase in the YFP signal with antibiotic gradients is explained by an increase in both cell density and volume of the biofilm.
(TIFF)

S8 Fig. Pyocins from competitor genotypes drive both attachment and cell damage in *P. aeruginosa*. Cell-free supernatant from WT PA14 (s14) promotes surface attachment of strain 4 when compared to supernatant from the respective pyocin-null genotype (s14Δpyo) as observed by two representative regions of each channel. Following the attachment phase we stained *yfp*-labeled cells with propidium iodide to test for cell damage (red). Images from each fluorescent channel were collected and processed using the same settings to ensure consistency. Scale bar is 20 μm. Experiments were repeated on different days to validate results.
(TIFF)

S9 Fig. Pyocin-induced attachment occurs on the top and bottom of the microfluidic device. Specifically, we see increased cellular attachment of YFP-labeled strain 4 in the presence of pyocin-containing cell-free supernatant from WT PA14 (s14) on both the bottom (glass) and top (PDMS) of channels, when compared to supernatant from the respective pyocin-null genotype (s14Δpyo). $p < 0.05$ in unpaired t tests at 5% significance. We show two representative images of each condition. Scale bar is 20 μm.
(TIFF)

S10 Fig. Comparison of standard assays (A) and peg assays (B) on mixing-induced biofilm formation. In standard assays, the biofilms measured are those attached to the edge of the wells in microtiter plates. In peg assays, the biofilms measured are those attached to pegs inserted into the wells. Here we show dose-dependent effects of strain mixing on the biofilm response of strains 1 and 4 (left) and 4 and 69 (right). Increased biofilm due to strain mixing is seen in both assays. Error bars are 95% confidence intervals of the mean. Find numerical values in S1 Data.
(TIFF)

S1 Table. Tryptic peptide fragments identified by mass spectrometry found by Protein Mass Spectrometry with homology to pyocin proteins.
(TIFF)

S2 Table. Natural isolates of *Pseudomonas aeruginosa* used in this study.
(TIFF)

S3 Table. Additional strains used in this study.
(TIFF)

Acknowledgments

We would like to thank Dan Cornforth and Sara Mitri for their comments on the manuscript. We thank Bodo Stern, Katharina Ribbeck, Andrew Murray, Joan Strassmann, David Queller, Julian Davies, Søren Sørensen, and Mette Burmølle for helpful discussions. We would also like to thank Jon Penterman and Pradeep Singh for the pyocin-null strain of PA14, Joseph Lam and the van Delden lab for the PAK strain and Qin Qi (MacLean lab) for the rifampicin resistant mutant of PAO1. Finally, KRF thanks Vlad Denic for afternoon adventures in protein purification and an inspiring conversation in the Forest Hills tennis club.

Author Contributions

Conceived and designed the experiments: NMO EMG JX RK WMD WK KRF. Performed the experiments: NMO EMG KRF. Analyzed the data: NMO EMG JX KRF. Contributed reagents/materials/analysis tools: RK WK. Wrote the paper: NMO RK WK KRF.

References

1. Costerton JW (1995) Overview of microbial biofilms. J Ind Microbiol 15: 137–140. PMID: 8519468
2. Kolter R, Greenberg EP (2006) Microbial sciences—The superficial life of microbes. Nature 441: 300–302. PMID: 16710410
3. Monds RD, O'Toole GA (2009) The developmental model of microbial biofilms: ten years of a paradigm up for review. Trends in Microbiology 17: 73–87. doi: 10.1016/j.tim.2008.11.001 PMID: 19162483
4. Nadell CD, Xavier JB, Foster KR (2009) The sociobiology of biofilms. FEMS Microbiol Rev 33: 206–224. doi: 10.1111/j.1574-6976.2008.00150.x PMID: 19067751
5. Hall-Stoodley L, Costerton JW, Stoodley P (2004) Bacterial biofilms: From the natural environment to infectious diseases. Nature Reviews Microbiology 2: 95–108. PMID: 15040259
6. Lopez D, Vlamakis H, Kolter R (2010) Biofilms. Cold Spring Harbor Perspectives in Biology 2: a000398. doi: 10.1101/cshperspect.a000398 PMID: 20519345
7. Romling U, Kjelleberg S, Normark S, Nyman L, Uhlin BE, et al. (2014) Microbial biofilm formation: a need to act. J Intern Med 276: 98–110. doi: 10.1111/joim.12242 PMID: 24796496
8. Beloin C, Ghigo JM (2005) Finding gene-expression patterns in bacterial biofilms. Trends in Microbiology 13: 16–19. PMID: 15639627
9. Karatan E, Watnick P (2009) Signals, Regulatory Networks, and Materials That Build and Break Bacterial Biofilms. Microbiology and Molecular Biology Reviews 73: 310–347. doi: 10.1128/MMBR.00041-08 PMID: 19487730
10. Elliott D, Burns JL, Hoffman LR (2010) Exploratory Study of the Prevalence and Clinical Significance of Tobramycin-Mediated Biofilm Induction in *Pseudomonas aeruginosa* Isolates from Cystic Fibrosis Patients. Antimicrobial Agents and Chemotherapy 54: 3024–3026. doi: 10.1128/AAC.00102-10 PMID: 20404125
11. Haddadin RNS, Saleh S, Al-Adham ISI, Buultjens TEJ, Collier PJ (2010) The effect of subminimal inhibitory concentrations of antibiotics on virulence factors expressed by *Staphylococcus aureus* biofilms. Journal of Applied Microbiology 108: 1281–1291. doi: 10.1111/j.1365-2672.2009.04529.x PMID: 19778348
12. Hoffman LR, D'Argenio DA, MacCoss MJ, Zhang ZY, Jones RA, et al. (2005) Aminoglycoside antibiotics induce bacterial biofilm formation. Nature 436: 1171–1175. PMID: 16121184

13. Kaplan JB (2011) Antibiotic-induced biofilm formation. International Journal of Artificial Organs 34: 737–751. doi: 10.5301/ijao.5000027 PMID: 22094552

14. Kaplan JB, Izano EA, Gopal P, Karwacki MT, Kim S, et al. (2012) Low levels of beta-lactam antibiotics induce extracellular DNA release and biofilm formation in *Staphylococcus aureus*. MBio 3: e00198–00112. doi: 10.1128/mBio.00198-12 PMID: 22851659

15. Kumar A, Ting YP (2013) Effect of sub-inhibitory antibacterial stress on bacterial surface properties and biofilm formation. Colloids and Surfaces B-Biointerfaces 111: 747–754.

16. Linares JF, Gustafsson I, Baquero F, Martinez JL (2006) Antibiotics as intermicrobial signaling agents instead of weapons. Proceedings of the National Academy of Sciences of the United States of America 103: 19484–19489. PMID: 17148599

17. Wang Q, Sun FJ, Liu Y, Xiong LR, Xie LL, et al. (2010) Enhancement of Biofilm Formation by Subinhibitory Concentrations of Macrolides in icaADBC-Positive and-Negative Clinical Isolates of *Staphylococcus epidermidis*. Antimicrobial Agents and Chemotherapy 54: 2707–2711. doi: 10.1128/AAC.01565-09 PMID: 20231401

18. Andersson DI, Hughes D (2014) Microbiological effects of sublethal levels of antibiotics. Nat Rev Microbiol 12: 465–478. doi: 10.1038/nrmicro3270 PMID: 24861036

19. Davies J, Spiegelman GB, Yim G (2006) The world of subinhibitory antibiotic concentrations. Curr Opin Microbiol 9: 445–453. PMID: 16942902

20. Fajardo A, Martinez JL (2008) Antibiotics as signals that trigger specific bacterial responses. Current Opinion in Microbiology 11: 161–167. doi: 10.1016/j.mib.2008.02.006 PMID: 18373943

21. Yim G, Wang HMH, Davies J (2007) Antibiotics as signalling molecules. Philosophical Transactions of the Royal Society B-Biological Sciences 362: 1195–1200.

22. Andersson S, Rajarao GK, Land CJ, Dalhammar G (2008) Biofilm formation and interactions of bacterial strains found in wastewater treatment systems. Fems Microbiology Letters 283: 83–90. doi: 10.1111/j.1574-6968.2008.01149.x PMID: 18422628

23. Burmolle M, Ren DW, Bjarnsholt T, Sorensen SJ (2014) Interactions in multispecies biofilms: do they actually matter? Trends in Microbiology 22: 84–91. doi: 10.1016/j.tim.2013.12.004 PMID: 24440178

24. Burmolle M, Webb JS, Rao D, Hansen LH, Sorensen SJ, et al. (2006) Enhanced biofilm formation and increased resistance to antimicrobial agents and bacterial invasion are caused by synergistic interactions in multispecies biofilms. Appl Environ Microbiol 72: 3916–3923. PMID: 16751497

25. Elias S, Banin E (2012) Multi-species biofilms: living with friendly neighbors. FEMS Microbiol Rev 73: 310–347.

26. Lee KWK, Periasamy S, Mukherjee M, Xie C, Kjelleberg S, et al. (2014) Biofilm development and enhanced stress resistance of a model, mixed-species community biofilm. Isme Journal 8: 894–907. doi: 10.1038/ismej.2013.194 PMID: 24152718

27. Little AEF, Robinson CJ, Peterson SB, Raffa KE, Handelsman J (2008) Rules of Engagement: Interspecies Interactions that Regulate Microbial Communities. Annual Review of Microbiology 62: 375–401. doi: 10.1146/annurev.micro.030608.101423 PMID: 18544040

28. Moller S, Sternberg C, Andersen JB, Christensen BB, Ramos JL, et al. (1998) In situ gene expression in mixed-culture biofilms: Evidence of metabolic interactions between community members. Applied and Environmental Microbiology 64: 721–732. PMID: 9464414

29. Pande S, Merker H, Bohl K, Reichelt M, Schuster S, et al. (2013) Fitness and stability of obligate cross-feeding interactions that emerge upon gene loss in bacteria. ISME J 8: 953–962. doi: 10.1038/ismej.2013.211 PMID: 24285359

30. Ren D, Madsen JS, de la Cruz-Perera CI, Bergmark L, Sorensen SJ, et al. (2014) High-Throughput Screening of Multispecies Biofilm Formation and Quantitative PCR-Based Assessment of Individual Species Proportions, Useful for Exploring Interspecific Bacterial Interactions. Microb Ecol 68: 146–154. doi: 10.1007/s00248-013-0315-z PMID: 24337804

31. Ren D, Madsen JS, Sorensen SJ, Burmolle M (2014) High prevalence of biofilm synergy among bacterial soil isolates in cocultures indicates bacterial interspecific cooperation. ISME J 9: 81–89. doi: 10.1038/ismej.2014.96 PMID: 24936766

32. Chandler JR, Heilmann S, Mittler JE, Greenberg EP (2012) Acyl-homoserine lactone-dependent eavesdropping promotes competition in a laboratory co-culture model. Isme Journal 6: 2219–2228. doi: 10.1038/ismej.2012.69 PMID: 22763647

33. Drescher K, Nadell CD, Stone HA, Wingreen NS, Bassler BL (2014) Solutions to the Public Goods Dilemma in Bacterial Biofilms. Current Biology 24: 50–55. doi: 10.1016/j.cub.2013.10.030 PMID: 24332540

34. Mitri S, Foster KR (2013) The genotypic view of social interactions in microbial communities. Annu Rev Genet 47: 247–273. doi: 10.1146/annurev-genet-111212-133307 PMID: 24016192

35. Nadell CD, Bassler BL (2011) A fitness trade-off between local competition and dispersal in *Vibrio cholerae* biofilms. Proceedings of the National Academy of Sciences of the United States of America 108: 14181–14185. doi: 10.1073/pnas.1111147108 PMID: 21825170

36. Foster KR, Bell T (2012) Competition, not cooperation, dominates interactions among culturable microbial species. Curr Biol 22: 1845–1850. doi: 10.1016/j.cub.2012.08.005 PMID: 22959348

37. Hibbing ME, Fuqua C, Parsek MR, Peterson SB (2010) Bacterial competition: surviving and thriving in the microbial jungle. Nature Reviews Microbiology 8: 15–25. doi: 10.1038/nrmicro2259 PMID: 19946288

38. Oliveira NM, Niehus R, Foster KR (2014) Evolutionary limits to cooperation in microbial communities. Proceedings of the National Academy of Sciences of the United States of America 111: 17941–17946. doi: 10.1073/pnas.1412673111 PMID: 25453102

39. Ratcliff WC, Denison RF (2011) Microbiology. Alternative actions for antibiotics. Science 332: 547–548. doi: 10.1126/science.1205970 PMID: 21527704

40. Bernier SP, Surette MG (2013) Concentration-dependent activity of antibiotics in natural environments. Front Microbiol 4: 20. doi: 10.3389/fmicb.2013.00020 PMID: 23422936

41. Cornforth DM, Foster KR (2013) Competition sensing: the social side of bacterial stress responses. Nature Reviews Microbiology 11: 285–293. doi: 10.1038/nrmicro2977 PMID: 23456045

42. Keller L, Surette MG (2006) Communication in bacteria: an ecological and evolutionary perspective. Nature Reviews Microbiology 4: 249–258. PMID: 16501584

43. Maynard Smith J, Harper D (2003) Animal signals. Oxford: Oxford University Press. ix, 166 p. p.

44. Darwin C (1859) On the origin of species by means of natural selection. London,: J. Murray. ix, 1, 502 p. p.

45. Burns JL, Gibson RL, McNamara S, Yim D, Emerson J, et al. (2001) Longitudinal assessment of *Pseudomonas aeruginosa* in young children with cystic fibrosis. J Infect Dis 183: 444–452. PMID: 11133376

46. Mahenthiralingam E, Campbell ME, Foster J, Lam JS, Speert DP (1996) Random amplified polymorphic DNA typing of *Pseudomonas aeruginosa* isolates recovered from patients with cystic fibrosis. J Clin Microbiol 34: 1129–1135. PMID: 8727889

47. Renders N, Verbrugh H, Van Belkum A (2001) Dynamics of bacterial colonisation in the respiratory tract of patients with cystic fibrosis. Infect Genet Evol 1: 29–39. PMID: 12798048

48. O'Toole GA, Kolter R (1998) Flagellar and twitching motility are necessary for *Pseudomonas aeruginosa* biofilm development. Molecular Microbiology 30: 295–304. PMID: 9791175

49. Savoia D, Zucca M (2007) Clinical and environmental Burkholderia strains: Biofilm production and intracellular survival. Current Microbiology 54: 440–444. PMID: 17457645

50. Lambertsen L, Sternberg C, Molin S (2004) Mini-Tn7 transposons for site-specific tagging of bacteria with fluorescent proteins. Environ Microbiol 6: 726–732. PMID: 15186351

51. Michel-Briand Y, Baysse C (2002) The pyocins of *Pseudomonas aeruginosa*. Biochimie 84: 499–510. PMID: 12423794

52. Penterman J, Singh PK, Walker GC (2014) Biological Cost of Pyocin Production during the SOS Response in *Pseudomonas aeruginosa*. Journal of Bacteriology 196: 3351–3359. doi: 10.1128/JB.01889-14 PMID: 25022851

53. Heo YJ, Chung IY, Choi KB, Cho YH (2007) R-Type pyocin is required for competitive growth advantage between *Pseudomonas aeruginosa* strains. Journal of Microbiology and Biotechnology 17: 180–185. PMID: 18051371

54. Kohler T, Donner V, van Delden C (2010) Lipopolysaccharide as Shield and Receptor for R-Pyocin-Mediated Killing in *Pseudomonas aeruginosa*. Journal of Bacteriology 192: 1921–1928. doi: 10.1128/JB.01459-09 PMID: 20118263

55. Qi Q, Preston GM, MacLean RC (2014) Linking System-Wide Impacts of RNA Polymerase Mutations to the Fitness Cost of Rifampin Resistance in *Pseudomonas aeruginosa*. Mbio 5: e01562. doi: 10.1128/mBio.01562-14 PMID: 25491352

56. Tseng BS, Zhang W, Harrison JJ, Quach TP, Song JL, et al. (2013) The extracellular matrix protects *Pseudomonas aeruginosa* biofilms by limiting the penetration of tobramycin. Environmental Microbiology 15: 2865–2878. doi: 10.1111/1462-2920.12155 PMID: 23751003

57. Stewart PS, Franklin MJ (2008) Physiological heterogeneity in biofilms. Nature Reviews Microbiology 6: 199–210. doi: 10.1038/nrmicro1838 PMID: 18264116

58. Migliore L, Rotini A, Thaller MC (2013) Low Doses of Tetracycline Trigger the *E. Coli* Growth: A Case of Hormetic Response. Dose-Response 11: 550–557. doi: 10.2203/dose-response.13-002.Migliore PMID: 24298230

59. Dwyer DJ, Belenky PA, Yang JH, MacDonald IC, Martell JD, et al. (2014) Antibiotics induce redox-related physiological alterations as part of their lethality. Proc Natl Acad Sci U S A 111: E2100–2109. doi: 10.1073/pnas.1401876111 PMID: 24803433

60. Dwyer DJ, Kohanski MA, Hayete B, Collins JJ (2007) Gyrase inhibitors induce an oxidative damage cellular death pathway in *Escherichia coli*. Molecular Systems Biology 3: 91. PMID: 17353933

61. Goh EB, Yim G, Tsui W, McClure J, Surette MG, et al. (2002) Transcriptional modulation of bacterial gene expression by subinhibitory concentrations of antibiotics. Proceedings of the National Academy of Sciences of the United States of America 99: 17025–17030. PMID: 12482953

62. Kohanski MA, Dwyer DJ, Collins JJ (2010) How antibiotics kill bacteria: from targets to networks. Nature Reviews Microbiology 8: 423–435. doi: 10.1038/nrmicro2333 PMID: 20440275

63. Kohanski MA, Dwyer DJ, Hayete B, Lawrence CA, Collins JJ (2007) A common mechanism of cellular death induced by bactericidal antibiotics. Cell 130: 797–810. PMID: 17803904

64. Kohanski MA, Dwyer DJ, Wierzbowski J, Cottarel G, Collins JJ (2008) Mistranslation of Membrane Proteins and Two-Component System Activation Trigger Antibiotic-Mediated Cell Death. Cell 135: 679–690. doi: 10.1016/j.cell.2008.09.038 PMID: 19013277

65. Tsui WHW, Yim G, Wang HHM, McClure JE, Surette MG, et al. (2004) Dual effects of MLS antibiotics: Transcriptional modulation and interactions on the ribosome. Chemistry & Biology 11: 1307–1316.

66. Kohanski MA, DePristo MA, Collins JJ (2010) Sublethal Antibiotic Treatment Leads to Multidrug Resistance via Radical-Induced Mutagenesis. Molecular Cell 37: 311–320. doi: 10.1016/j.molcel.2010.01.003 PMID: 20159551

67. Ezraty B, Vergnes A, Banzhaf M, Duverger Y, Huguenot A, et al. (2013) Fe-S Cluster Biosynthesis Controls Uptake of Aminoglycosides in a ROS-Less Death Pathway. Science 340: 1583–1587. doi: 10.1126/science.1238328 PMID: 23812717

68. Imlay JA (2015) Diagnosing oxidative stress in bacteria: not as easy as you might think. Curr Opin Microbiol 24C: 124–131.

69. Keren I (2013) Killing by bactericidal antibiotics does not depend on reactive oxygen species (vol 339, pg 1213, 2013). Science 340: 1404–1404.

70. Liu YY, Imlay JA (2013) Cell Death from Antibiotics Without the Involvement of Reactive Oxygen Species. Science 339: 1210–1213. doi: 10.1126/science.1232751 PMID: 23471409

71. Dong TG, Dong S, Catalano C, Moore R, Liang X, et al. (2015) Generation of reactive oxygen species by lethal attacks from competing microbes. Proc Natl Acad Sci U S A 112: 2181–2186. doi: 10.1073/pnas.1425007112 PMID: 25646446

72. Imlay JA (2013) The molecular mechanisms and physiological consequences of oxidative stress: lessons from a model bacterium. Nature Reviews Microbiology 11: 443–454. doi: 10.1038/nrmicro3032 PMID: 23712352

73. Penterman J, Nguyen D, Anderson E, Staudinger BJ, Greenberg EP, et al. (2014) Rapid Evolution of Culture-Impaired Bacteria during Adaptation to Biofilm Growth. Cell Reports 6: 293–300. doi: 10.1016/j.celrep.2013.12.019 PMID: 24412364

74. West SA, Griffin AS, Gardner A, Diggle SP (2006) Social evolution theory for microorganisms. Nature Reviews Microbiology 4: 597–607. PMID: 16845430

75. Callaway TR, Edrington TS, Anderson RC, Harvey RB, Genovese KJ, et al. (2008) Probiotics, prebiotics and competitive exclusion for prophylaxis against bacterial disease. Anim Health Res Rev 9: 217–225. doi: 10.1017/S1466252308001540 PMID: 19102792

76. Kamada N, Chen GY, Inohara N, Nunez G (2013) Control of pathogens and pathobionts by the gut microbiota. Nature Immunology 14: 685–690. doi: 10.1038/ni.2608 PMID: 23778796

77. Gareau MG, Sherman PM, Walker WA (2010) Probiotics and the gut microbiota in intestinal health and disease. Nat Rev Gastroenterol Hepatol 7: 503–514. doi: 10.1038/nrgastro.2010.117 PMID: 20664519

78. Saeidi N, Wong CK, Lo TM, Nguyen HX, Ling H, et al. (2011) Engineering microbes to sense and eradicate *Pseudomonas aeruginosa*, a human pathogen. Molecular Systems Biology 7: 521. doi: 10.1038/msb.2011.55 PMID: 21847113

79. Liberati NT, Urbach JM, Miyata S, Lee DG, Drenkard E, et al. (2006) An ordered, nonredundant library of *Pseudomonas aeruginosa* strain PA14 transposon insertion mutants. Proceedings of the National Academy of Sciences of the United States of America 103: 19931–19931.

80. Benoit MR, Conant CG, Ionescu-Zanetti C, Schwartz M, Matin A (2010) New Device for High-Throughput Viability Screening of Flow Biofilms. Applied and Environmental Microbiology 76: 4136–4142. doi: 10.1128/AEM.03065-09 PMID: 20435763

81. Webb JS, Thompson LS, James S, Charlton T, Tolker-Nielsen T, et al. (2003) Cell death in *Pseudomonas aeruginosa* biofilm development. Journal of Bacteriology 185: 4585–4592. PMID: 12867469